UNIVERSITY OF LIVERPOOL

Examination of mitochondrial and cellular response to metabolic stresses: changes in mitochondrial membrane potential by modulators of ischaemic preconditioning and metabolic stress-induced extracellular nucleotide accumulation.

Thesis submitted in accordance with the requirements of the University of Liverpool for the degree of Doctor in Philosophy by Christopher John Eric Thompson.

2013

I would like to dedicate this thesis to my family whom without their support and encouragement this would still be unwritten. This is especially true of Amy Williams and my daughter Isla who have helped me all the way and made sure that this thesis was submitted in time.

I would like to thank Dr. Alec Simpson for the opportunity to work in his laboratory and develop the techniques, critical thinking and analytical skills required in scientific research. Dr Helen Burrell's support in developing techniques, scientific reasoning and producing this thesis was invaluable. I would also like to thank Dr John Qyale, Dr Tomoko Kamishima and Dr Alex Laude for their support and tutelage. Lastly I am grateful to Dr Rachel Carter for her instruction and support in working with chick embryos.

Contents

1. Abstract

1.1. Introduction

Cardiac and cerebral ischaemia can induce cellular hypoxia which results in injury potentially via apoptosis. In 2004, this accounted for 12.9 million (21.9%) of the world's deaths. Brief periods of ischaemia are known to protect cells from a subsequent and more sustained ischaemic event. This action is known as ischaemic preconditioning (IPC). Pharmacological agents can be used to manipulate IPC. Diazoxide is well documented to promote IPC, while 5-hydroxydecanoyl (5-HD) abolishes diazoxide-induced IPC. The mitoK_{ATP} channel, the sarcoK_{ATP} channel or succinate dehydrogenase are implicated in facilitating IPC. Actions of these agents are likely to converge on mitochondrial function. Also, during hypoxia it is widely reported that extracellular ATP becomes elevated. Whilst the activity of ATP via P2 signalling is well documented along with the activity of adenosine via A receptors, little attention has been paid to extracellular ADP or potential P2Y signalling arising from hypoxia. The aim of this study was to:

1. Establish the influence of diazoxide and 5-HD on mitochondrial membrane potential ($\Delta\psi_m$).
2. Investigate the generation of extracellular nucleotides during hypoxia.
3. Generate a cardiomyocyte (CM) model in which IPC and hypoxia-related nucleotide modulation could be characterised.

1.2. Methods

To measure $\Delta\psi_m$, tetramethylrhodamine, ethyl (TMRE) signalling was measured using a microplate reader. Hypoxia was replicated by metabolic poisoning (4 mM cyanide, 10 mM 2-deoxyglucose (2-DG) and 5 µM ionomycin) and the resulting extracellular nucleotide was measured using ATP monitoring reagent (AMR, ViaLight) and a Berthold tube luminometer (LB955). HL-1 cells and primary chick

CMs were examined to determine if they could be used as a contractile, cultured myocyte model.

1.3. Results

The IPC-inducing agent, diazoxide, induced significant depolarisation (F/F_0=0.098, auc. 7.86±1.0%) and surprisingly so did the antagonist, 5-HD ($F/F_{0=}$0.046, auc. 3.13±0.6%). When used in combination, 5-HD negated the substantial diazoxide induced depolarisation (F/F_0=0.036, auc. 5.08±0.7%). After metabolic poisoning, the observed extracellular ATP was elevated from 5±1 nM to 60±6 nM. The ADP concentration was much greater than the observed ATP and was also elevated from 259±31 nM to 4202±394 nM during chemical induced hypoxia (CIH). Oxidised ATP (oATP) reduced the extracellular ATP and ADP concentration by 53±16% and 40±32%, respectively. Primary chick CMs offered a more appropriate CM model compared to HL-1 cells. Chick CMs displayed contractile activity and positive CM specific antibody staining.

1.4. Discussion

The data is consistent with a diazoxide-induced depolarisation arising from potassium channel modulation, while 5-HD appears to modulate $\Delta\psi_m$ as a metabolic agent rather than as a channel inhibitor. The presence of relatively large concentrations of extracellular ADP after CIH, suggest that $P2Y_{1,6,11}$ signalling may be significant in hypoxia. The extracellular nucleotides appear to arise not from ecto-enzyme activity or connexin release but via an oATP-inhibited mechanism. This suggests a potential linkage with $P2X_7$ receptors. Isolated chick primary CMs produced a beating myocyte culture expressing cardiomyocyte markers. This model system has the potential to be used with recombinant probes in order to monitor cell and mitochondrial function during hypoxia.

2. Abbreviations

$[Ca^{2+}]_c$	Cytoplasmic calcium concentration
$[Ca^{2+}]_m$	Mitochondrial calcium concentration
$[K^+]_m$	Mitochondrial potassium concentration
$\Delta\psi_m$	Mitochondrial membrane potential
2-DG	2-Deoxyglucose
3-NPA	3-Nitropropionic acid
5-HD	5-hydroxydecanoate
5-HD-CoA	5-Hydroxydecanoyl-coenzyme A
acyl-CoA	Acetyl coenzyme A
ADP	Adenosine diphosphate
AK	Adenylate kinase
ALP	Alkaline phosphatase
AMP	Adenosine monophosphate
ANT	Adenine nucleotide translocase
Ap_5A	Diadenosine pentaphosphate
ARL 67156	6-*N*,*N*-Diethyl-D-β,γ-dibromomethylene ATP trisodium salt
ATP	Adenosine triphosphate
BSA	Bovine serum albumin
Ca^{2+}	Calcium ion

CABG	Coronary artery bypass graft
$CaCl_2$	Calcium chloride
CFTR	Cystic fibrosis transmembrane conductance regulator
cGMP	Cyclic guanosine monophosphate
CICR	Calcium induced calcium release
CIH	Chemically induced hypoxia
CM	Cardiomyocyte
CN	Cyanide (sodium)
CNS	Central nervous system
DAPI	4',6-Diamidino-2-phenylindole
$d^{\cdot}H_2O$	Distilled water
DMEM	Dulbecco's modified Eagle medium
DMSO	Dimethyl sulfoxide
DNA	Deoxyribonucleic acid
E-C	Excitation-contraction
EDTA	Ethylenediaminetetraacetic acid
EGTA	Ethylene glycol tetraacetic acid
eN	5’-nucleotdiase
E-NPP	Ecto-nucleotide pyrophosphatase/phosphodiesterase
E-NTPDase	Ecto-nucleotide triphosphate diphosphohydrolase
ER/SR	Endoplasmic/Sarcoplasmic reticulum

ESc	Embryonic stem cells
ETC	Electron transport chain
ETF	Electron transferring flavoprotein
ETF-Q	Electron transfer flavoprotein-Q
FAD(H)	Flavin adenine dinucleotide (reduced)
FCCP	Carbonyl cyanide p-(tri-fluromethoxy)phenyl-hydrazone
FCS	Fetal calf serum
FFA	Flufenamic acid
GDP	Guanosine diphosphate
GTP	Guanosine triphosphate
H_2O	Water
HBS	HEPES-buffered Saline
HPLC	High performance liquid chromatography
HUVEC	Human umbilical vein endothelial cells
I-R	Ischaemic reperfusion
IMAC	Inner-membrane anion channel
IMM	Inner mitochondrial membrane
IMS	Intramembrane space
IP_3R	Inositol trisphosphate receptor
IPC	Ischaemic preconditioning
K^+	Potassium ions

K_{ATP} channel	Potassium ATP channel
KCl	Potassium chloride
K_i	Inhibition constant
KCO	Potassium channel opener
K_m	Michaelis-Menten constant
MAM	Mitochondria associated membranes
MCU	Mitochondrial calcium uniporter
MEM	Modified Eagle medium
MF-20	Sarcomeric myosin heavy chain antibody
$MgCl_2$	Magnesium chloride
$MgSO_4$	Magnesium sulphate
MHC	Myosin heavy chain
mitoK_{ATP}	Mitochondrial potassium ATP channel
MODS	Multiple organ dysfunction syndrome
MOPS	3-(N-morpholino) propanesulfonic acid
mPTP	Mitochondrial partial transition pore
mt[AEQ]WT	Mitochondrial aequorin plasmid wildtype
Na_2HPO_4	Disodium phosphate
NaCl	Sodium chloride
NAD^+ (H)	Nicotinamide adenine dinucleotide (reduced)
NaOH	Sodium hydroxide

NCX	Na^+/Ca^{2+} exchanger
NDPK	Nucleoside diphospate kinase
NE	Norepinephrine
NEAA	Non-essential amino acid
NF-κB	Nuclear factor-KappaB
NO	Nitric Oxide
NOS	Nitric oxide synthase
O_2	Oxygen
$O_2^{\cdot}$	Superoxide anions
OH^-	Hydroxyl radicals
OMM	Outer mitochondrial membrane
ONOOH	Peroxynitrous acid
P1 or P2	Purinergic Receptors
P/S	Penicillin/Streptomycin
PBFI	Potassium-binding benzofuran isophthalate
PDE_5	Phosphodiesterase Type 5
PEP	Phosphoenolpyruvate
P_i	Inorganic Phosphate
PI	Propidium Iodide
PKC or G	Protein Kinase C or G
Q	Ubiquinone

RLU	Relative luminescence units
RNA	Ribonucleic acid
ROI	Region of interest
ROS	Reactive oxygen species
RyR	Ryanodine receptor
sarcoK$_{ATP}$	Sarcomeric potassium ATP channel
SDS	Sodium dodecyl sulfate
SERCA	Sarcoplasmic reticulum calcium transport ATPase
siRNA	Short interfering RNA
SNAP	S-nitroso-N-acetylpenicillamine
SNP	Sodium nitroprusside
SRCE	Store-regulated calcium entry
SUR	Sulfonylurea receptor
TCA	Tricarboxylic acid cycle
TMRE	Tetramethylrhodamine ethyl ester
Tris-(H)Cl	Tris(hydroxymethyl)aminomethane (hydro)chloride
UCP	Uncoupling protein
UDP	Uridine diphospohate
UTP	Uridine triphospohate
VDAC	Voltage-dependent anion channel

3. Figures

4. Equations

5. Introduction

5.1. Ischaemia

Ischaemia occurs when a tissue receives an insufficient supply of blood. Reduced blood supply arises as a consequence of disease or trauma. Subsequently, tissues can become hypoxic or anoxic and thus starved of oxygen. The tissue will then suffer injury, which is triggered by an ischaemic cascade. The ischaemic cascade, induced by hypoxia, is a series of biochemical changes which involve the loss of ATP synthesis (and inversely elevation of ADP, AMP, and P_i). This involves a switch to anaerobic metabolism and can result in mitochondrial damage, collapse of the $\Delta\psi_m$ and $[Ca^{2+}]_m$ overload, and activation of the caspase-dependent apoptosis cascade [1, 2].

In 2004, 7.2 million (12.2%) of the world's deaths were attributed to cardiac ischaemia and 5.7 million (9.7%), to cerebrovascular or stroke related disease, of which 85% were the result of ischaemic injury [3]. In the United Kingdom, coronary artery disease is the biggest killer and is attributed to 94,000 deaths, annually. It is estimated that 2.6 million people, in the UK, are living with coronary artery disease and for every 1 in 5 men and 1 in 7 women, will prove to be fatal.

Cardiac ischaemia occurs when the heart receives insufficient blood flow, most commonly as a result of atherosclerosis or acute coronary syndrome. The symptoms vary depending upon the exact cause but generally include chest pain (angina pectoris) that radiates through the arm and back, limited ability for physical activity, and nausea without vomiting. In the cardiovascular system, ischaemic damage to the myocytes is well documented, however myocytes are not the only cell affected. Due to their localisation, endothelial cells are also subjected to ischaemia and the resulting pathological events [4]. During periods of hypoxia, endothelial cells release autacoids which modulate the environment as a result of elevated $[Ca^{2+}]_c$, ATP depletion and channel modulation [5].

In cerebrovascular disease, interruption of the blood supply, for more than 10 seconds, can induce unconsciousness and, for more than 1 to 2 minutes, irreversible brain damage. Cerebral ischaemia can be either focal, which is localised to a single

region and induced by cerebral vessel occlusion, or a global episode, which encompasses wide areas and arises from dramatically reduced or halted blood flow.

Ischaemia is potentially reversible, if the blood flow recovers and as a consequence cellular energy demands are met. There is only a small window for recovery before cellular damage is irreversible and can result in cell death. In highly metabolic active tissue, this can occur in fewer than 2 to 3 minutes; As such the most common sites of ischaemic injury are the cardiac and cerebral systems. Ischaemia also affect the gastrointestinal system, kidneys and extremities of the limbs (fingers and toes).

Paradoxically, restoration of blood supply can also cause damage, which can be more severe than if induced by the original ischemia. This reperfusion injury will be discussed in more detail later (see 5.1.2 Reperfusion Injury)

5.1.1. Ischaemic Risk Factors

Ischaemia can be induced by several medical conditions including: atherosclerosis, embolism, thromboembolism, coronary artery disease, anaemia, diabetes, high blood pressure and blood vessel compression (from tumour growth).

5.1.1.1. Atherosclerosis

Atherosclerosis frequently precedes either acute or chronic ischemia due to the onset of various coronary syndromes. Atherosclerosis is a common disorder where fat, cholesterol, and other substances build up in the walls of arteries and whilst originally considered a lipid storage disease, is attributed to inflammatory responses [6, 7]. Over time, these plaques can block the arteries and result in acute ischaemic conditions such as myocardial infarction and stroke [8-10].

Atherosclerosis develops as illustrated in Figure 5-1. Atherosclerosis develops with increased low-density lipoprotein and very low-density lipoprotein accumulation in the sub endothelial space and the subsequent recruitment of monocytes. The monocytes differentiate into macrophages that then engulf low-density lipoproteins and cholesterol deposits [11]. The atherogenic lipoproteins infiltrate the sub-

endothelial space and become oxidised [12]. The modified oxidised lipoproteins induce an autoimmune response, stimulating macrophage lipoprotein uptake, resulting in the formation of foam cells [13]. As foam cells coalesce, they form fatty streaks and ultimately atheromatous plaques. The plaques grow larger over time, occluding the artery or becoming unstable and forming a thrombosis or embolism. For a complete review please see Glass and Witztum (2001) [14]. One consequence of macrophage activation is the release of mitogen and chemo-attractants that result in the recruitment and proliferation of smooth muscle cells.

5.1.1.2. Coronary artery disease

Coronary artery disease or heart disease and its sequelae: myocardial infarction, ischaemia and heart failure, are the leading causes of morbidity and mortality in mankind [15].

Coronary heart disease and other cardiac pathologies can lead to either acute or chronic heart failure. Acute heart failure develops rapidly (within hours and days) and as compensatory mechanisms cannot establish, it is life threatening. Acute insult arises from insults such as, acute myocardial infarctions and arrhythmias and can require pharmacological and surgical intervention. Chronic or long term heart failure occurs over months or years, rather than the rapid acute failure. The heart can undergo adaptive responses to compensate for the failings. Whilst these afford a level of protection and preserve function, in the long term they are often insufficient to maintain the function of the heart. Chronic heart failure can present as either ‘compensated’, where the symptoms are stable and many overt features are absent, or ‘decompensated’ where the injury shows deterioration and can present as acute episodes. For a full review including management, assessment and treatment see Millane *et al.* (2000) [16].

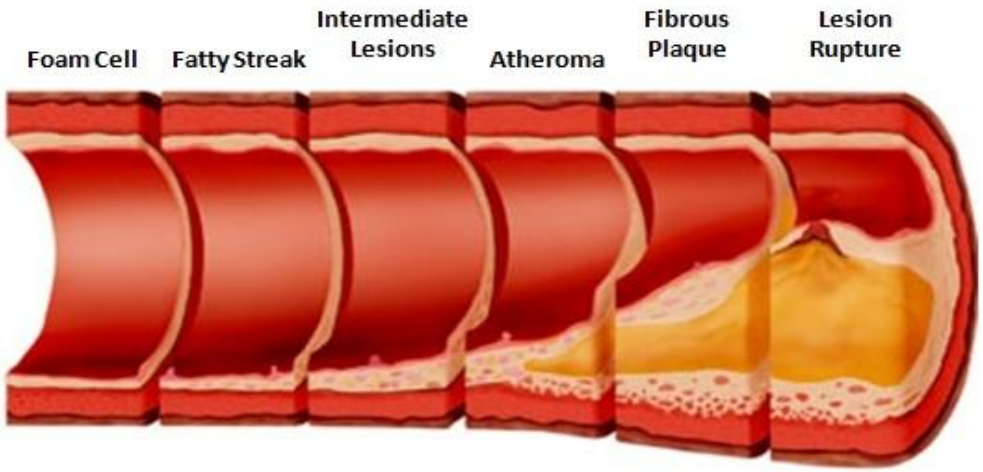

Figure 5-1. The development of atherosclerosis, from foam cell to rupture.

The development of arterial atherosclerosis occurs in arterial vessels, with the development and localisation of foam cells. The fatty streak can worsen, resulting in occlusion of the vessel with the growth of the atheroma. Adapted from Koenig and Khuseyinova [17]

5.1.2. Reperfusion Injury

Cells subject to ischaemic insult are subsequently prone to ischaemic reperfusion (I-R) injuries. The restoration of blood flow, reperfusion, is necessary to prevent irreversible damage, such as necrosis and cell death that are associated with prolonged ischaemia. While reperfusion is essential and instigates recovery, it can also exacerbate injury through oxidative damage, physical damage, tissue damage, cell dysfunction and death.

Under normal circumstances, mitochondria remove cellular calcium to modulate signalling and mitochondrial function, through allosteric activation of the enzymes regulating oxidative phosphorylation and ATP synthesis (pyruvate dehydrogenase, isocitrate dehydrogenase, and α-ketoglutarate dehydrogenase, stimulation of the ATP synthase (Complex V), α-glycerophosphate dehydrogenase, and the adenine nucleotide translocase (ANT)) [18-21]. During ischaemia, glycolytic ATP production cannot match cellular demand, and alongside decreased ATP, lactic acid accumulation is observed [1]. Lactic acid lowers the pH, triggering the Na^+/H^+ antiporter, elevating $[Ca^{2+}]_c$ [1, 22]. During re-oxygenation, the $\Delta\psi_m$ is restored and the accumulated of $[Ca^{2+}]_c$ is sequestered by the mitochondria. Calcium overload can also be seen via an increased calcium transient amplitude (as the result of elevated action potential duration and store loading), loss of sarcoplasmic reticulum (SR) calcium transport ATPase (SERCA) activity, or the loss of calcium-induced calcium release (CICR) through the loss of micro-domains, resulting in elevated signalling amplitude [23-26].

During reperfusion, rapid repolarisation occurs and results in a large uptake of calcium along with mitochondrial overload. This is detrimental to the cells and can result in mitochondrial pathology [27, 28].

Elevated $[Ca^{2+}]_c$ can induce altered gene transcription as seen in cardiac hypertrophy and multi organ system failure [29-31]. In the short term, the effects of calcium overload can result in the physiological uncoupling of the mitochondria, compromising the organelle's ability to generate ATP [28]. Originally the damage observed was attributed to increased membrane permeability, but is now

attributed to the formation of the mitochondrial partial transition pore (mPTP). The formation of this pore is nearly inevitable during I-R injury as the ideal conditions for its formation and opening are $\Delta\psi_m$ depolarisation, high oxygen, low ATP and high reactive oxygen species (ROS) generation [32]

The mPTP is a, non-selective, 3 nm pore located on the inner mitochondrial membrane (IMM), permeable to molecules smaller than 1.5 kDa. Its opening can be transient in nature and of a low conductance and can afford cardiac protection by limiting mitochondrial calcium overload and related ROS production [1, 33-35]. Despite the benefits, the formation of the mPTP can induce $\Delta\psi_m$ depolarisation, reduce ATP synthesis, and potentially reduce swelling of the matrix, which would otherwise result in the loss of the membrane integrity, cristae unfolding and would lead to mitochondrial membrane rupture. The loss of the mitochondrial membranes can culminate in either necrotic cell death or the release of apoptogenic factors (cytochrome c) [36-39]. Whilst the mPTP is the end mechanism and proposed mechanism for cellular damage ($\Delta\psi_m$ depolarisation, swelling and rupture), the presence of ROS can play a critical role. Despite being discussed as a potential IPC trigger, ROS generation is associated with mPTP formation [40, 41]. Mitochondrial calcium overload elevates nitric oxide (NO) synthesis which inhibits Complex I and IV of the electron transport chain (ETC, see section 5.3.6) resulting in ROS generation [19].

In the cardiovascular system, I-R can ‘stun’ the myocardium. It was originally described by Heyndrickx, in 1975, as “prolonged post ischaemic dysfunction of viable tissue salvaged by reperfusion” [42]. Stunning involves a loss in ATP re-synthesis, contractility and micro-vascular function. Micro-vascular dysfunction, where the blood supply never returns to pre-ischaemic rates, arises from vasoconstriction, involving platelet and leukocyte activation [43-47]. Reperfusion injury can induce arrhythmias, typically after thrombolytic treatment or myocardial re-vascularisation surgery. I-R injury often occurs following ischaemic insult, resulting from surgeries such as, angioplasty, organ transplantation and bypass surgery (typically coronary artery bypass graft (CABG) surgery). Despite the inherent I-R risks, patients receiving reperfusion treatment show improved recovery,

compared to those who did not receive treatment, emphasising the importance of reperfusion, despite the associated risks [43].

Central nervous system (CNS) ischaemia contributes to the morbidity and mortality of victims of strokes, head trauma and cranial ischaemic events. CNS ischaemia is characterised by disruption of the blood brain barrier. I-R injury can induce cerebral oedema, elevated intracranial pressure and leukocyte migration. This presents, as exacerbated loss of sensory, motor and cognitive function [48].

Severe I-R inflammation can induce systematic inflammatory response syndrome or even multiple organ dysfunction syndrome (MODS). In intensive care units, MODS accounts for, 30 to 40% of mortalities [49]. A devastating remote organ injury, MODS, commonly affects the pulmonary system and after 24 to 72 hours of respiratory insufficiency, multi-organ failure follows [50].

5.1.3. Ischaemic-Reperfusion Physiology

Several risk factors attribute to I-R injury, with various potential consequences, as discussed in section 5.1.2. Despite this, the pathology can be described by alterations of cellular, vascular, leukocyte and compliment activation.

5.1.3.1. Cellular Activation

During ischaemia, the decrease in ATP synthesis modulates ATP ionic pump action resulting in calcium, sodium and water entry and induces ROS synthesis, via adenine nucleotide catabolism [51]. The altered calcium handling induces elevations of intracellular calcium concentrations and entry through the L-type channel, which results in mitochondrial calcium overload and the associated pathology as discussed [52]. In cardiac tissue, I-R also modulates the myocardial metabolism, delaying functional recovery [53].

In the failing heart protein expression is altered including the down regulation of uncoupling protein (UCP) (UCPs 2 and 3; see section 5.2.1) [54, 55]. The loss of UCPs can affect the proton leak across the IMM and as such have shown significant

importance in I-R injury [56]. UCP knockout mice subjected to I-R injury have shown elevated ROS generation, whilst over-expression causes reduced generation [57, 58]. The UCPs have also been proposed to play a role in heart failure, but in a paradoxical fashion to in I-R, with down regulation enhancing energetic efficiency (tricarboxyic acid cycle (TCA) and ATP synthesis) whilst allowing ROS generation [59].

As discussed, NO concentrations can be elevated in I-R injury and can result in ROS synthesis can have direct effects, NO, the endothelium-derived relaxing factor (EDRF) induces smooth muscle relaxation, alongside inhibiting complex IV and so electron movement (see section 5.3.5) whilst is also believed to act as a protective factor via direct opening of the K_{ATP} channel, an effect analogous with diazoxide [60-62].

Within minutes of I-R insult, ROS synthesis, including superoxide anions ($O_2^{\cdot -}$), hydroxyl radicals (OH^-) and peroxynitrite, is elevated [63]. Elevated ROS production, is related to increased leukocyte activity and ATP degradation [64]. Under normal circumstances, ATP degradation forms hypoxanthine, which is oxidised by xanthine dehydrogenase, forming xanthine via the substrate nicotinamide adenine dinucleotide (NAD^+). In ischaemia, xanthine dehydrogenase is replaced with xanthine oxidase, which produces ROS through its substrate oxygen [65]. ROS production is also elevated by the increased pool of hypoxanthine, which upon reperfusion, in combination with the elevated oxygen level, is converted to ROS [51]. ROS synthesis is a negative factor, acting both as an oxidising and reducing agent. Damage to the cell membrane and sarcolemma arises from impaired membrane-bound enzyme systems and leukocyte stimulation through endothelial platelet activation factors [65-67].

Peroxynitrate is formed from NO and superoxide and whilst it is not a free radical it is a powerful oxidant and is much more reactive than its parent molecules [68, 69]. Peroxynitrate can exert direct oxidative modulation in the form of peroxynitrous acid (ONOOH), or indirectly via decomposition into highly ROS (hydroxyl radical, nitrogen dioxide) [60]. Oxidative modulation can arise from inhibition of complex I,

II, III and V (ATP synthase), whilst paradoxically complex IV which is inhibited by NO, peroxynitrate appears to exert no inhibitory effect but potentially acting as a catalyst [70-75]. Peroxynitrate is also known to modulate the TCA cycle via inhibition of the enzyme aconitase (thus inhibiting the citrate to iso-citrate step), along with being a putative inducer of mPTP formation and opening, and is apoptogenic [61, 62, 76-81].

5.1.3.2. Vascular Activation

At the vascular level, I-R induces pro-inflammation gene expression (adhesion molecules and cytokines), whilst down regulating 'protective' gene products (thrombomodulin and nitric oxide synthase (NOS)). These changes result in vasoconstrictive responses [47, 50]. The signalling cue for the described response is attributed to extracellular ATP and elevated adenosine concentrations and signalling pathways [82, 83].

5.1.3.3. Leukocyte Activation

Reperfusion can induce leukocyte activation. Leukocytes interact with endothelial cells through well defined steps namely rolling, firm adhesion and transmigration [64]. Activation and accumulation induces vessel narrowing via leukocyte-endothelial cell adhesion, increasing micro-vascular permeability and toxic extra-vascular ROS release.

5.1.3.4. Compliment activation

The compliment system is a key aspect of the innate immune system, primarily cytotoxic and apoptotic activities [84]. Complement activation following I-R is associated with a myriad of pathological conditions including myocardial infarction, atherosclerosis, hemorrhagic shock and pulmonary injury [85-88].

Inflammatory mediators released during I-R induce compliment activation and generate changes in vascular homeostasis [89]. Compliment activation occurs along 3 routes called classical, alternative and lectin compliment activation [89]. In

ischaemia, it is the antibody-independent alternative pathway that is activated, which leads to formation of complement component 3 (C3) fragments.

Inflammation is a negative effect on cells since, in ischemia, it has been demonstrated to exacerbate tissue injury, affect arterial occlusion and acts as an independent risk factor of pathologies such as atherothrombotic stroke [90-92].

The anaphylatoxin fragments C3a and C5a activate the complement system, activating either: complement receptor type 1 (or CD35), membrane cofactor proteins (CD46). Compliment activation can amplify the inflammatory response and modulate vascular homeostasis via nuclear factor-kappa B (NF-κB), leukocyte adhesion molecule transcription and pro-inflammation cytokines (interleukin-1, -6 and tumor necrosis factor alpha (TNF-α)) [93, 94].In rat models, C3 fragments were shown to stimulate leukocytes, whilst C5 fragments were released in direct response to ROS [85, 95, 96].

5.1.4. Cardioprotection

Several endogenous cardio-protective mechanisms exist. IPC arises from brief periods of ischaemia, as first described in 1986 by Murry *et al.*, who observed a reduction in infarction size following 4, 5 minute cycles of circumflex occlusion and reperfusion [97]. Ischaemic protection is suggested to act through pathways, including activation of G protein-linked phospholipase C coupled receptor, tyrosine kinase pathways and protein kinase C (PKC) [98]. IPC releases the inactivation of redox-sensitive TCA cycle enzymes, reduces loss of mitochondrial respiration function, and prevents the release of cytochrome c, and prevents alterations in mitochondrial structure [99].

Protection occurs in two phases, acute and delayed. Acute protection occurs in a 1-2 hour window after the initial insult. This is attributed to elevated adenosine signalling and downstream PKC activation [100, 101]. Delayed conditioning, arises 24 hours post ischaemic insult and lasts for an extended period. Resulting from chronic hypoxia, delayed preconditioning is the secondary window of protection [102]. The protection afforded is not as potent as the first window but cell survival

is still promoted [103]. In brief, delayed IPC follows the paradigm that freely diffusible molecules, generated during IPC, triggers cellular adaptation, thus activating the PKC signal cascade. This alters gene expression and the synthesis of protective proteins, such as NO synthase and heat shock proteins [50, 104]. For a detailed and cardiomyocyte focused review, see Baxter's 2001 paper [104].

Preconditioning is reported to afford protection and recovery from I-R insult by reducing infarct size, preserving vascular endothelial function, decreasing neutrophil accumulation, and reducing apoptosis [97, 105-107]. Several therapeutic treatments are currently used and being developed to combat injury resulting from both, ischaemia and reperfusion. The existing cardio-protective mechanisms include the use of IPC, calcium preconditioning, potassium (K^+) channel opener (KCO), delayed preconditioning, adaptive preconditioning, ischaemic post- conditioning, and Na^+/H^+ inhibitors.

IPC offers protection through increased vascular function, whilst reducing apoptosis. In CABG patients, reperfusion arrhythmias were significantly reduced, following IPC [108, 109].

5.1.4.1. Calcium preconditioning

Transient elevations of intracellular calcium induce calcium preconditioning [110, 111]. This form of protection arises from significant functional recovery and decreased lactate dehydrogenase. The calcium dynamics is a strong PKC activator, conferring protection from ischaemic injury [112].

5.1.4.2. Post-conditioning

Perceived as a new concept and area of research, post conditioning was originally reported by Sewell, in 1955 [113-115]. Post conditioning is potentially very useful clinical tool by reducing I-R injury as late as 6 to 48 hours after focal and global insult respectively [116, 117]. Research suggests that post conditioning is as effective as pre conditioning in reducing the size of infarction and preserving endothelial function [117]. Post conditioning is believed to affect a broad range of

triggers, offering anti-arrhythmic protection, whilst reducing ROS production and deleterious effects associated with I-R injury [118]. For detailed historical and research reviews see Zhao's 2003 and 2009 papers [116, 117].

5.1.5. Medical Intervention

When administered prior to ischaemia, KCO such as diazoxide and pinacidil, afford acute protection [15, 119-124]. The use of KCO has been recorded to aid function and compliance by over 50% following I-R insult [125]. The role of K^+ influx and the associated IPC is presently unknown, but is known to affect mitochondrial ion movement and to improve coronary flow through the mechanisms as outlined in section 5.4.2 [126].

Inhibiting the multi-facetted leukocyte insult is a very powerful tool. Protection arises from the use of anti-TNF-α antibodies, which inhibit receptor engagement, leukocyte-endothelial interactions (intercellular adhesion molecule 1), and reduce lipoxin activation (aspirin) along with leukocyte adhesion molecule synthesis (aspirin and glucocorticods) [127, 128].

NO treatment affords protection by directly opening the K_{ATP} channel, improving endothelial function or reducing leukocyte activation. NO derived treatment has been shown to occur in cardiac, cerebral and renal tissues [129-131]. While the exact pathway of NO protection is unknown it is attributed to cyclooxygenase-2 activation, arising from the synthesis of prostanoids (prostaglandin (PG) $–E_2$ and $–I_2$) [132-137]. NO can offer cellular protection; however in excess it can exhibit deleterious effects, on tissue recovery, via ROS generation.

In response to ROS damage, antioxidant treatments are currently being investigated with mixed results. Success in reducing organ failure, in post haemorrhagic shock and rejection in renal transplantation has been observed in patients treated with the antioxidant superoxide dismutase [138-140].

Complement activation therapy is a novel therapeutic option. In rat myocardial experiments, complement component 3 (C3) convertase inhibitor, reduced

infarction size by 44%, while complement component 5 (C5) antibody treatment reduced post CABG operation mortality [141].

While several of the treatments described have only shown promise as IPC agents in experimental models, KCO, which inhibit multi-facetted leukocyte and antioxidant treatments, have all shown positive effects in therapeutic medical intervention.

5.2. Mitochondria

Mitochondria were originally named 'bioblasts' by Richard Altmann in 1894 before the name mitochondria was coined by Carl Benda [142, 143]. Mitochondria are important as not only do they play a critical role in I-R injury and are therefore targets of cardioprotection, they are the fundamental site of cellular respiration [144]. The importance of mitochondria to cardioprotection is linked to their role in cellular respiration, control of apoptosis and calcium dynamics [144-147].

5.2.1. Architecture

Mitochondria are typically 0.5 to 1 μm in diameter and 7 μm long. They appear as discrete rod-like structures or as extended tubes that break and reform. They are motile and continually fuse and break apart. Mitochondrial abundance is related to the aerobic needs of the tissue. Mitochondria have a highly ordered structure as seen in Figure 5-2 and discussed below.

Mitochondria are made from two phosphlipid bilayers, distinct in both appearance and physio-chemical properties. The outer mitochondrial membrane (OMM) is made up of a ratio of proteins and phospholipids at a ratio of 1:1. This forms a widely permeable membrane to ions and molecules smaller than 5000 Da, whilst the passage of larger molecules is regulated by the voltage-dependent anion channel (VDAC) [148]. The VDAC channel was first discovered by Schein, in 1976, and is multifunctional in both metabolic function and also apoptosis [149-151]. Proposed to be involved in apoptosis by Shimizu (1999), the VDAC channel has now been shown to be involved in both intrinsic (responding to stimulation such as $[Ca^{2+}]_c$ and ROS) and extrinsic (TNFα and death receptor) apoptosis [152, 153]. Alongside being an aspect of apoptosis, the VDAC channel and ANT are thought to form the mPTP [154].

The IMM is made up of a 4:1 ratio of proteins to phospholipids. It encloses the mitochondria and where it convolutes it forms the cristae. The IMM is highly impermeable and entry is only via channels and transporters. UCP are

mitochondrial transporters located on the IMM [155]. Whilst UCP1 is expressed in brown adipose tissue, UCP2 and 3 are found in a variety of cell types, notably those utilizing β-oxidation [155]. The UCPs act according to their name as they are fatty acid anion transporters on the IMM. They provide an alternative means for proton re-entry that is not coupled to ATP synthesis and, subsequently, they can induce $\Delta\psi_m$ uncoupling as they drive thermogenic activity [156, 157]. Whilst the UCPs are thermogenic they also afford protection to mitochondria by inducing mild uncoupling and by limiting ROS generation [158].

The two membranes form an intramembrane space (IMS) or perimitochondrial space, a compartmentalisation between the mitochondria and cytoplasm. The IMS has a role in oxidative phosphorylation, acting as a store for protons ejected from the mitochondrial matrix. It generates the proton motive force, which is the drive for ATP synthesis. The cristae form a larger surface area for the enzymatic reactions of oxidative phosphorylation and ATP synthesis. The matrix is a highly concentrated mixture of enzymes, mitochondrial DNA, ribosomes and it is the site of aspects of cellular respiration (oxidation and the TCA cycle).

5.2.2. Micro-domains and Related Structures

The endoplasmic reticulum (ER) or SR is an extensive network of cisternae and microtubules and is the site of protein synthesis. It is also the site of calcium signalling via the D-myo-inositol-1,4,5-trisphosphate receptor (IP_3R) and ryanodine receptor (RyR) [159-162]. It is now well established that mitochondria have an intimate relationship, both spatially and functionally, with elements of the ER/SR [163, 164]. The close association forms “hotspots” between the ER or SR and the mitochondria, thus producing calcium micro-domains. The regions of elevated concentrations of calcium induce mitochondrial uptake by the low affinity uniporters [165]. The close apposition between the ER/SR and mitochondria was shown to be formed by tethered junctions of 10 to 25 nm [166-168]. The close contacts are referred to as the mitochondria associated membranes (MAM) and are the sites for calcium signalling and lipid transfer [169-171].

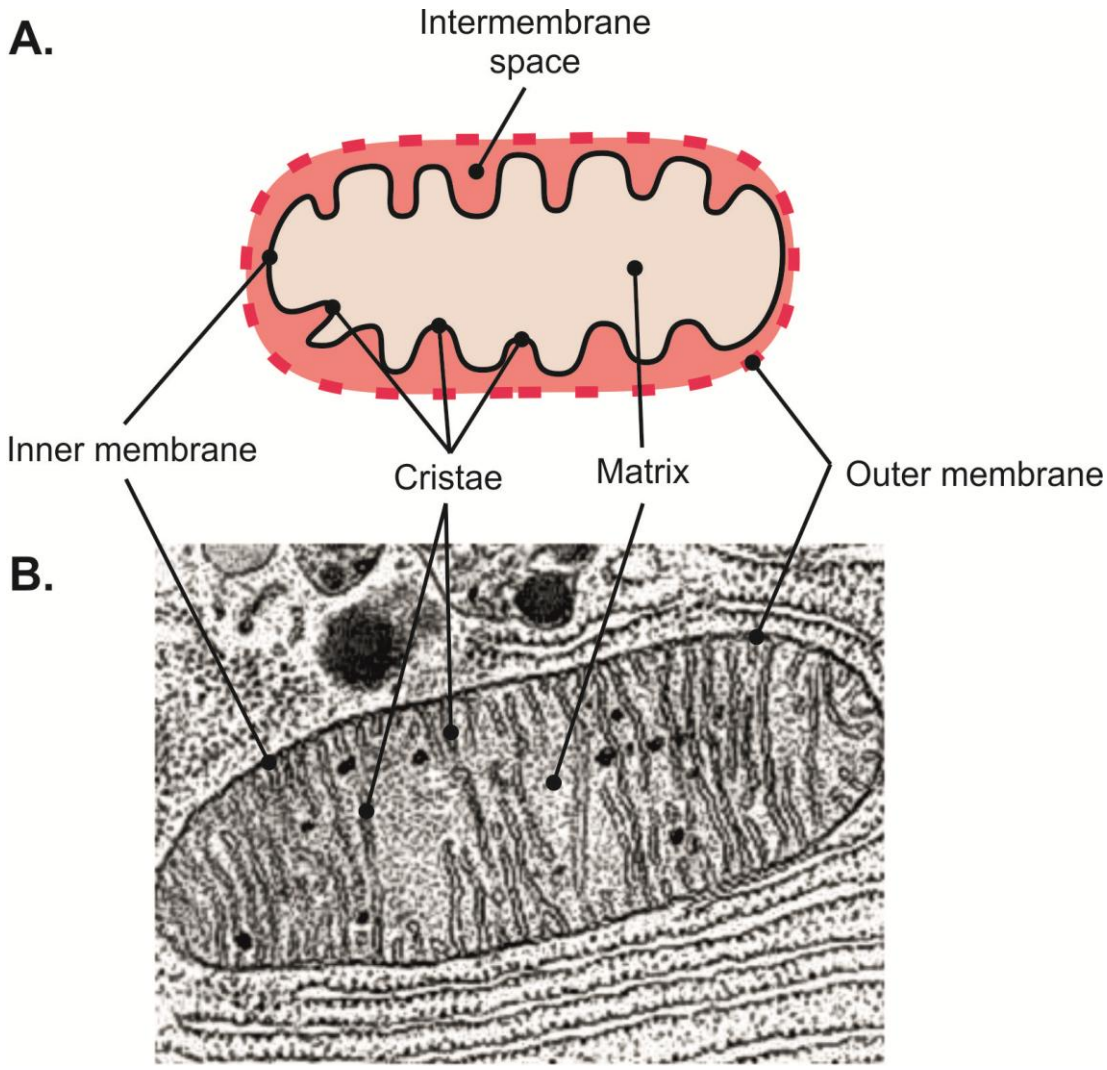

Figure 5-2. Illustration and electron microscope image of mitochondrial architecture.

A) Diagrammatic view of mitochondria, with the major architecture: outer and inner membranes (OMM, IMM), intramembrane space (IMS), cristae and matrix. B) Electron microscope image of a typical mitochondria in profile.

5.3. Cellular Respiration

The "father of modern chemistry," Antoine Lavoisier originally characterised the composition of the air we breathe and studied energy conservation and transformation in cells [172].

Living cells acquire and use energy in a process, known as energy metabolism. The metabolism of glucose and fatty acids occurs through: glycolysis, β-oxidation, the TCA cycle and the ETC, as summarised in Figure 5-3. The synthesis of ATP occurs through two main processes called oxidative or substrate-level phosphorylation. Oxidative phosphorylation occurs in the mitochondria and is the main source of ATP. Driven by redox reactions, ATP is synthesised from ADP and P_i. In substrate-level phosphorylation, ATP is synthesised through the transfer of high-energy phosphoryl groups from high-energy compounds to ADP. This occurs during glycolysis and the TCA cycle.

Respiration is the process of releasing energy from the breakdown of glucose, fatty acids, glutamine and ketone bodies. Respiration constantly takes place in every living cell in order to supply the required energy. In aerobic respiration, all products of nutrient degradation converge at the TCA cycle. In the TCA cycle, acetyl-CoA is oxidized to CO_2, reducing the electron transporting coenzymes (NAD^+ and flavin adenine dinucleotide (FAD)) to their energy donating states (NADH and $FADH_2$).

$$Glucose + O_2 \rightarrow CO_2 + H_2O + Energy$$

Anaerobic respiration is a form of respiration using electron acceptors other than oxygen. For the ETC to function, an exogenous final electron acceptor must be present to allow electrons to pass through the system. Alternative final electron acceptors have smaller reduction potentials than oxygen and as such less energy is released per oxidized molecule.

$$Glucose \rightarrow Lactic\ Acid + Energy$$

The respiration rate is dictated not only by the concentration of ADP and calcium, but it has also been noted that electron availability is a critical factor [173-176].

Cardiac tissue predominantly generates ATP from β-oxidation of fatty acids [177-180]. Whilst this is balanced in normal physiology, cardiac tissue can utilize several energy sources including, glucose, lactate, glutamate and even ketone bodies during atypical and pathological conditions, as discussed in 5.6.2 [180-187].

The heart's ability to function efficiently is highly dependent on the level of cellular ATP, with 2% of the cellular ATP pool turned over with every heart beat and at maximal cardiac output, the entire pool is turned over every few seconds [188-190]. During increased cardiac output, the ADP/P_i concentration is not sufficient to meet demand, therefore an alternative mechanism, called calcium-regulated cardiac activity, acts as a "real-time" ATP regulator to ensure that demand is met by controlling the electron production in the TCA cycle [191].

5.3.1. Glycolysis

In the cytosol, glycolysis converts one molecule of glucose into 2 pyruvate molecules. This yields, a net profit of 2 ATP molecules, as summarised in Equation 5-1.

$$Glucose + 2NAD^+ + 2P_i + 2ADP \rightarrow 2\mathrm{P}yruvate + 2NADH + \mathbf{2}\boldsymbol{ATP} + 2H^+ + 2H_2O$$

Equation 5-1. Glycolysis

Initially, ATP is used to facilitate glycolysis, but twice as much ATP is generated than is consumed overall. ATP is generated through substrate-level phosphorylation as phosphoenolpyruvate (PEP) is converted to pyruvate. For complete oxidation, the pyruvate molecules are transported to the mitochondrial matrix and converted into acetyl-CoA by pyruvate dehydrogenase. In aerobic conditions, the pyruvate molecules are transported into the mitochondrial matrix, where they subsequently participate in the TCA cycle.

5.3.2. Beta-Oxidation

In 1904, Knoop showed that fatty acid oxidation is a process by which two-carbon units are progressively removed from the carboxyl end of a fatty acid molecule [192]. This oxidation pathway was confirmed by Dakin, whilst the generation of acetyl-CoA and the steps were defined by Lynen *et al.* in 1953 [193-195]. Beta-oxidation is the main process of fatty acid oxidation and notably occurs, in cardiac and skeletal muscle [182].

Beta-oxidation consists of four reactions and generates the common intermediary, acetyl-CoA, that enters the TCA cycle at the citrate synthase enzyme (Figure 5-7). In conjunction, a shortened acyl-CoA molecule is synthesised and FAD and NAD^+ are reduced as illustrated in Figure 5-5.

5.3.3. Glutamate

The most abundant amino acid, glutamine, is found in abundance in intracellular pools [196-200]. Glutamine, via phosphate-dependent glutaminase within the mitochondrial matrix, is converted to glutamate [201, 202]. As either a precursor or substrate, glutamate can be utilised in cellular respiration via glutamate dehydrogenase and enters the TCA cycle as α-ketoglutarate (see Figure 5-6) [201]. In the liver and kidney, glutamate can be converted to glucose where the appropriate enzymatic machinery is located, as illustrated in the checked section of Figure 5-6 [203].

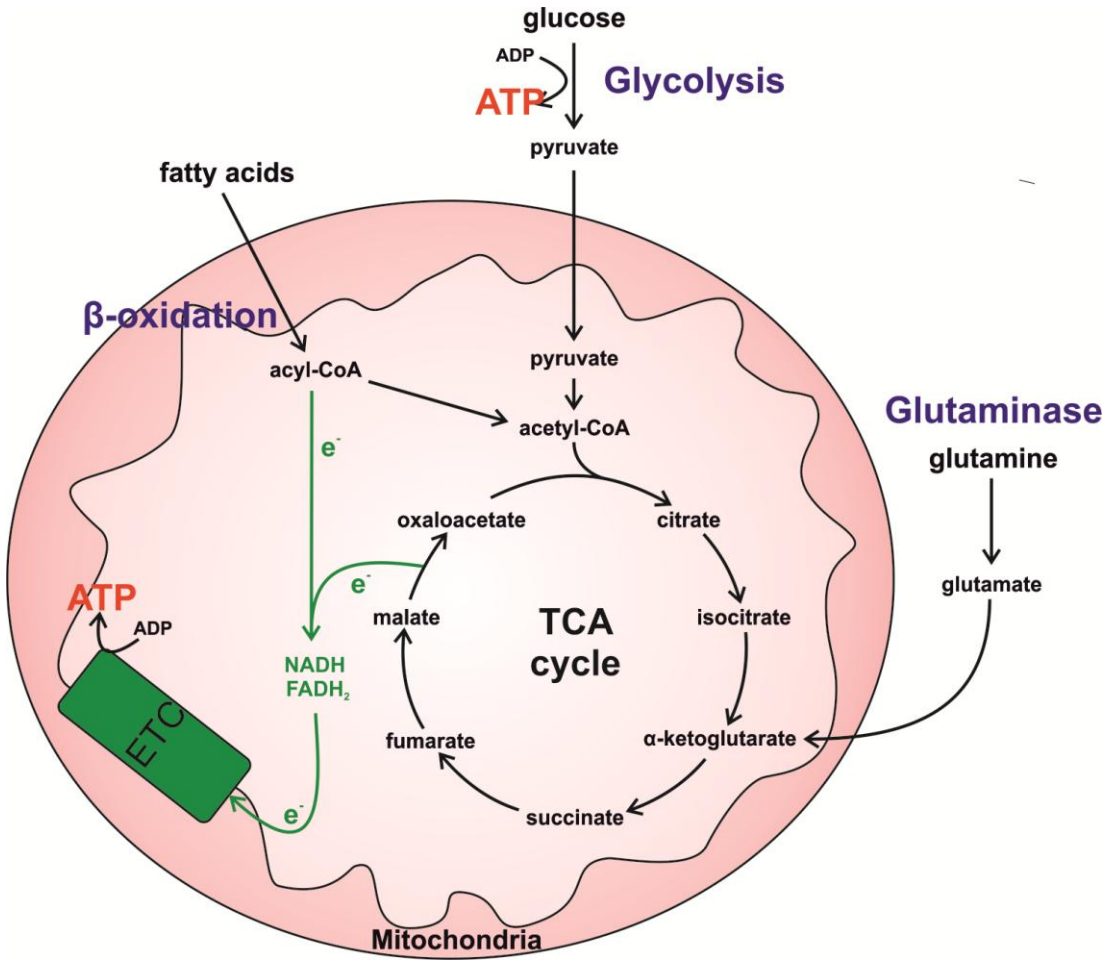

Figure 5-3. Overview of cellular energy metabolism through glycolysis, β-oxidation and glutaminase and the interaction with the tricarboxylic acid (TCA) cycle and electron transport chain (ETC).

The diagram presents a simplistic overview of cellular respiration with the energy sources, glucose, fatty acids and glutamate, their enzymatic pathway and entry into the TCA cycle and ETC. The sites of ATP synthesis are highlighted in red text, whilst electron pathways and reduced electron carriers are in green.

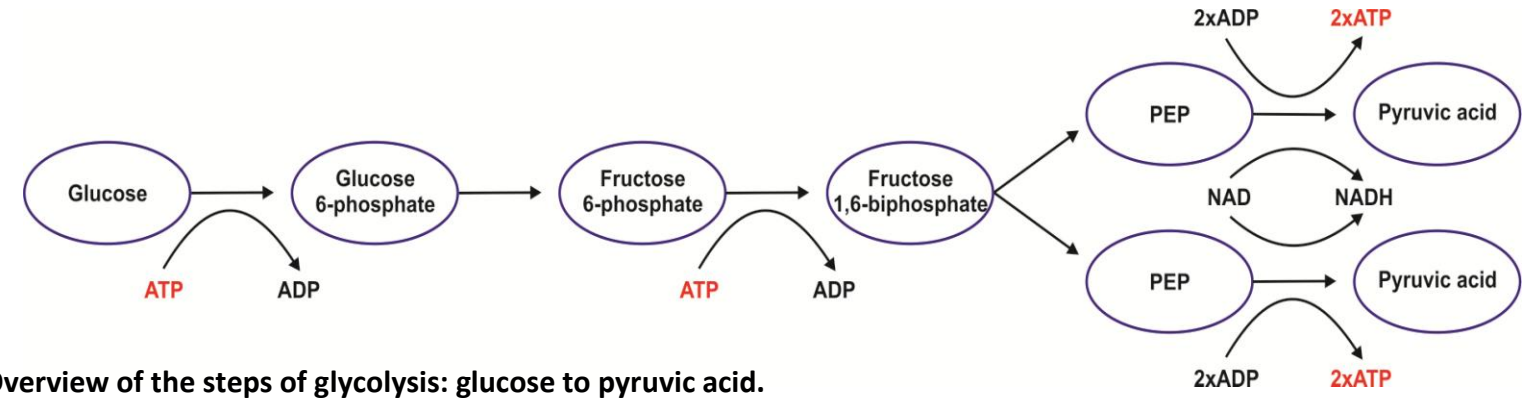

Figure 5-4. Overview of the steps of glycolysis: glucose to pyruvic acid.

In glycolysis a single glucose molecule, is degraded into 2 pyruvate molecules, via a series of reactions. ATP is initially used to dephosphorylate glucose and fructose-6-phosphate, but is replaced during substrate-level phosphorylation. Phosphoenolpyruvate (PEP).

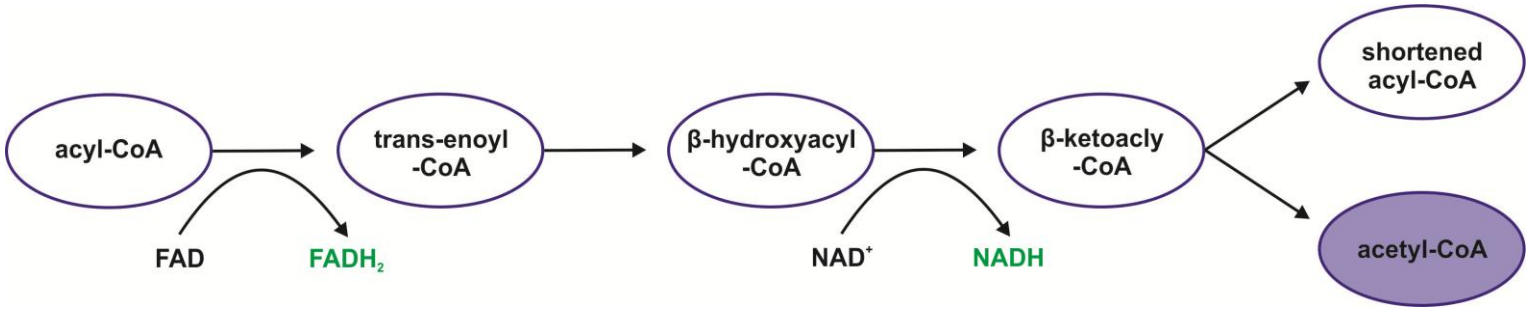

Figure 5-5. Diagrammatic view of the steps involved in β-oxidation: acyl-CoA to acetyl-CoA.

In β-oxidation acyl-CoA is converted, via a series of enzymatic and electron donating stages, to acetyl-CoA. Acetyl CoA then enters the ETC.

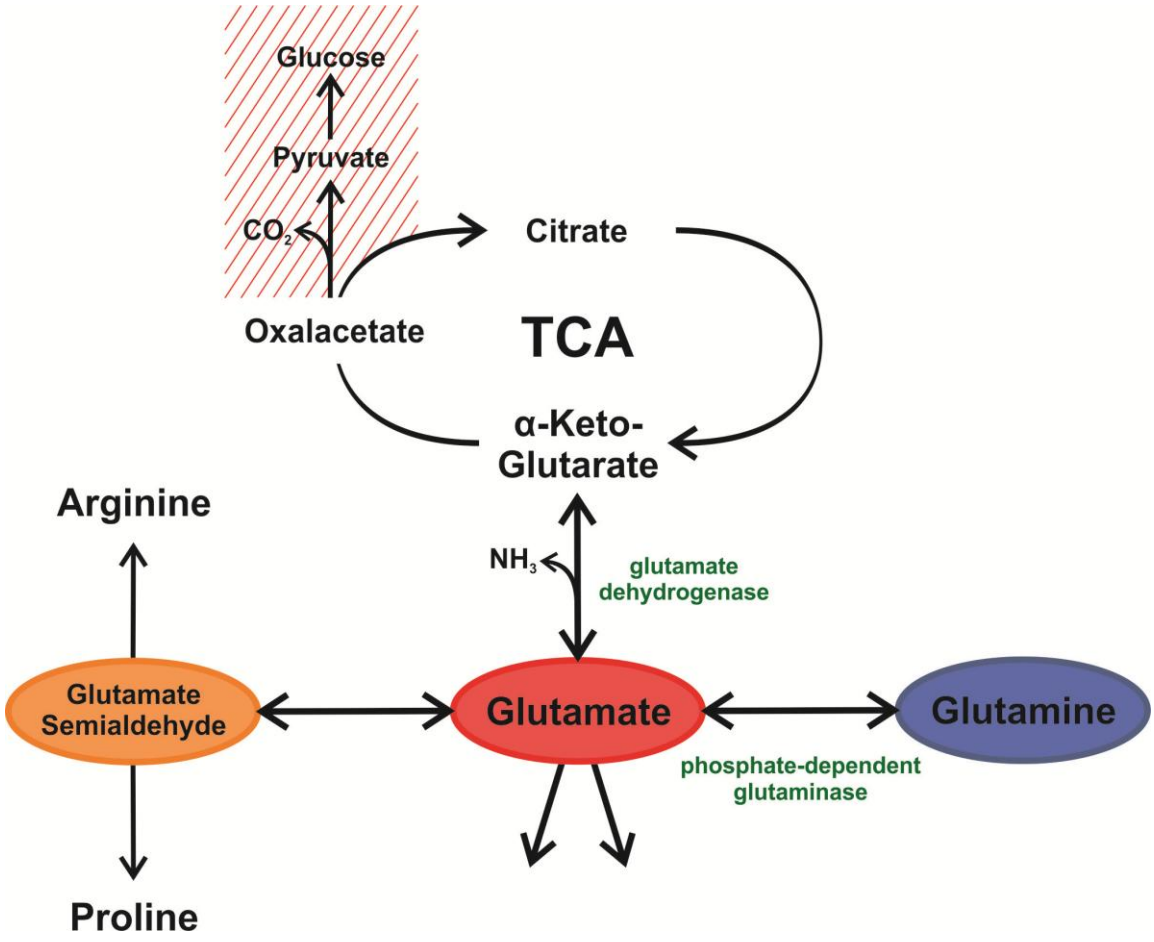

Figure 5-6. Overview of glutamate metabolism and involvement in the TCA cycle.

The diagram presents a simplistic overview of glutamine derived glutamate and its involvement in cellular respiration. Glutamate itself acts as a both a substrate or precursor in metabolism. The enzymes are donated by green text and the formation of glucose is highlighted in the red hatched area (this only occurs in the kidney and liver).

5.3.4. Tricarboxylic Acid Cycle

The TCA or Krebs cycle was named after its discoverer, Sir Hans Krebs. Krebs based this cycle on four main observations in the 1930s [204].In the TCA cycle, a series of sequential reactions oxidise fuel molecules and release electrons. This reduces the coenzymes, NAD^+ and FAD, converting them to their energy rich forms, NADH and $FADH_2$, seen in the equation below.

$$Pyruvate \rightarrow 3NADH + 1FADH_2 + \mathbf{1}\boldsymbol{ATP} + CO_2$$

Equation 5-2. TCA cycle

Consisting of eight reactions, as summarised in Figure 5-7, the cycle begins with condensation of acetyl-CoA and oxaloacetate to generate citrate. The following seven reactions regenerate oxaloacetate and include four oxidation reactions. The oxidation reactions generate the reduced NADH and $FADH_2$ coenzymes. In addition, through substrate-level phosphorylation, a guanosine triphosphate (GTP) molecule is formed. The GTP molecule readily transfers a phosphate group to ADP to produce ATP.

5.3.5. Oxidative Phosphorylation

Oxidative phosphorylation is essentially, the reduction of oxygen through a series of redox reactions and cellular respiration (energy transformations) across the ETC. The entire process can be surmised in the equation below.

$$2H_2 + O_2 \rightarrow 2H_2O$$

Equation 5-3. Oxidative Phosphorylation

The important aspect of oxidative phosphorylation is not the formation of water, but the chemiosmosis of protons across the IMM and the resulting unbalanced proton distribution [205, 206]. The proton movement generates the mitochondrial

proton motive force, through pH gradient and electrical potential. As described by Boyer, and illustrated in Figure 5-8, proton efflux and influx, down the gradient, provides the energy for ATP synthesis at the F_1F_O complex [207, 208].

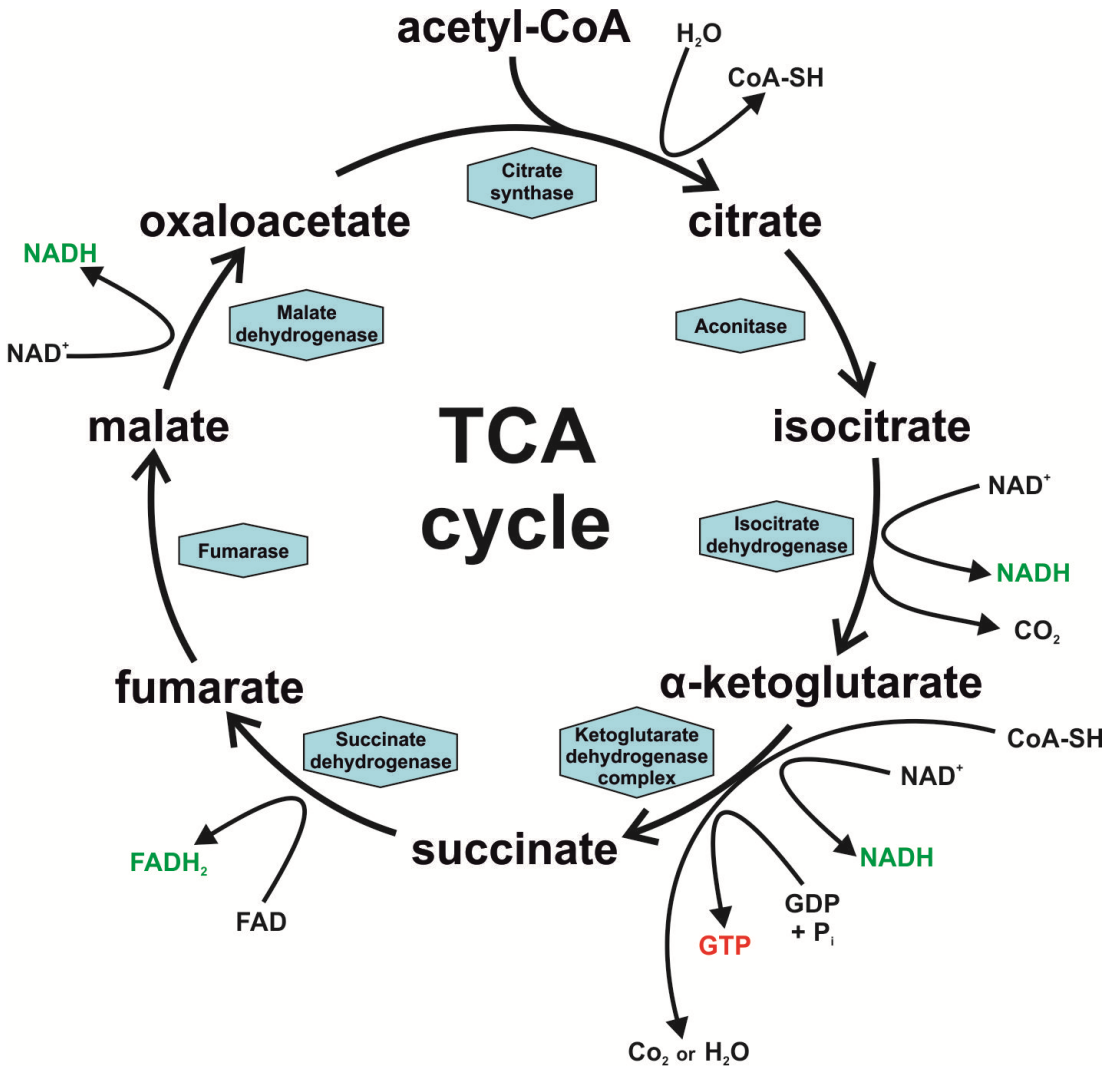

Figure 5-7. An overview of the tricarboxylic acid (TCA) or Krebs cycle.

The diagram illustrates an overview of the enzymatic steps of the tri-cyclic acid (TCA) cycle, converting citrate (C6) to oxaloacetate (C4). The reduced electron donors (NADH and $FADH_2$) and GTP produced are highlighted in red text. The dehydrogenase enzymes are named in the hexagonal boxes and the substrates are the oval sections. CoA-SH is shortened coenzyme A, NAD^+ is nicotinamide adenine dinucleotide, NADH is the reduced NAD^+, FAD is flavin adenine dinucleotide, $FADH_2$ is reduced FAD.

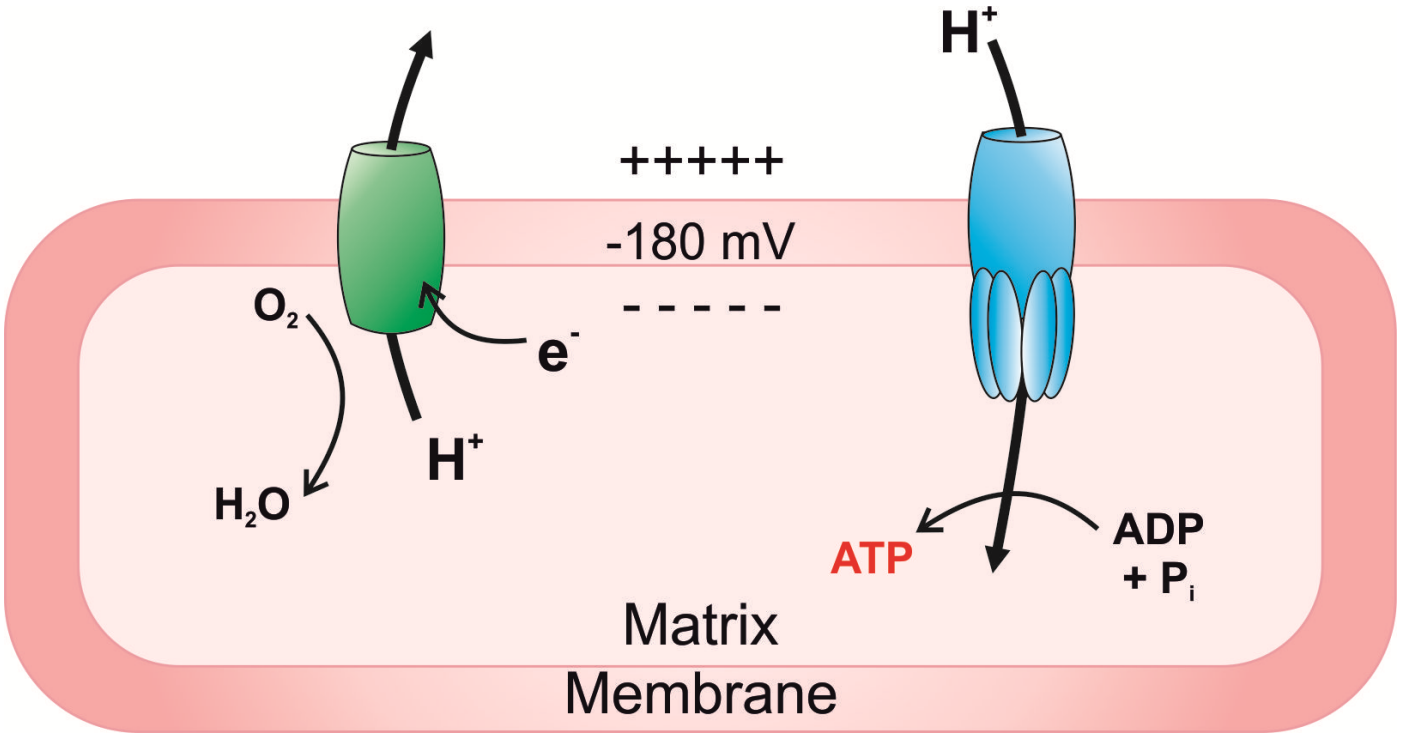

Figure 5-8. Oxidative phosphorylation: proton efflux and influx across the inner mitochondrial membrane.

Oxidative phosphorylation is summarised by the efflux of protons through the complexes of the electron transport chain (ETC) and proton influx along with the resulting ATP synthesis via ATP synthase. Explain what the green and blue things are in the membrane.

5.3.6. The Electron Transport Chain (ETC)

The ETC couples electron transfer between an electron donor (the reduced coenzymes, NADH or $FADH_2$) and an electron acceptor (oxygen) with the movement of protons across the IMM. This process is called oxidative phosphorylation as ADP is phosphorylated to ATP using the energy of the oxidative steps. Figure 5-8 summarises the $\Delta\psi_m$ and the efflux and influx of protons that drive ATP synthesis during this process.

The original ETC model proposed a freely diffuse and independent series of complexes, located in the inner mitochondrial membrane. However it is now perceived to exist as a highly-ordered structure of interacting enzymes. This structure increases the efficiency and efficacy of electron transfer [209-212]. The ETC is a sequence of redox reactions between protein complexes I to IV. These complexes are illustrated in Figure 5-10 and discussed below.

5.3.6.1. Complex I

Complex I (NADH-coenzyme, ubiquinone (Q) oxidoreductase or NADH dehydrogenase), is the first protein in the ETC [213]. The reaction begins with the oxidation of NADH, which donates two electrons, reducing coenzyme Q10 or Q to ubiquinol (QH_2), as described in Equation 5-4. This redox reaction results in the efflux of four protons into the IMS of the mitochondria through undefined mechanisms that seemingly involve conformational changes of the complex [214].

$$NADH + Q + 5H^+_{matrix} \rightarrow NAD^+ + QH_2 + 4H^+_{IMS}$$

Equation 5-4. Complex I of ETC

5.3.6.2. Complex II

Complex II, which is also called succinate-Q oxidoreductase or succinate dehydrogenase is the second entry point of the ETC. Complex II is unique as it is also involved in the TCA [215]. At complex II, succinate is oxidised to form fumarate and again reduces Q to QH_2.

$$Succinate + Q \rightarrow Fumarate + QH_2$$

Equation 5-5. Complex II of ETC

This reaction produces the electron donor $FADH_2$. Whilst the reduced coenzyme donates an electron, the energy release does not support proton efflux.

The third and final entry point into the ETC is the electron transfer flavoprotein-Q oxidoreductase (ETF-Q oxidoreductase). This enzyme accepts electrons from the electron transferring flavoprotein (ETF), forming QH_2, at the surface of the IMM, as described in the equation below [216, 217]. ETF-Q oxidoreductase is significant in β-oxidation as it is the entry route for electron donation from, acetyl-CoA dehydrogenases [218, 219].

$$ETF_{reduced} + Q \rightarrow ETF_{oxidised} + QH_2$$

Equation 5-6. ETF-Q oxidoreductase

5.3.6.3. Complex III

Complex III, also known as Q-cytochrome c oxidoreductase, cytochrome c reductase or cytochrome bc1 complex, catalyses the redox reaction of QH_2 and cytochrome c, as described in Equation 5-7 [220].

$$QH_2 + 2Cyt\ c_{Oxidase} + 2H^+_{matrix} \rightarrow Q + 2Cyt\ c_{reduced} + 4H^+_{IMM}$$

Equation 5-7. Complex III of ETC

The reaction is more complex than the other complexes, as it occurs in two steps, which doubles proton efflux [221, 222]. In the first step QH_2 is oxidized, donating one electron to cytochrome c, whilst the second reduces Q to ubisemiquinone (Q^-). This initial step releases two protons from the QH_2 into the IMS. In step two, the Q^- intermediate remains bound to the complex and the molecule of QH_2. As previously, the redox reaction occurs but the second electron reduces the bound Q^- and gains two proton from the matrix to form a QH_2 molecule [223].

5.3.6.4. Complex IV

Complex IV or cytochrome c oxidase is the final protein in the ETC. The last complex acts to mediate the reduction of the terminal electron acceptor, oxygen, to water. [224]. The redox reaction, of oxygen and cytochrome c aids in establishing the proton gradient by directly inducing proton efflux while consuming matrix protons during oxygen reduction, as described by Equation 5-8.

$$4\ Cyt\ c_{reduced} + \ O_2 + \ 8\ H^+_{matrix} \ \rightarrow \ 4\ Cyt\ c_{oxidised} + \ 2\ H_2O + 4\ H^+_{IMM}$$

Equation 5-8. Complex IV of ETC

5.3.7. ATP Synthase

ATP synthase is the last enzyme in the oxidative phosphorylation pathway. This complex utilizes the energy held in the proton gradient, to synthesise ATP, as described below.

$$\mathrm{ADP} + \ \mathrm{P_i} + \ 4\ \mathrm{H^+_{IMS}} \ \rightleftharpoons \ \mathrm{ATP} + \mathrm{H_2O} + 4\ \mathrm{H^+_{matrix}}$$

Equation 5-9. ATP synthesis by ATP synthase

The described phosphorylation reaction is an equilibrium, which shifts direction depending on the proton motive force. With a high proton gradient and $\Delta\psi_m$, the

reaction proceeds as desired, from left to right, resulting in the synthesis of ATP via proton influx [225]. In the absence of a proton-motive force, the ATP synthesis reaction reverses. In this instance, ATP is hydrolysed and the channel acts to efflux protons into the IMS, to preserve $\Delta\psi_m$. The ATP synthase protein is a complex made from a F_0 membrane embedded portion and the F_1 headpiece, which is the site of ATP synthesis.

To summarise, each molecule of glucose subject to cellular respiration generates a potential 36 molecules of ATP if incomplete redox reactions, free radical generation, and the ADP concentration are ignored. Glycolysis is responsible for the production of only 2 molecules of ATP, whilst β oxidation (of fatty acids) generates approximately 14 ATP molecules and the remaining 20 ATP molecules arise from oxidative phosphorylation (NADH and $FADH_2$).

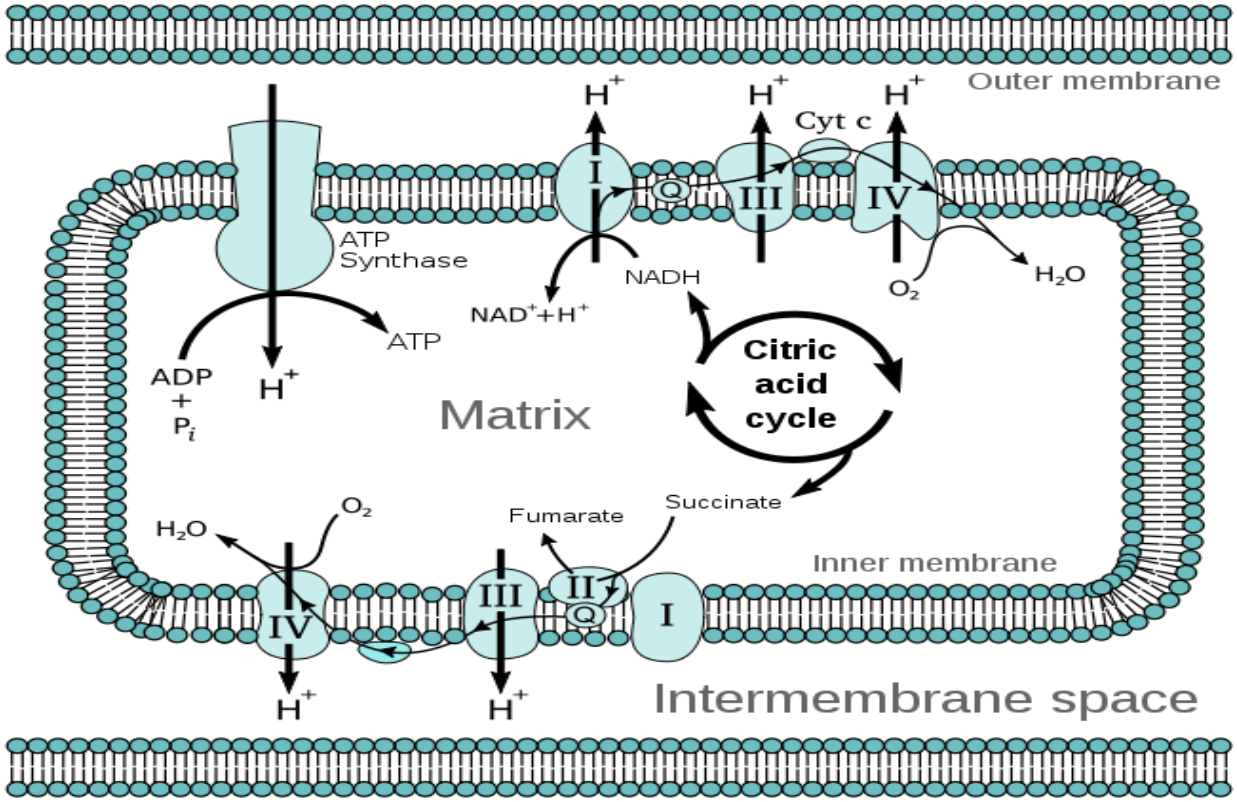

Figure 5-9. An overview of the electron transport chain (ETC) within mitochondria and entry of NADH and succinate.

An overview of the enzymes involved in the electron transport chain (ETC). The architecture and relationship of complex I to IV, in relationship to each other, the ATP synthase channel and citric acid cycle. The two entry points of the ETC are illustrated: the NADH electron donator interaction with complex I and succinate interaction with complex II.

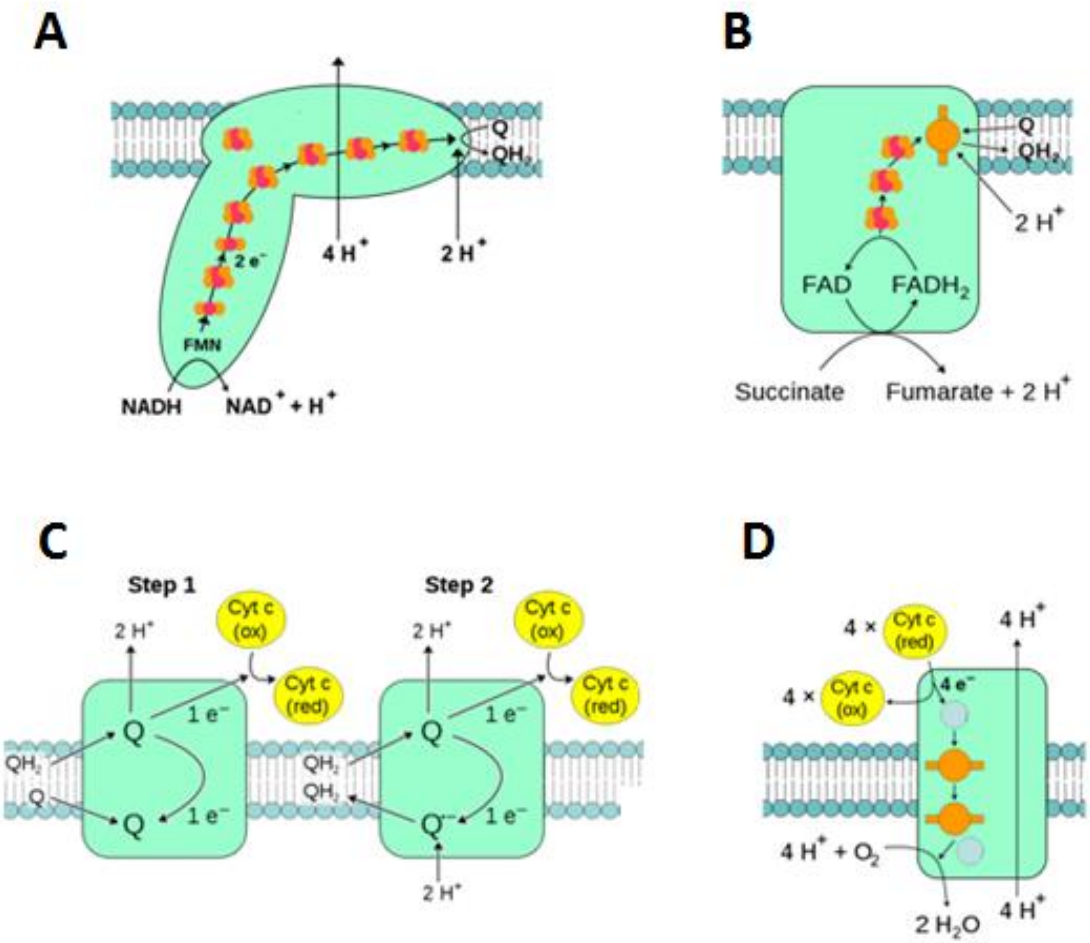

Figure 5-10. The complex's I to IV forming the electron transport chain (ETC).

Graphical representation of the four complexes that form the electron transport chain (ETC) on the inner mitochondrial membrane (IMM). A) Complex I shows the structure of the enzyme and flow of electrons, donated by the reduced NADH, resulting in the efflux of 4 protons (H^+) and reduction of ubiquinone (Q) to ubiquinol (QH_2). B) Complex II is the site of Succinate entry into the ETC, reducing FAD to $FADH_2$, resulting in proton removal from the matrix and the formation of QH_2. C) Complex III illustrates the 2 step process in the transport of electrons and the efflux of four H^+ ions. D) The complex IV enzyme is the final step in the ETC resulting in the formation of two water (H_2O) molecules and the efflux of four H^+ ions. FMN is flavin mononucleotide, is a prosthetic group of some flavoproteins, cyt c is cytochrome c, a heme protein which acts as an electron transfer molecule, reduced (red) and oxidised (ox).

5.4. Mitochondrial Membrane Potential

A proton gradient is generated by the efflux of protons across the IMM by complex I, III and IV of the ETC (Figure 5-9). The electrochemical gradient generated drives ATP synthesis via the F_1F_0-ATP synthase [226]. The $\Delta\psi_m$, established by the proton pumps, needs to be maintained at more than 80% to maintain ATP synthesis [227]

5.4.1. Potassium Cycle

In mitochondria, K^+ plays a vital role in regulating the mitochondrial matrix volume and the $\Delta\psi_m$. Mitochondrial homeostasis of potassium is governed by 5 different mechanisms, as illustrated in Figure 5-11. These mechanisms include the opening of a mitoK_{ATP}, via K^+ "leakage"; the potassium-hydrogen (K^+/H^+) antiporter, which ejects excess K^+ in order to regulate the matrix volume; P_i entry via the P_i/OH exchanger (driven by K^+ induced alkalisation of the matrix); and the $\Delta\psi_m$, which at approximately -190mV drives K^+ influx via the Eyring rate theory (Equation 5-10). In this final mechanism a 10% decrease in $\Delta\psi_m$ results in a 32% decrease in K^+ diffusion [228, 229].

$$J = fPC_{10}\, e^{u/2}$$

Equation 5-10. Erying rate theory

At high potentials, greater than 100mV, the flux of cations (**J**) can be described by a simple exponential function of membrane potential (**Δψ**). Where **u** denotes -zFΔψ/RT, **P** is permeability constant, $\mathbf{C_{10}}$ the bulk ion concentration and f describes the portioning into the energy wells at the surface of the membrane.

5.4.2. Protection Mediators

In 1983, Noma first discovered the K_{ATP} channels located on the sarcolemma in cardiac myocytes. He proposed that they were potential key effectors in IPC, affording protection from ischaemia, shortening action potential durations and reducing calcium influx into the cytoplasm [15, 98]. Several studies have mimicked the protective effect of IPC using pharmacological K_{ATP} channel activators and inhibited using channel blockers.

Further research has implicated the mitochondrial K^+ channel ($mitoK_{ATP}$) and not the $sarcoK_{ATP}$ as the key IPC effectors [230]. The ability for $mitoK_{ATP}$ channels to be end effectors is supported by experimental work with the $mitoK_{ATP}$ selective KCO opener, diazoxide. Diazoxide affords cardioprotection without reduction in observed action potential duration while being inhibited by the presence of channel blockers [15, 121-123].

The $mitoK_{ATP}$ channel, located on the IMM, is believed to have a similar structure to the $sarcoK_{ATP}$ but despite the research over the last 10 years, it has yet to be isolated and the structure confirmed [228]. The $mitoK_{ATP}$ channels are proposed to exhibit similar gating properties to the $sarcoK_{ATP,}$ but with a smaller conductance of approximately 10 pS [228, 231].

There appears to be a paradox as opening of potassium channels would potentially lead to depolarisation and a reduction in ATP synthesis. However, it is possible that potassium channel opening leads to a compensatory mechanism that affords protection [232, 233]. Channel opening offers tight coupling between proton pumping and ATP synthesis and requires an impermeable IMM. The opening of the $mitoK_{ATP}$ channel must modulate mitochondrial function in a manner that supersedes energy loss observed in $\Delta\psi_m$ depolarisation as described in Figure 5-12 [234].

5.4.2.1. Matrix swelling

It is well documented that the opening of the mitoK$_{ATP}$ channel can induce matrix swelling via electrophoretic potassium uptake and the K^+/H^+ antiporter [235, 236]. The potassium influx is accompanied by weak acid (to maintain an electro-neutral environment) and water accumulation, leading to matrix swelling. Mitochondrial swelling preserves cellular respiration, through improved oxidative metabolism, increasing ADP translocation and ATP synthesis. This results from a closer association between the IMM and OMM [236-239].

5.4.2.2. Calcium Overload

The opening of the mitoK$_{ATP}$ has been demonstrated to reduce $\Delta\psi_m$ and subsequently blunt mitochondrial calcium overload, as modulated by KCO such as diazoxide [235, 240, 241]. Calcium release from preloaded mitochondria may occur via an alternative channel, postulated to be the cyclosporine A-sensitive mPTP [240]. The mechanism of reducing mitochondrial calcium has been attributed to an approximate 20mV decrease in the $\Delta\psi_m$, which reduces the driving force of calcium entry [98, 233].

5.4.2.3. ROS production

Elevated ROS production has been shown to be altered by mitoK$_{ATP}$ channel modulation. The opening affords ROS-induced cardioprotection via PKC signalling and is abolished by the presence of the ROS inhibitor L-nitro-arginine [242-244].

5.4.2.4. Mitochondrial Partial Transition Pore

A proposed end effecter of mitoK$_{ATP}$ channel modulation is the formation and partial opening of the mPTP and the resulting protective effects associated with the $\Delta\psi_m$ depolarisation, which occur prior to rupture and apoptosis [33, 245, 246].

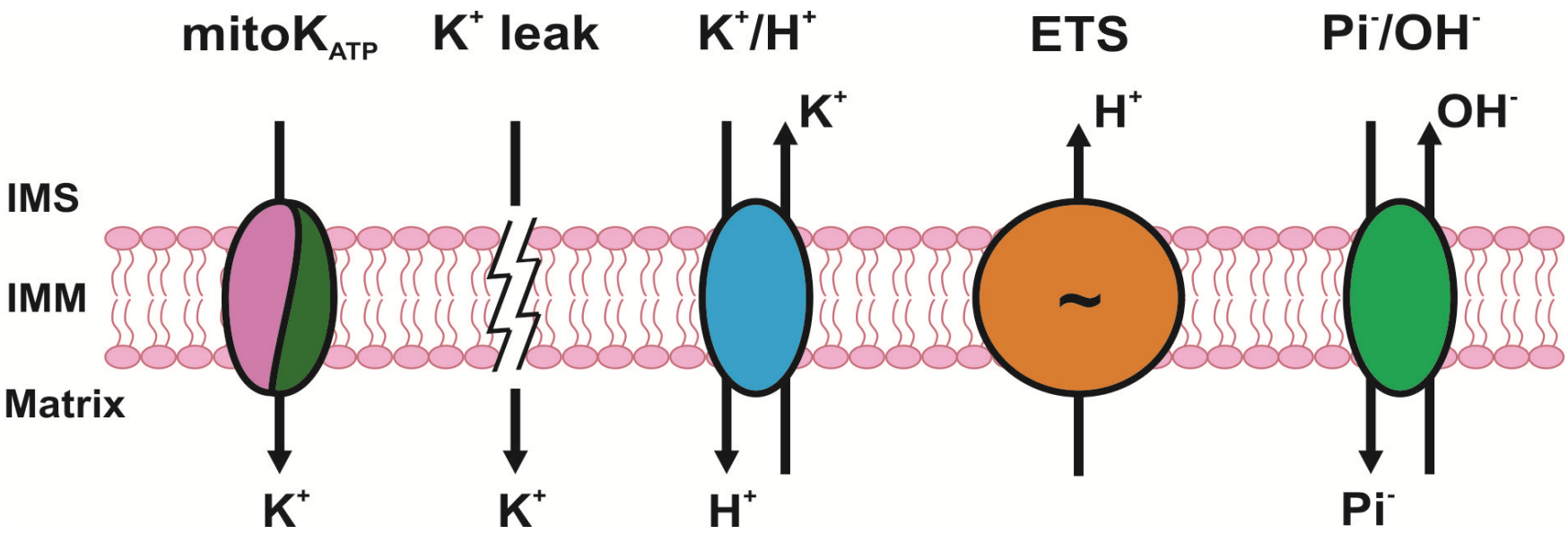

Figure 5-11. Mitochondrial potassium transport: the K^+ cycle

In mitochondria, potassium is vital in regulating $\Delta\psi_m$ and cell volume. The potassium concentration and gradient is regulated by the mitoK$_{ATP}$ channel, K^+ "leakage", potassium-hydrogen (K^+/H^+) antiporter, ETC ejecting protons, and P_i entry via the P_i/OH^- exchanger. K^+ denotes potassium ions, H^+ denotes protons, P_i denotes inorganic phosphate and OH^- denotes hydroxide.

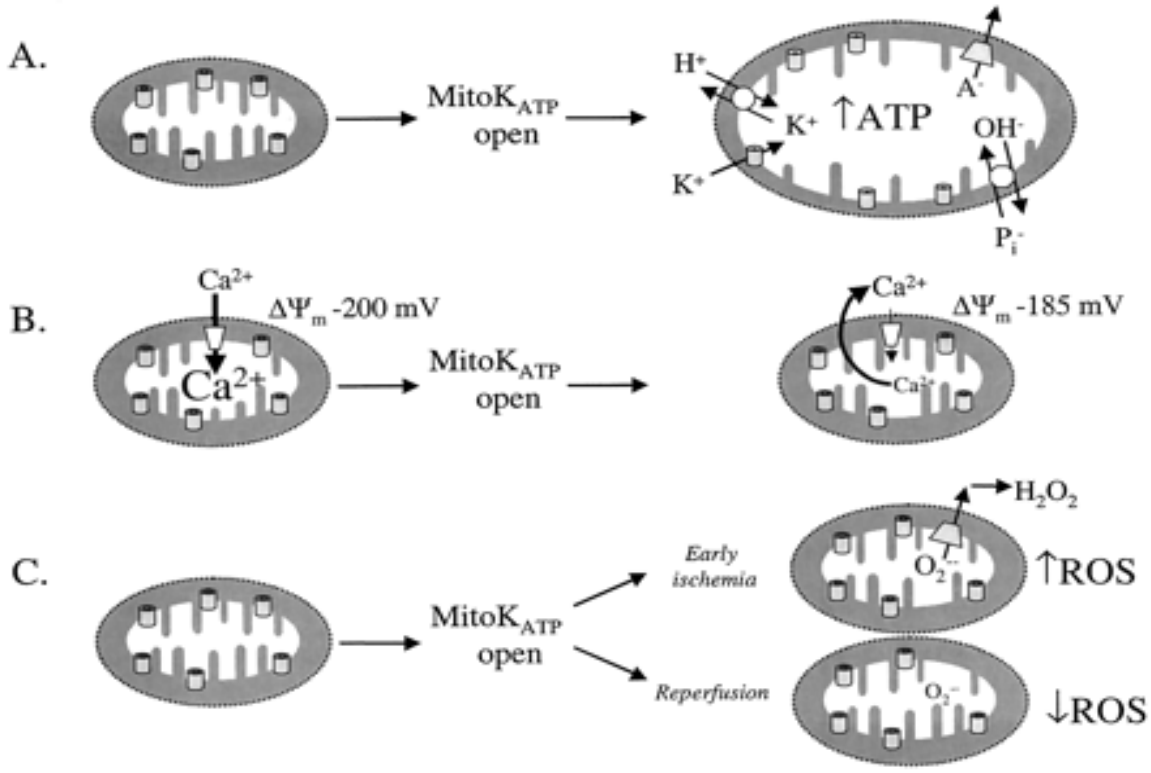

Figure 5-12. Putative mechanisms of mitoK$_{ATP}$ channel mediated ischaemic protection.

To protect the mitochondria, and cell, during ischaemia and reperfusion the putative mechanisms have been proposed. A) Mitochondrial volume, determined by the balance between salt influx and efflux from the matrix, may be adjusted to optimize energy production or minimize energy loss. B) Mitochondrial calcium overload may be slowed by depolarization of the $\Delta\psi_m$, and calcium release may be initiated by permeability transition pore opening. C) ROS production by the mitochondria may be enhanced during early ischaemia to trigger protection but inhibited during reperfusion to mitigate damage. Adapted from O'Rourke [98].

5.4.3. Potassium Channel Modulators

The opening of the mitoK$_{ATP}$ channel, resulting in K^+ influx was initially proposed by Gross *et al.*, in 1999 [230].

Following this, KCO openers (nicarandil and diazoxide) have been utilised as pharmacological IPC agents [15, 120-124]. Diazoxide has since been proposed as a mitochondrial specific KCO, modulating the mitoK$_{ATP}$ channel only. This is supported by a lack of action potential shortening associated with sarcoK$_{ATP}$ opening and an abrogation of the effects presence of specific mitoK$_{ATP}$ blocker 5-HD [121, 122, 247, 248].

5.4.3.1. Diazoxide

The pharmacological IPC associated with diazoxide, is suggested to result from direct modulation and opening of the mitoK$_{ATP}$ channel. Data published by Moreau *et al.* (2005) has supported the potential of direct modulation, of the mitoK$_{ATP}$ channel by diazoxide having demonstrating that it binds to sulfonylurea receptor 1 and 2A (SUR-1, -2a), proposed channel subunits [249-251] .

Although diazoxide irrefutably induces IPC, the exact mechanism of action remains elusive. In 1999, D'hahan demonstrated diazoxide modulation of the sarcoK$_{ATP}$ channel occurred, but only in the presence of elevated ADP, which serves as an essential cofactor [252]. Suzuki *et al.* (2003) reported diazoxide to have a K_m of 840 µM, for the sarcoK$_{ATP}$ channel [253]. Alongside modulation of potassium channels, diazoxide is now believed to potentially affect several mechanisms, including: partial inhibition of succinate dehydrogenase, upstream ROS synthesis, generation of PKC and opening of the transient mPTP [34, 41, 144, 254-256].

It is diazoxides metabolic effects that have gathered interest as an alternative explanation of the associated IPC. Forbes *et al.* (2001) and Hanley *et al.* (2002), amongst others, have demonstrated that diazoxide inhibits succinate dehydrogenase, thereby inhibiting complex II of the ETC (see 5.3.6) and affording IPC via mitochondrial depolarisation [41, 239, 254, 257-263].

5.4.3.2. 5-hydroxydecanoic acid

In 1991, McCullough first described 5-HD as an "ischemia selective inhibitor of mitoK$_{ATP}$ channels" [264]. Following this and its proven ability to abrogate pharmacological IPC, 5-HD was promoted as a putative specific mitoK$_{ATP}$ channel blocker [228, 265, 266]. It has been documented to negate diazoxide induced potassium influx, but the presence of ATP and magnesium is required [120, 237].

Contrary to this, several papers have proposed that, 5-HD opposes diazoxide induced pharmacological IPC, by modulating β-oxidation (described in section 5.3.2) and acting as a partial substrate. This concept is supported by the fact that ischaemic and pharmacological preconditioning can be abolished by trimetazidine, a 3-ketoacyl-CoA inhibitor [267, 268]. Lehtihet *et al.*, in 2003, documented IPC inhibition by glibenclamide. Glibenclamide showed dose dependent inhibition of carnitine-palmitoyl transferase 1 (CPT-1) in β-cells, thus preventing fatty acid transport across the OMM [269]. It is not clear if 5-HD, in its active form, can enter the mitochondria and prevent β-oxidation [237].

Whilst 5-HD is well documented to abrogate pharmacological IPC and although originally believed to close the mitoK$_{ATP}$ channel, it is now perceived to modulated β-oxidation. The presence of 5-HD can inhibit β-oxidation which is proposed to inhibit IPC whilst paradoxically elevated β-oxidation may also be responsible. The succinate dehydrogenase inhibitor 3-nitropropionic acid (3-NPA) induced IPC, was prevented by the presence of 5-HD [266]. When metabolised 5-HD forms 5-HD-CoA, and depending on the isomer formed, it can act as a weak substrate or an inhibitor of β-oxidation [254, 270]. The L-isomer forms a substrate for fatty acid oxidation, whilst the D-isomer can result in a bottleneck of the pathway [237, 270-273]. This suggests that 5-HD is potentially not a direct inhibitor of the mitoK$_{ATP}$ channel but rather a metabolic antagonist of diazoxide-induced succinate dehydrogenase inhibition [254, 262, 263, 270, 272, 274].

5.4.4. Cyclic GMP Modulators

A critical element of preconditioning and resulting cardiac protection is NO driven cGMP-dependent protein kinase G (PKG) activation [275-277]. In CMs, cGMP-dependent PKG signalling exerts positive ionotrophic, negative metabolic and functional effects [278-280]. The opening of the mitoK$_{ATP}$ channel is a proposed end effector of PKG in preconditioned hearts compared to non-conditioned hearts and as such is a proposed mechanism of IPC [281-283].

Whilst guanylate cyclase-driven cGMP production is the main signalling pathway of NO, it can also can affect signalling and cellular physiology via direct NO action or peroxynitrate signalling, as previously discussed in section 5.1.3 [60]. As a proposed mitoKATP channel opener, this is believed to modulate calcium signalling amongst other downstream signalling effects. These include cardiac excitability or downstream effects of PKG activation such as modulation of the L-type channel, inhibition of mPTP formation and a reduction in mitochondrial swelling and ROS production [241, 284-291].

The cGMP concentration can be modulated by several means, including NO activation of guanylate cyclase, or hydrolysis via phosphodiesterase type 5 (PDE$_5$, which preferentially hydrolyzes cGMP) [292]. Zaprinast (ZAP) inhibits PDE$_5$ cGMP hydrolysis (maximal inhibition, I_C=10 μM), resulting in elevation of cGMP concentration even under basal conditions [278, 293].

Protein kinase G is proposed to increase mitoK$_{ATP}$ channel activity, via PKG-dependant phosphorylation, but requires the presence of cGMP and ATP [232, 290]. Whilst NO has been shown to induce cGMP activation as the trigger for mitoK$_{ATP}$ in patch clamp models and CMs, it has paradoxically been shown to have no comparable effect in whole cell models [290, 294-296].

The exogenous NO donors, S-nitroso-N-acetylpenicillamine (SNAP) and sodium nitroprusside (SNP), are both known to induce cGMP-dependent PKG activation via the activation of guanylate cyclase [288, 290, 297, 298]. The use of the guanylyl cyclase inhibitor 1H-[1,2,4]oxadiazolo[4,3-a]quinoxalin-1-one or ODQ confirms

SNAP as a NO donor [232, 299]. As NO can modulate several pathways PKG inhibitors, KT5823, (*Rp*)-8-Br-PETP-cGMPS and (Rp)-pCPT-cGMP, were utilized to inhibit cGMP-PKG activation, confirming this pathway over other potential routes [290, 300]. The cGMP-PKG pathway was corroborated by the PKG activator, (Sp)-8-Br-PET-cGMP, which mimicked the observed effects induced by NO [300].

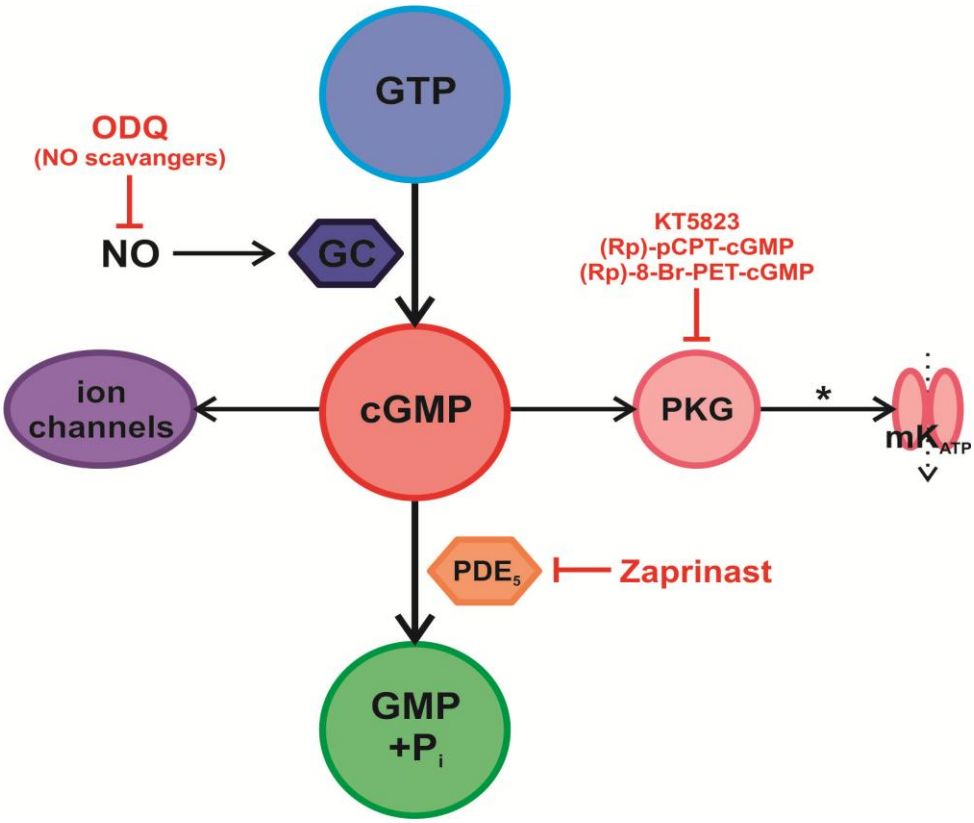

Figure 5-13. Proposed cyclic GMP (cGMP) dependent activation pathway of protein kinase (PK) and site of inhibitors.

Diagram of the nitric oxide (NO) and cyclic GMP (cGMP) activation of protein kinase G (PKG). Cyclic GMP, and subsequently PKG, can be elevated through NO donor stimulation of guanylate cyclase (GC) and inhibition of phosphodiesterase type 5 (PDE_5) cGMP hydrolysis using zaprinast. The mitochondrial potassium ATP channel ($mitoK_{ATP}$) is proposed to be activated via PKG-dependent phosphorylation is donated by *.

5.5. Extracellular Nucleotides

The concept of purines as extracellular signalling molecules was instigated by Drury and Szent-Gyorgyi in 1929 [301]. Subsequently ATP was recognised as the elusive source of cellular energy and emerged as a key extracellular signalling molecule [301]. They documented the effect of extracellular purines (adenosine and AMP) on the heart and found that they pronounced chronotrophic effects and vasodilatory action on the microvasular [301]. Numerous studies have since documented the role of nucleotides and the expression of receptors ubiquitous to all mammalian tissue and essentially all cells in vertebrate organisms [302-305].

Nucleotide signalling mediates a multitude of biological processes. Depending on the expression of particular purinoceptors many varying responses may arise from a single agonist. Purinoceptor signalling affects a plethora of responses including smooth muscle relaxation and contraction, ion transport, inflammation and immune responses, cardiac function and cell proliferation [302].

5.5.1. Purino Receptors

ATP and other nucleotides act via cell surface purinoceptors, which are senstive to nucleotides in the range of 10-80 μM [306]. The purino receptors consist of two main families, P1 and P2, defined by their agonist sensitivity, first indicated in the different actions of purines [307]. The receptors were documented by Burnstock in 1978 and given the nomenclature “P1-purinoceptors” and “P2-purinoceptors” before P1 (A) and P2 respectively [308]. The adenosine sensitive P1 or A receptors were initially identified in brain slices and are made up of 4 G protein coupled receptors; $A_{1, 2A, 2B \text{ and } 3}$ [302, 309, 310]. In mammalian tissues, the ATP, ADP, UTP and UDP receptor family, P2, comprises of the P2X ligand-gated ion channels ($P2X_{1-7}$), and P2Y G-protein coupled receptor ($P2Y_{1, 2, 4, 6, 11-14}$) [302, 311-315]. The receptor sub-family structure and nucleotide sensitivity is illustrated in Figure 5-14, (for a full review see Ralevic and Burnstock (1998)) [302].

$P2Y_2$, $P2Y_{11}$ and P2X receptors in their various forms are sensitive to ATP, whilst only $P2Y_1$, $P2Y_6$ and $P2Y_{11}$ are ADP receptors. However the P2X channels exhibit sensitivity to ADP, but it is a weak agonist compared to ATP [316, 317]. There is widespread evidence that the $P2Y_1$ receptors respond selectively to ADP while ATP acts is antagonistic [318].

5.5.2. Nucleotide Release

Constitutive release of nucleotides occurs in resting cells. The basal level of ATP is dependent on basal release and signal termination, is reported to be 1 to 10 nM at the peri-cellular space without bulk diffusion into the extracellular space [304, 314, 319, 320]. The extracellular nucleotide concentration and signal termination is precisely regulated by receptor de-sensitisation and down regulation, nucleotide reuptake, and extracellular interconversion by a family of ecto-enzymes [304].

It is widely documented that extracellular ATP release occurs in a plethora of cells including, epithelial, endothelial, astroyctes, fibroblasts, CMs, and various other tissues [321-323]. The extracellular ATP concentration has been reported to be nearly four times greater in hypoxic cardiac tissue when compared to cells in normoxic conditions [324].

Using mathematical modelling it has been suggested that, ADP and AMP are released in-conjunction with ATP [325]. It has also been shown that at the cell surface, ADP and GDP are detectable at concentrations equal to or greater than their respective triphosphates [319].

Despite continuing research, the exact source and mechanism of nucleotide release is yet to be defined, but several non-lytic and apoptotic mechanisms have been proposed including 1) mechanical stimulation and ATP channel release, 2) electro-diffusion through ion channels, 3) facilitated diffusion by nucleotide specific ATP binding cassette transporters and 4) vesicular release, as illustrated in Figure 5-15 [315, 322, 326].

5.5.2.1. Mechanical Stimulation ①

The first documented occurrence of ATP release in response to mechanical stimulation, was observed during sustained exercise in human forearm musculature [327]. The concept of non-lytic ATP release was strengthened by the pioneering work with perfused endothelial cells [328-330]. Following these initial studies, ATP release has now been observed in a variety of tissues including umbilical vein, endothelia, epithelia and fibroblasts [331-336]. Of the cell lines in which ATP release has been observed, epithelial cells are particularly sensitive to sheer stress [315].

5.5.2.2. ATP Binding Cassette ②

The ABC transporters are an alternative mechanism of release. Of the ABC transporters, it is the cystic fibrosis transmembrane conductance regulator (CFTR) that has received the most attention. Whole-cell and single channel electrophysiological patch clamp experiments have suggested ATP conductance occurs in the regions that exhibit the presence of CFTRs [289, 337]. Despite early indication, studies using native, heterologously expressed or highly purified CFTRs, showed that ATP conductance remained [338-340]. To further disprove the involvement of CFTRs, the extracellular ATP concentration is comparable in normal, cystic fibrosis and CFTR-null cells [333, 334, 341]. It appears that CFTRs are not the direct sites of ATP release, but the multiple drug resistance protein (MDR) confers control over ATP efflux since ATP release is reduced in the presence of MDR-1 inhibition [315, 342].

5.5.2.3. Vesicle Trafficking ③

Vesicle trafficking and exocytosis are also a putative mechanism of nucleotide release. In astrocytes, vesicular ATP release is well established [343, 344]. It has been demonstrated to occur in the vascular endothelium, as it reduced in the presence of vesicle inhibitors (monensin and *N*-ethylanalemide) [323, 345, 346]. Whilst the 'selectivity' of the inhibitors is disputed, vesicle trafficking remains as a potential release mechanism.

5.5.2.4. Ion Channels ④

Adenosine triphosphate and other nucleotides are proposed to move through ion channels such as hemi-, stretch- or voltage-channels. Despite early research, stretch-activated cation channels show no close association to ATP release [347, 348]. Both directly and indirectly, VDACs are ATP conduits [349, 350]. In murine cells, VDAC-1 knockouts and inhibition reduce but not fully inhibit ATP release, suggesting multiple mechanisms of release [351, 352].

Connexin and pannexin channels and the $P2X_7$ receptor are all proposed mechanisms of ATP release under both basal and stimulated conditions [353, 354]. Connexons are 1 to 1.5 nm pores, formed from the oligmerisation of 6 connexins [355, 356]. The union of two adjacent hemichannels on cytoplasmic membranes form gap junctions [357], forming large conductance channels with the same permeability as the hemichannels (<1kDa). The opening of the channel is a ligand-gating reaction which can switch between its open and closed state in less than a millisecond [358]. The most widely distributed connexin, of the 13 subsets, is connexin 43. It is expressed in a majority of cell types including CM and fibroblast [359]. The channels can also form non-junctional or 'unopposed' hemichannels and these have been shown to open under both physiological and pathological conditions [360].

The channel has been shown to have a higher than expected substrate conductance and both the hemichannel and channel is now a proven mechanism of ATP release [355, 360-366]. The channel can be modulated by the presence of either 100 µM flufenamic acid (FFA) or EGTA, opening and closing the hemichannel respectively [362, 364]. The presence of gap-junction inhibitors have been shown to have mixed results with inhibitors such as FFA and carbenoxolone affording no modulation on the extracellular ATP. This has been seen in several cell types including endothelial and polymorphonuclear leukocytes cells [367-369]. ATP release is also reduced in the presence of gap peptides (Cx26, 30 and 43) and in knockout mice [364, 370-376].

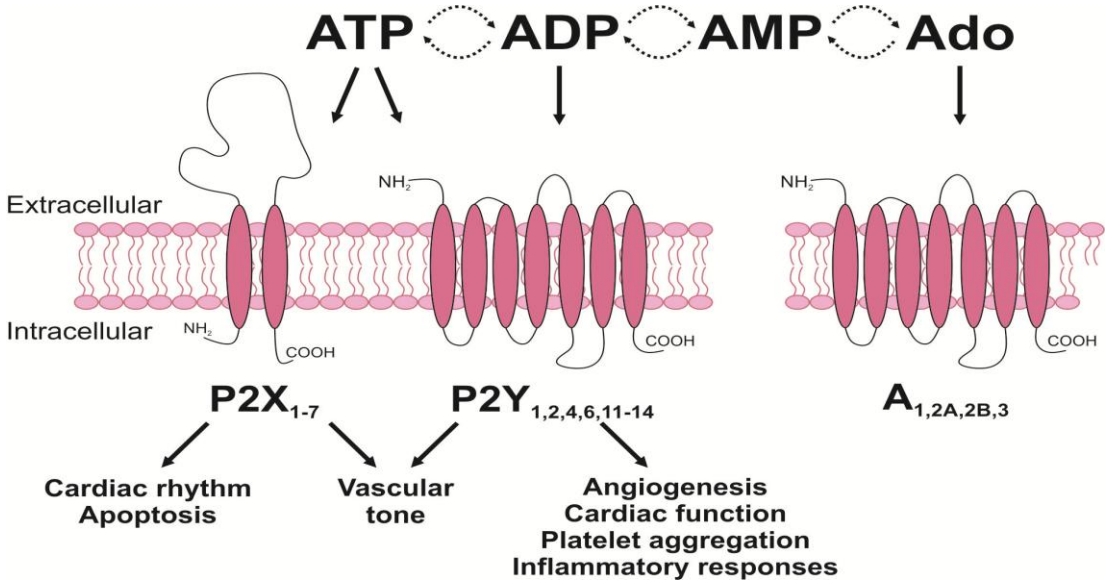

Figure 5-14. Purinoceptor family subtypes, P2X, P2Y and A and their structure and nucleotide sensitivity.

Nucleotides mediate signalling and downstream signalling. Nucleotide signalling acts via a series of ionotropic P2X receptors and metabotropic P2Y receptors, classified by their affinity to ATP and ADP whilst adenosine acts on its own G-protein-coupled nucleoside-selective receptors.

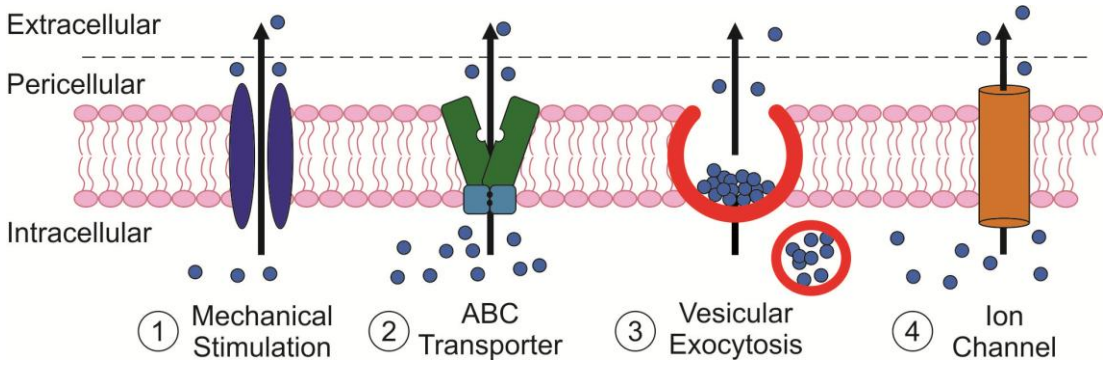

Figure 5-15. Four putative non-lytic nucleotide release mechanisms.

Proposed non-lytic nucleotide-releasing pathways: ① mechanical stimulation, ②facilitated diffusion by nucleotide-specific ATP binding cassette (ABC) transporters, ③ vesicle trafficking and exocytosis secretions and ④ ion channels.

5.5.3. Extracellular Nucleotide Function

The nucleotides responsible for the observed ischaemic effects, such as vasodilatory and chronotrophic modulation, are believed to be attributed to ATP and the products of its degregation, adenosine and AMP [82, 83, 323]. Early research on nucleotide signalling studied the effect on a variety of tissue, notably on coronary, vascular tissue and platelet aggregation [377-379].

ATP signalling is a proposed candidate of cardiovascular effects, both vasodilation and innate immune response activation, as discussed in 5.1.3 [301, 330, 380, 381]. ATP has been shown to induce hyperventilation, bradycardia, hypotension and apnea, via P2X stimulation [301, 382-384]. Alongside elevated ATP, adenosine is also released during hypoxia and shown to induce hyperaemia, increased blood flow [301, 383, 385, 386].

The co-release of ATP and norepinephrine (NE) or acetylcholine occurs in the sympathetic and parasympathetic nervous system, respectively, and can induce an excitatory (P2X) or sedative (P2Y) response [332]. In apoptosis, the $P2X_7$ receptor acts as a non-selective ion pore of leukocytes, whilst the $P2X_5$ and $P2X_7$ receptors induces proliferation, differentiation or apoptosis, respectively in stratified epithelium [387, 388]. ADP signalling via $P2Y_1$ and $P2Y_{12}$ is critical in haemostasis. ADP induces platelet aggregation, which can form a platelet plug and repair damage but can lead to thrombosis formation and vascular occlusions, which manifest as strokes and cardiac infarctions [389-391]. In epilepsy, activation of P2X receptors induces generalised motor seizures, whilst ATP acts as a mechano-transducer in bone function [382]. In cancer patients, exogenous ATP treatment has had positive effects by reducing cachexia (weight loss, muscle atrophy, fatigue and weakness) and improving survival rates [392].

5.5.4. Ecto-nucleotides

Once released, ecto-nucleotidases convert ATP into ADP, AMP and adenosine. Although this reduces ATP signalling, all of the products exert their own

pharmacological effects [382]. This makes the overall effect of ATP addition or release potentially very complex.

Nucleotide concentrations in the extracellular matrix are modulated by several ecto-enzymes at both the cell surface and within the extracellular environment [304, 393].

De-phosphorylation or nucleotide hydrolysis is regulated by several enzymes: ecto-nucleotide triphosphate diphosphohydrolase (E-NTPDase), ecto-nucleotide pyrophosphatase/phosphodiesterase (ENPP), alkaline phosphatase (ALP) and ecto-5'-nucleotdiase (eN) families [21]. Maximal activity is observed in the presence of divalent cations, calcium and magnesium, and exhibit a K_m in the low micro-molar range [304].

$$ATP \rightleftharpoons ADP \rightleftharpoons AMP \rightleftharpoons adenosine$$

Equation 5-11. Nucleotide hydrolysis and synthesis

Nucleotide synthesis, or phosphorylation (where Equation 5-11 runs right to left), was originally believed to be a strictly intracellular process, but other work shows that extracellular ATP synthesis may occur [394]. This process is mediated by the following phosphorylation enzymes: adenylate kinase (AK), nucleoside diphosphate kinase (NDPK) and F_1F_0 ATP synthase.

5.5.4.1. Hydrolysis

The E-NTPDase family (or ecto-apyrase; Figure 5-16) dephosphorylate a variety of nucleoside tri- and di-phosphates in the presence of divalent cations (calcium and magnesium). The E-NTPDases contain an actin-hsp 70-hexokinase β- and γ-phosphate binding motif and highly conserved apyrase regions [395]. The subfamilies exhibit different specificity and ability for nucleotide hydrolysis. E-NTPDase 1 (CD_{39} or vascular ATPDase) converts ATP>AMP with only a modest appearance of ADP. It hydrolyses ATP at a molecular ratio 1:0.8 (ATP:ADP). In contrast, E-NTPDase 2 (or CD39L1, ecto-ATPase) converts ATP>ADP with minimal AMP accumulation with a ratio of 3:1 (ATP:ADP) [304, 396]. E-NTPDase3 (or

CD39L3, HB6) and E-NTPDase8 (or hepatic ATPDase) are a secreted proteins, which hydrolyse ATP to AMP with transient ADP accumulation [320, 397, 398]. Several inhibitors have been developed to inhibit E-NTPDase enzymes hydrolysis. Suramin, a non-competitive inhibitor of ATPase, exhibits a K_i=53 μM.

The ecto-nucleotide pyrophosphatase/phosphodiesterase (E-NPP or PDNP, PC-1; Figure 5-17) family consists of 3 subfamilies. E-NPP_{1-3} requires calcium binding at the EF hand and is optimal within an alkaline pH. E-NPP_1 and E-NPP_3 hydrolyse, ATP>AMP with a K_m=13-50 μM, whist E-NPP2 (or autotaxin) hydrolyses ATP>ADP>AMP, but neither facilitate AMP>adenosine hydrolysis [396, 399-403]. The E-NPP enzymes exist either as a membrane protein or via proteolytic cleavage, as a soluble protein, notably E-NPP_2 [304, 404].

ALP (Figure 5-17) is a homodimeric enzyme, requiring divalent cation binding at catalytic sites, for ATP>ADP>AMP>adenosine hydrolysis [322]. The family consists of 4 members (non-specific, intestinal, placental and germ cell) expressed as either GPI-anchored or soluble enzymes [400]. Alkaline phosphatases exhibit a K_m= low millmolar [304].

It is known that eN (also known as CD_{73}; Figure 5-17) occurs as both GPI anchored and soluble forms and drive adenosine accumulation via AMP>adenosine hydrolysis, expressing a K_m =14±3 μM [306, 405, 406].

5.5.4.2. Synthesis

The transphosphorylating enzyme, AK transfers phosphate groups between adenine based nucleotides (ATP + AMP ⇌ 2ADP; proportional to Mg^{2+} concentration) [407]. The AK family exists as both a soluble and membrane bound enzyme, with AK1 being cytosolic and AK2 located to the internal mitochondrial space [322]. In epithelial cells, AKs exert a K_m=43 μM (ADP) and K_m = 23 μM (ATP), but primarily drive ATP synthesis [408].

The NDPK enzyme, expressed on the plasma membrane or a soluble form (NDP), converts ATP + UDP ⇌ ADP + UTP.

The F_1F_0 complex is comprised of a 500 kDa central F_0 and water soluble F_1 "head piece" that requires oxidative phosphorylation ($NADH/FADH_2$) to convert ADP to ATP. It is not solely located to mitochondria andhas been shown to be expressed by endothelial cells [394]. Partial inhibition of ADP>ATP phosphorylation can be achieved in the presence of oligomycin [408]. Diadenosine pentaphosphate (Ap_5A) also reduces ADP>ATP phosphorylation by inhibiting both AK and F_1F_0 activity [409].

5.5.4.3. Nucleotide Enzyme inhibitors

ATP hydrolysis has been shown to be inhibited by the presence of ebselen (2-phenyl-1,2-benzisoselenazol-3(2H)-one). Ebselen inhibits ATP hydrolysis by approximately 60% when used at concentrations less than 100 µM [410]. Ebselen is reported to have negligible effects on ecto-ATPase and AK activity, whilst it inhibits NDPK hydrolysis with a K_i=7.6±3 µM [411]. Ebselen is also documented to affect various biological activities including NOS, PKC, NADPH oxidase[412].

6-*N*,*N*-Diethyl-D-β,γ-dibromomethylene ATP trisodium salt (ARL 67156) is postulated as a 'non-specific inhibitor of ectonucleotidases', a 'non-specific ecto-triphosphate nucleotidase inhibitor', an 'inhibitor of the E-NTPDases', a 'specific inhibitor of E-NTPDase1 and or E-NTPDase2', and a 'selective ecto-5'-nucleotidase inhibitor' [400, 413-419]. ARL 67156 can attenuate ATP and ADP hydrolysis, NTPase substrates and decrease ATP- and ADPase activity [398, 419, 420]. Despite the evidence, the influence of ARL 67156 on ecto-nucleotides, remains uncertain, but is a weak competitive inhibitor of E-NTPDase1, E-NTPDase3 and E-NPP1, and does not modulate E-NTPDase2, E-NPP3 and ecto-5'-nucleotidase activity [304, 421, 422].

The ALP inhibitor levamisole has been shown to inhibit hydrolysis of both AMP to adenosine and ADP to AMP [405, 423-425].

Acting in a concentration-dependent manner, Ap_5A is an AK inhibitor which causes 69±5%, 80% and 100% inhibition at 100 µM, 300 µM and 500 µM respectively [306, 408, 426, 427]. Preventing ATP to ADP hydrolysis, Ap_5A is a competitive inhibitor and a non-competitive inhibitor of AK synthesis.

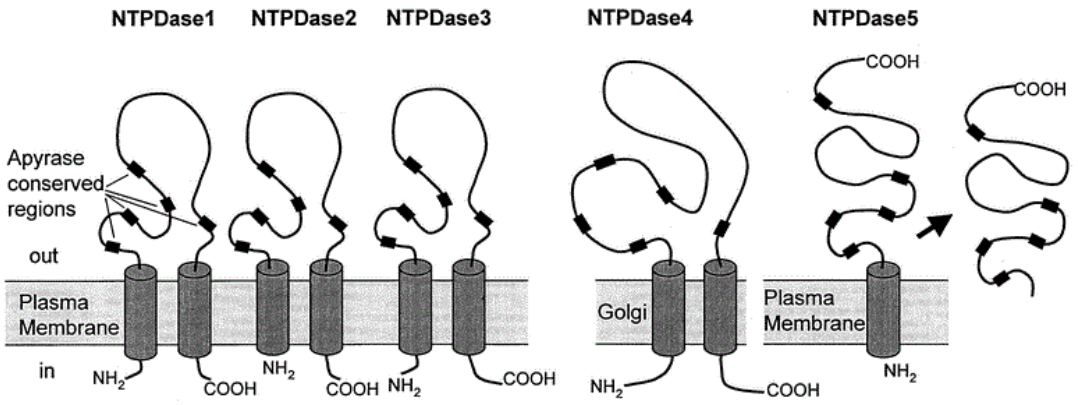

Figure 5-16. E-NTPDase family substrates and structures

Predicted membrane topography and catalytic properties of members of the E-NTPDase family. Enzymes may occur as homomultimers. E-NTPDase5 occurs as a soluble protein (arrow). Adapted from Zimmermann [304].

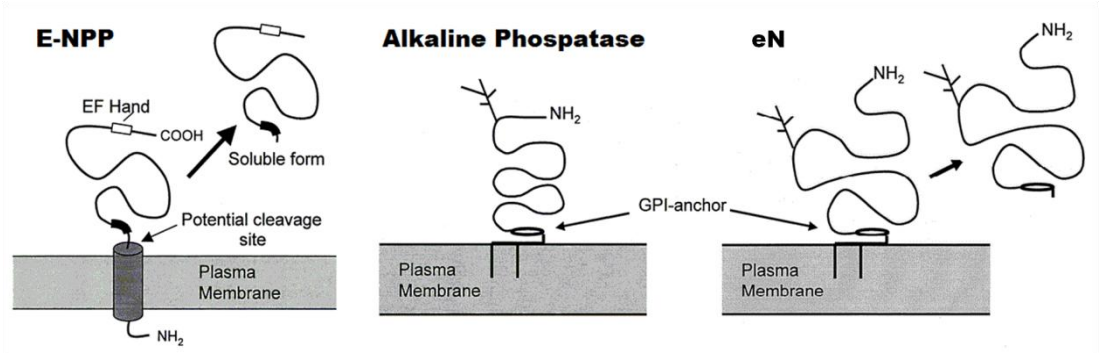

Figure 5-17. Nucleotide hydrolysis enzymes structures: ecto-nucleotide pyrophosphatase/phosphodiesterase (E-NPP), alkaline phospatase (ALP) and 5'-nucleotidase (eN).

Predicted membrane topography and catalytic properties of members of the ecto-nucleotide pyrophosphatase/phosphodiesterase (E-NPP), alkaline phosphatise (ALP) and 5'-nucleotidase (eN). The enzymes may occur as dimers and may become transformed into soluble proteins by proteolytic cleavage or endogenous GPI-specific phospholipase. Adapted from Zimmermann [304].

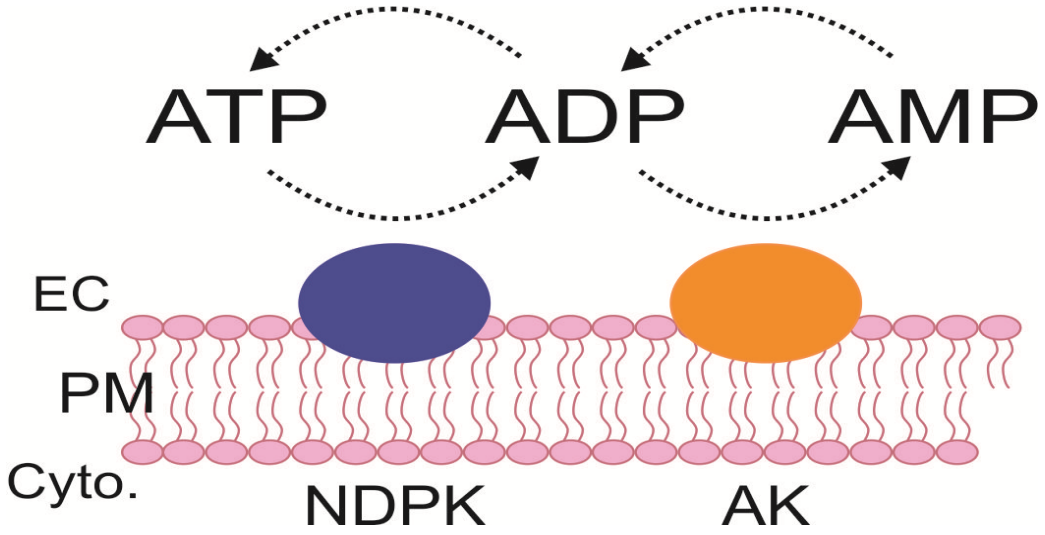

Figure 5-18. Nucleotide synthesis enzyme activity by nucleoside diphosphate kinase (NDPK) and adenylate kinase (AK).

The action of the nucleotide conversion enzymes, nucleoside diphosphate kinase (NDPK) and adenylate kinase (AK) on ATP, ADP and AMP. The enzymes are proposed to act in both directions, hydrolysing and synthesising nucleotides.

5.6. Cardiac Cells

The heart is a complex muscular organ consisting of 3 layers, the pericardium (a connective tissue layer surrounding the heart), the myocardium (muscular tissue) and the endocardium (inner endothelium).

The myocardium is a collection of adapted CMs, which form concentric layers of muscle tissue. Myocytes are approximately 100x20 μm in size and exhibit a striated subcellular structure. They contain large numbers of mitochondria and are fatigue resistant. Individual CMs are connected by intercalated discs forming structural junctions (desmosomes) and gap junctions, which allow electrical conductance and generate a functional syncytium across the cells.

The contractile apparatus in myocytes is composed of actin and myosin filaments, which form the M and Z lines and the A, H and I bands of a sarcomere. At regular intervals along the Z lines, there are transverse (T) tubules, which are highly organised, three dimensional invaginations of the plasma membrane. T-tubules are separated from each other by approx 2 μm long mitochondria and junctional SR [428]. T tubules form a close proximity with the terminal cisternea of the SR, the site of excitation-contraction (E-C) coupling [428].

5.6.1. Excitation-Contraction Coupling

By converting the electrical excitation (action potential) of the heart into a physical contraction of CM, the E-C coupling propels blood around the body. Originating with an action potential, the E-C coupling activates the voltage-gated Na^+ channel, inducing Na^+ influx, rapid depolarisation of the cell membrane, opening the L-type voltage-gated calcium channels, triggering a rise in $[Ca^{2+}]_c$, above 100 nM [429, 430].

The calcium influx (which accounts for less than 20% of total calcium) opens the RyR-2 channel, resulting in a further elevation in $[Ca^{2+}]_c$, as a calcium “spark”, via CICR from the sacroplasm [429, 431, 432]. Calcium entry occurs over 1 to 2 ms and

over the following 10 ms, facilitated by the T-tubule structure, the $[Ca^{2+}]_c$ substantial increases, which generates cardiac contraction.

The contractile apparatus in muscle is made from the actin and myosin filaments forming cross bridges according to the sliding filament theory. The elevated $[Ca^{2+}]_c$ binds troponin C, inducing a conformational change, which causes troponin I dissociation and exposes the actin binding site. Contraction is brought about as the myosin head subsequently forms a cross bridge and generates a 'working stroke' and longitudinal sliding of the filaments. As the action potential repolarises, the $[Ca^{2+}]_c$ concentration drops below the 100 nM threshold, unbinding from troponin C and again blocking the binding site, which results in relaxation.

The decrease in $[Ca^{2+}]_c$ occurs through a loss of L-type channel activation and parallel uptake via the SERCA channel and Na^+/Ca^{2+} exchanger (NCX). Of the calcium, 80% is sequestered by the SR and 20% extruded into the extracellular environment [429].

5.6.2. Cardiac Energy Demands

Cardiac tissue is energetically demanding and the ATP pool is turned over in approximately 10 seconds under normal conditions [182, 185, 186]. The ATP supply is mainly derived from oxidative phosphorylation, which accounts for 90%, whilst the TCA cycle and glycolysis generation attributed the remaining 10% [189, 433].

The main source of ATP in cardiac tissues is derived from β-oxidation of fatty acids, such as triacylglycerol and very low density lipids [177-179]. Fatty acid is accumulated in the heart via passive diffusion and a proton carrier-mediated pathway via the fatty acid translocase (FAT) and fatty acid transport protein (FATP). For a full review please see the referenced papers [179, 434]. While fatty acids are the hearts predominate source of energy (70-95%), due to its high energy demand, the heart acts as an "omnivore" and takes energy from a variety of carbon sources including glucose and glutamate [180-187]. The regulatory pathways which control the physiological and pathological switch in energy sources are still elusive, although insulin and pyruvate dehydrogenase are known to be involved [180].

During hypoxia and ischaemia, despite the loss of oxygen and reduced ATP synthesis, β-oxidation remains the major source of energy [435, 436]. Whilst this is the case, glucose derived ATP is elevated which has the beneficial effect of requiring less oxygen than fatty acid ATP generation [180].

5.6.3. Primary Cardiomyocytes

Heart tissue was first cultured in 1912, when Burrows placed pieces of explanted embryonic chick hearts in culture and observed that single, individual cells migrated away from the explants [437]. It was not until 1952 that CMs were isolated from foetal hearts and the isolation protocol was subsequently developed, where CMs were cultured as their component cells for extended periods [438-440].

In the developing chick heart, contractility can begin within 33-38 hours of incubation of a fertilised egg. This occurs in a cluster of cells within a restricted region at the right postero-ventral edge of the primitive ventricle. The cardiac cells found in this region are significantly differentiated, inducing pacemaker potential, and generating a bioelectric potential and contractility [441, 442]. With a short embryonic phase and their relative costs, chick CMs have since been used to study cardiac physiology, pharmacology and metabolic parameters [443-445].

The neonatal rat CM model permits the study of many of the morphological, biochemical and electrophysiological characteristics [446-449]. Neonatal CMs offer a preferential model compared to adult CMs as a typical rat litter of 10–20 neonatal pups provides sufficient tissue and is comparatively less expensive than CMs isolated from adult rats. Neonatal CMs also offer easier isolation, sensitivity to Ca^{2+} and a stable phenotype that is contractile [450, 451].

Despite their advantages, CM isolation techniques and Langendorff preparations are time consuming, costly, and limited to cells with adult characteristics. The isolation method is not fully specific and a heterogeneous population is regularly isolated, with non CMs (fibroblast, leukocytes) overgrowing the desired CMs in culture. However the presences of fibroblasts have been shown necessary for proper CM growth and function [452, 453]. During their embryonic stage,

fibroblasts secrete factors such as, fibronectin, collagen and heparin-binding EGF-like growth factor (HEEGF), which collaboratively promote CM proliferation via β1 integrin signalling [454]. The adult heart is prominently two thirds fibroblasts, which act as a mechanical scaffold and co-ordinate CM function [455-457]. Primary populations also appear to lose their contractile ability and are susceptible to oxidative and mechanical injury. Cells can also be damaged by the enzymatic solutions used in the digestion process [439, 458-461].

5.6.4. Embryonic Stem Cells

Embryonic stem cells (ESc), originally derived from undifferentiated cells from murine embryos, can be kept in permanent culture if grown on feeder layer cells (fibroblasts) [462-464]. Cultured ESc form embryoid bodies which can be investigated as either a culture population or dispersed single cells. The cell express a pattern of cardiac-specific markers and in early development spontaneous contraction is observed [465, 466].

Despite the potential of ESc, there are associated limitations as undifferentiated stem cells exhibit no electrical activity or spontaneous beating and only express certain markers. Likewise, M-band or T-tubule-formation may not be not finalised [463, 467, 468]. Differences in ion channel expression and biophysical characteristics have also been noted and over time Esc appear to exhaust their ability to proliferate and CM phenotype deteriorates [452, 469-471].

5.6.5. Cardiomyocyte Cell Lines

Several alternatives to primary CM isolation have been developed as discussed below. Cell lines however are subject to limitations including limited ability to be passaged, low recovered from frozen stock, loss of phenotype, and minimal or nonexistent contractile activity.

Cell lines, such as the P19 and MC29 (avian CMs), are useful tools for studying cardiomyocyte development and differentiation. Studies using these populations were limited by a loss of phenotype and contractile ability [466, 472-474]. Quail

CMs have been utilized in experiments, allowing up to 60 passages, before the cells begin to lose CM markers [475].

The H9c2 cell line is a sub clone derived from BDIX rat heart tissue and is a well established CM model [476-478]. In culture, the cells form typical and parallel spindle-shaped confluent cultures, but lack gap junctions, caveolae or T-tubules. They also form only stress fibres and not myofibrils [479, 480]. The AT1, atrial tumour cell line, was developed from differentiated myocytes that had been maintained from serial propagations of ectopic grafts. The cell line succeeded and they retained their cardiac (atrial) phenotype and capacity to proliferate, however they lacked the ability to be continually passaged or reconstituted from frozen stores [472, 481].

Claycomb *et al.* have developed a new cell line, HL-1, isolated from the existing AT-1 CM line. These cells are a hybrid of embryonic and adult CM's, exhibiting CM morphology with a single central nucleus, contractile myofibrils, intercalating discs, express myosin heavy chain (MHC), Cx43, and CM electrophysiological characteristics [482]. The HL-1 cell line has been extensively cultured and appear to be viable following unlimited passaging (at least p240), maintaining their phenotype with synchronous and spontaneous contraction in culture [472, 475]. With the discussed attributes, the HL-1 cells offer a viable atrial CM model and are a working model for studying apoptosis, cell cycle, calcium dynamics and hypoxia & oxidative stress [483-486].

5.6.6. Cardiomyocyte Morphology and Markers

To confirm the phenotype of cultured cells, the literature was studied to confirm specific antibodies and morphology of CMs in culture, in conjunction with observing spontaneous beating.

In vivo CM aggregate to form thick, highly refractive cells. These can be either round or spindle shaped, uni-nuclated cells with a fine granular cytoplasm and long actin filaments interrupted by osmiophilic dense bodies. They may also contain striated myofibrils and pseudopodia processes [487-490]. In cultures, the expression of

muscle specific sub structures increases after approximately 3 to 7 days as pre-myofibrils are replaced by CM iso-forms that mature to express myocyte banding (A-, I-Z-I) and ultimately contractile activity [491].

Cell shape and morphology are intimately linked with certain aspects of cell function such as E–C coupling [492]. Figure 5-19 represents photographs of CMs in culture. Isolated (Day 0) cells are typically “rod” shaped with rectangular “stepped” ends and clear cross-striations. Day 1 CMs remain rod-shaped with clear cross-striations, and after 6 days the ends become progressively rounded [493]. Figure 5-19b shows a population of CMs after 16 days in culture, with thin membranous pseudopodia developing and projecting into the local environment. With increasing time, the pseudopodia spread laterally and also start to appear at other positions on the cell. In general, more than 50% of myocytes cultured remain rod-shaped after 7 days in culture. However, this is highly dependent on the quality of the isolation and varies considerably depending on the CM species and culture conditions.

Once mature, the CMs are identifiable by the presence of MHC, sarcomeric α-actinin and the prevalence of troponin T [459, 494-497]. Sarcomeric α- actinin, is a specific marker for skeletal and cardiac muscle actinins, which are microfilament proteins. Figure 5-20A illustrates the labelling of the highly ordered Z lines and dots in the stress fibres, whilst the sarcomeric myosin heavy chain antibody (MF-20) stains the myosin filaments (Figure 5-20B) [498].

Troponin T, a CM specific marker, targets an element of the regulatory protein that associates with actin, forming only partially organised patterns [494, 495, 499, 500]. Troponin T also acts as a cardiac-specific marker for necrotic damage and was recently identified as a sensitive diagnostic tool for early myocardial damage monitoring, as the concentration in plasma is increased by 1,000 – 10,000 fold within 3 hours of injury [501, 502]. In conjunction with CM specific antibodies, Cx43 can be utilized to reflect electrical conductivity potential between CMs as it stains the Cx43 hemichannel, labelling intact electro-mechanism and coupling [494].

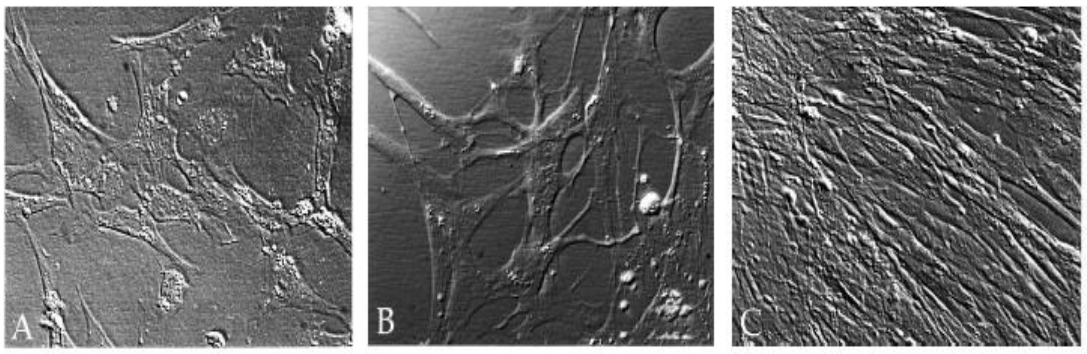

Figure 5-19. CM morphology micrographs of chick cardiomyocytes at 2, 4 and 9 days in culture.

Typical morphology of chick CMs after A) 2 days, B) 4 days and C) 9 days in culture. Micrographs were obtained using Hoffman modulation contrast optics. Adapted from Eatman *et al.* [503].

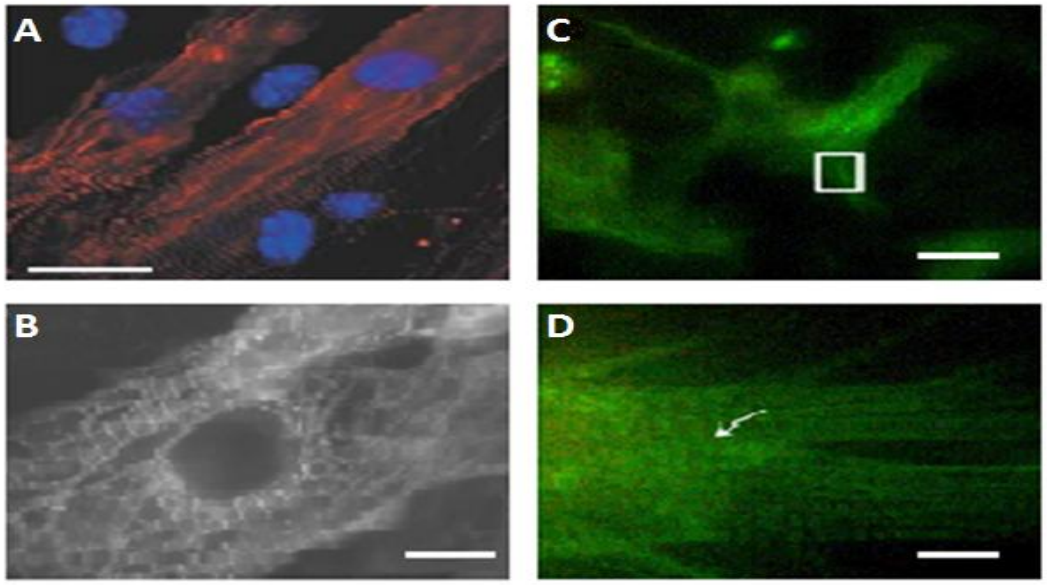

Figure 5-20. Cardiomyocyte immunofluorescence staining with sarcomeric α-actinin, MF20 and troponin T.

Immunofluorescence of: A) sarcomeric α-actinin, B) MF20 confirmed the presence of myosin and C, D) troponin T staining (anti-cardiac-troponin T mAb). Scale bar (A) 15 µM, (B, D) 10 µM (C) 25 µM. Adapted from Laugwitz, K.L., *et al.*, Jones & Kennedy and Zhu, D. *et al.* [494, 498, 500].

5.7. Research background

5.7.1. Mitochondrial Membrane Potential Dyes

Probes for $\Delta\psi_m$ need to be easily detectable and distributed across the IMM. TMRE is a cell-permeant, cationic dye, that is readably sequestered by active mitochondria [504]. TMRE accumulates within the mitochondria, binding to both aspects of the IMM, due to its charge and solubility, giving an improved accuracy [505-507]. As a $\Delta\psi_m$ dye, TMRE provides an improvement upon its predecessor R123, which inhibits F_1F_0-ATPase activity.

TMRE exhibits a shift in the emitted (576 nm) fluorescence in response to changes in membrane potential by increasing during hyperpolarisation and decreasing during depolarisation, Figure 5-21 [508]. When used at higher concentrations (greater than 150 nM) in 'quenching mode', the dye accumulates within mitochondria in sufficient concentration to form aggregates, thus quenching some of the fluorescent emissions of the aggregated dye [507]. Under these conditions, once dye is loaded into mitochondria, subsequent MMP depolarization results in dye release, unquenching the loaded probe, transiently increasing fluorescent signal. Conversely, mitochondrial hyperpolarization result in elevated dye entering the mitochondria, resulting in further quenching and a decreased fluorescent signal. At quenching mode concentration, TMRE exhibits a non-linear fluorescence, allowing dynamic and acute effects of experimental treatments on $\Delta\psi_m$ to be measured [504, 509-512].

5.7.2. Mitochondrial Membrane Potential Modulators

Experimentally, the $\Delta\psi_m$ can be modulated using the depolarizing and hyperpolarizing agents cyanide and oligomycin respectively [507]. Cyanide is a complex IV inhibitor, which acts by inducing cytochrome oxidase to complex with cytochrome α_3. The inhibition of complex IV prevents the flow of electrons through the ETC (Figure 5-22A) and consequently prevents proton efflux (Figure 5-22B) [513, 514]. Oligomycin is a natural antibiotic, obtained by isolation from *Streptomyces*

diastatochromogenes. Oligomycin blocks proton conductance by binding to the oligomycin sensitivity-conferring protein (OSCP) of the F_1F_0-ATPase complex (subunits 6 and 9 of F_0). It thereby inhibits ATP synthesis and results in hyperpolarisation (Figure 5-22B) [173, 515]. At high concentrations, oligomycin inhibits the plasma membrane Na^+/K^+-ATPase pump but does not affect the Na^+-dependent ADP/ATP exchanger or K^+-dependent phosphatase activity.

Carbonyl cyanide *p*-(tri-flluromethoxy)phenyl-hydrazone (FCCP) is a protonophore and, as such, a potent un-coupler of oxidative phosphorylation in mitochondria [516, 517]. The presence of FCCP dissipates the mitochondrial proton gradient, thus reducing the driving force of ATP synthesis [516, 518-524]. The presence of FCCP induces a marked depolarisation of the $\Delta\psi M$ to approximately -60 mV [525-528]. It is postulated that the FCCP bypasses mitoK_{ATP} channel opening, by 'short-circuiting' the channel and inducing depolarisation through a parallel leak [233].

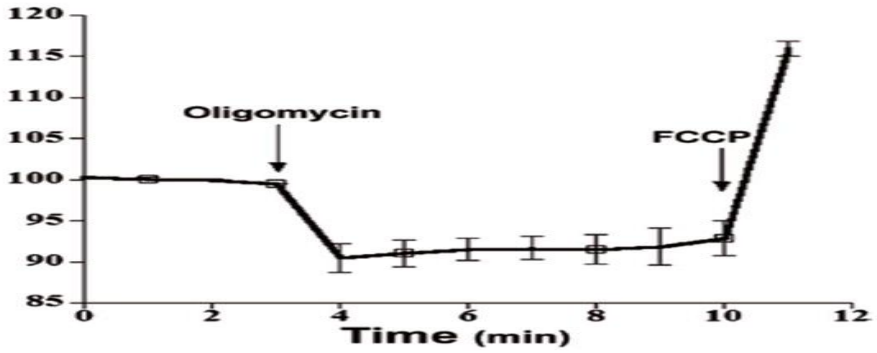

Figure 5-21. The effect of the hyperpolarising agent (oligomycin) and depolarising agent (FCCP) on fluorescence in 'quench mode'.

The change (Δ) in Rhod123 fluorescence was measured in individual mitochondria, in response to stimulation with FCCP (depolarising agent) and oligomycin (hyperpolarising agent). Adapted from Perry *et al*. (2011) [507].

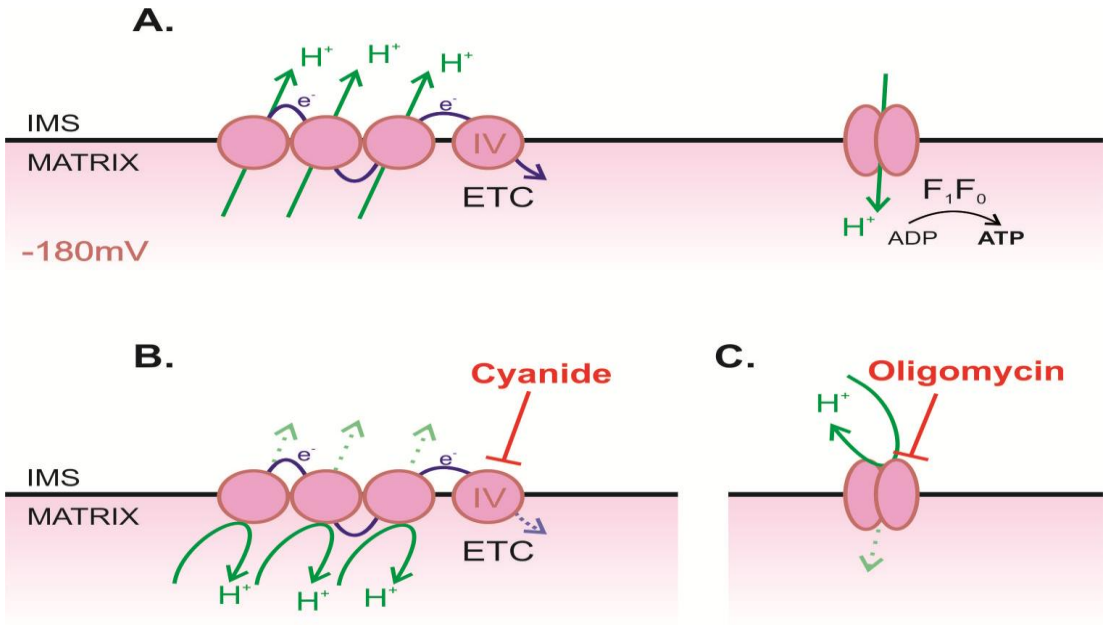

Figure 5-22. Illustration of A) ETC and proton dynamics under normal conditions and in the presence of B) sodium cyanide and C) oligomycin.

Diagrammatic illustration of the effects on the ETC complex IV and ATP synthase apparatus. The dashed arrows represent the original flow of protons (green arrows) and electrons (blue arrows).

5.7.3. Manipulating ATP Synthesis

As discussed above, cyanide is a potent $\Delta\psi_m$ depolarising agent that acts through inhibition of electron transport [513, 514]. 2-DG acts as a competitive inhibitor of glycolysis [529]. Phosphorylation of 2-DG by hexokinase produces 2-DG-phosphate which, unlike glucose-6-phosphate, is not further metabolised [530]. When used in conjunction with each other, cyanide and 2-DG induce CIH thus replicating events observed in ischaemia [531-534].

Produced by bacterium *Streptomyces conglobatus*, ionomycin is a calcium selective ionophore, mobilizing calcium from internal stores and elevating $[Ca^{2+}]_c$. Early studies assumed that ionomycin directly facilitated calcium transport across the plasma membrane [535-537]. Recent studies have subsequently shown that ionomycin also induces store-regulated calcium entry (SRCE) when used at concentrations around 100 nM, and it is ionophoretic when used above 1 μM [538, 539]. At concentrations above 10 μM, ionomycin possibly elicits ATP release through positive feedback via the $P2X_7$ channel and exocytosis, triggered by elevated $[Ca^{2+}]_c$ [540].

5.7.4. Measuring Nucleotides

Quantification of ATP release is complicated and often hindered by mechanical perturbations such as routine cell culture, which result in unintended ATP (nucleotide) release [315]. Measuring the nucleotide concentration is also difficult as the concentration in the extracellular bulk phase often does not coincide with the concentration at the cell surface. Several methods exist to measure released nucleotides [306, 341, 393, 394, 408, 541-545].

Firefly luciferase assays utilizing the ATP specific luciferase-luciferin enzymatic reaction are widely used and are an extremely sensitive technique [394]. This reaction has been adapted to quantify ADP using phosphoenolpyruvate and pyruvate kinase to convert ADP to ATP, thus allowing observation of ADP alongside ATP [408]. The classic luciferase assay has also been adapted to quantify real-time ATP release in the presence of excess soluble luciferase-luciferin and further

improved by anchoring the luciferase molecule to the plasma membrane [541-544]. In addition to the luciferase assay, high performance liquid chromatography (HPLC) provides a platform for measuring the overall pattern of nucleotides.

In quantifying the nucleotide concentration in the human umbilical vein endothelial cells *(HUVEC), ATP concentrations of 1-10 nM and 5-200 nM have been observed under basal and stimulated conditions respectively [341, 393, 545]. The extracellular nucleotide concentrations in epithelial cells have been observed with nucleotides concentrations approximately, ATP≈10 nM, ADP≈40 nM, AMP≈70 nM and adenosine ≈200 nM [306].*

5.7.5. Measuring Calcium

As a ubiquitous second messenger, Ca^{2+}-signalling is involved in several pathways including ion channel gating, E-C coupling and contractile activity. It is necessary to have a working protocol for measuring it during normal dynamics to allow changes that may arise in atypical conditions induced by arrhythmias and ischaemia.

Fluorescent indicators began with quin-2 and the synthesis of trappable calcium indicators, based on a fluorophore and carboxylic acid group that bind Ca^{2+} [546] Fluorescent dyes are easily loaded and through the presence of acetoxy-methyl ester (AM). The ester, which is removed by endogenous esterases, masks the carboxylic acid making the molecule lipophilic trapping the acid form of the dye in the cell [547-550].

The dyes have acknowledged limitations including dye leakage, cell toxicity and behaviour as Ca^{2+}-buffers [551, 552]. The development of modern dyes, with higher quantum yields, have reduced the drawback associated with dyes, but not removed them.

5.7.5.1. Fura-2

The calcium sensitive fluorescent ratio-metric dye fura-2 exhibits a spectral shift in presence and absence of calcium, thus enabling the calcium concentration to be

accurately calculated using the Grykiewicz equation (Equation 5-12) [549, 550, 553, 554]. Despite the developments, there are still potential issues with partially hydrolyzed dye not acting as a calcium indicator, and leakage over time (45% loss over 30 minutes) [550].

$$[Ca^{2+}]\, nM = K_d \times \left(\frac{(R - R_{min})}{(R_{max} - R)}\right) \times Sfb$$

Equation 5-12. Grykiewicz equation

The Grykiewicz equation allows the conversion of 340nm and 380nm excitation derived emission (510nm) to actual Ca^{2+} concentration. $\mathbf{K_d}$, describes Ca^{2+} binding (225nM at 37^{o}C) [549], **R**= 240/280 nm ratio, $\mathbf{R_{min}}$ = 340/380 ratio under calcium-free conditions, $\mathbf{R_{max}}$ = 340/380 nm ratio under Ca^{2+}-saturated conditions and **Sfb** denotes the ratio of baseline fluorescence (380nm) under Ca^{2+}-free and -bound conditions.

5.7.5.2. Fluo-4

Fluo-4, an analogue of fluo-3, offers high fluorescence emission allowing use at lower concentrations. The dye exhibits a large dynamic range between 100 nM to 1 µM and a K_d = 345 nM. Despite its advantages as a single excitation/emission dye, photo-bleaching, dye leakage and compartmentalisation are issues associated with fluo-4.

5.7.5.3. X-Rhod-1

The long-wavelength calcium indicator, X-Rhod-1, is a derivative of Rhod-2. It is very useful for measuring $[Ca^{2+}]_m$ and, due to its positive charge, it is sequestered into mitochondria [555, 556].

X-Rhod-1 exhibits an excitation spectra peak at 585nm and an emission peak at 602nm with a K_d=700 nM (22°C) enabling $[Ca^{2+}]_m$ to be observed in the micro molar range. X-Rhod-1 can detect the mobilization of intracellular calcium stores and excitatory stimulation of smooth muscle, which would saturate fluo-3 and rhod-2 signalling [557-559]. The low-affinity indicator also has a quick ion dissociation rate, allowing rapid calcium changes to be tracked [558].

5.7.5.4. Aequorin

Aequorin is a Ca^{2+} sensitive marker that is isolated from *Aequorea aequorea* [560-562]. Aequorin measurement is limited to large and robust cells that can withstand the insult of microinjection [547]. Compared to other fluorescent dyes, aequorin is more sensitive and harmless in biological systems [563, 564].

Advances in genetics have allowed the mapping of aequorin and the development of a working plasmid. In 1992, Rizzuto *et al.* generated a mitochondrial targeted aequorin plasmid, fusing apoaequrion with the targeting presequence of subunit VIII of human cytochrome c oxidase [565, 566]. A mitochondrial specific aequorin offered a relatively non-traumatic procedure for introducing a specific and sensitive $[Ca^{2+}]_m$ marker [547, 552].

Aequorin is a 30 kDa globular molecule with a hydrophobic core cavity that accommodates coelenterazine. The aequorin molecule is made from 4, helix-loop-helix EF hand domains, forming two β sheets [562, 564, 567]. Aequorin has three Ca^{2+} binding domains but only two Ca^{2+} ions are needed to exhaust the luminescence and induce irreversible conformational transition [563, 564, 568].

Reconstitution of the inert apoaequorin with coelenterazine generates the Ca^{2+} sensitive aequorin [546, 551, 569]. In the presence of Ca^{2+}, aequorin undergoes an irreversible reaction generating light, with the emission 469nm and by-products carbon dioxide (CO_2) and coelenteramide (a blue florescent protein; Figure 5-1) [163, 547, 564]. To quantify the observed luminescence subject to Allen and Blinks (1977) theory, the calibration curve converts the relative luminescence to $[Ca^{2+}]_m$ [568, 570, 571].

$$[Ca^{2+}] = \frac{\left[\left(\frac{L_0}{(L_{max})}\right)^{1/3} + \left(K_{TR}\left(\frac{L_0}{(L_{max})}\right)^{1/3}\right) - 1\right]}{\left[K_R - \left(K_R\left(\frac{L}{(L_{max})}\right)^{1/3}\right)\right]}$$

Equation 5-13. Aequorin Calibration

The equation is derived from Allen and Blinks theory where: **$[Ca^{2+}]$** equals the calculated calcium concentration, **L_0** equals the peak luminescence per second, **L_{max}** equals the total luminescence observed, **K_R** equals the dissociation constant for the first calcium ion to bind and **K_{TR}** equals the binding constant of the seconds calcium ion to bind. The **K_R** and **K_{TR}** constants are determined values, specific to the coelenterazine and aequorin isoforms.

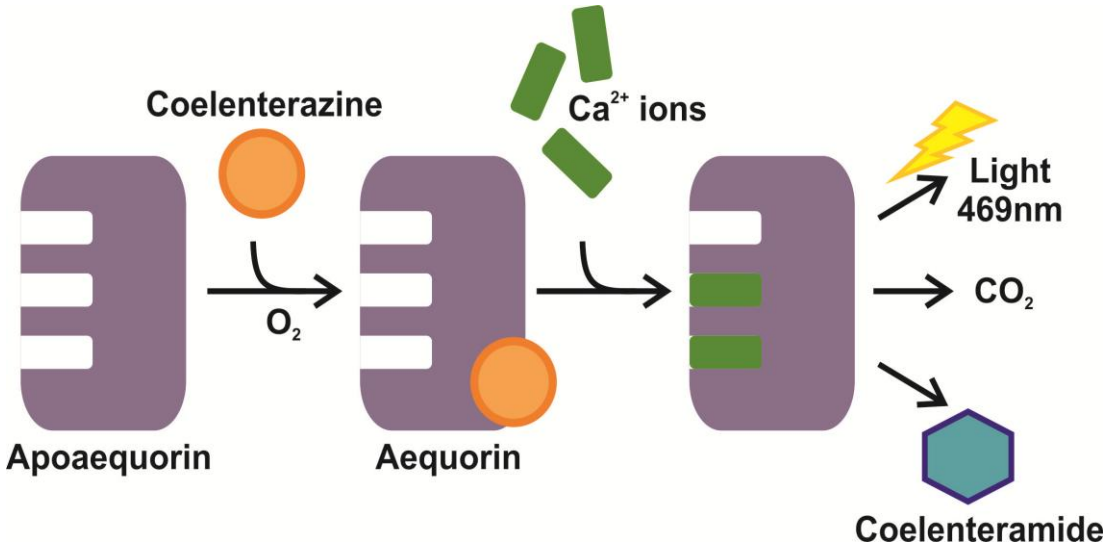

Figure 5-23. Illustration of the reconstitution and activation of aequorin from apoaequorin.

The diagram illustrates the reconstitution of apoaequorin and coelenterazine to produce the calcium sensitive aequorin. In the presence of calcium [Ca^{2+}] ions, the aequorin undergoes an irreversible reaction which generates coelenteramide, CO_2 and emitted light λ=469nm.

5.7.6. Cell Lines

5.7.6.1. EA.hy926

The HUVEC EA.hy926 cell line is a permanent human endothelial cell line that was established by fusion of primary human umbilical vein cells with a thioguanine-resistant clone of A549 [572]. Ea.hy926 cells have been maintained for more than 100 population doublings, providing a durable cell line. The cells demonstrate the highly differentiated function and characteristics of human endothelium [572-576].

5.7.6.2. HeLa

The HeLa cell line is the first immortal cancer cell line which hasa stable genome during continuous cultivation, since 1951 [577, 578]. HeLa cells have been selected due to their documented history as a proven model and physiological attributes allowing the measurement of intracellular calcium, $\Delta\psi_m$, and cellular functions of interest [549, 579, 580]. The HeLa cell line provides a viable working model since they are capable of NOS synthesis and, similar to cardiac tissue, predominantly derive ATP from β-oxidation [299, 581].

5.7.6.3. HL-1 cells

The HL-1 cell line is a hybrid of both embryonic and adult CMs as discussed in section 5.6.5. They offer a potential model for use in this study as, whilst exhibiting a CM specific phenotype and contractile function, they also offer the ability to be continually passaged.

5.7.6.4. Swiss 3T3

Swiss 3T3 cells are an immortal line of fibroblast-like cells developed in 1962 by Todaro & Green that have since become a standard fibroblast cell line [582, 583]. The Swiss 3T3 cells offer a useful non-CM model.

5.8. Hypothesis and Research Aims

5.8.1. Ischaemic Preconditioning

Diazoxide is well documented to promote IPC and the presence of 5-HD abolishes the protection induced by diazoxide [15, 120-124, 228, 247, 248, 264-266]. Diazoxide is known as a KCO and its IPC function is associated with opening of the mitoK$_{ATP}$ channel. However, some reports suggest it may be via the opening of the sarcoK$_{ATP}$ channel or inhibition of succinate dehydrogenase (section 5.4.2) [252-254, 258].

Surprisingly, there is very little evidence for diazoxide modulating $\Delta\psi_m$, which would be expected from mitoK$_{ATP}$ channel opening and resulting K^+ influx [15, 120-124, 584]. Similarly, 5-HD is supposed to close the mitoK$_{ATP}$ channel; therefore 5-HD should be seen to abolish the effect of diazoxide on the $\Delta\psi_m$. 5-HD has been proposed to have other actions than closing the mitoKATP, such as modulating β-oxidation [254, 262, 263, 270, 272, 274].

Since the fundamental action of diazoxide and 5-HD effect on $\Delta\psi_m$ has not been directly studied, the first aim was to establish whether diazoxide and 5-HD really influenced $\Delta\psi_m$. A notable feature of the proposed mitoK$_{ATP}$ is that it is activated by cGMP. The next aim was to examine if the action of diazoxide, 5-HD and cGMP are consistent with a cGMP-activated mitoKATP channel mediating IPC.

5.8.2. Extracellular Nucleotides

It is widely accepted that extracellular ATP is elevated during hypoxia (up to a four fold increase can occur). The presence of nucleotides, notably ATP and adenosine, in the extracellular environment induce a range of P2 receptor mediated signalling including vascular tone, angiogenesis, vascular remodelling, cardiac function, and positive ionotrophic effects [321, 585-589]. Extracellular ATP is the main element of observed P2 signalling. However, it has been shown that the presence of ADP can contribute to vascular tone (P2Y$_{11}$, [589-591]), platelet aggregation (P2Y$_1$, [592,

593]), proinflamatory action ($P2Y_{11}$, [588]) and is also implicated on migraine pain via P2Y receptor activation ([594]).

A great deal of research has focused on ATP signalling and changes during pathology, such as decreasing cytoplasmic ATP and an increasing extracellular ATP, which have been observed during hypoxia [595]. Recent mathematical modelling has suggested that other nucleotides can be released alongside ATP [325]. Lazarowski et al. (2000) has also shown ADP at concentrations equal to or greater than ATP within the extracellular environment [319].

Despite the known effects of ADP signalling via P2Y receptor activation and its unique and distinct pharmacology, the elevation of ADP in response to ischaemia appears to have received minimal attention.

The major aim of the project is to look at this section was to observe the extracellular nucleotide concentration during CIH, confirming the presence of ADP alongside ATP in the extracellular environment. The pathways by which extracellular nucleotides accumulate and the influence of ecto-enzyme activity and release are examined.

5.8.3. Cardiomyocytes

In this thesis the effect of CIH and $\Delta\psi_m$ are being examined in endothelial and HeLa cell models. However ischaemia and preconditioning is mainly relevant to cardiac tissue and nucleotide release from the heart is likely to dominate the cardiac vascular pharmacology.

A CM model in which IPC and nucleotide generation and release can be examined would be extremely useful. Also there are many unresolved issues regarding cardiac metabolism, mitochondrial function and ATP generation that could be investigated using a suitable myocytes model.

Cultured CM cell lines have many advantages over acutely isolated myocyte preparations. Currently the use of cell cultures is taking on increasing relevance due

to the versatility, economy and convenience of the methodology, as compared to whole animal experiments and primary CM isolation [493]. In experimental terms it offers, homogenous population (removing interference from non-myocytes), reduced loss of membrane proteins expression (from damage during isolation) and offer a platform for longer term studies [493, 596].

While immortalised cardiac cell lines such as HL-1 cells are commercially available, there are still associated issues which primary CM cultures offer an alternative, along with being more physiologically relevant both structurally and functionally to the living organism [452, 466, 469-475, 479, 481, 597, 598]. Rat neonatal myocytes have provided a useful model of cardiomyocyte morphological, biochemical, electrophysiological and are well-established in studying the toxicity of drugs [446-448]. However, there is an associated cost, regulatory issue and complex isolation procedures that limit the utility of this model. Stem cells offer an ideal model allowing CM models to be studied as either cultured populations or dispersed single cells. Whilst ESc express CM specific markers, they are limited by the altered ion channel expression and biophysical characteristics [465, 466]. The chick CM models are limited by time consuming isolation and preparation protocols. However, technique developments offer a low costs, limited regulatory restrictions and easy to generate CMs model.

The HL-1 cell line provides a convenient model and has already been used in hypoxia studies, however chick CMs were also examined as primary cell offer several advantages on commercial cell lines.

6. Methods

6.1. Solutions

Claycomb Culture Media — 10% FCS, 1% P/S, 1% NE (0.1 mM) and L-Glutamine (2 mM)) [472].

Culture Media (CMs) — MEM, 5% FBS, 1% P/S and 5 mM Glucose.

Culture Media (EA.hy926) — DMEM supplemented with 10% FCS, 1% P/S and 2 mM L-glutamine, replaced every 2 days [572]. Passaged at a dilution of 2.0 $x10^6$ cells approximately every 4 to 5 days.

Culture Media (HeLa) — DMEM supplemented with 10% Heat inactivated FCS, 1% P/S and 1% nonessential amino acids (NEAA) [580]. Passaged at a dilution of approximately 1.5 $x10^6$ cells every 3 days.

Culture Media (Swiss 3T3) — DMEM supplemented with 10% FCS and 1% P/S [599]. Passaged at a dilution of 2.5 $x10^6$ cells, every 3 to 4 days.

Digestion Buffer SH — 50 mM Tris-HCl, 100 mM NaCL, 10 mM $MgCl_2$ and 1 mM dithioerythritol.

EB buffer — 10 mM Tris-Cl, pH 8.5.

Enzyme Solution — Perfusion media, HBS (without HEPES), 30 mg Collagenase II per 10 ml.

Freezing Solution — 90% FCS, 10% Dimethyl sulfoxide (DMSO).

HEPES-buffered Saline (HBS) — 145 mM NaCl, 5 mM KCl, 1 mM Na_2HPO_4, 1 mM $MgSO_4$, 10 mM HEPES. The buffer was then titrated to pH 7.55 at 22^oC. At time of use 10 mM Glucose and 1 mM $CaCl_2$ or 1 mM EGTA was added.

Heraeus incubator	5% CO_2 and 37^{o}C.
HPLC Solvent A	8 mM tetrabutylammonium hydrogen sulphate, 17 mM KH_2PO_4, pH 5.3.
HPLC Solvent B	8 mM tetrabutylammonium hydrogen sulphate, 100 mM KH_2PO_4, pH 5.3 and 10% methanol.
Isolation Media	500 ml liquid Hams media, 125 mg Fetuin, 10mg Ascorbic Acid, 5g BSA, 5 ml P/S.
Luria Bertani (LB) agar	40 g/L agar (w/v 37.5%), casein enzymic hydrolysate (25%), sodium chloride (25%), yeast extract (12.5%).
Luria Bertani (LB) broth	25 g/L**,** w/v casein enzymic hydrolysate (40%), sodium chloride (40%), yeast extract (20%).
Opti-MEM	Reduced Serum Media buffered with HEPES, sodium bicarbonate and supplemented with hypoxanthine, thymidine, sodium pyruvate, L-glutamine, trace elements and growth factors.
Phosphate buffered saline (PBS)	A simple salt solution containing phosphate ions that buffer the pH to 7.2, whilst providing an osmotic pressure.
Potassium HEPES	5 mM NaCl, 145 mM KCl, 1 mM KH_2PO_4, 1 mM $MgSO_4$, 10 mM HEPES. The buffer was titrated to pH 7.55 at 22^{o}C. 5 mM Glucose and 1 mM $CaCl_2$ or 1 mM EGTA were added at the time of use.
Soybean inhibitor	25 mg soybean inhibitor/ 100 ml PBS.

TBE buffer	100 mM Tris base, 90 mM boric acid and 1 mM EDTA.
Trypsin/EDTA	0.05% trypsin and 0.02% ethylenediaminetetraacetic acid (EDTA).
Wash Media	Claycomb media, 5% FCS and 1% P/S.
Buffer P1	50 mM Tris-Cl, 10 mM EDTA, 100 µg/ml RNase A and 0.1% LyseBlue (v/v).
Buffer P2	200 mM NaOH, 1% SDS (w/v).
Buffer P3	3 M potassium acetate.
Buffer QBT	750 mM NaCl, 50 mM MOPS, 15% isopropanol (v/v) and 0.15% Triton X-100 (v/v).
Buffer QC	1M NaCl, 50 mM MOPS and 15% isopropanol (v/v).
Buffer QF	1.25 M NaCl, 50 mM Tris-Cl and 15% isopropanol (v/v).
Buffer TE	10 mM Tris-Cl and 1 mM EDTA.

6.2. Cell Preparation

6.2.1. Cells Culture

All cells were cultured in sterile T75 flasks with vented caps (Corning) and labelled: cell type, passage number, cell dilution and date of seeding. Cells were incubated at 37^{o}C in 5% CO_2 (CO_2:air ratio) unless stated otherwise. Once the cells were 100% confluent, they were sub-cultured, as described in, 6.2.2 Passaging and sub-culturing.

6.2.2. Passaging and sub-culturing

The culture media was aspirated and the cells washed with 10 ml of PBS. The PBS was then aspirated and 4 ml of trypsin/EDTA added. The cells were incubated for 2 minutes. The flask was then tapped to help remove the cells from the flask. Once the cells had detached, they were pipetted gently up and down, to break up any remaining clumps. The cells were re-suspended in fresh culture media at a ratio of 2.0 x10^{6} cells.

6.2.3. Freezing cells

Cells not required for immediate use, were frozen down and stored, using liquid nitrogen. The cells were trypsinised (as outlined above) and re-suspended in 10 ml of culture media, before being centrifuged at 190x g, for 5 minutes. The supernatant was aspirated and the cell pellet re-suspended in 1 ml of freezing solution. The cells were transferred to a sterile cryovial labelled: cell type, passage number and date of freezing. Cryovials were frozen down to -80^{o}C using a "Mr Frosty" filled with isopropanol, which allows freezing at steady 1^{o}C increments. After 48 hours at -80^{o}C, the frozen cells were transferred to liquid nitrogen stores, until required.

6.2.4. Thawing cells

Cells (HeLa, EA.hy926 and Swiss 3T3) from frozen stocks (as described above) were defrosted rapidly in a water bath at 37^{o}C. Once defrosted, the cell suspension was transferred drop wise into a T75 flask, containing 20 ml of pre-warmed media. The cells were incubated overnight to allow healthy cells to adhere to the flask. The following morning, the DMSO contaminated media was replaced with fresh culture media.

When thawing EA.hy926 cells, the cells were transferred to 10 ml of pre-warmed culture media and centrifuged at 190x g, for 5 minutes. The supernatant was aspirated and the cell pellet was re-suspended in 20 ml of fresh culture media in a T75 culture flask.

6.3. HL-1 Cell Preparation

6.3.1. Cell culturing

HL-1 cells were cultured in complete Claycomb media and were supplemented daily with a fresh 25% extra, Claycomb media. As the HL-1 cells exhibit low adhesion levels, the flasks were pre-coated with 0.02% gelatin and 0.5% v/v fibronectin (6 ml for a T75 and 2 ml for a T25), 24 hours prior to cell culture use. The gelatin/fibronectin layer forms a competent extracellular matrix, for the cardiomyocytes to adhere and acts as an insoluble cue for the formation of actomycin [491].

6.3.2. Passaging cells

Once confluent, the Claycomb culture media was aspirated and the cells briefly rinsed with 6 ml of trypsin/EDTA to remove any un-adhered cells. This was then replaced with a further 3 ml of fresh trypsin/EDTA before being incubated for 2 minutes. A final 3 minute trypsin/EDTA wash was applied. Once the cells were in suspension, 3 ml of soybean inhibitor was added to inhibit any further the trypsin/EDTA action. The cell suspension was repeatedly mixed using a pipette. The flask was further rinsed with 5 ml of wash media, which was added to the cell suspension, before being centrifuged at 500x g, for 5 minutes. The resulting supernatant was aspirated and the cell pellet re-suspended in Claycomb culture media, before being transferred to pre-coated flasks at a seeding density of $1x10^6$ cells.

6.3.3. Freezing and thawing cells

Confluent cells were frozen down and thawed as described in their respective sections. However, when cells were thawed, the cell culture medium was replaced after 4 hours.

6.4. Primary Myocytes

6.4.1. Isolation and Digestion

The primary myocyte isolation protocol was based upon a method that was originally published by DeHann in 1967 and refined by Laugwitz *et al.* (2005). The protocol was further modified as described below [494, 498, 600].

Twenty four hours prior to myocyte isolation, the culture plates were pre-coated with 0.02% gelatin and 0.5% v/v fibronectin, to improve cell attachment. Fertilised eggs were maintained in a Multihatch (mark II) at 37^{o}C in a humid environment (approximately 60%) for 8 days, allowing the embryo's heart to develop. Once ready the chicks were euthanised, in accordance to Schedule 1 of the Animals (Scientific Procedures) Act 1986, and the hearts dissected out. The isolated hearts were rinsed in Tyrodes salt buffer and pooled in a 35mm diameter dish, containing pre-warmed culture media. Using warmed media doubles the cell viability, in comparison to being maintained on ice [459, 498].

The pooled hearts were transferred, into a 15 ml centrifuge tube (Tube A), containing 5 ml of enzyme solution. Tube A was then slowly rotated for 10 minutes at 37^{o}C [510]. The initial enzymatic wash was discarded. A further 5 ml of enzyme solution was added and rotated for a further 10 minutes. The supernatant was then transferred to *Tube B,* which contained 5 ml of soybean inhibition (to inhibit the enzymatic digestion), and mixed through repeated inversion. The solution was centrifuged at 50x g, for 10 minutes. The resulting supernatant was discarded and the cell pellet re-suspended, in 1 ml of culture media. The protocol was repeated between 6 to 8 times, until the dissected hearts were reduced to a single conglomerate.

6.4.2. Cell culturing

Following isolation and digestion, the isolated cells were suspended in 10 ml of culture media and centrifuged at 50x g for 10 minutes. The cell pellet was re-

suspended in 10 ml of isolation media and cultured for 1 hour in a 100 mm culture dish at 37^{o}C. This step removed non-myocyte cells, which adhered to the plate [601]. The CM rich supernatant was collected and centrifuged at 50x g, for 10 minutes. The cells were then re-suspended in culture media (supplemented with 2 mM L-glutamate) plated, and incubated for 24 hours. After the first 24 hours the media was replaced with fresh culture media. The elimination of L-glutamate facilitates CM culture, whilst reducing fibroblast proliferation [490, 497]. The media was replaced every 24 hours.

6.4.3. Heart Cryostat sampling

Chick hearts were micro-dissected from E8 embryos ensuring all vessels are removed. Isolated the hearts were rinsed in Tyrodes salt buffer. Once rinsed the tissue was dehydrate via a graded ethanol series (10%, 20%, 50% 95% and 100%) washes for 2 hours each [602]. Before the samples were embedded they were subject to two 20 minute xylene washes, 'a clearing step' to remove alcohol. The tissue was then embedded in melted paraffin, at 60^{o}C.

To section cardiac samples the cryostat was set to -20^{o}C. Frozen samples were mounted onto the specimen chuck using optimal cutting temperature compound and loaded onto the specimen holder. With the cryo-microtome blade set at 10^{o}, 30 µM 'rough cuts' were taken to produce a flat section. Once the aspect of the heart wanting to be measured was achieved 'fine sectioning' 10 µM thin sections were cut, with the anti-roll plate down. Desired sections were collected by pressing them onto prepared slides. With tissue samples mounted onto slides they were subsequently stained as desired with specific antibodies as described in section 6.10.1

6.5. Calcium Measurements

6.5.1. Calcium Indicators

To measure cell and organelle calcium dynamics, several techniques were adopted, including the use of Ca^{2+} sensitive fluorescent indicators Fura-2, fluo-4 and x-rhod-1. Depending on the nature of the experiment and selected indicator the fluorescence was measured either using a FlexStation 3 (section 6.9.2) or Leica confocal microscope system (section 6.10).

The cells were cultured as previously described (section 6.2.1). When working with the FlexStation 3, cells were plated at a dilution of 4.0 $x10^6$ cells, for 24 to 48 hours prior to use. For confocal microscope use, cells were cultured in glass based 35 mm petri dishes, 27mm diameter coverslips, at a dilution of 2.0 x 10^6 cells. Once confluent, the culture media was replaced with HBS and the cells were loaded with the chosen indicator, as shown in Figure 6-4.

During the loading of the fluorescent indicators (Fura-2 and Fluo-4) cells were incubated in presence of 0.0125% pluronic F127 and 200 µM sulfinpyrazone. Following loading, the HBS was replaced with fresh HBS, containing sulfinpyrazone. The cells were then incubated for a further period allowing de-esterification to occur, ensuring the indicator was hydrolysed..

6.5.2. Mitochondrial aequorin

As an alternative to X-Rhod-1, mitochondrial targeted aequorin was used to measure $[Ca^{2+}]_m$.

Cells were cultured at a 1.0 $x10^6$ cells dilution, on 16mm diameter round glass coverslips, located in 12 well-plates and incubated for 24 hours, prior to transfection. Once 50% to 60% confluent, the cells were transfected with the mt[AEQ]WT plasmid using the transfection reagent, GeneJuice®. A ratio of 1 µg to 3 µl, (plasmid to GeneJuice® transfection reagent) ensured maximal transfection efficiency, with minimal cytotoxcicty. The mt[AEQ]WT plasmid was incubated at

room temperature in Opti-MEM (50 µl per well), for 5 minutes. For every well (coverslip) 3 µl of GeneJuice® was added to the Opti-MEM-plasmid mix. The resulting solution was gently mixed, by repeated inversion, before being added drop wise to the cell culture. Transfected cells were incubated for 48 hours and prior to experimentation the aequorin was activated. Apoaequorin was activated by incubating the cells, in the absence of light, for 2 hours, in HBS supplemented with 10 mg/ml BSA and 6 µM native coelenterazine (Figure 5-23) [603].

6.6. Plasmid Preparation

6.6.1. Agar Plates

15 ml of LB agar was supplemented with either 51.6 µM kanamycin or 143 µM ampicillin. This was then poured into a 150mm non-coated petri dish and allowed to set for 5 minutes. The dish was then set for a further 20 minutes, under the UV light of a closed culture hood. The finished plates were stored upside-down at 4^{o}C, until required.

6.6.2. Plasmid generation

Filter paper impregnated with plasmid, was folded into quarters and fitted into a 200 µl modified pipette tip. The modified tip allowed the filter paper to rest above any eluted solution. With the filter paper in place, 10 ml of d.H_2O was added to the paper, and centrifuged at 370x g, for 5 minutess within a 0.6 ml eppendorf tube.

From the extracted plasmid rich solution, 5 µl was added to 50 µl DH5α competent E.coli, stored on ice. The bacteria were then heat shocked, at 42^{o}C for 40 seconds and then returned to the ice, for a further 2 minutes. During the freeze-thaw process the *E.Coli* bacteria becomes transiently competent, enabling DNA uptake. The plasmid enriched bacteria was cultured in the shaker incubator at approximately 300rpm, at 37^{o}C, for 2 hours. The expanded culture were plated on agar plates, using a sterile glass spreader, and incubated, inverted, overnight at 37^{o}C [604]. As the bacterial colonies become established, discrete single colonies were picked and added to 6 ml of LB broth, supplemented with the corresponding antibiotic. The starter culture was maintained in the shaker incubator over night.

Bacterial cultures were incubated and expanded until a sufficient bacterial pellet was produced, normally over a period of 4 to 5 days, of successive expansion. Bacteria were harvest by centrifuging cultures at 6000x g, for 10 minutes. The bacterial pellet was treated using a Qiagen plasmid purification maxi prep kit to

isolate the plasmid (section 6.6.3). The purified plasmid purity and plasmid concentration measured using a NanoDrop 1000 fluorospectrometer (section 6.6.4).

Plasmid enriched bacteria samples were stored for future expansions. To achieve this from the final broth a 5 ml sample was centrifuged at 6000x g, for 10 minutes. The resulting bacterial pellet was re-suspended in LB broth, supplemented with more than 20% glycerol (v/v) and stored at -80^{o}C.

6.6.3. Plasmid Extraction

To extract the plasmid, the bacterial cell pellet was re-suspended in, 10 ml Buffer P1. To this 10 ml Buffer P2 was added and mixed by vigorous inversion of the tube 6 times and the suspension incubated for 5 minutes, at 22^{o}C. To this 10 ml chilled Buffer P3 was added and mixed, by vigorously inverting the tube. The resulting lysate was poured into a QIAfilter Cartridge and incubated for 10 minutes, at 22^{o}C. During this time a HiSpeed Maxi Tip was equilibrated, by adding 10 ml Buffer QBT and allowed to empty. The plunger was then inserted into the QIAfilter Cartridge and the cell lysate syringed into the equilibrated, HiSpeed Maxi Tip. Once the lysate entered the resin of the HiSpeed Maxi Tip, 60 ml of Buffer QC was added to the QIAfilter Cartridge and allowed to empty under gravitational force.

To elute the plasmid from HiSpeed Maxi Tips, 15 ml Buffer QF was added and the plasmid rich elute collected. The plasmid was precipitated, by adding 10.5 ml isopropanol. The elute and isopropanol solutions were mixed and incubated for 5 minutes, at 22^{o}C. The solution was then transferred to a 30 ml syringe with a QIAprecipitator Maxi Module attached and syringed under constant pressure. This was then repeated by passing 2 ml of 70% ethanol through the QIAprecipitator Maxi Module. The membrane of the QIAprecipitator Maxi Module was dried by repeatedly passing air through the syringe. Fitting the QIAprecipitator to a 5 ml syringe, 1 ml of Buffer TE was passed through into a 1.5 ml eppindorf tube. The plasmid rich elute was passed through the QIAprecipitator filter a second time to maximise the concentration of plasmid extracted.

6.6.4. Plasmid Quantification

To quantify plasmid concentration and purity a NanoDrop 1000 fluorospectrometer (ThermoScientific) was used. The NanoDrop measures the DNA nucleotide fluorescence at the absorbance wavelength (260nm) and quantifies the concentration of the plasmid, using the following equation:

$$Plasmid\ (\mu g/\mu L) = Absorbance \times 50 \times dilution\ factor$$

6.6.5. Plasmid Gels

Plasmid construction was confirmed by running samples through electrophoresis agarose gels. The mt[AEQ]WT plasmid was initially segmented, using restriction endonuclease EcoR1. A single EcoR1 unit has the enzyme activity to completely cleave 1 µg of plasmid, every hour, at 37^{o}C. The plasmid, at a concentration less than 10 µg was mixed with 1 µl endonuclease EcoR1 and the digestion Buffer SH. The samples were incubated for 1 hour, in a water bath, at 37^{o}C. In parallel to the sample, an 'uncut' control was incubated in the absence of EcoR1 restriction endonuclease.

During plasmid digestion, the agarose gel was prepared. Agarose was dissolved at 1% w/v (adequate for 250bp to 12kbp) in 50 ml TBE buffer and heated in the microwave, for 1 minute. Once dissolved, 17 µM SYBR safe was added, allowing for DNA visualization. The gel was poured to a depth of 3-5mm, into a clean plate and the comb located, to a depth of 0.5-1mm above the bottom of the plate. Once the gel set, the comb was removed and the plate located on the stage of the electrophoresis tank. The bath was filled with TBE buffer, to a depth which covered the gel, as illustrated in Figure 6-2.

To the outside wells, 5 µl of 1Kb Ladder DNA marker was loaded. The Ladder gives a reference scale of 300bp to 10Kbp. To the 10 µl samples, 2.5 µl of 5x GelPilot loading dye, was added and mixed by repeated pipetting. From the samples 5 µl was loaded into desired wells in the agarose gel.

Electrophoresis gels were run using a 97V electrical field. The plasmid fragments were separated according to size along the gel, which was ran for between 1 to 2 hours, until the segments were clearly separated. The gels were then photographed using a UV light box and Nikon digital camera.

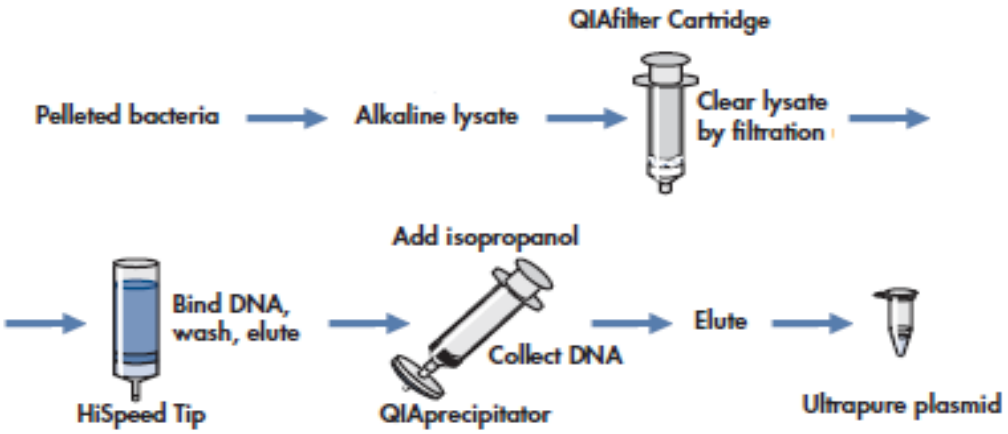

Figure 6-1. Diagrammatic overview of the Qiagen HiSpeed plasmid extraction procedure.

Diagrammatic overview of extracting plasmid from bacterial pellet through: alkaline lysate, filtration, DNA binding, wash and elution, precipitation and elution. Adapted from HiSpeed® Plasmid Purification Handbook (2005).

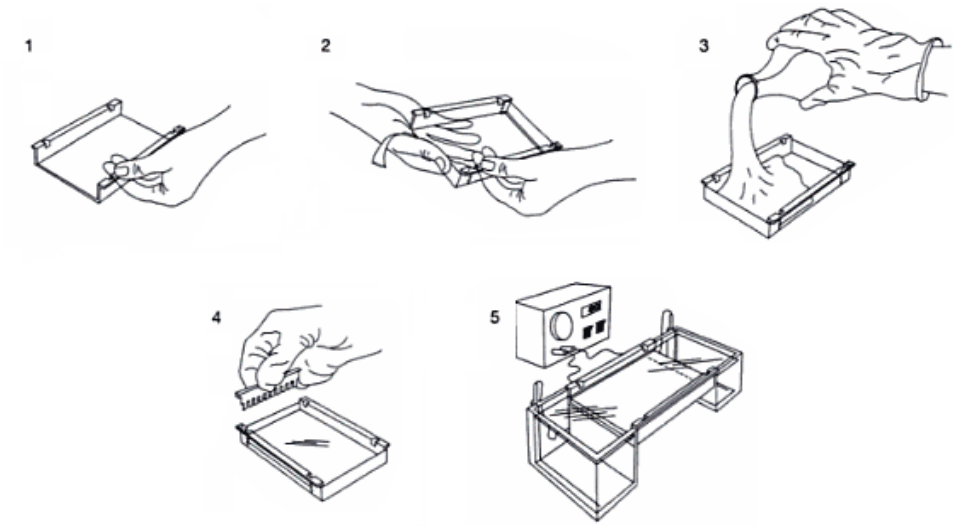

Figure 6-2. Pouring and running an agarose gel

Diagrammatic overview of pouring an agarose gel. 1) clean the plate, 2) seal the ends, 3) pour in 3-5mm agarose gel, 4) position the comb and 5) once finished and prepared the gel is ready to run. Adapted from Molecular Cloning: A Laboratory Manual [3rd Edition] Figure 5-3.

6.7. Mitochondrial Membrane Potential

6.7.1. TMRE

To measure $\Delta\psi_m$, cells were cultured in black walled 96 well culture plates, at a density of 2.0 x10^6 cells (as described in section 6.2.1). Once confluent, the culture media was replaced with, 200 µl per well, HBS supplemented with 3 µM TMRE. The cells were incubated for 20 minutes, at 22^oC. The TMRE HBS was replaced with, 100 µl HBS, and incubated for a further 15 minutes, to allow de-esterification [232, 510].

6.7.2. Mitochondrial Membrane Potential Modulators

Once loaded with TMRE, the cell plate was located in the FlexStation. The automated plate reader then made experimental additions from the compound plate, whilst recording the TMRE fluorescence.

The fluorescence was measured for 5 minutes, to generate a base line. At 300 seconds, the selected agonists were added from the compound plate. The agonists were 5 times concentrated, as added at a 1.0 x10^6 cells dilution giving the final concentrations: 100 µM SNP, 20 µM SNAP, 20 µM ZAP, 500 µM 5-HD, 500 µM DZ, 6 µM oligomycin and 4 mM cyanide. Along with the agonist additions a mock addition, (HBS, vehicle control), was made during each experimental repeat to enable direct comparison. The reagents were used in isolation and as various combinations. The resulting fluorescence was recorded for 20 minutes. At the end of each experimental run, 10 µM FCCP was added and the signal measured for a further 5 minutes.

The data recorded from the FlexStation 3 was then manipulated and expressed as F/F_0, as described in section 6.9.2.

6.8. Nucleotide Release and Quantification

6.8.1. Cell poisoning

EA.hy926 cells were cultured in 12 well culture plates (see section 6.2.1). Once confluent, the culture media was replaced with 200 µl HBS, containing 150 µM promidium Iodide (PI) and incubated, for 1 hour. During the incubation period, the cells were subjected to a poison cocktail consisting of: 4 mM cyanide, 10 mM 2-DG and 5 µM ionomycin, over a window of 5 to 40 minutes. At the end of the poisoning protocol, samples were taken from each well. The nucleotide concentration was then assayed, using either a tube luminometer (see 6.9.3) or HPLC (see 6.9.5).

6.8.2. Nucleotide Interconversion

To study the potential effect of endogenous interconversion enzymes the nucleotide assay experiment, as above, was repeated in the presence of selected inhibitors. The inhibitors were added to the wells at the beginning of the 1 hour poisoning protocol at the desired concentration: 10 mM levamisole, 30 µM ebselen, 100 µM, ARL 67156 and Ap_5A.

Before Ap_5A can be used nucleotide phosphates contaminants need to be removed. Ap_5A stock was cleaned using 20 units of alkaline phosphatase in a total volume of 100 µl dephosphorylation buffer (50 mM Tris–HCl, 1 mM EDTA, pH 8.5) for 60 min at 37^{o}C prior to use [605-607]

6.8.3. Inhibition of nucleotide release

The nucleotide assay as described in section 6.8.1, was also repeated in the presence of the connexin and pannexins blocker 100 µM flufanamic acid (FFA) or the $P2X_7$ channel inhibitor, 100 µm oATP [608-610].

6.8.4. Cell Permeability

To measure the cell permeability two mechanisms were used. The first was to measure the apoptotic markers caspase 3/7, a marker of mitochondrial outer membrane permabilisation [611, 612]. In conjunction with taking a sample for nucleotide measurement, a 20 µl sample of the HBS buffer solution was taken. To this equal parts of Caspase-Glo® 3/7 reagent was added and the solutions mixed by repeated inversion. The samples were then recorded using the Berthold tube luminometer, as discussed in section 6.9.3.

Following nucleotide sample collection the PI supplemented HBS buffer was replaced with HBS containing 2 µM Calcein AM. The cells were then stored at 4^{o}C, prior to being imaged using a LEICA DMIRB microscope with excitation filter 494nm (calcein) and 535nm (PI).

6.8.5. Cell quantification

Once the samples were taken and the calcein and PI staining was imaged (see above), the cell number was recorded. This allowed for accurate comparison between experiments.

The buffer was replaced with, 500 µl Trypsin/EGTA and incubated for 3 minutes. The 12 well plate was then tapped to help remove the cells adherent to the plate. Once the cells had detached, they were pipetted up and down, to break up any remaining clumps. The cells in suspension were then counted using a haemocytometer, as described below.

6.8.6. Haemocytometer

To quantify cell concentration in suspension a Neubauer haemocytometer was used. To prepare the counting chambers, the coverslips were fixed into place so that 'Newton's rings' were visible. The cell suspension was then thoroughly mixed before adding approximately 10 µl to the edge of the coverslips. The chamber then fills via capillary action.

It is essential that the cell suspension is dilute enough, that the cells are not overcrowded, but more than 100 are counted (giving statistically significant readings). Using a 40 times objective, on the microscope, the grid was visible and cells brought into the plane of view. In counting the cells the average of 3 large (red) squares, illustrated in Figure 6-3, was taken. Only cells within the squares and touching the top and right boundary were counted, any that were in contact with the bottom or left boarder, were disregarded. Having established a cell number ($\boldsymbol{n}$), the cell concentration was calculated, using Equation 6-1, adjusting for any sample dilutions.

$$\underset{(cells\ mL^{-1})}{cell\ concentration} = \left(\frac{n}{0.1}\right) \times 1{,}000$$

Equation 6-1. Cell count

The equation is calculated by dividing the cell number ($\boldsymbol{n}$), by the volume of the size of the square (1mm^2), multiplied by the depth (0.1mm) of the cell chamber. This was then multiplied by 1000 converting the units from millimetre to millilitre.

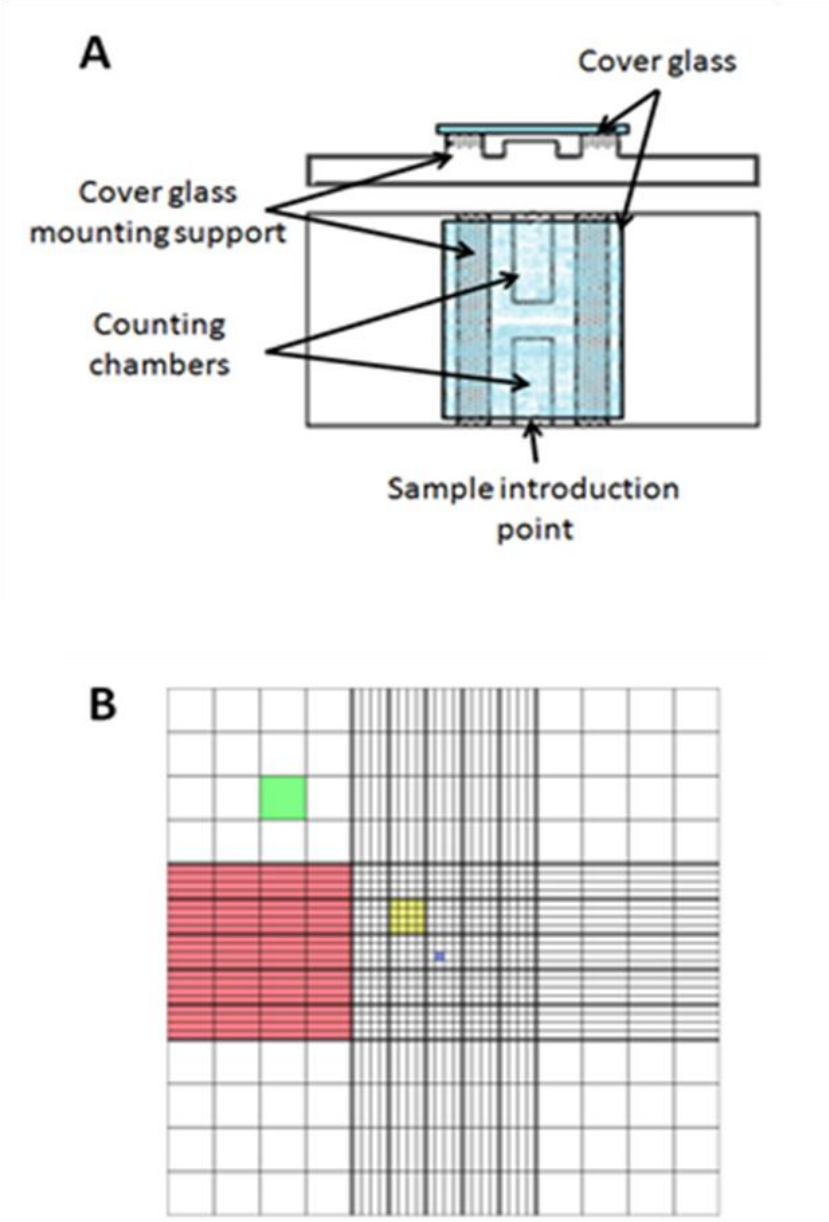

Figure 6-3. Haemocytometer, cell counting

A) Diagram of a haemocytometer, showing the position of the coverslip in relation to the counting chamber. B) haemocytometer grid with a depth of 0.1mm, and the red square (1mm^2), green square (0.0625mm^2), yellow square (.0.4mm^2) and blue square (0.0025mm^2).

6.9. Measuring Fluorescence & Luminescence

6.9.1. Fridge Luminometer

This purpose built luminometer, was used to detect the luminescence emitted from mt[AEQ]WT. Transfected cells were initially incubated with ceolenterazine to reconstitute activate aequorin, as described in section 6.5.2.

Once ready, coverslips were loaded into the purpose-built perfusion chamber, heated to 37^{o}C using a thermocirculator. A 35mm diameter, thickness #1 glass coverslips, was fixed on the top of the perfusion chamber, using silica gel. The perfusion chamber was filled with HBS, with any air being forced out. The chamber was then located, immediately below the photocathode of the photomultiplier tube (PMT, EMI type 9789). The PMT detects the emitted luminescence. The PMT was housed in a light insulated, modified fridge, which maintained the PMT at a constant low temperature. Cold air was passed across the PMT face, to prevent condensation. The above modifications reduced any noise interference, giving a low and stable dark count, of 1 to 5 counts per second. Connected to the PMT, a voltage supply (EMI PM28B) provided a regulated 1200 – 1500I current. A fast pre-amplifier, amplified current pulses, before being transmitted to an EMI C660 amplifier-discriminator. The amplifier-discriminator rejected slow fluctuations. The aequorin luminescence was captured by the photon counter (SR400) and displayed as photometric traces of counts, set at 1 count per second.

Once the cells were placed in the luminometer chamber, a base line luminescence was recorded. Reagents were introduced using a peristaltic pump. Additions were made for 2 minutes, to ensure the solution in the chamber was fully exchanged. At the end of each experiment, the cells were permeabilised with water containing only 10 mM calcium chloride. This lysed the cells and discharged any remaining aequorin enabling calibration of the signal. The data was saved as an ASCII text file and then imported to Excel. The raw data (RLU), was calibrated and converted to $[Ca^{2+}]_m$ µM, using the following equation [613].

$$[Ca^{2+}]_M\ \mu M = \left(\frac{-3.5}{\left(\log 10 \left(\frac{RLU - DC}{\sum RLU - DC} \right) \right)} \right) + 0.5$$

Equation 6-2. Converting mt[AEQ]WT derived RFU to $[Ca^{2+}]_m$.

To calculate the precise $[Ca^{2+}]_m$ µM the RLU obtained from the luminometer were introduced into the above equation. RLU denote the relative luminescence detected whilst DC denotes the dark count observed in a cell free system, (equalling 5 RLU).

6.9.2. FlexStation 3

The FlexStation 3 (Molecular Devices) is an automated microplate reader that allowed for the real time measurement of fluorescence, whilst making automated experimental additions.

The fluorescence of the various dyes, Fura-2, Fluo-4, x-Rhod-1 and TMRE, was measured using the FlexStation 3. Cells were cultured in black walled 96 well plates, at a 4.0 $x10^6$ cell dilution. Once confluent, the cells were loaded with the required dye, as described in sections 6.2.1 and 6.7. The culture plate was then located in the FlexStation 3.

The reagents were five times concentrated, as they were added at a ratio of 1 in 5, to give the desired final concentrations. The reagents were used alone and in various combinations as required. Once prepared, the fluorescence was recorded using Softmax Pro software, Flex mode, allowing the addition of compounds alongside recordings. The programme setup is described in Figure 6-6 and the fluorescent settings in Figure 6-5.

The resulting fluorescence was plotted as F/F_0, (fluorescence (F) divided by the average fluorescence during the base line reading from 0 to 300 seconds). This was

then normalised to the control mock additions to eliminate any addition artefacts and to allow comparison between repeats.

6.9.3. Tube Luminometer

Following incubation in the presence of the poison cocktail (as described in 6.8.1), a 2 µl sample of the buffer was collected. The sample was combined with 20 µl of ATP monitoring reagent (AMR, ViaLight®). The AMR emits light, relative to the ATP concentration. The emitted relative light units (RLU), was measured using a Berthold tube luminometer (LB955) and detected using a photon counter, with a 380 to 630nm spectral range. For optimal luciferase activity, the luminometer was maintained at an ambient temperature (18^{o}C to 22^{o}C).

Subsequent to the ATP RLU measurements, 10 µM phosphoenolpyruvate (PEP) and 10 units pyruvate kinase (PK), were added to the tubes. The enzymes converted ADP to ATP and the resulting luminescence recorded.

For each sample the mean bioluminescence was taken from the measurements and then converted from RLU into nucleotide concentration, using the calibration curves produced, as discussed below.

6.9.4. Calibration curves

Calibration curves were constructed from serial ATP and ADP dilutions, 1 pM to 10 mM. The curves generated, were then used to convert the RLU to nucleotide concentrations.

The ATP calibration curve was plotted as, ATP concentration against RLU (Figure 8-1). The ADP calibration curve plotted ADP standards against ATP equivalence (Figure 8-1). The ATP equivalence was calculated from the RLU generated from ADP converted to ATP minus the original count. Both curves were described by a Boltzmann curve of best fit, due to their sigmoidal shape and from this the nucleotide concentration was calculated, Equation 6-3.

6.9.5. High Performance Liquid Chromatography

Nucleotide species were separated and quantified using High Performance Liquid Chromatography (HPLC; Shimadzu), in parallel to the tube luminometer. The protocol used, is based on the based that published by Lazarowski *et al.* [319].

A 50 µl sample of buffer solution, from cells subjected to poisoning, as described in section 6.8.1, was collected. The buffer sample was heat treated at 100^{o}C, for 10 minutes, using a heat block Thermo Cycler (PTC-200, Peltier). Heat treating the samples, inhibited any subsequent nucleotide interconversion. The samples were then treated with 10% Perchloric Acid (5.8M) for 30 seconds, at 22^{o}C. The samples were then centrifuged at 1500x g, at 4^{o}C, for 10 minutes. The supernatant was then collected ready for nucleotide sampling.

The treated samples were transferred into HPLC vials and loaded in the auto-sampler. The ASI-100 automated sample injector (Dionex), sequentially ran the samples through a Hypersil BDS C18 column (5 µm, 150x4.6mm). The ion pairing mobile phase was developed at 1 ml/minute from: 0 to 4 minutes in 100% solvent A and 4 to 30 minutes in 100% solvent B. The solvents were added using a P680 HPLC pump (Dionex). The nucleotides ATP and ADP were eluted at 23 minutes and 14 minutes, respectively [319, 614]. The absorbance was measured at 254 nm and monitored on-line, using a Dionex UVD 170U detector.

6.10. Confocal Microscopy

Images were acquired using an inverted Leica SP2 AOBS, 2 -photon laser scanning confocal microscope.

Live cell imaging was recorded using the confocal microscope. The cells were cultured on glass bottom 35mm petri dishes, as described in section 6.5.1- Calcium Indicators. Once loaded with the Ca^{2+}-sensitive indicators, culture dishes were placed on the microscope stage and the cells located within the plane of focus. Live fluorescence was recorded in 'real time' capture mode at the relevant fluorescence as described in Figure 6-5. at described laser lines and emission bands or where to find them.

6.10.1. Immunofluorescence

Immunofluorescence was used to label cell structures in both cultured cells and cryostat sections, using the antibodies described in Figure 6-7 and Figure 6-8.

Prior to immunofluorescence staining, cells were fixed using PFA. Cells were cultured on 16mm diameter round glass coverslips at 2.0 x 10^6 cells. Once confluent the cells were washed, 3 times in PBS. The coverslips were then bathed for 15 minutes, in 1 ml of 4% PFA/PBS (v/v), at 22^{o}C. The PFA was replaced with, 1 ml 50 mM ammonium chloride (NH_4Cl), for 20 minutes. The ammonium chloride reduces potential auto-fluorescence, quenching free aldehydes [615]. The fixed cells were permeabilised with 0.2% TritonX-100, for 4 minutes. The coverslips were washed 3 times, for 2 minute in PBS.

Once permeabilised, the cells were blocked in a 10% v/v, serum/PBS solution and incubated for 30 minutes, at 22^{o}C, in the absence of light. The serum was specific to the host of the secondary antibody. This was replaced with a 5% serum/PBS solution, containing the primary antibody(s) and incubated for 30 minutes, at 22^{o}C, in the absence of light. The coverslips were washed, 3 times in PBS, for 4 minutes. Following this they were incubated in 5% serum/PBS, with the desired secondary antibody(s), for a further 30 minutes, as before.

When the primary antibodies were generated from the same host species, direct staining was used. In direct staining, the primary and secondary antibodies were incubated in succession. If two structures were labelled the staining protocol was repeated after the initial staining. Where the antibodies were generated from different host species, indirect staining was used. This method involved co-incubation of the primary antibodies, followed by the secondary antibodies.

Once stained the coverslips were subject to a further 3 PBS, 4 minute washes. The coverslips were then immersed in PBS and twice in $d.H_20$. Excess water was removed using filter paper. The coverslips, were mounted on 26 mm by 76 mm superfrosted slides using, 15 µl moviol with 4',6-Diamidino-2-phenylindole (DAPI, 1/2000).

Fixed and labelled cells were located on the confocal microscope stage and imaged using the 63 time oil immersion objective. The cells were captured using sequential imaging at 1024 by 1024 format. Sequential mode removed any bleeding between the fluorescence emission channels, ensuring there was no interference between labels.

Dye	Incubation Time	De-esterify Time	Temperature
Fura-2 (2.5 µM)	45 minutes	15 minutes	37°C
Fluo-4 (2 µM)	45 minutes	30 minutes	22°C
x-Rhod-1 (1 µM)	60 minutes	30 minutes	37°C

Figure 6-4. Table outlining the protocol for calcium dyes.

The table records the varying concentration levels and incubation times and conditions of the 3 different calcium sensitive fluorescent indicators utilised.

Dye	Excitation	Emission	Cut Off
Fura-2	340/380 nm	510 nm	455 nm
Fluo-4	488 nm	530 nm	515 nm
x-Rhod-1	540 nm	600 nm	570 nm
TMRE	549 nm	574 nm	570 nm

Figure 6-5. Table of dye excitation and emission.

The table shows the excitation and emission of the dyes used with the FlexStation 3 and the cut-off.

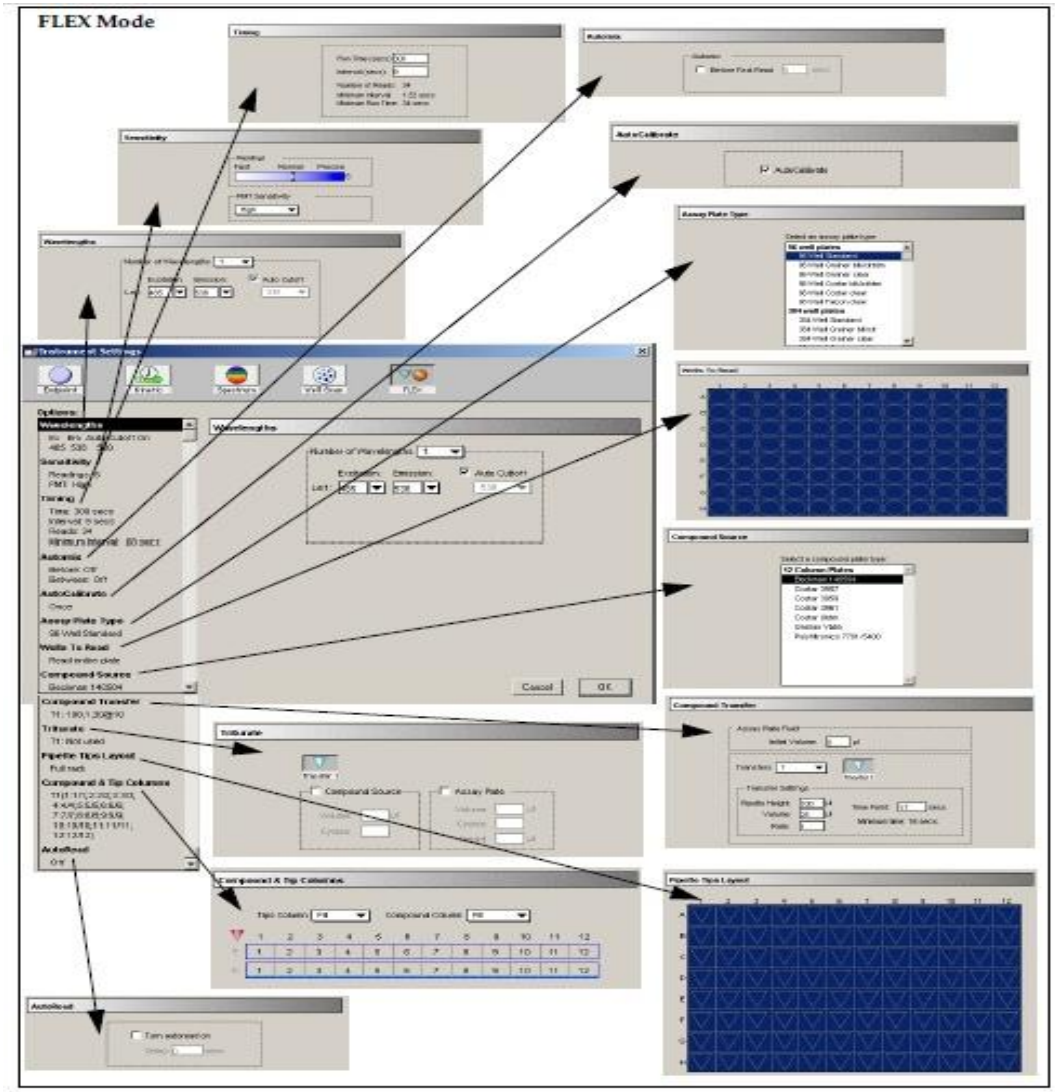

Figure 6-6. Overview of the FlexStation 3 software, Softmax Pro, settings.

FlexStation 3, SoftMax Pro, Flex mode, programme was set with the appropriate, excitation and emission wavelength. The Sensitivity was set to readings: 6 and PMT: medium, whilst Timing establishes the total run time, Time: 1500s and Interval: minimal interval. The Automix and AutoCalibrate were left off, while the Assay Plate Type was set as 96 Well Standard and Wells To Read set dependant on how many columns were cultured. The Compound Source left as “Beckman 140504” and Compound Transfer set to 2 Transfers; transfer 1: pipette height = 200 µl, volume = 25 µl, rate = 2 and time point 300secs and transfer 2: pipette height = 200 µl, volume = 30 µl, rate = 2 and time point 1500secs. Triturate was not used, Pipette Tips Layout full rack, Compound & Tip Columns set so the tips column and compound fill are the same for each column and AutoRead off.

Primary Antibodies	Host Species	Notes
anti-Troponin T	Rabbit	Cardiac isoform Ab-1 (clone 13-11) [616]. *(Thermo Scientific MS-295-P0)*
anti-sarcomeric α-Actinin	Mouse	Derived from clone EA-53. *(Sigma A7811)*
anti-myosin heavy chain	Mouse	Sarcomeric specific [617, 618] *(DSHB MF-20)*

Figure 6-7. Table of primary antibodies for immunofluorescence labelling.

The primary antibodies used and their respective host species and any additional information regarding the generation.

Host Species	Reactivity	Label or Dye	Excitation/ Emission
Goat	anti-rabbit*	Alexa Fluor® 488 (A-11012)	495/519 nm
Goat	anti-mouse*	Alexa Fluor® 488 (A-11001)	495/519 nm
Goat	anti-mouse*	Alexa Fluor® 594 (A-11008)	590/617 nm

Figure 6-8. Table of secondary antibodies for immunofluorescence labelling.

The secondary antibodies bind to the primary antibody, depending on their reactivity. They are labelled with an Alexa Flour® green or red tag, detectable at the set excitation and emission values. *All reactivity was IgG target isotype.

6.11. Statistics and Data Presentation

6.11.1. Plotted Data

In several circumstance the average from multiple and comparable experiments was plotted to represent the observed results. In several circumstances a line of best fit was applied to the data, including the Boltzmann Curve as described below.

$$x(\ Nucleotide\ Log_M\ ) = \left(\left(Ln\left(\left(\frac{A1 - A2}{y - A2}\right) - 1\right)\right)dx\right) + x0$$

Equation 6-3. Boltzmann curve

The Boltzmann curve describes the sigmoidal curve of best fit where: **y** is the function, **A1** is the low y limit, **A2** is the high y limit, **x0** is the inflexion point and **dx** is the width.

In some instances the data was not comparable and so typical and representative traces have been displayed. The data is displayed as a scatter graph and a smoothed trace applied to remove noisy, irregular data using a Fast Fourier Transform (FFT) filter. FFT Filter smoothing is accomplished by removing Fourier components with frequency's higher than a cut-off frequency, calculated from the below equation.

$$\boldsymbol{F_{cutoff} = \frac{1}{n\Delta t}}$$

Equation 6-4. The Fast Fourier transform equation

The equation describes the cut-off frequency, where **n** denotes the number of data points, set at 5, and **Δt** is the time or spacing between two adjacent data points.

6.11.2. Outliers

Outliers were defined by Grubb as, a numerical observation that appears to deviate markedly from other members of the sample in which it occurs [619]. To test for outliers the Grubbs' test, or normed residual test, was applied to detect a single outlier in a univariate data set that follows an approximately normal distribution [1, 2]. Grubbs' test is defined for the hypothesis that H_0: is that there are no outliers in the data set, whilst H_a: there is exactly one outlier. The test is defined by *Equation 6-5* and *Equation 6-6.*

$$G = \frac{\max |Y_i - \bar{Y}|}{s}$$

Equation 6-5. Grubbs' test for outliers

The Grubbs' test statistic is the largest absolute deviation from the sample mean in units of the sample standard deviation, with ***Ȳ*** *denoting the sample mean and* ***s*** *the standard deviation.*

$$G > \frac{(N-1)}{\sqrt{N}} \sqrt{\frac{\left(t_{\alpha/(2N).N-2}\right)^2}{N-2+\left(t_{\alpha/(2N).N-2}\right)^2}}$$

Equation 6-6. Grubbs' test for outlier significance.

For the two-sided test the hypothesis of no outliers (**H0**) is rejected, based on a significance level (**α**) of 0.05, if the above equation is proven. ***tα/(2N)****.* ***N-2*** *denotes the critical value of the* ***t*** *distribution with (****N-2****) degrees of freedom and a significance level of* ***α/(2N)****.*

7. Results - $\Delta\psi_m$

7.1. Introduction

The mitoK$_{ATP}$ channel has yet to be isolated and its' structure confirmed. However, it is postulated to mediate diazoxide-induced IPC [228]. Whilst mitochondrial depolarisation may seem paradoxical in affording IPC, there are several compensatory mechanisms proposed to be activated in response to the opening of the mitoK$_{ATP}$ channel, matrix swelling, reduced Ca^{2+} overload and ROS production (for full details please see section 5.4.2) [232-234].

Diazoxide is believed to afford IPC via mitoK$_{ATP}$-induced depolarisation, supported by inhibition by the 'specific' mitoK$_{ATP}$ blocker [121, 122, 247, 248]. Surprisingly, there is very little evidence for diazoxide modulating $\Delta\psi_m$, which would be expected from mitoK$_{ATP}$ channel opening and resulting K^+ influx [15, 120-124, 584]. 5-HD inhibits diazoxide-IPC via the mitoK$_{ATP}$ channel and therefore would negate $\Delta\psi_m$ depolarisation, however recent data suggests that 5-HD is not as selective as perceived but may act via modulation of β-oxidation, as discussed in section 5.4.3.2 [41, 228, 239, 254, 257-263, 265, 266, 270, 272, 274].

The mitoK$_{ATP}$ channel is sensitive to cGMP-PKG activation and the presence of cGMP elevating agents induces mild depolarisation. Subsequently the NO donors, SNAP and SNP and PDE$_5$ inhibitor zaprinast were used to induce cGMP-induced mitoK$_{ATP}$ channel modulation [275-277].

As such the effect of diazoxide and 5-HD on modulation of $\Delta\psi_m$ was examined. Secondary to this was to study the effect of diazoxide, 5-HD and cGMP to ensure they are consistent with cGMP-activated mitoK$_{ATP}$ channel.

7.2. TMRE Controls

The initial aim was to confirm that TMRE can be used to measure $\Delta\psi_m$ in HeLa cells [507, 510, 620-622]. To examine TMRE's function as a $\Delta\psi_m$ indicator, known depolarising and hyperpolarising agents, sodium cyanide and oligomycin respectively, were used to induce increases and decreases in $\Delta\psi_m$ [525-528].

Cells were loaded with TMRE (3 μM), as described in the methods section 6.7.1 and $\Delta\psi_m$ measured using the FlexStation3, automated microplate reader. The observed fluorescence data was presented as normalised mean trace of F/F_0 and the percentage change of the area under the curve (auc.) as compared to the control (mock additions).

The representative trace of F/F_0 and overall effects following the addition of sodium cyanide and oligomycin are illustrated as green and orange traces, respectively, in Figure 7-1. Cyanide induced depolarisation resulted in a large upward shift in TMRE (F/F_0=0.13 and auc. 14.3±2.56%). The addition of oligomycin induced a negative shift in the observed fluorescence (F/F_0=-0.05 and auc. -5.01±1.8%).

Sodium cyanide and oligomycin modulated $\Delta\psi_m$ as expected when using TMRE in "quenching mode" as described in section 5.7.1 [173, 507, 513-515]. The results confirm a working protocol, allowing the measurement of dynamics in relative changes of $\Delta\psi_m$ [507, 623-625].

The effect of the vehicles used in the experiments (ethanol and DMSO) were investigated (Figure 7-2). Both vehicles provoked negligible effects on the observed fluorescence F/F_0. Whilst the lack of change confirms that the vehicles alone induce little to no $\Delta\psi_m$ modulation, the addition of FCCP induced $\Delta\psi_m$ depolarisation as expected [516, 517, 525-528]. FCCP typically induces considerable depolarisation, to approximately -60 mV [525-528]. The addition of FCCP acts as an internal control, confirming TMRE function.

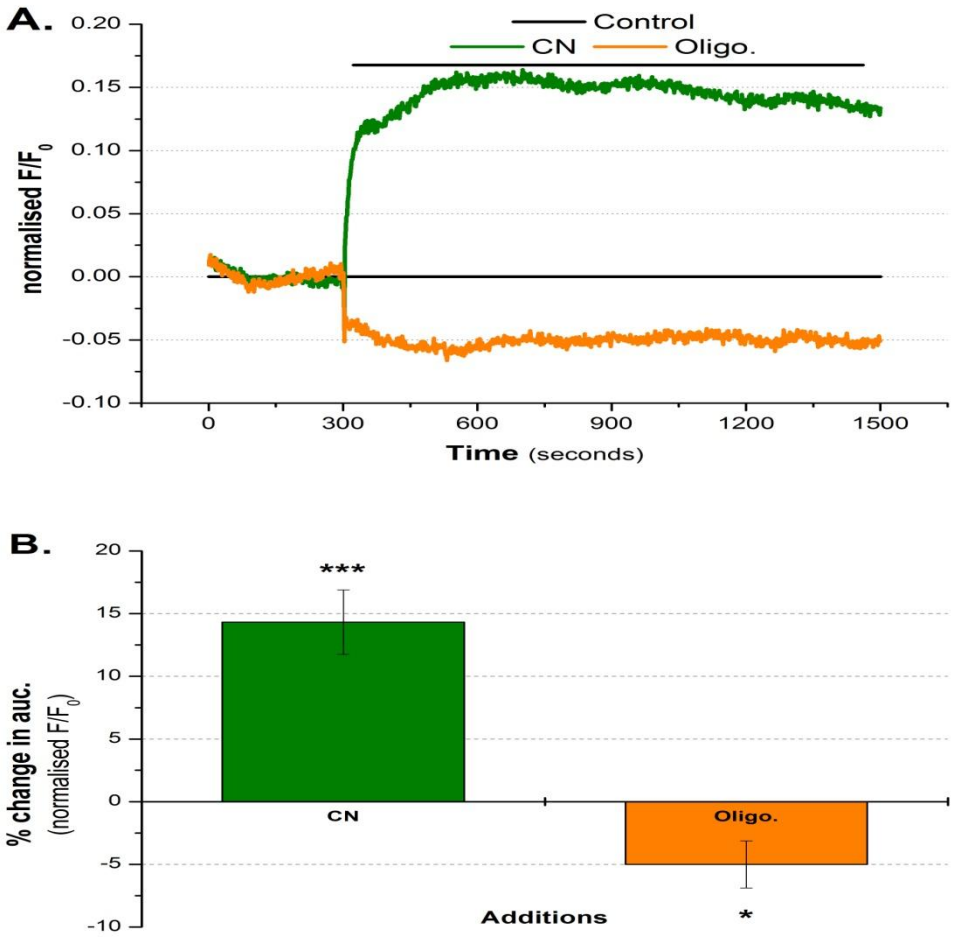

Figure 7-1. Sodium cyanide (depolarisation) induces a positive shift in TMRE fluorescence and oligomycin (hyperpolarisation) a negative shift, measured in HeLa cells.

HeLa cells were cultured in black walled 96 well plates. Once confluent, the cells were loaded with 3 µM TMRE. The response to the depolarising and hyperpolarising agents, 4 mM sodium cyanide (CN) and 6 µM oligomycin (Oligo) were observed, in HBS. A) The $\Delta\psi_m$ is represented as TMRE F/F_0 normalised to the mock addition trace to eliminate addition artefacts. B) The bar graph indicates the $\Delta\psi$m, represented as the percentage change in the integrated F/F_0 compared to the control mock addition. Error bars represent S.E.M. from the mean of at least 6 repeated experiments. T-test: *P<0.05, **P<0.01 and ***P<0.001, compared to the control, 0% auc. change.

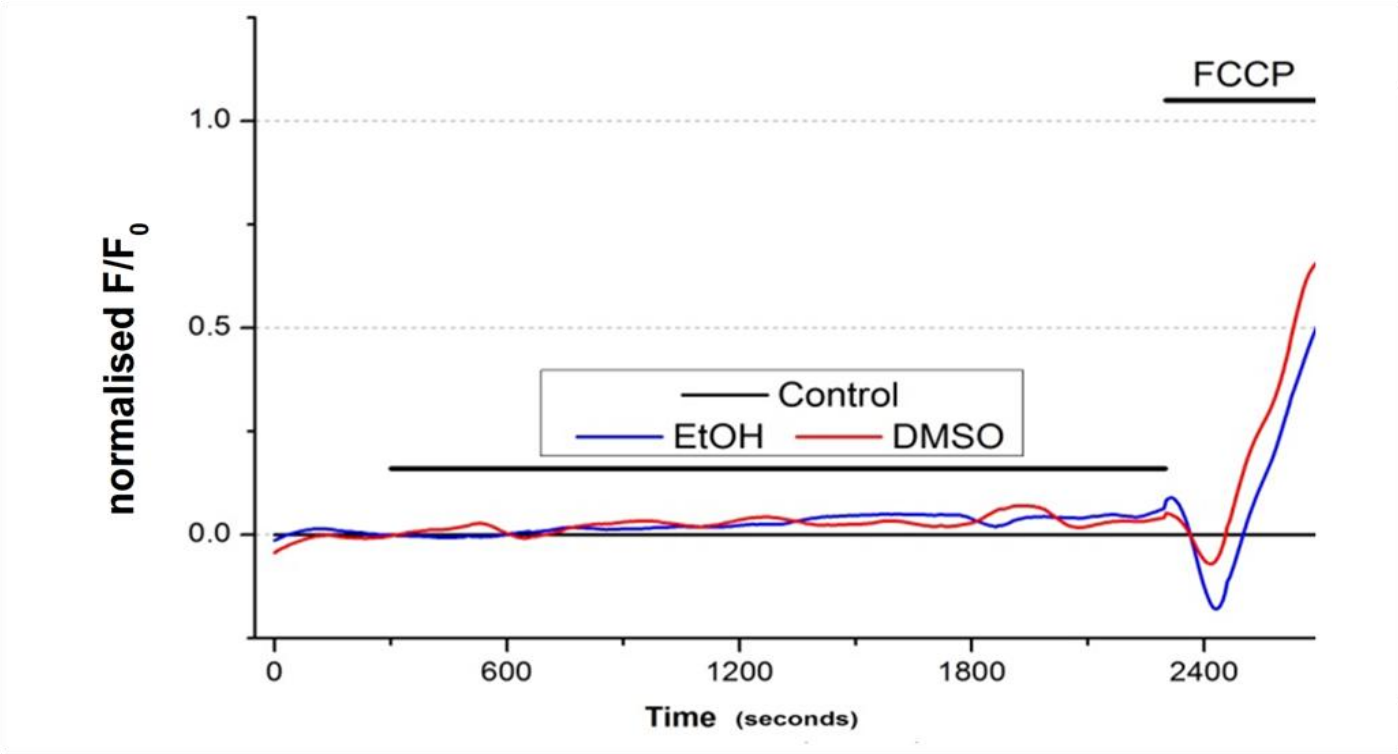

Figure 7-2. Representative trace of the effects of the vehicles (ethanol (EtOH) and dimethyl sulfoxide (DMSO)) on $\Delta\psi_m$ in HeLa cells.

HeLa cells were cultured in black walled 96 well plates. Once confluent, the cells were loaded with 3 µM TMRE. The TMRE fluorescence was recorded whilst EtOH and DMSO were added (at maximal concentrations used in experiments), in HBS at 37^{o}C. The $\Delta\psi_m$ is represented as TMRE F/F_0, the mean of 3 experimental repeats. The solid bar indicates the mock, EtOH and DMSO addition, and 10 µM FCCP.

7.3. Ischaemic Preconditioning and $\Delta\psi_m$

In an attempt to understand the mechanisms of pharmacological IPC by diazoxide, and the ability for 5-HD to negate it, the modulation of the $\Delta\psi_m$ was studied using TMRE loaded HeLa cells.

The addition of diazoxide triggered significant depolarisation as represented by an upward shift in TMRE (F/F_0=0.098 or auc. 7.86±1.0%; Figure 7-3). The presence of 5-HD also induced a loss of the $\Delta\psi_m$ as observed by an increase in the TMRE fluorescence also ($F/F_{0=}$0.046 or auc. 3.13±0.6%; Figure 7-3). When used in combination, diazoxide and 5-HD, the TMRE fluorescence increased (F/F_0=0.036 or auc. 5.08±0.7%; Figure 7-3), to a level similar when subjected to 5-HD alone.

Thus it appears that 5-HD opposed the depolarisation induced by diazoxide. Surprisingly 5-HD alone actually depolarised the mitochondria as well. This would indicate that the modest depolarisation seen in the presence of 5-HD and 5-HD with diazoxide does not modulate IPC. The larger depolarisation induced by diazoxide alone could still be important and significant in its function to bring about IPC.

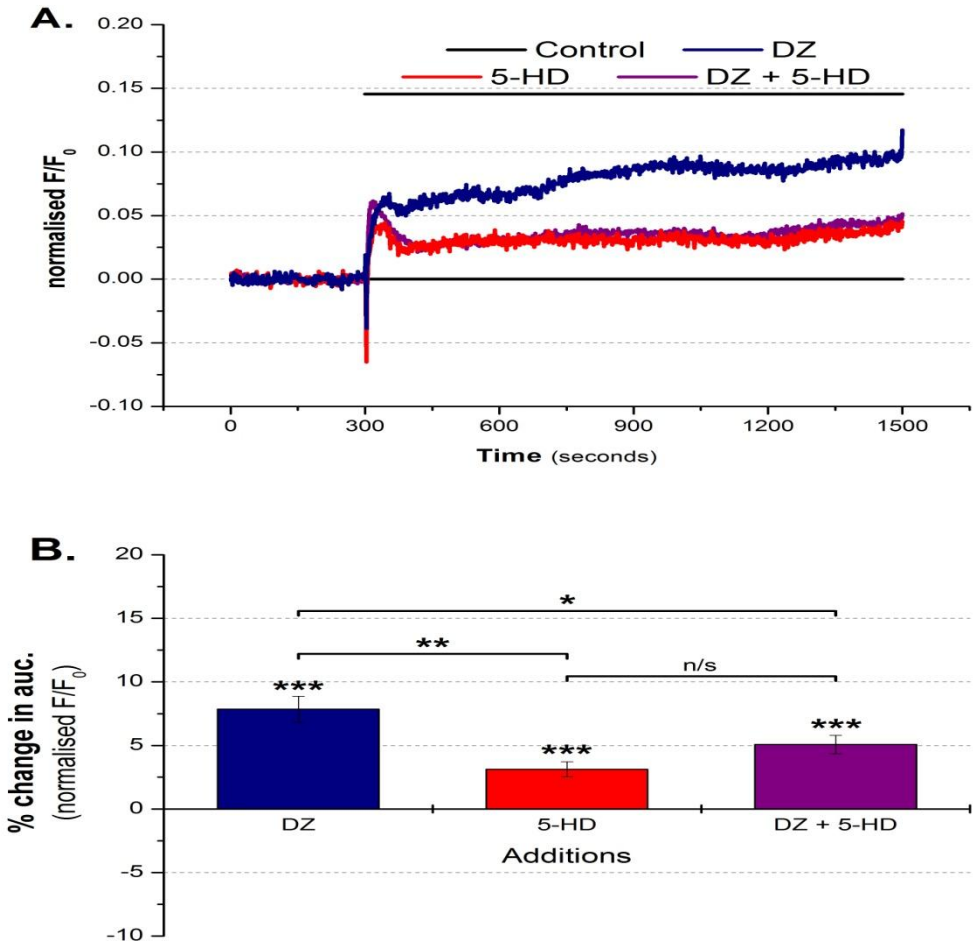

Figure 7-3. $\Delta\psi_m$ dynamics in the presence of putative mitoK$_{ATP}$ channel modulators, diazoxide (DZ) and 5-HD in HeLa cells.

HeLa cells were cultured in black walled 96 well plates. Once confluent, the cells were loaded with 3 µM TMRE. The $\Delta\psi_m$ was observed in the presence and absence of channel modulators, 500 µM diazoxide, 500 µM 5-HD, either in isolation or in combination with each other, and measured in HBS at 37^{0}C. A) The $\Delta\psi_m$ is represented as TMRE F/F$_0$ normalised to the mock addition trace to eliminate addition artefacts. B) The bar graph indicates the $\Delta\psi$m, represented as the percentage change in the integrated F/F$_0$ compared to the control mock addition. Error bars represent S.E.M. from the mean of at least 6 repeated experiments. T-test: *P<0.05, **P<0.01 and ***P<0.001, compared to the control, 0% auc. change.

7.4. Ischaemic Preconditioning and $\Delta\psi_m$ Modulators

To measure the effects and to allude to the potential mechanism of action, the $\Delta\psi_m$ modulation exhibited by diazoxide and 5-HD was recorded in the presence of either sodium cyanide or oligomycin.

When monitoring the presence of multiple $\Delta\psi_m$ modulators, cells were initially challenged with either cyanide or oligomycin. Their effects when used in isolation are discussed in section 5.7.2 and illustrated in Figure 7-1. When used in combination, the TMRE fluorescence is significantly elevated in comparison to the effects observed in the presence of either sodium cyanide or oligomycin alone, (F/F_0=0.6, 61.92±3% auc.; Figure 7-4).

The exaggerated depolarisation is attributed to F_1F_0ATPase inhibition by oligomycin. Under normal conditions, oligomycin prevents proton influx, whilst cyanide prevents proton efflux, as illustrated in Figure 7-5A. During depolarisation of mitochondria the proton motive forces result in the F_1F_0ATPase complex working in reverse, using ATP rather than producing it and pumping protons out of the matrix, as the mitochondria try to maintain the $\Delta\psi_m$. Under these circumstances the presence of oligomycin results in an elevated depolarisation as both reagents act to prevent proton efflux, as illustrated in Figure 7-5B [626].

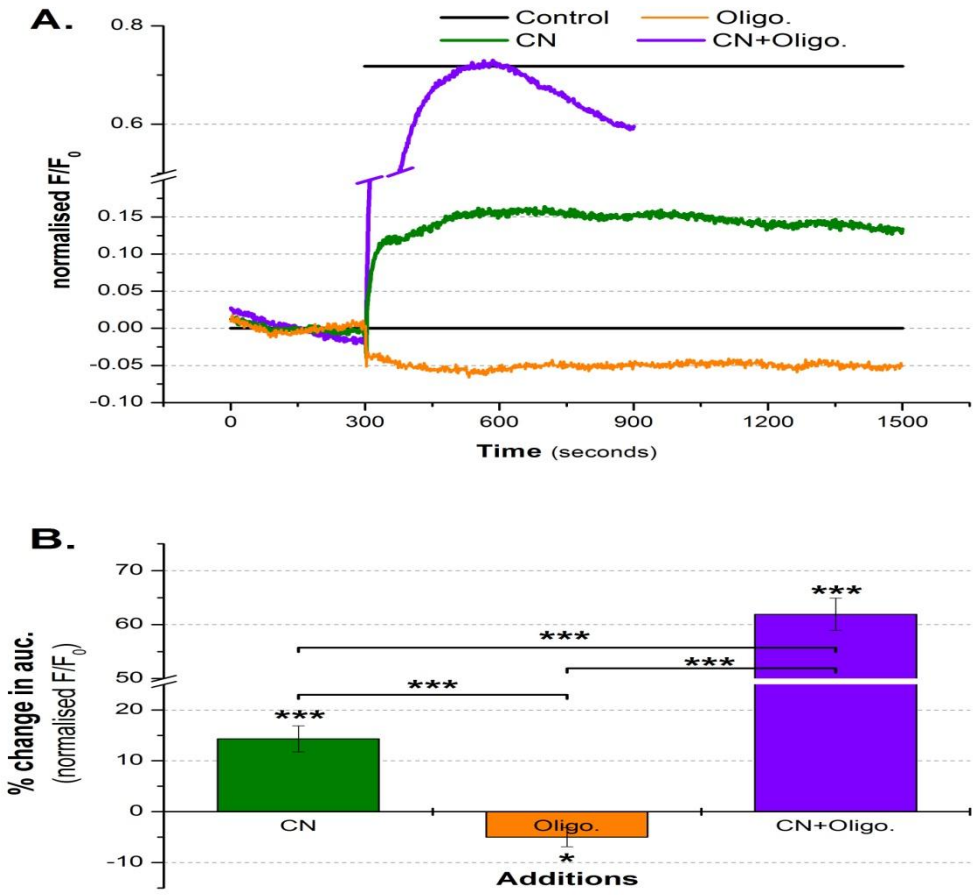

Figure 7-4. Sodium cyanide in combination with oligomycin induced an elevated a positive shift (depolarisation) in TMRE fluorescence, compared to their use in isolation, in HeLa cells.

HeLa cells were cultured in black walled 96 well plates. Once confluent the cells were loaded with 3 µM TMRE. The response to the depolarising and hyperpolarising agents, 4 mM sodium cyanide (CN), 6 µM oligomycin (Oligo), either in isolation or in combination with each other, was measured in HBS at 37^0C. A) The $\Delta\psi_m$ is represented as TMRE F/F_0 normalised to the mock addition trace to eliminate addition artefacts. B) The bar graph indicates the $\Delta\psi$m, represented as the percentage change in the integrated F/F_0 compared to the control mock addition. Error bars represent S.E.M. from the mean of at least 6 repeated experiments. T-test: *P<0.05, **P<0.01 and ***P<0.001, compared to the control, 0% auc. change.

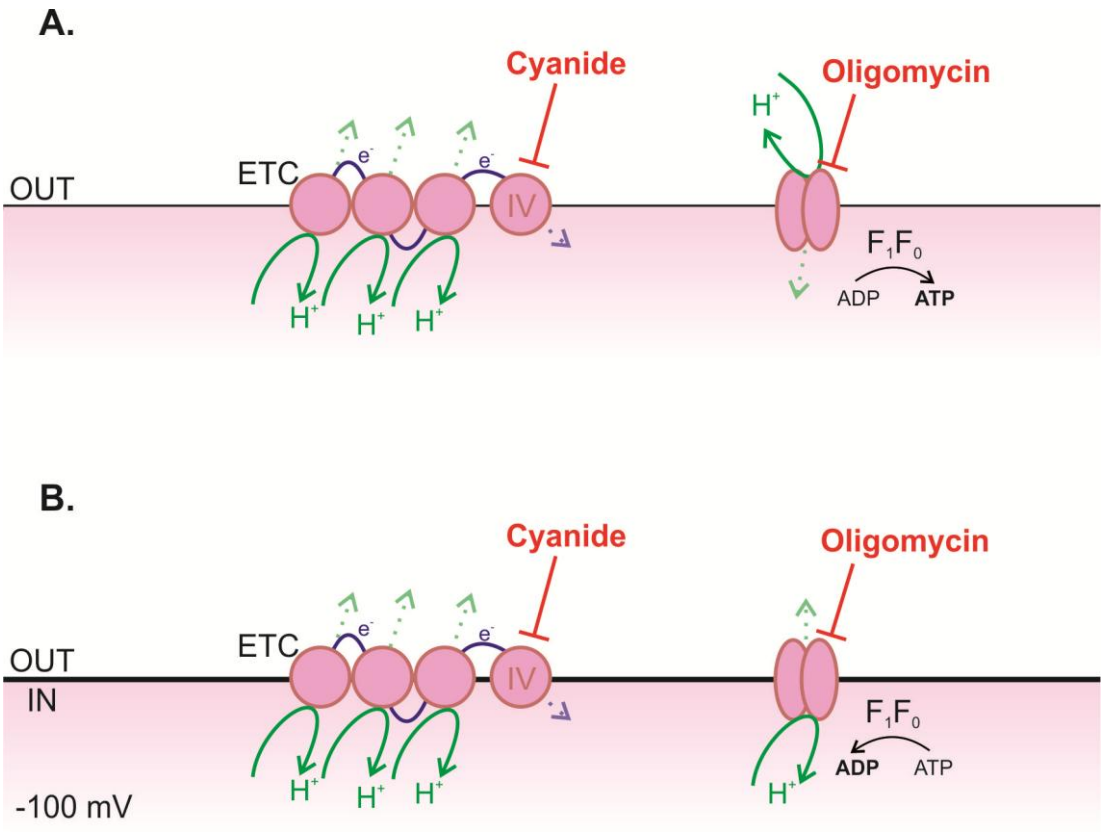

Figure 7-5. Illustration of sodium cyanide and oligomycin modulation on proton movement, across the IMM under normal and depolarised conditions.

Diagrammatic illustration of the effects on the ETC complex IV and ATP synthase apparatus by CN and oligomycin, in A) normal $\Delta\psi_m$ and B) depolarised, -100 mV, mitochondria. The dashed arrows represent the original flow of protons (green arrows) and electrons (blue arrows). Also note the reversal of ADP>ATP, to ATP>ADP.

When challenged with cyanide and diazoxide, there was enhanced loss of $\Delta\psi_m$ in comparison to the actions of either agent alone (F/F_0=0.35, 35.35±7.5% auc.; Figure 7-6). 5-hydroxydecanoic acid caused a small reduction on cyanide-induced depolarisation that did not reach statistical significance (F/F_0=0.09, 9.14±1.6% auc.; Figure 7-6).

The IPC agent diazoxide and the inhibitor 5-HD's effect on $\Delta\psi_m$ were also examined in the presence of oligomycin. Diazoxide exhibited a slower but, overall a similar amplitude of depolarisation as compared to its addition alone (F/F_0=0.07, 6.67±3.5% auc.; Figure 7-6). Whilst oligomycin slowed diazoxide depolarisation, 5-HD retarded oligomycin-associated hyperpolarisation (F/F_0=-0.02, -2.08±2.4% auc.; Figure 7-6).

Depolarisation was significantly greater in the presence of both cyanide and diazoxide in comparison to the changes driven by the reagents alone. The depolarisation is larger (35.35±7.5% auc.; Figure 7-6) but not significantly different to the additive effects (24.8±4.9% auc.).

The hyperpolarisation induced by oligomycin reflects continued proton extrusion with no compensatory proton influx. The present of oligomycin had minimal effect on diazoxide-derived depolarisation, whereas 5-HD appeared to partially relieve the oligomycin-induced hyperpolarisation.

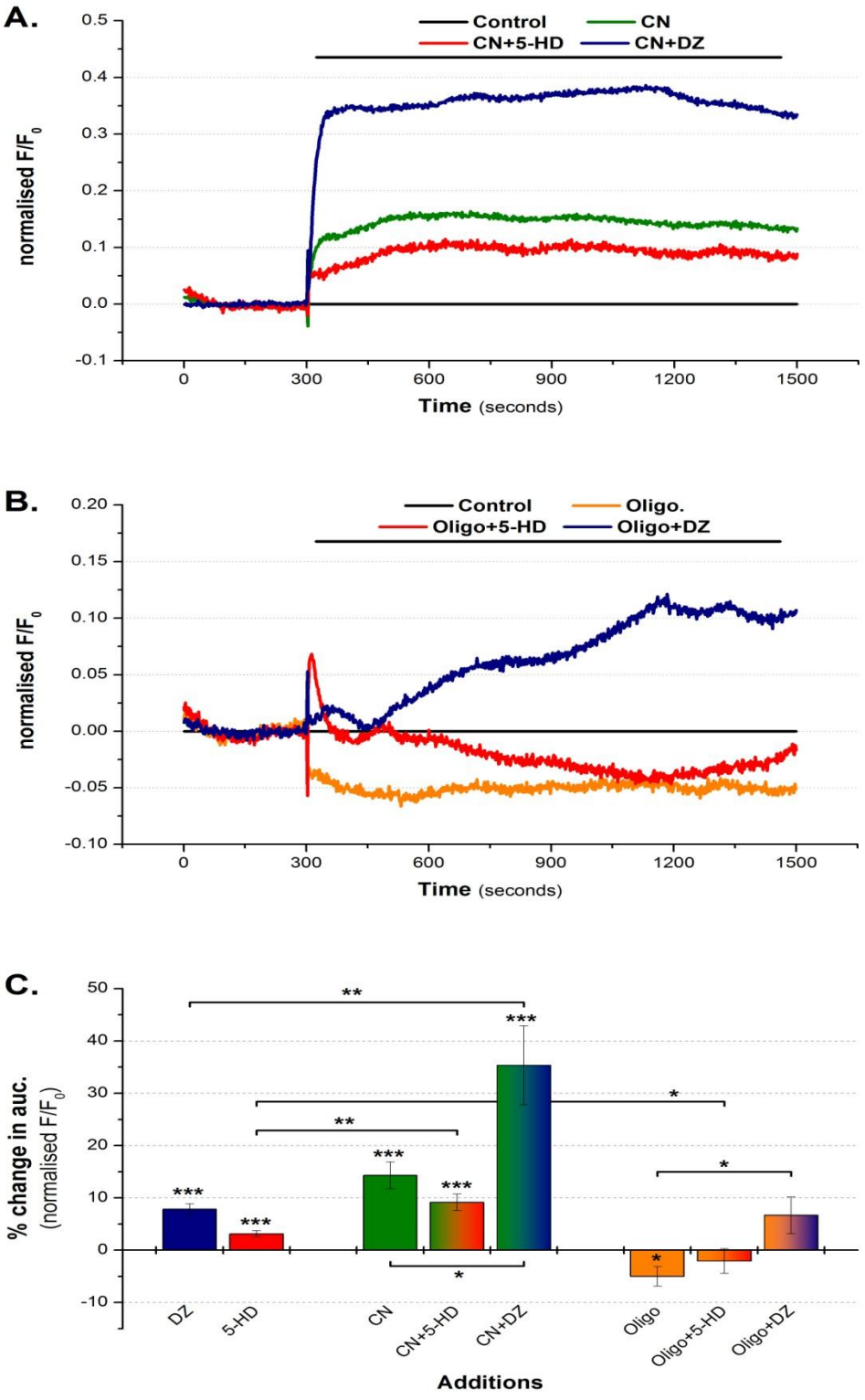

Figure 7-6. The effect of diazoxide (DZ) and 5-HD on sodium cyanide-depolarisation and oligomycin-hyperpolarisation in HeLa cells.

HeLa cells were cultured in black walled 96 well plates. Once confluent the cells were loaded with 3 µM TMRE. The response to 500 µM DZ and 500 µM 5-HD, on 4 mM sodium cyanide (depolarisation), 6 µM oligomycin (hyperpolarisation) , was measured , in HBS at 37^0C. A) The $\Delta\psi_m$ is represented as TMRE F/F_0 normalised to the mock addition trace to eliminate addition artefacts. B) The bar graph indicates the area under the curve of DZ, 5-HD, CN and oligomycin, alone and in various combinations additions, compared to the mock additions. The $\Delta\psi$m is represented as the percentage change in the integrated F/F_0 compared to the control mock addition. Error bars represent S.E.M. from the mean of at least 6 repeated experiments. T-test: *P<0.05, **P<0.01 and ***P<0.001, compared to the control, 0% auc. change.

7.5. Cyclic GMP Modulation

Since cGMP was reported to modulate mitoK_{ATP} channels, agents that increase cGMP were used to establish whether this pathway has any impact on $\Delta\psi_m$. To study the effect of cGMP on the $\Delta\psi_m$, the exogenous NO donors, (SNAP and SNP), and the PDE5 inhibitor (zaprinast) were used to induce cGMP-dependent PKG activation, as illustrated in Figure 5-13 [288, 290].

The presence of the cGMP modulators induced a small but significant $\Delta\psi_m$ depolarisation; SNAP (F/F_0=0.02, 2.2%±0.5 auc.; Figure 7-7), SNP (F/F_0=0.05, 4.9%±1.6 auc.; Figure 7-8) and zaprinast (ZAP, F/F_0=0.03, 2.8%±0.8 auc.; Figure 7-9).

Incubation with both SNAP and diazoxide had no further significant effect on the $\Delta\psi_m$ potential. However, when looking at the trace and auc. the TMRE shift was half of that seen in the presence of diazoxide alone (F/F_0=0.05,4.4%±1.8 auc.; Figure 7-7). SNAP had no significant effect on 5-HD-depolarisation (F/F_0=0.04, 6.2%±3 auc.; Figure 7-7).

The presence of SNP and diazoxide or 5-HD both induced significant depolarisation (F/F_0=0.05, 5%±1.8 auc.) and (F/F_0=0.05, 5.5%±1.6 auc.), respectively, as seen in Figure 7-8. The addition of SNP attenuates diazoxide effect on $\Delta\psi_m$, whilst 5-HD-depolarisation was not altered.

Zaprinast and diazoxide induced significant depolarisation of the $\Delta\psi_m$, whilst slowing observed TMRE fluorescence reaching the same overall level as observed in the presence of diazoxide only (F/F_0=0.04, 5.3%±2.3 auc.; Figure 7-9). Zaprinast and 5-HD depolarised the $\Delta\psi_m$ to the same degree as observed in the presence of either zaprinast or 5-HD alone (F/F_0=0.05, 4%±1.2 auc.; Figure 7-9).

As SNAP, SNP and zaprinast elevate cGMP by different routes the small depolarisation observed in their presence can be attributed to elevated cGMP.

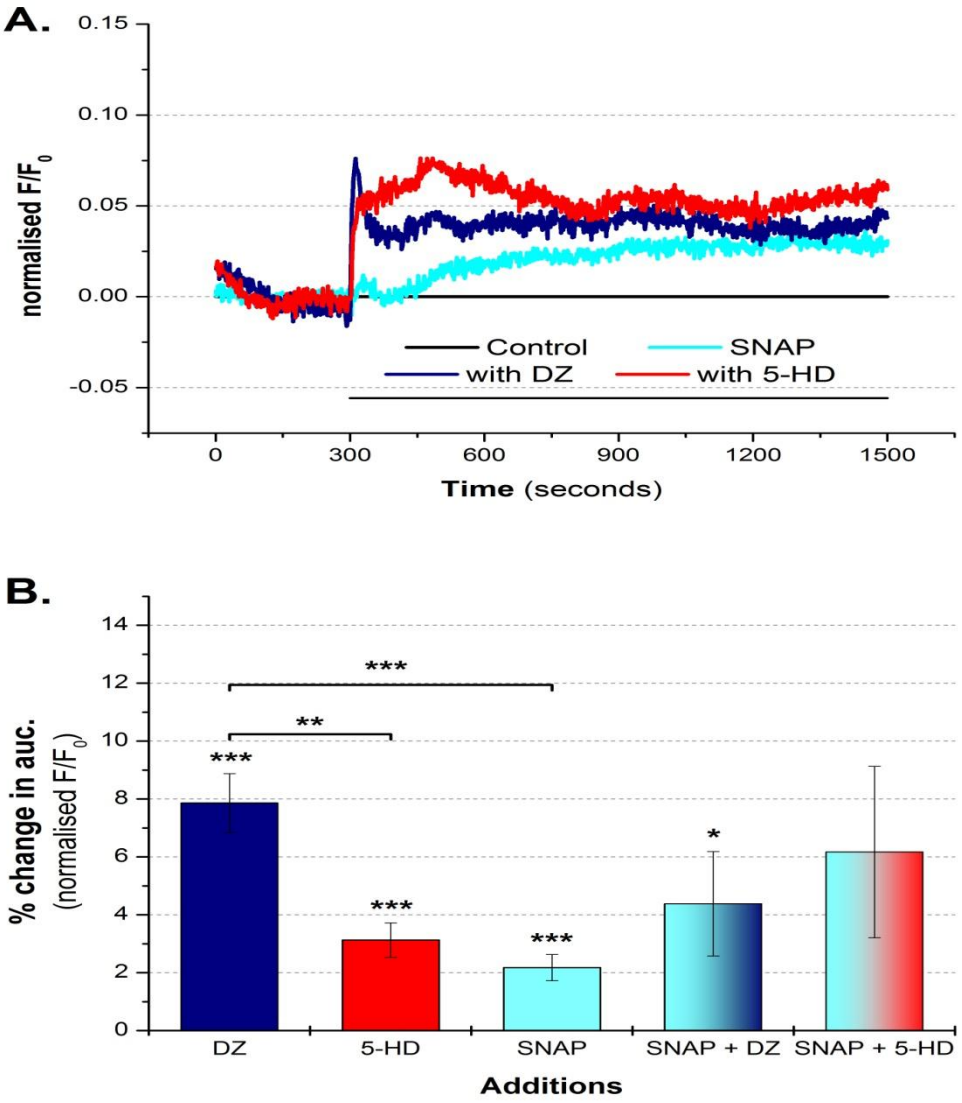

Figure 7-7. The effect of cGMP modulator SNAP (depolarisation), on $\Delta\psi_m$ alone and in-conjunction with diazoxide or 5-HD in HeLa cells.

HeLa cells were cultured in black walled 96 well plates. Once confluent the cells were loaded with 3 µM TMRE. The addition of 20 µM SNAP in the presence or absence of either 500 µM diazoxide or 500 µM 5-HD was recorded, in HBS at 370C. A) The $\Delta\psi$m is represented as TMRE F/F_0 normalised to the mock addition trace to eliminate addition artefacts. B) The bar graph indicates the $\Delta\psi$m, represented as the percentage change in the integrated F/F_0 compared to the control mock addition. Error bars represent S.E.M. from the mean of at least 6 repeated experiments. T-test: *P<0.05, **P<0.01 and ***P<0.001, compared to the control, 0% auc. change.

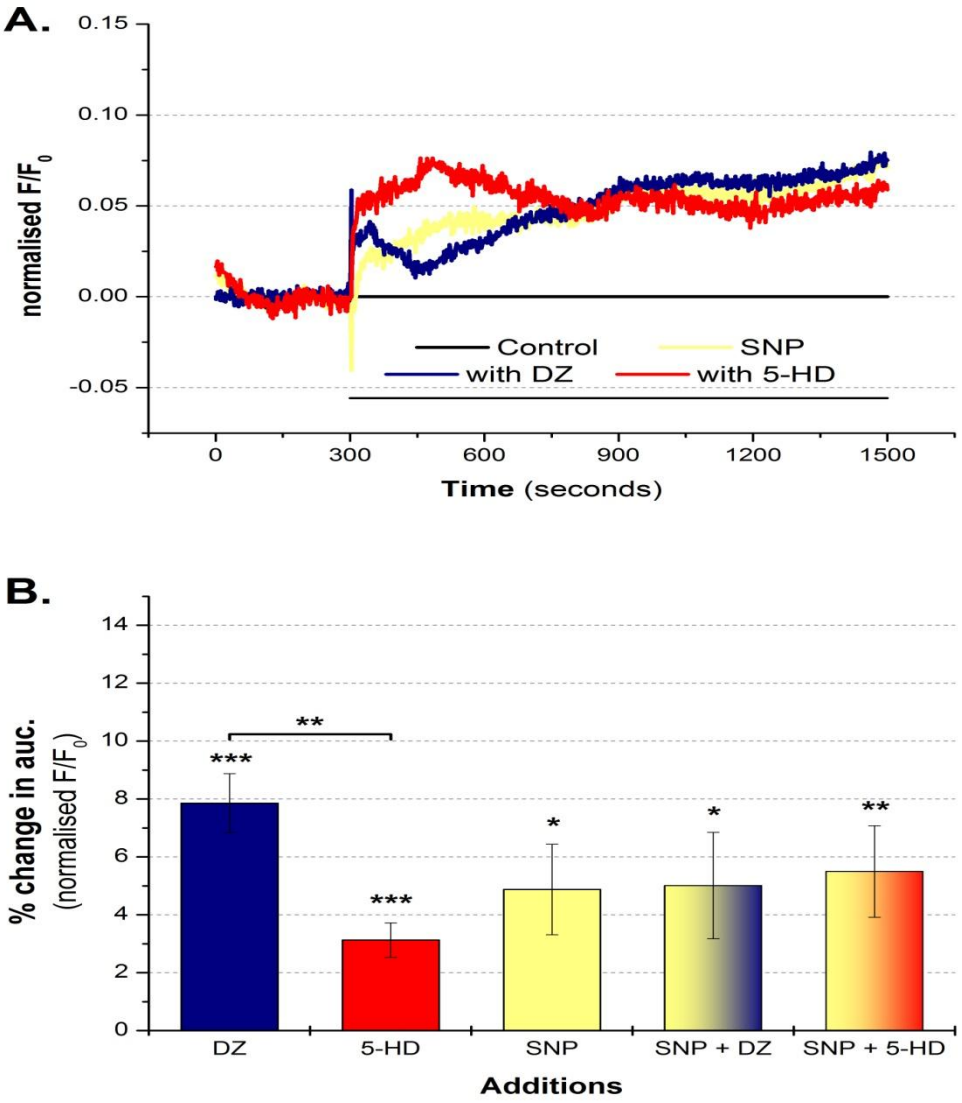

Figure 7-8. The effect of cGMP modulator SNP (depolarisation), on $\Delta\psi_m$ alone and in-conjunction with diazoxide or 5-HD in HeLa cells.

HeLa cells were cultured in black walled 96 well plates. Once confluent the cells were loaded with 3 µM TMRE. The addition of 100 µM SNP in the presence or absence of either 500 µM diazoxide or 500 µM 5-HD, was recorded, in HBS at 37^0C. A) The $\Delta\psi_m$ is represented as TMRE F/F_0 normalised to the mock addition trace to eliminate addition artefacts. B) The bar graph indicates the $\Delta\psi$m, represented as the percentage change in the integrated F/F_0 compared to the control mock addition. Error bars represent S.E.M. from the mean of at least 6 repeated experiments. T-test: *P<0.05, **P<0.01 and ***P<0.001, compared to the control, 0% auc. change.

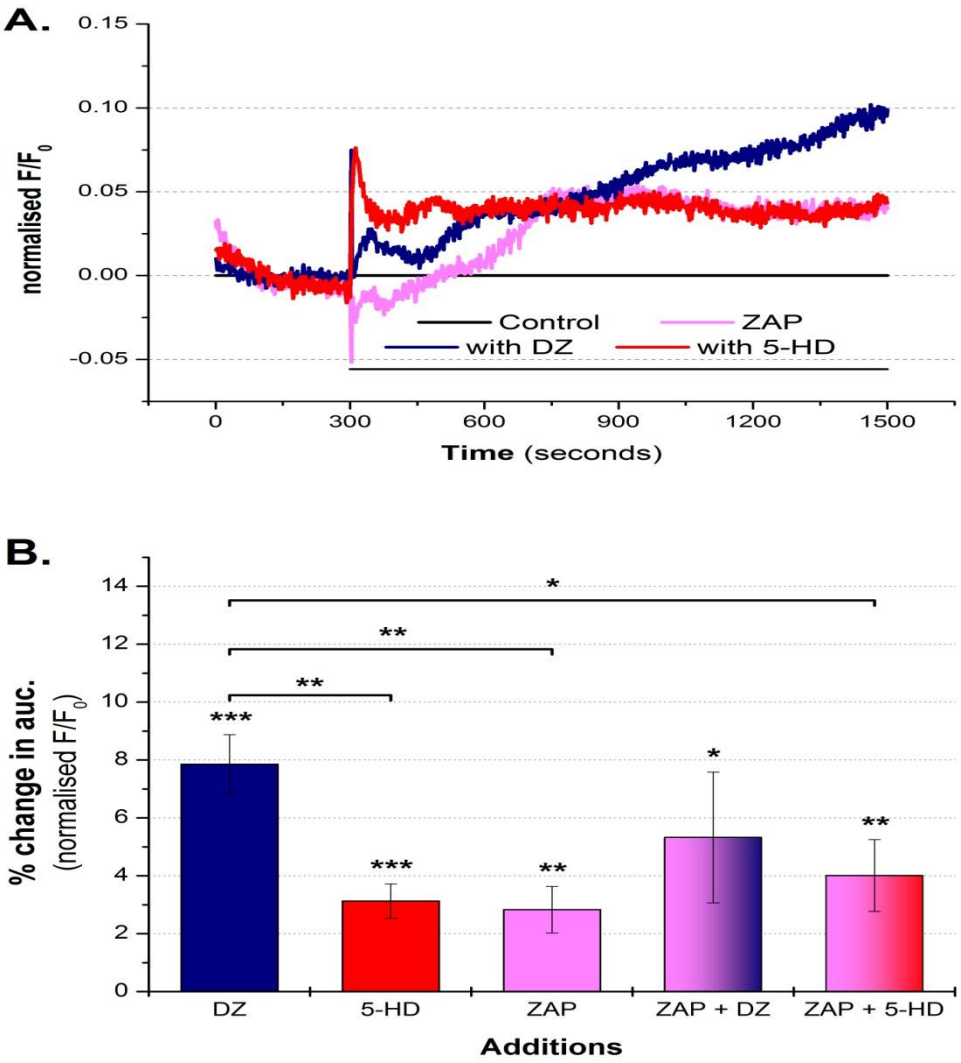

Figure 7-9. The effect of cGMP modulator, zaprinast (ZAP, depolarisation), on $\Delta\psi_m$ alone and in-conjunction with diazoxide or 5-HD in HeLa cells.

HeLa cells were cultured in black walled 96 well plates. Once confluent the cells were loaded with 3 µM TMRE. The addition of 20 µM ZAP in the presence or absence of either 500 µM diazoxide or 500 µM 5-HD, was recorded, in HBS at 37^0C. A) The $\Delta\psi_m$ is represented as TMRE F/F_0 normalised to the mock addition trace to eliminate addition artefacts. B) The bar graph indicates the $\Delta\psi$m represented as percentage variance of the integrated F/F_0 compared to the control mock addition. Error bars represent S.E.M. from the mean of at least 6 repeated experiments. T-test: *P<0.05, **P<0.01 and ***P<0.001, compared to the control, 0% auc. change.

7.6. FCCP Modulation

As discussed, FCCP is a protonophore and an effective un-coupler of mitochondrial oxidative phosphorylation [510, 516-519, 524]. The presence of FCCP induces a large depolarisation of the $\Delta\psi_m$, from -180 mV to approximately -60 mV [525-528]. As such FCCP was used as a control at the end of each experimental run and also to examine any modulation deriving from the presence of $\Delta\psi$m modulating agents.

The addition of FCCP induced a large and rapid depolarisation of the $\Delta\psi_m$ F/F_0 (0.49±0.05; Figure 7-10). The presence of diazoxide slightly elevated the overall depolarisation (F/F_0=0.57±0.1 or auc. 14.4±3%; Figure 7-10). Pre-treatment with 5-HD prior to FCCP-depolarisation, resulted in no significant deviation from the depolarisation induced by FCCP alone (F/F_0=0.5±0.1 or auc. 1.6±0.4%; Figure 7-10). Pre-treatment with both diazoxide in combination with 5-HD resulted in a transient increased depolarisation, before recovering back to the level of depolarisation observed in its absence (F/F_0=0.77±0.05 or auc. 57±4%; Figure 7-10).

There was no discernible difference of FCCP-depolarisation in either the absence or the presence of cyanide (F/F_0=0.46±0.1 or auc. -3.9%±0.7); or cyanide in combination with 5-HD (F/F_0=0.48±0.1 or auc. 6%±1.3; Figure 7-11). However, the presence of cyanide and diazoxide induced significantly elevated depolarisation (F/F_0=0.48±0.1 or auc. 6%±1.3; Figure 7-11). Similar effects were observed in the presence of oligomycin alone (F/F_0=0.51±0.1 or auc. 8.5%±1.2), 5-HD (F/F_0=0.37±0.1 or auc. -9.6%±1.1). Treatment with oligomycin in combination with diazoxide induced elevated depolarisation (F/F_0=0.76±0.1 or auc. 63%±7; Figure 7-12).

The effect on FCCP driven depolarisation was measured in the presence of the cGMP modulators alone and in combination with either diazoxide or 5-HD (SNAP Figure 7-13, SNP Figure 7-14 and zaprinast Figure 7-15). The cGMP modulators all exhibited minimal effect on FCCP-depolarisation (SNAP F/F_0=0.47±0.1 or auc. -6.7%±1, SNP F/F_0=0.52±0.1 or auc. +4.2%±1 and zaprinast F/F_0=0.59±0.1 or auc. +10%±2). The presence of diazoxide in combination with the cGMP modulators elevated the observed TMRE fluorescence: SNAP (F/F_0=0.61±0.1 or auc. +28%±3);

SNP (F/F_0=0.69±0.02 or +50%±4); zaprinast (F/F_0=0.79±0.1 auc. +62%±8). Pre-incubation with SNP in combination with 5-HD had minimal effect on the observed $\Delta\psi_m$ (F/F_0=0.34±0.03, -10%±3 auc.); whilst SNAP and zaprinast reduced the FCCP driven depolarisation (SNAP F/F_0=0.35±0.1 or auc. -27%±4 and zaprinast F/F_0=0.32±0.03 or auc. -20%±2).

Initially FCCP was used as a control however, the data yielded some interesting results as illustrated in Figure 7-16. Whilst the shift in depolarisation was significantly reduced as $\Delta\psi_m$ is already depolarised, the presence of both cyanide and diazoxide resulted in elevated overall FCCP-depolarisation (Figure 7-16B).

The presence of diazoxide alone showed a moderate, but not significant, elevation in the observed FCCP-derived depolarisation. When used in combination with other agents, notably with cyanide or SNP, the overall FCCP-depolarisation was elevated. The elevated depolarisation arose from increased shift in F/F_0 depolarisation rather than $\Delta\psi_m$ depolarisation arising from the presence of the selected agents. This elevated depolarisation occurs because the FCCP induced depolarisation was additive to that already induced by diazoxide.

5-HD alone also exhibited no effect on $\Delta\psi_m$ depolarisation induced by FCCP. Pre-incubation with 5-HD in combination with oligomycin or zaprinast significantly reduced the overall FCCP-induced depolarisation (Figure 7-12, Figure 7-15 and Figure 7-16B), whilst the shift in FCCP-depolarisation is reduced in the combined presence of SNAP and 5-HD (Figure 7-13 and Figure 7-16A).

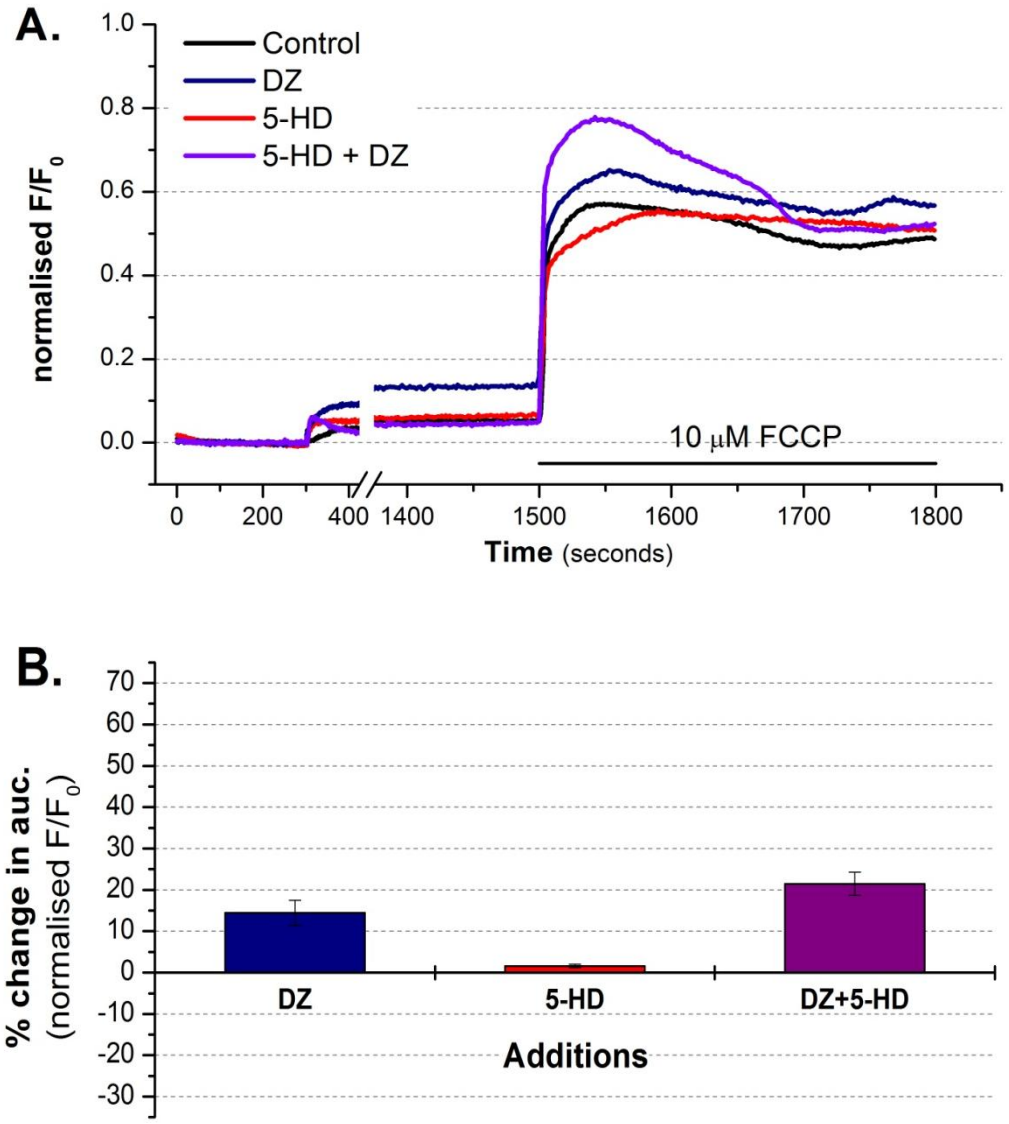

Figure 7-10. FCCP depolarisation modulation by the presence of diazoxide (DZ), 5-HD and DZ and 5-HD, in HeLa cells.

HeLa cells were cultured in black walled 96 well plates. Once confluent the cells were loaded with 3 µM TMRE. The response to 10 µM FCCP was measured, on cells in the presence of the channel modulators, 500 µM diazoxide, 500 µM, 5-HD and diazoxide and 5-HD in combination and was measured as: A) the $\Delta\psi$m is represented as TMRE (F/F_0). B) The solid bar indicates the addition of 10 µM FCCP. The $\Delta\psi$m is represented as the percentage change compared to the 10 µM FCCP alone. Error bars represent S.E.M. from the average of at least 6 repeat experiments. T-test: *P<0.05, **P<0.01 and ***P<0.001, compared to the control, 10 µM FCCP.

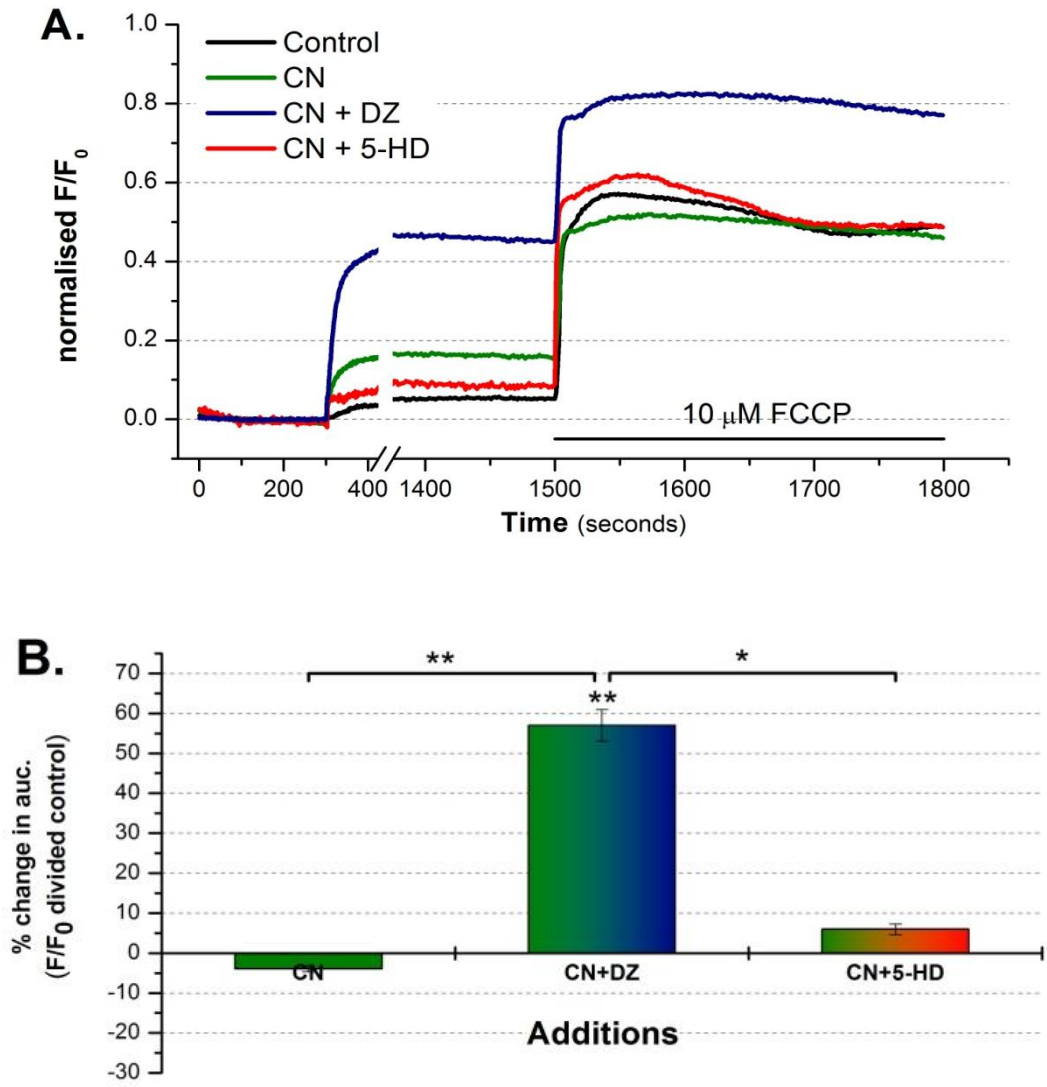

Figure 7-11. FCCP depolarisation modulation by the presence of sodium cyanide (CN, no effect) alone and in conjunction with diazoxide (DZ, which elevated depolarisation) or 5-HD (no effect) in HeLa cells.

HeLa cells were cultured in black walled 96 well plates. Once confluent the cells were loaded with 3 µM TMRE. The response to 10 µM FCCP was measured, on cells in the presence of 4 mM sodium cyanide alone and with either 500 µM diazoxide or 500 µM 5-HD. A) The $\Delta\psi$m is represented as TMRE (F/F_0). B) The solid bar indicates the addition of 10 µM FCCP. The $\Delta\psi$m is represented as the percentage change compared to the 10 µM FCCP alone. Error bars represent S.E.M. from the average of at least 6 repeat experiments. T-test: *P<0.05, **P<0.01 and ***P<0.001, compared to the control, 10 µM FCCP, or as indicated by bar, other agents.

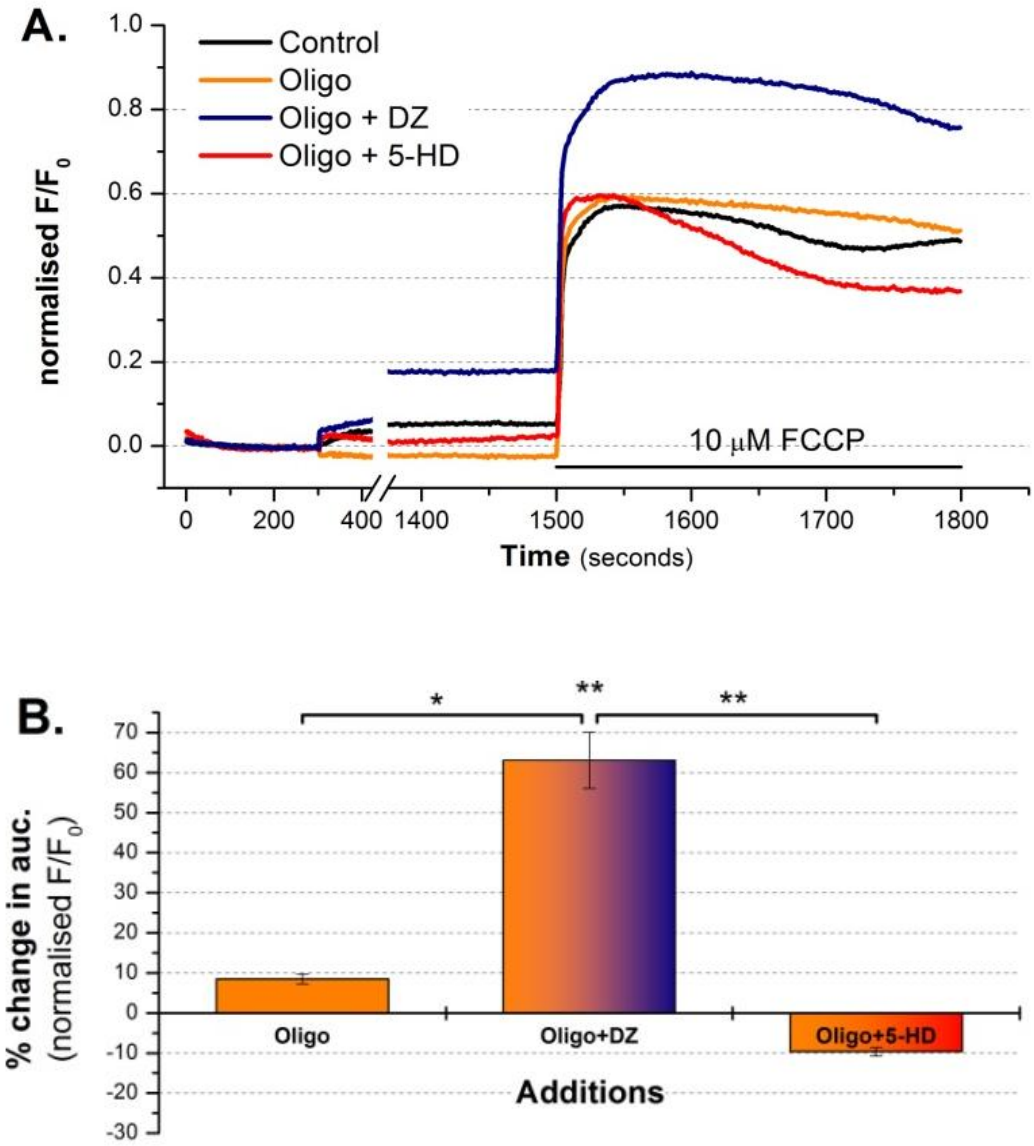

Figure 7-12. FCCP depolarisation modulation by the presence of oligomycin (no effect) alone and in conjunction with diazoxide (DZ, which elevated depolarisation) or 5-HD (no effect) in HeLa cells.

HeLa cells were cultured in black walled 96 well plates. Once confluent the cells were loaded with 3 µM TMRE. The response to 10 µM FCCP was measured, on cells in the presence of 6 µM oligomycin alone and with either 500 µM diazoxide or 500 µM 5-HD. A) The $\Delta\psi$m is represented as TMRE (F/F_0). B) The solid bar indicates the addition of 10 µM FCCP. The $\Delta\psi$m is represented as the percentage change compared to the 10 µM FCCP alone. Error bars represent S.E.M. from the average of at least 6 repeat experiments. T-test: *P<0.05, **P<0.01 and ***P<0.001, compared to the control, 10 µM FCCP, or as indicated by bar, other agents.

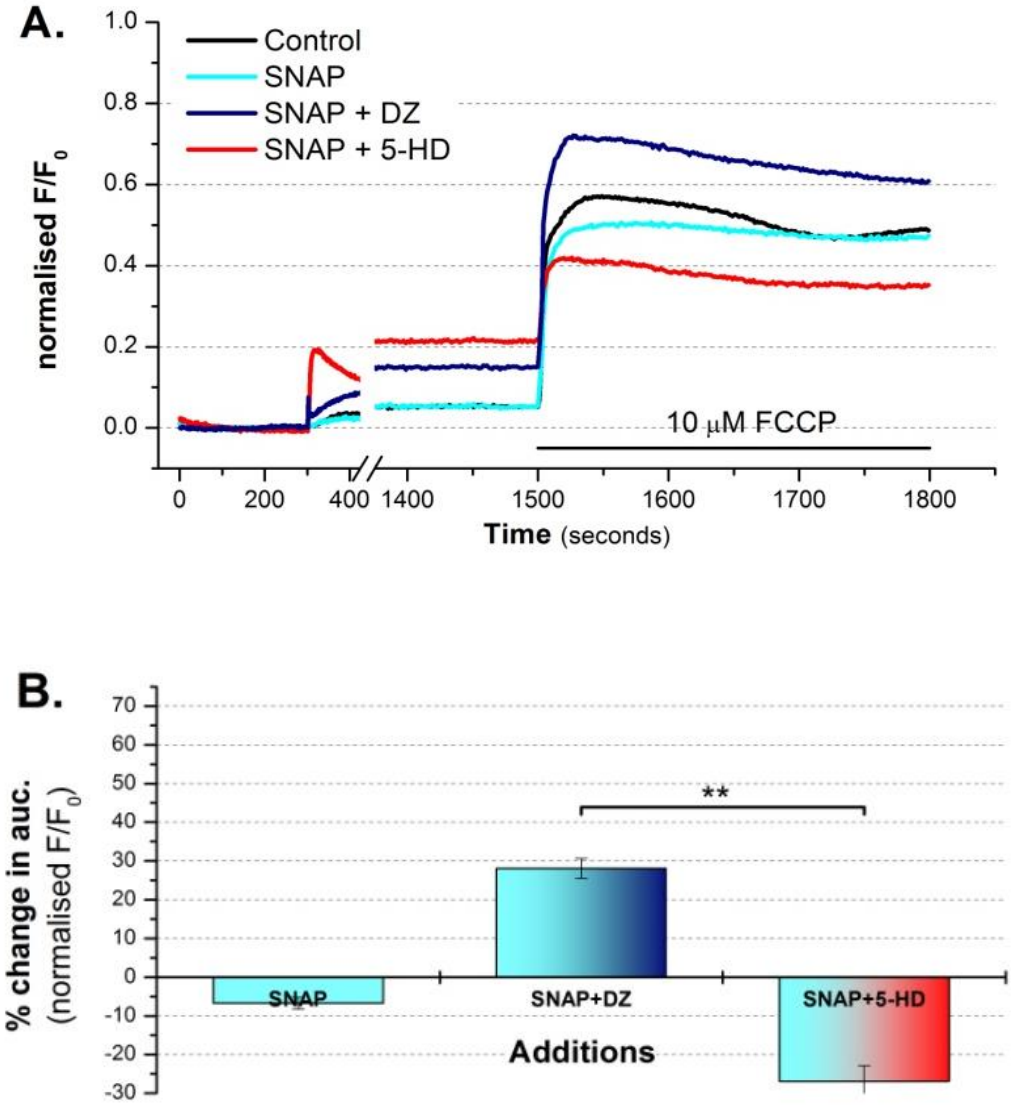

Figure 7-13. FCCP depolarisation modulation by the presence of SNAP (no effect) alone and in conjunction with diazoxide (DZ, which elevated depolarisation) or 5-HD (no effect) in HeLa cells.

HeLa cells were cultured in black walled 96 well plates. Once confluent the cells were loaded with 3 µM TMRE. The response to 10 µM FCCP was measured, on cells in the presence of 20 µM SNAP cyanide alone and with either 500 µM diazoxide or 500 µM 5-HD. A) The $\Delta\psi$m is represented as TMRE (F/F_0). B) The solid bar indicates the addition of 10 µM FCCP. The $\Delta\psi$m is represented as the percentage change compared to the 10 µM FCCP alone. Error bars represent S.E.M. from the average of at least 6 repeat experiments. T-test: *P<0.05, **P<0.01 and ***P<0.001, compared to the control, 10 µM FCCP, or as indicated by bar, other agents.

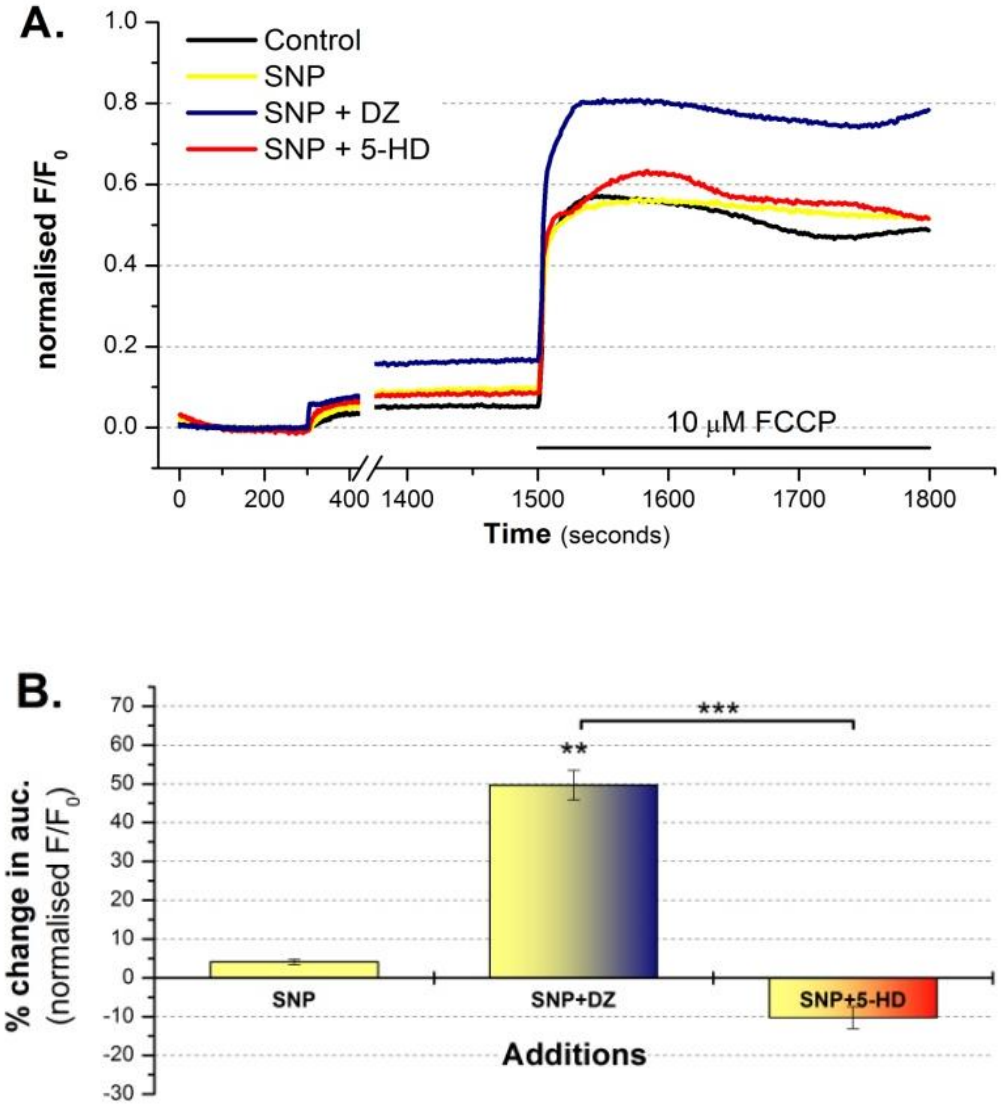

Figure 7-14. FCCP depolarisation modulation by the presence of SNP (no effect) alone and in conjunction with diazoxide (DZ, which elevated depolarisation) or 5-HD (no effect) in HeLa cells.

HeLa cells were cultured in black walled 96 well plates. Once confluent the cells were loaded with 3 µM TMRE. The response to 10 µM FCCP was measured, on cells in the presence of 100 µM SNP cyanide alone and with either 500 µM diazoxide or 500 µM 5-HD. A) The $\Delta\psi$m is represented as TMRE (F/F_0). B) The solid bar indicates the addition of 10 µM FCCP. The $\Delta\psi$m is represented as the percentage change compared to the 10 µM FCCP alone. Error bars represent S.E.M. from the average of at least 6 repeat experiments. T-test: *P<0.05, **P<0.01 and ***P<0.001, compared to the control, 10 µM FCCP, or as indicated by bar, other agents.

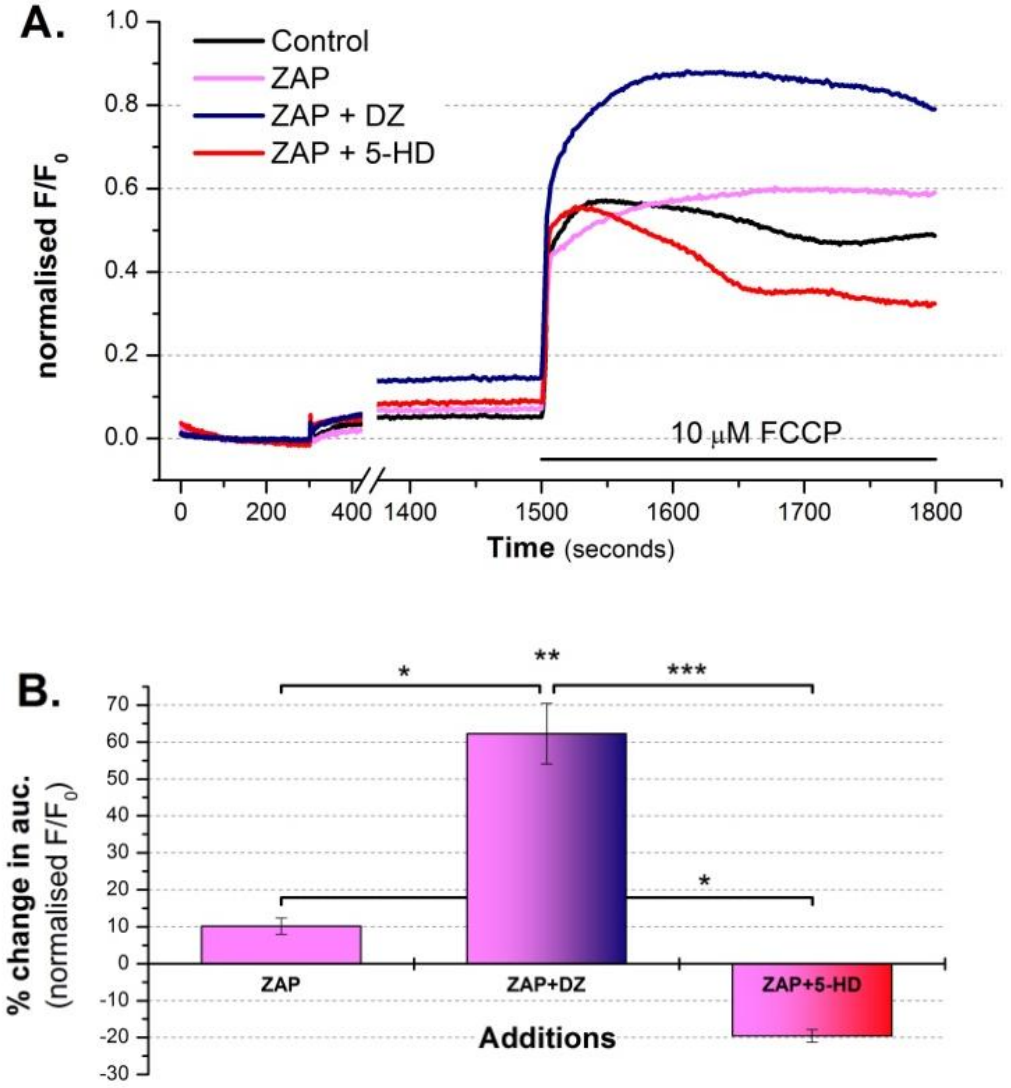

Figure 7-15. FCCP depolarisation modulation by the presence of zaprinast (ZAP, no effect) alone and in conjunction with diazoxide (DZ, elevated depolarisation) or 5-HD (no effect) in HeLa cells.

HeLa cells were cultured in black walled 96 well plates. Once confluent the cells were loaded with 3 µM TMRE. The response to 10 µM FCCP was measured, on cells in the presence of 20 µM ZAP cyanide alone and with either 500 µM diazoxide or 500 µM 5-HD. A) The $\Delta\psi$m is represented as TMRE (F/F_0). B) The solid bar indicates the addition of 10 µM FCCP. The $\Delta\psi$m is represented as the percentage change compared to the 10 µM FCCP alone. Error bars represent S.E.M. from the average of at least 6 repeat experiments. T-test: *P<0.05, **P<0.01 and ***P<0.001, compared to the control, 10 µM FCCP, or as indicated by bar, other agents.

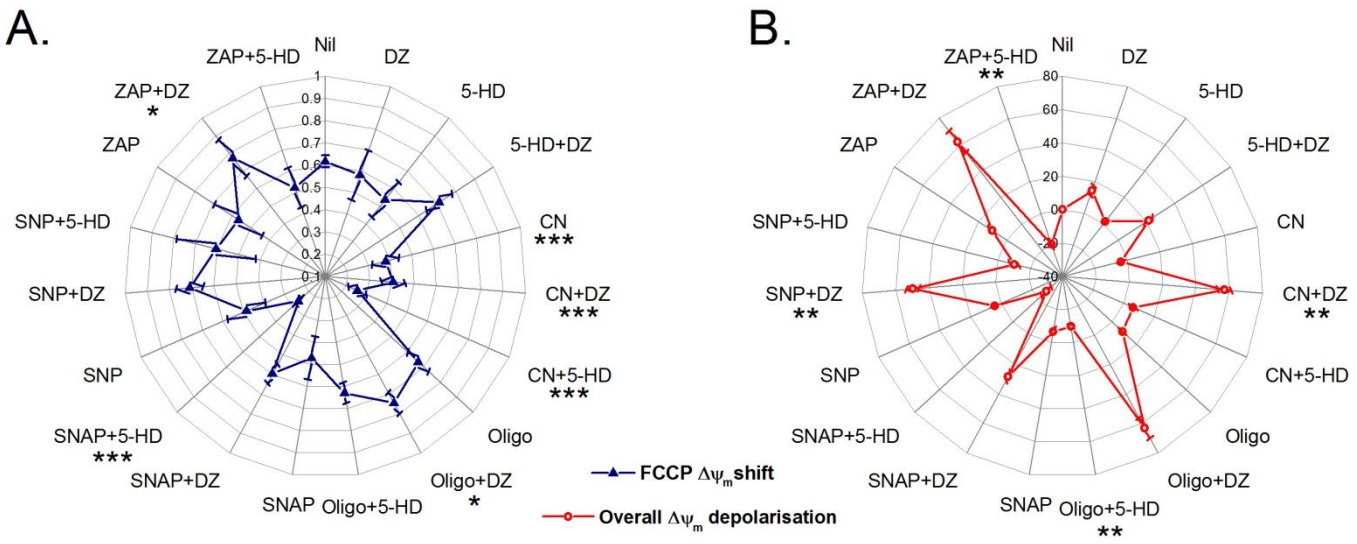

Figure 7-16. Comparison of the shift (A, blue) and overall (B, red) FCCP induced depolarisation and the effect of the presence of various $\Delta\psi_m$ modulators in the presence or absence of diazoxide or 5-HD, in HeLa cells.

HeLa cells were cultured in black walled 96 well plates. Once confluent the cells were loaded with 3 µM TMRE. The response to 10 µM FCCP was measured, on cells in the presence of 4 mM cyanide (CN), 6 µM oligomycin (Oligo), 20 µM SNAP, 100 µM SNP or 20 µM zaprinast (ZAP) alone or in combination with 500 µM diazoxide (DZ) or 500 µM 5-HD. A) The shift in $\Delta\psi_m$ depolarisation F/F_0 following the addition of 10 µM FCCP is displayed, whilst B) illustrates the overall F/F_0 depolarisation observed. Error bars represent S.E.M. from the average of at least 6 repeat experiments. T-test: *P<0.05, **P<0.01 and ***P<0.001, compared to the control, 10 µM FCCP.

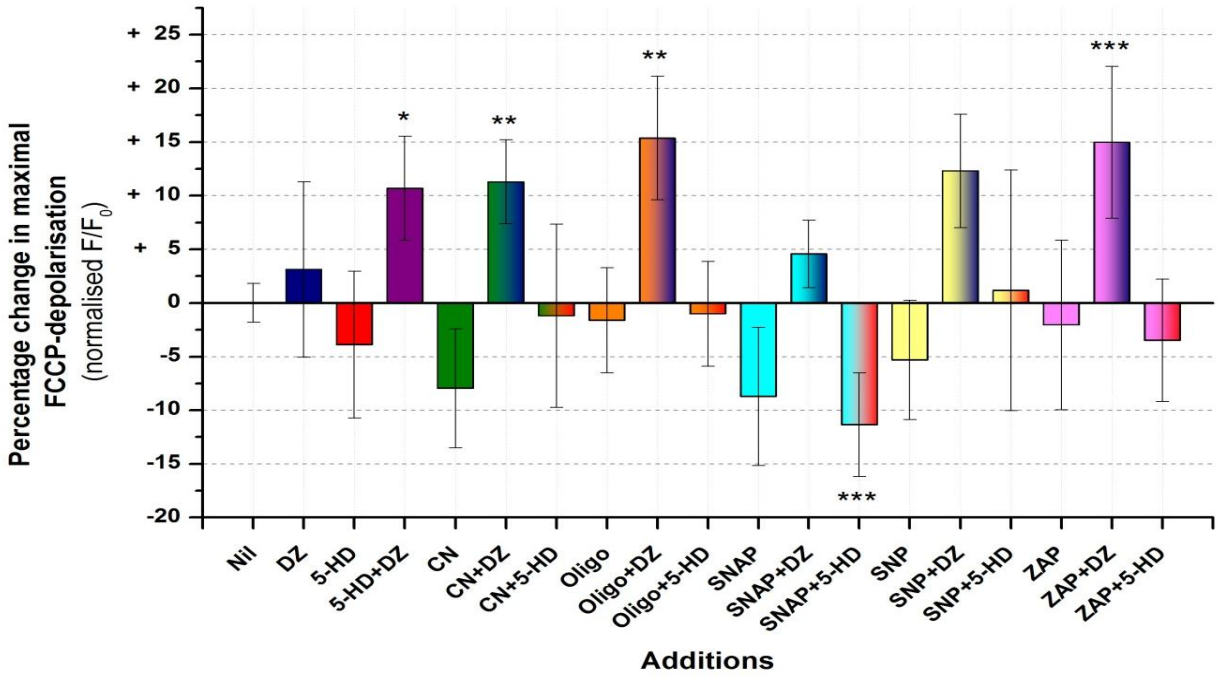

Figure 7-17. Comparison of the shift if FCCP-driven depolarisation, relative to the cells pre-exposure to various $\Delta\psi_m$ modulators in the presence or absence of diazoxide or 5-HD, in HeLa cells.

HeLa cells were cultured in black walled 96 well plates. Once confluent the cells were loaded with 3 µM TMRE. The response to 10 µM FCCP was measured, on cells in the presence of 4 mM cyanide (CN), 6 µM oligomycin (Oligo), 20 µM SNAP, 100 µM SNP or 20 µM zaprinast (ZAP) alone or in combination with 500 µM diazoxide (DZ) or 500 µM 5-HD. The shift in FCCP-driven depolarisation is represented as the percentage change in F/F_0 compared to the control FCCP addition alone. Error bars represent S.E.M. from the average of at least 6 repeat experiments. T-test: *P<0.05, **P<0.01 and ***P<0.001, compared to the control, 10 µM FCCP.

7.7. Conclusions

Diazoxide induces substantial $\Delta\psi_m$ depolarisation (Figure 7-3). Based on a resting $\Delta\psi_m$ of -180 mV and FCCP inducing depolarisation to -60 mV, diazoxide induces depolarisation to approximately -150 mV. The loss of $\Delta\psi_m$ is consistent with mitoK_{ATP} opening and subsequent K^+ influx. Depolarisation is assumed to be the contributing factor of pharmacological IPC, synonymous with diazoxide, irrespective of the mechanism of depolarisation [15, 120-124, 584].

Diazoxide in conjunction with cyanide enhanced the observed depolarisation (Figure 7-6). As cyanide inhibits complex IV of the ETC, if diazoxide depolarisation arose from modulation of the ETC (most likely complex II), would the same degree of elevated depolarisation be observed? However, the $\Delta\psi_m$ depolarisation is more logical if diazoxide acts in a complimentary manner, indicative of a KCO. Unlike when used with cyanide, oligomycin reduces diazoxide-induced depolarisation. The modulation of depolarisation is indicative of diazoxide generating K^+ influx at a time of reduced proton influx (oligomycin), potentially via the mitoK_{ATP} opening.

Diazoxide-induced $\Delta\psi_m$ modulation is attenuated by 5-HD in the manner that it inhibits IPC [228, 264-266]. Despite 5-HDs perceived specificity, recent publications have suggested that the antagonistic effects of 5-HD on diazoxide derived IPC may arise from metabolic actions rather than as a K^+ channel blocker (see section 5.4.3) [2, 4, 5, 237, 254, 262-264, 266-274]. 5-HD's ability to impair oligomycin-hyperpolarisation, suggests that the net effect maybe decreased proton flux. This might arise from a direct effect at the F_1F_0 ATPase or by a reduction in NADH supply. The effect of 5-HD on β-oxidation might mediate such an effect on the latter. Since 5-HD reduced the oligomycin-induced hyperpolarisation, this is not consistent with any inhibition of a K^+ channel, the commonly proposed site of action for this drug.

5-HD induced small depolarisation in the measured $\Delta\psi_m$, consistent with it exerting metabolic actions rather than a K^+ channel inhibitor. If under basal conditions the

channel was closed or nonexistent or open then there would be no $\Delta\psi_m$ modulation or even hyperpolarisation (from reduce K^+ influx).

7.7.1. Cyclic GMP & IPC

In the absence of specific mitoK_{ATP} channel modulators or molecular strategies, the cGMP-PKG activation pathway was used as a control [281-283]. The addition of the cGMP modulating agents (SNAP, SNP and zaprinast) were selected to induce mitoK_{ATP} channel opening, allowing observation of the effects of diazoxide and 5-HD in relation to direct activation of the proposed channel, mitoK_{ATP}. The presence of cGMP modulators induced mild depolarisation, consistent with cGMP-PKG opening of mitoK_{ATP}. However without confirming the precise mechanism of action the modulation of diazoxide or 5-HD-induced $\Delta\psi_m$ is inconclusive.

Diazoxide-cGMP modulator depolarisation could be explained by competitive inhibition, if cGMP acts as a partial agonist relative to diazoxide activation of the putative mitoK_{ATP} channel. If, for example diazoxide binds to SUR1 and SUR2A (putative channel subunits) this could be the site of cGMP-dependent channel opening [249-251]. The critical factor is the relatively small effect and the statistical power, which requires further experimentation to establish if the observed cGMP inhibited diazoxide-depolarisation is a genuine effect.

Cyclic GMP derived depolarisation was not modulated by the addition of 5-HD. This may be as any modulation of $\Delta\psi_m$ is obscured by 5-HD derived depolarisation. Depolarisation induced by the combination of the cGMP-elevating agents and 5-HD could suggest a common pathway, explaining why there is no additional modulatory or inhibitory effects. Alternatively the cGMP modulators could induce cGMP-dependent mitoK_{ATP} channel opening which is negated by 5-HD.

7.7.2. FCCP Depolarisation

The addition of FCCP was initially used as an internal control to induce large $\Delta\psi_m$ depolarisation (to approximately to -60 mV) at the end of each experiment however it yielded some interesting results [516, 517, 525-528].

FCCP depolarisation was modulated by the presence of diazoxide and 5-HD. The data supports the findings that diazoxide is predominantly a mitochondrial KCO. If diazoxide were to act on the ETC there would be no additive or compounding depolarisation as induced by FCCP and cyanide. However the modulation of two independent depolarising mechanisms such as the ETC (FCCP) and mitoK_{ATP} channel (diazoxide) would explain the additional shift in depolarisation observed.

The antagonistic effect to FCCP-depolarisation afforded by 5-HD is interesting for the fact that the action only arises while in the presence of other $\Delta\psi_m$ modulating agents and not by 5-HD alone. It could be that the β-oxidation in the HeLa cell model plays a crucial role or that 5-HD is acting as a channel blocker.

8. Results - Extracellular Nucleotides

8.1. Introduction

During hypoxia the extracellular concentration of ATP is known to be increased (up to 4 fold) and via purinoceptor activation induces a range of downstream dynamics events [301, 324]. Whilst elevated extracellular ATP and subsequent P2 dynamics is a well-documented event, minimal attention has been paid to extracellular ADP and its' distinct pharmacology via $P2Y_{1,6,11}$ receptor activation(vasodilation, platelet aggregation and proinflamatory action) [82, 83, 301, 316, 317, 321, 323, 324, 383, 385, 386, 585-594].

With both nucleotides having different if not opposing signalling it is important to look at their concentration and accumulation in response to metabolic stressing. Recent mathematical modelling has suggested that alongside ATP other nucleotide including ADP accumulate which has even been shown at concentrations equal to or greater than ATP [319, 325].

Subsequently one of the main aims of this section is to look at the extracellular nucleotide concentration during CIH and determine if ADP is present alongside ATP. The cause of extracellular nucleotide accumulation was also examined with regard to ecto-enzyme activity and release.

8.2. Calibration Curves

To measure nucleotide release the sensitivity of the luciferase assay, AMR VIALIGHT®, was examined and standard curves for ATP and ADP were generated.

In a cell-free assay, the light emitted after addition of AMR Vialight® to serial dilutions of ATP (1 pM – 10 µM) was recorded. There was a significant fit to a Boltzmann curve (R^2=1; Figure 8-1A). To quantity the concentration of ADP, the ADP in the sample was converted to ATP as described in the methods (section 6.9.4). The additional ATP was then determined after measurement of the original ATP present in the sample. To allow for the non-linearity of the ATP calibration curve ADP standards were converted to ATP to give an ATP equivalence curve. Sample ADP measurements were then measured against this curve, Figure 8-1B. This approach allowed ADP concentration above 10 nM to be reliably measured.

To further confirm the concentration of nucleotides, the signal measured by luminometry was compared to the area under the curve (auc.) after HPLC at the relative elution times for ATP (18.5 minutes) and ADP (14 minutes). The HPLC system showed a lower sensitivity compared to the tube luminometer protocol. The ATP samples were only measurable down to the 0.1-1 µM range whilst ADP was measurable at concentrations in the 1-10 µM range for HPLC, in comparison to the picomolar and nanomolar ranges for ATP and ADP respectively, when using luminometry.

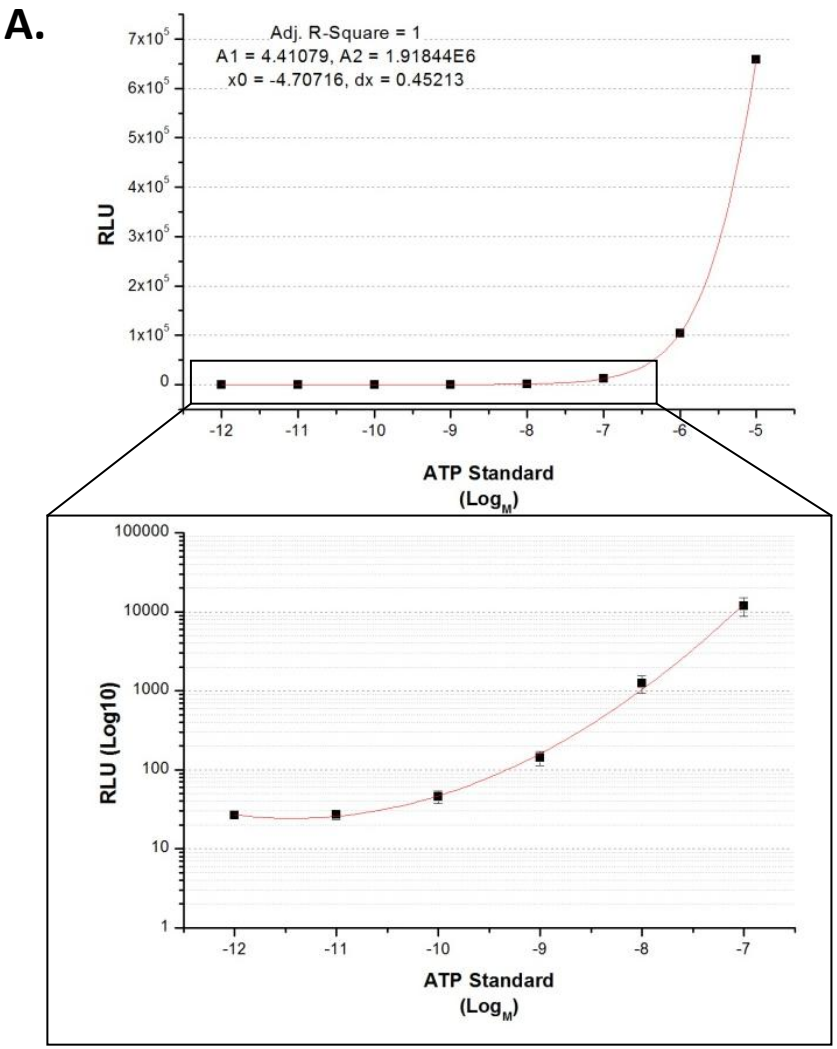

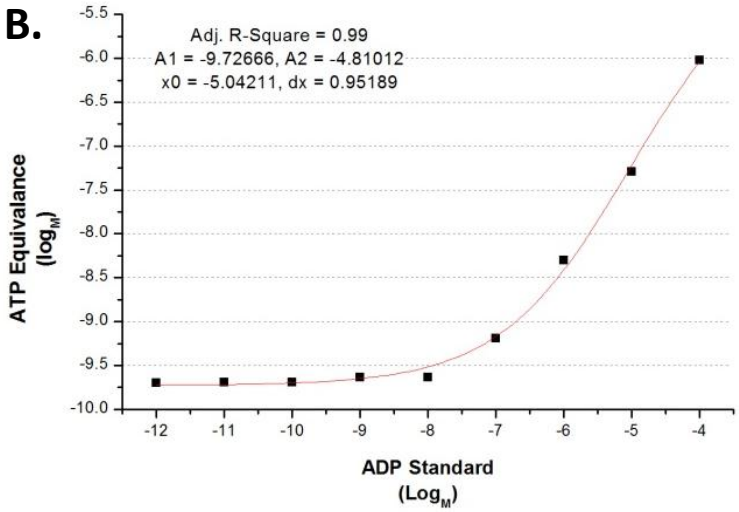

Figure 8-1. Standard Curves generated in the Tube Luminometer system for ATP (A) and ADP (B).

In HBS supplemented with propidium iodide (PI, 150 µM) cell free samples of nucleotides were ran through the Berthold tube luminometer. Serial concentrations of ATP (1 pM – 10 µM) and ADP (1 pM – 100 µM) were added to tubes containing 20µl AMR. To the ADP samples 33.3µl PK and 5.8µl PEP was added converting ADP to ATP and re-measured. A) The ATP standard was plotted as ATP Log_M against RLU and B) the ADP standard as ATP equivalence. The data plotted is the mean of 3 repeats and a Boltzman standard curve was applied to both.

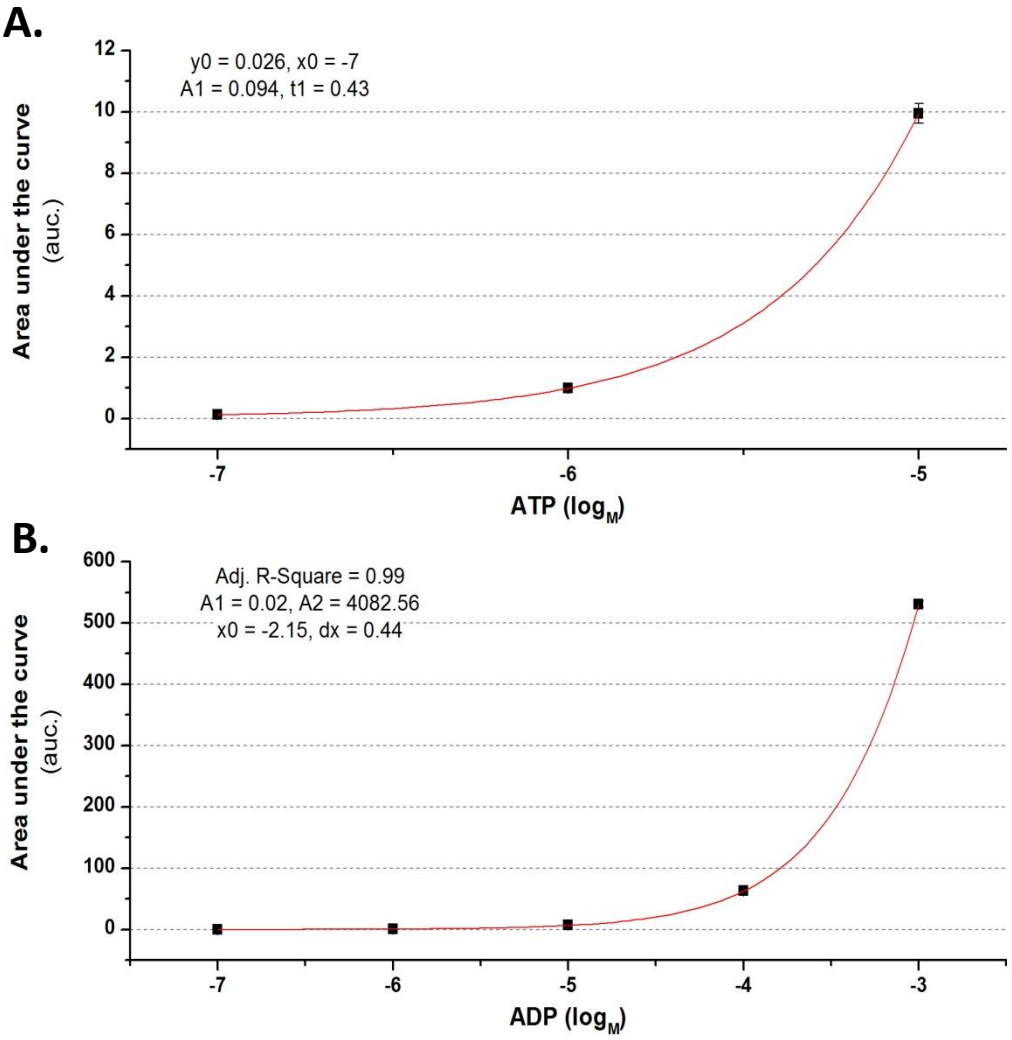

Figure 8-2. Standard Curves generated in using HPLC for known ATP (A) and ADP (B) standards.

In HBS supplemented with propidium iodide (PI, 150 µM) cell free samples of nucleotides were ran and separated by HPLC via a Hypersil BDS C18 column, with ATP and ADP eluting at 18.5 minutes and 14 minutes. A) The ATP standards (log_M) plotted against the area under the curve (auc.) as recorded from λ=254 nm at 18.5 minutes. B) The ADP standards (log_M) were ran through the HPLC and plotted as auc. as measured at the elution point 14 minutes. The data plotted is the mean of 3 repeats and to the ATP data an exponential growth curve was applied whilst to the ADP data a Boltzman standard curve was used.

8.3. Poisoning and Nucleotide Release

The released extracellular nucleotide concentration was measured in the presence of metabolic poison, cyanide and 2-DG (which act to chemically induce hypoxia) supplemented with ionomycin, and compared to release under control conditions (in the absence of metabolic poisoning). These initial experiments allowed the observation of the basal concentrations of extracellular nucleotides (ATP and ADP) including any release arising from mechanical perturbations [315].

Under conditions of basal release, the measured extracellular nucleotide concentrations after 40 minutes assay period were 5±1 nM (ATP) and 259±31 nM (ADP; Figure 8-3D). An initial elevation of ATP occurred, which is suggestive of mechanical stimulation during the experimental protocol, in line with the work published by Lazarowski et al. (2003) [315]. For each experiment ATP and ADP were measured at a time zero nil addition control (T_0-NAC), to the left of the curves. The T_0-NAC measurement of ATP and ADP fell into the range of 1 to 25 nM and 250 to 550 nM, respectively. This acts as an internal control for elevated extracellular nucleotides resulting from mechanical perturbations.

Incubation with cyanide in combination with 2-DG, for up to 40 minutes, had no observable effect on the concentrations of extracellular nucleotides compared to the control (Figure 8-3B). Previous experiments have indicated that metabolic poisoning with cyanide and 2-DG sufficient to induce an immediate effect on cellular ATP [534, 627]. In order to induce metabolic stress ionomycin was added to the poison cocktail. Ionomycin alone induced a gradual elevation of ATP and ADP, which peaked after 40 minutes with maximum concentration of 36±6 nM and 2816±402 nM, respectively (Figure 8-3C). One feature of the poison cocktail was that it led to a much quicker increase in the release of ATP and ADP as observed in the initial 0 to 20 minute poisoning. In the presence of cyanide, 2-DG and ionomycin the extracellular ATP and ADP concentrations in EA.hy923 cells was significantly elevated in parallel to each other with overall concentrations at 40 minutes of 60±6 nM (ATP) and 4202±394 nM (ADP; Figure 8-3D).

As expected, the extracellular ATP and ADP concentration was significantly elevated in the presence of the poison cocktail in comparison to the summation of release in response to ionomycin alone and cyanide in combination with 2-DG.

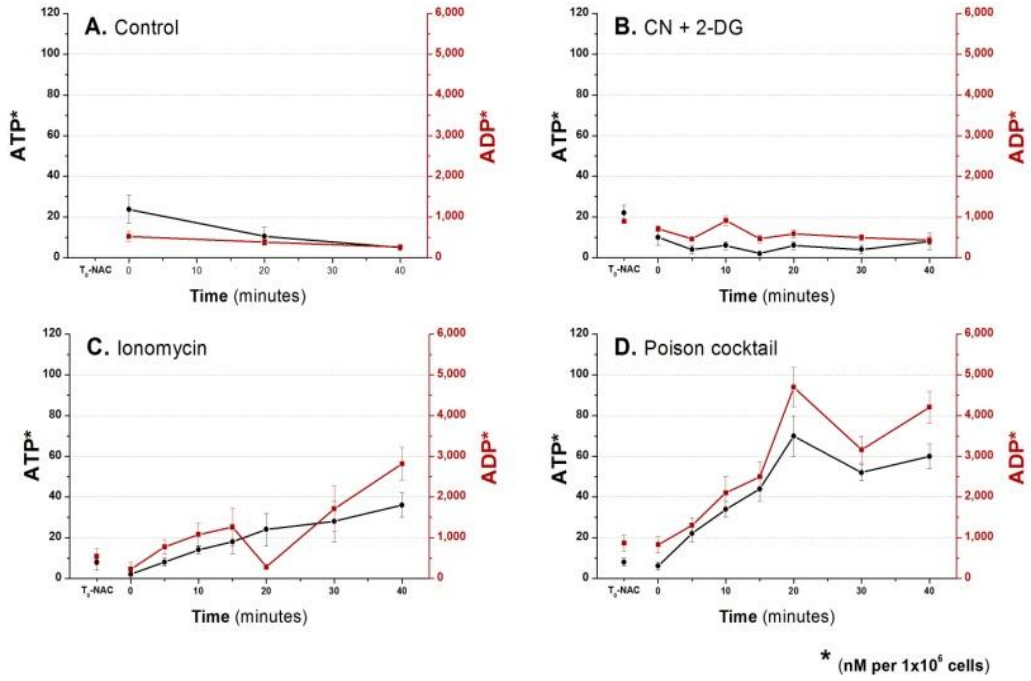

Figure 8-3. Extracellular nucleotide concentration under A. basal conditions and in the presence of B. CN + 2-DG, C. oligomycin and D. poison cocktail, in EA.hy926 cells.

EA.hy926 cells were cultured in 12 well plates until confluent. Once confluent, nucleotide release in response to poisoning was measured, in HBS, via tube luminometry. The effect of the extracellular nucleotide concentration was measured under A. basal conditions and in the presence of B. 4 mM Cyanide and 10 mM 2-DG, C. 5 µM Ionomycin and D. the poison cocktail (cyanide, 2-DG and ionomycin). The left hand scale and black trace represent the measured extracellular ATP (nM), whilst ADP is represented on the right hand scale and red trace (nM). T_0-NAC denotes the time zero nil addition control. Error bars represent S.E.M. from the average of at least 6 repeat experiments.

8.4. HPLC Confirm of Poisoning

To corroborate the extracellular nucleotide concentrations measured using tube luminometry, samples were also measured using HPLC. The ATP concentration following metabolic poisoning, 0 to 40 minutes, was not detectable using HPLC. The calibration curve was sensitive down to the 100 nM range, where as the observed ATP concentration in luminometry was less than 100 nM, below the threshold for HPLC. In comparison the ADP concentration was measurable using HPLC. The observed ADP concentration was recorded to similar levels as seen using tube luminometry (Figure 8-2).

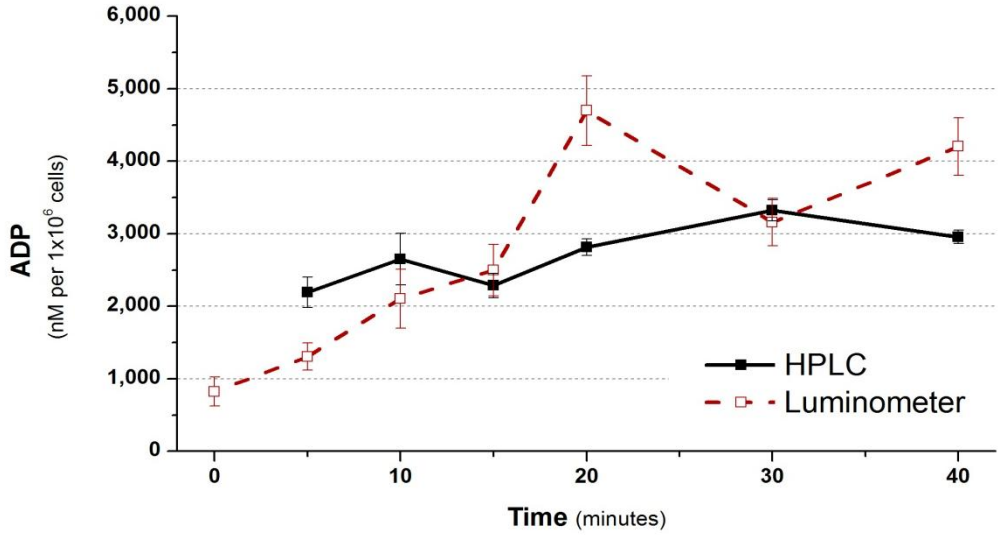

Figure 8-4. Extracellular ADP concentration following metabolic poisoning, measured using HPLC (black line) and luminometry (red dashed line).

EA.hy926 cells were cultured in 12 well plates until confluent. Once confluent, nucleotide release in response to poisoning was measured, in HBS. The effect of the extracellular nucleotide concentration was measured over a period of 0 to 40 minutes of metabolic poisoning (4 mM cyanide, 10 mM 2-DG and 5 µM ionomycin). The black line represents the ADP concentration calculated using HPLC, whilst the red dashed line from luminometry. Error bars represent S.E.M. from the average of 3 repeat experiments.

8.5. Ecto-nucleotide Inhibitors

Since the concentration of extracellular ADP was higher than expected experiments were performed to determine if the observed ADP was derived from metabolism of ATP. The extracellular nucleotide concentrations were observed in the presence and absence of ecto-enzyme inhibitors levamisole, ARL 67156 or ebselen during metabolic poisoning.

In the continued presence of levamisole the observed extracellular concentration of ATP became elevated after only 5 minutes of poisoning, and an increased accumulation of extracellular ATP was seen compared to poisoning alone (Figure 8-5A). The overall ATP concentration was elevated by 43% (86±10 nM with levamisole compared to 60±6 nM in the control). The extracellular ADP concentration was also elevated in the first 5 minutes of metabolic poisoning, resulting in an increase of 39% (2934±97 nM; Figure 8-5B). The presence of the ecto-nucleotide inhibitor ARL 67156 significantly elevated the nucleotide concentration, notably after 10 minutes with the final concentration at 40 minutes increased by 103% (122±16 nM, ATP) and 58% (6648±194 nM, ADP; Figure 8-6). The presence of ebselen had a less pronounced effect on the nucleotide concentration compared to levamisole or ARL 67156, with smaller modulation of the extracellular ATP (16±2%, 70±10 nM) and ADP concentration and ADP (15±5%, 4836±1340 nM; Figure 8-7).

Levamisole is an ATP hydrolysis inhibitor and as such it was expected that levamisole would lead to an increased concentration of measurable ATP. If any of the observed ADP concentration had been derived from alkaline phosphatase hydrolysis of ATP, it would be expected that a reciprocal decrease in ADP concentration would be observed. However, the concentration of both nucleotides was elevated, raising the possibility that both nucleotides are released in response to metabolic poisoning rather than levamisole-modulated hydrolysis. Instead, the preserved ADP concentration could also be explained by levamisole inhibiting ADP to AMP hydrolysis. Again if extracellular ADP had been derived from hydrolysis of ATP the presence of ARL 67156 would be expected to reduce the observed ADP.

The results however showed that while ATP was significantly elevated during inhibition of extracellular hydrolysis, the ADP concentration was also elevated. While ARL 67156 is reported to inhibit ATP to ADP hydrolysis, it has also been shown inhibit ADP to AMP hydrolysis, thus possibly explaining the ADP elevation [398, 400, 413-420]. The presence of ebselen had a small effect on the extracellular ADP concentration, suggesting that again either the observed ADP arises from mechanisms other than ATP hydrolysis, or that the ebselen-inhibited ecto-enzymes (NDPK) are not a pronounced pathway of extracellular nucleotide 'recycling'.

As means to potentially induce 'full' inhibition of ecto-enzyme modulation on extracellular nucleotide concentrations, cells were subjected to metabolic poisoning in the presence of all three inhibitors, levamisole, ARL 67156 and ebselen. The concentration of extracellular ATP and ADP during metabolic poisoning is illustrated in the absence and presence of the enzyme inhibitors, Figure 8-8.

In the presence of the ecto-enzyme inhibitors a substantial elevation in the extracellular nucleotide concentrations was observed. There was a large and rapid rise in observed ATP up to 20 minutes where the extracellular concentration plateaued at approximately 200 nM, a 333% increase compared to the absence of the inhibitors (Figure 8-8A). The measured ADP concentration was also modulated by the ecto-enzyme inhibitors and over the first 15 minutes showed a parallel increase to ATP, peaking at 9436±1018 nM. However, this does not then level out but appears to be gradually decreasing over the remaining course of the experiment, but still the extracellular concentration was on average 181% greater than during poisoning alone (7624 nM; Figure 8-8B).

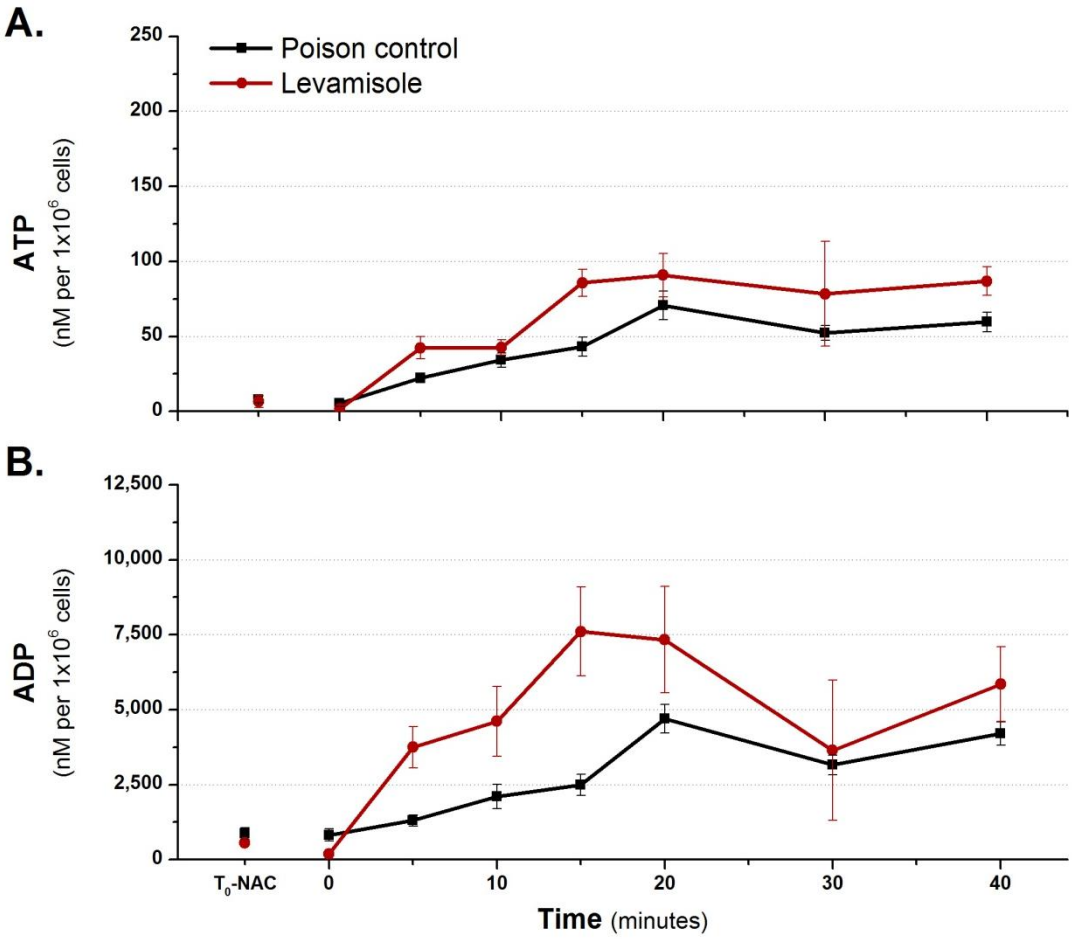

Figure 8-5. Extracellular nucleotide concentration following metabolic poisoning in the presence and absence of the inhibitor levamisole, in EA.hy926 cells.

EA.hy926 cells were cultured in 12 well plates until confluent. Once confluent, nucleotide release in response to poisoning was measured, in HBS, via tube luminometry. The effect of the poison cocktail (4 mM cyanide, 10 mM 2-DG and 5 µM ionomycin) on extracellular nucleotide concentration (A. ATP and B. ADP) was recorded in the presence and absence of 10mM levamisole. The data plotted is the mean of 27 (poison control) and 6 (levamisole) with S.E.M. error bars. T_0-NAC denotes the time zero nil addition control.

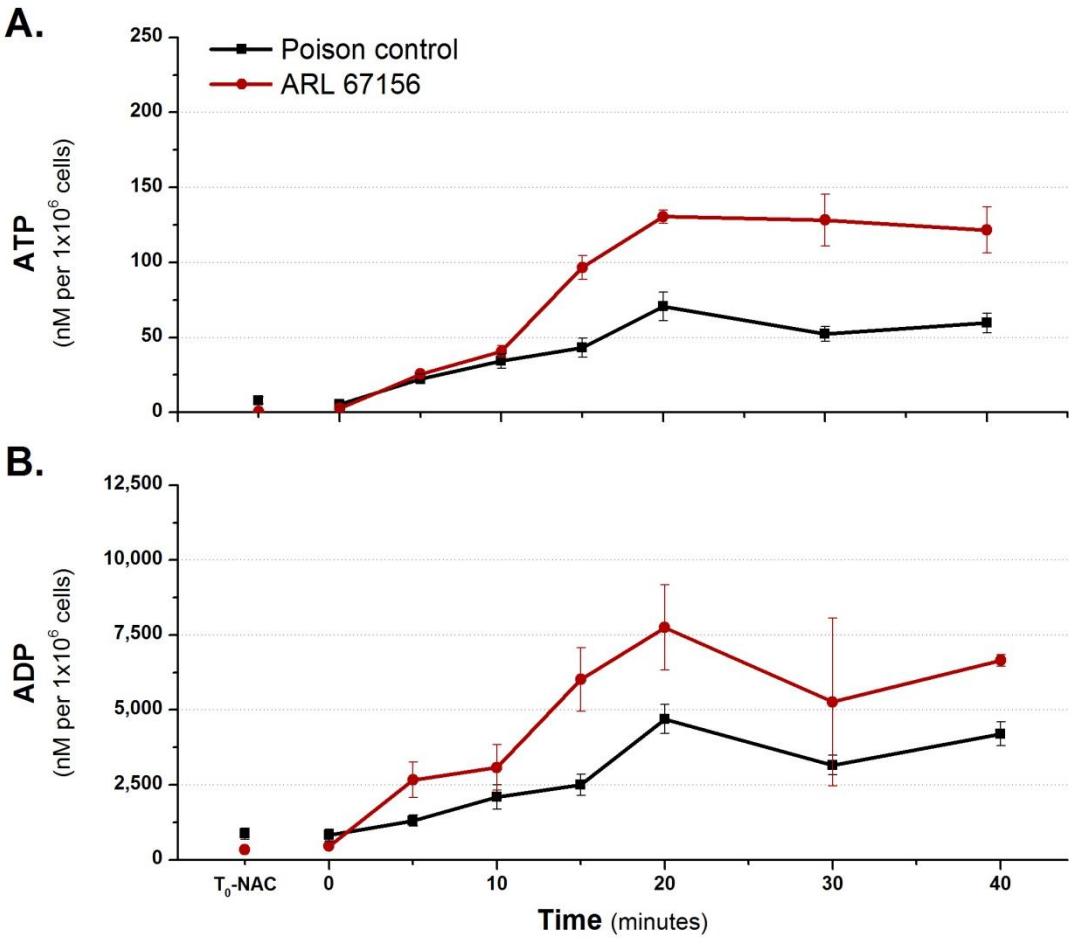

Figure 8-6. Extracellular nucleotide concentration following metabolic poisoning in the presence and absence of the inhibitor ARL 67156, in EA.hy926 cells.

EA.hy926 cells were cultured in 12 well plates until confluent. Once confluent, nucleotide release in response to poisoning was measured, in HBS, via tube luminometry. The effect of the poison cocktail (4 mM cyanide, 10 mM 2-DG and 5 µM ionomycin) on extracellular nucleotide concentration (A. ATP and B. ADP) was recorded in the presence and absence of 100 µM ARL 67156. The data plotted is the mean of 27 (poison control) and 6 (ARL 67156) with S.E.M. error bars. T_0-NAC denotes the time zero nil addition control.

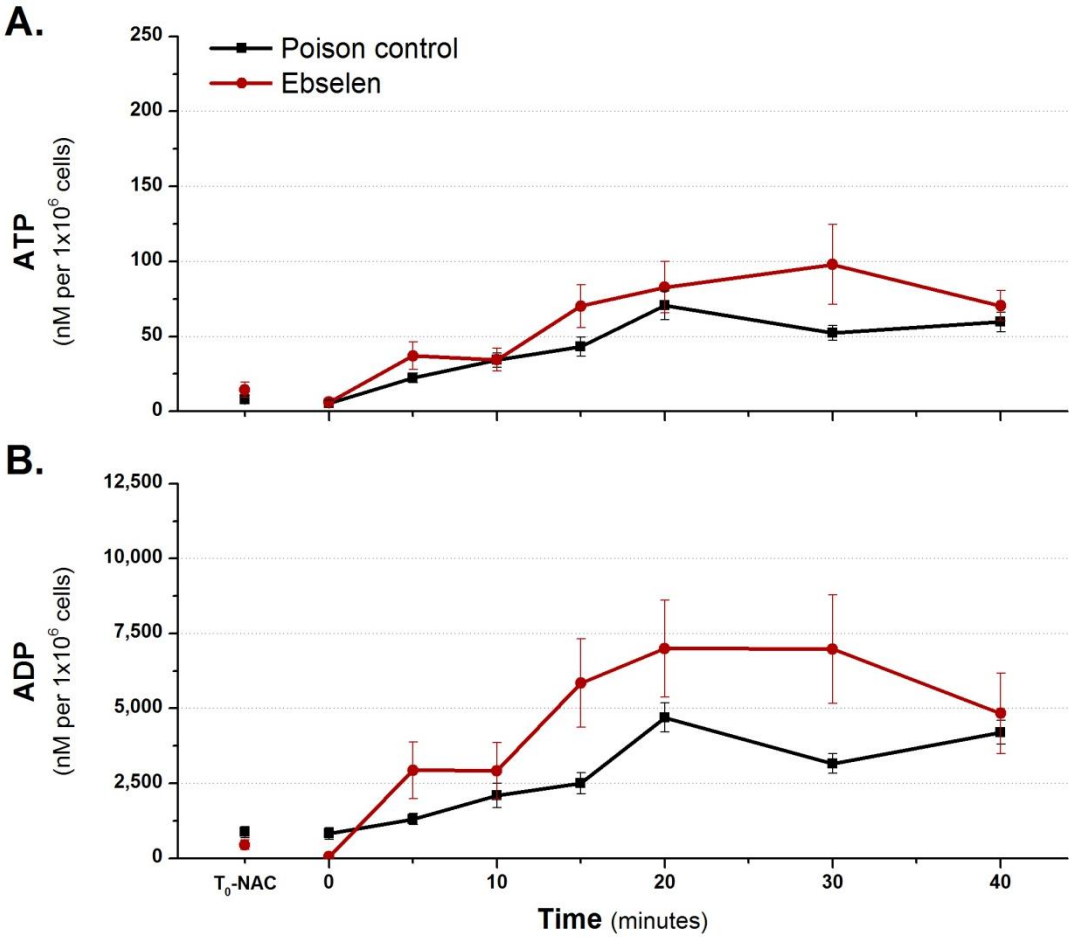

Figure 8-7. Extracellular nucleotide concentration following metabolic poisoning in the presence and absence of the inhibitor ebselen, in EA.hy926 cells.

EA.hy926 cells were cultured in 12 well plates until confluent. Once confluent, nucleotide release in response to poisoning was measured, in HBS, via tube luminometry. The effect of the poison cocktail (4 mM cyanide, 10 mM 2-DG and 5 µM ionomycin) on extracellular nucleotide concentration (A. ATP and B. ADP) was recorded in the presence and absence of 30µM ebselen. The data plotted is the mean of 27 (poison control) and 6 (ebselen) with S.E.M. error bars. T_0-NAC denotes the time zero nil addition control.

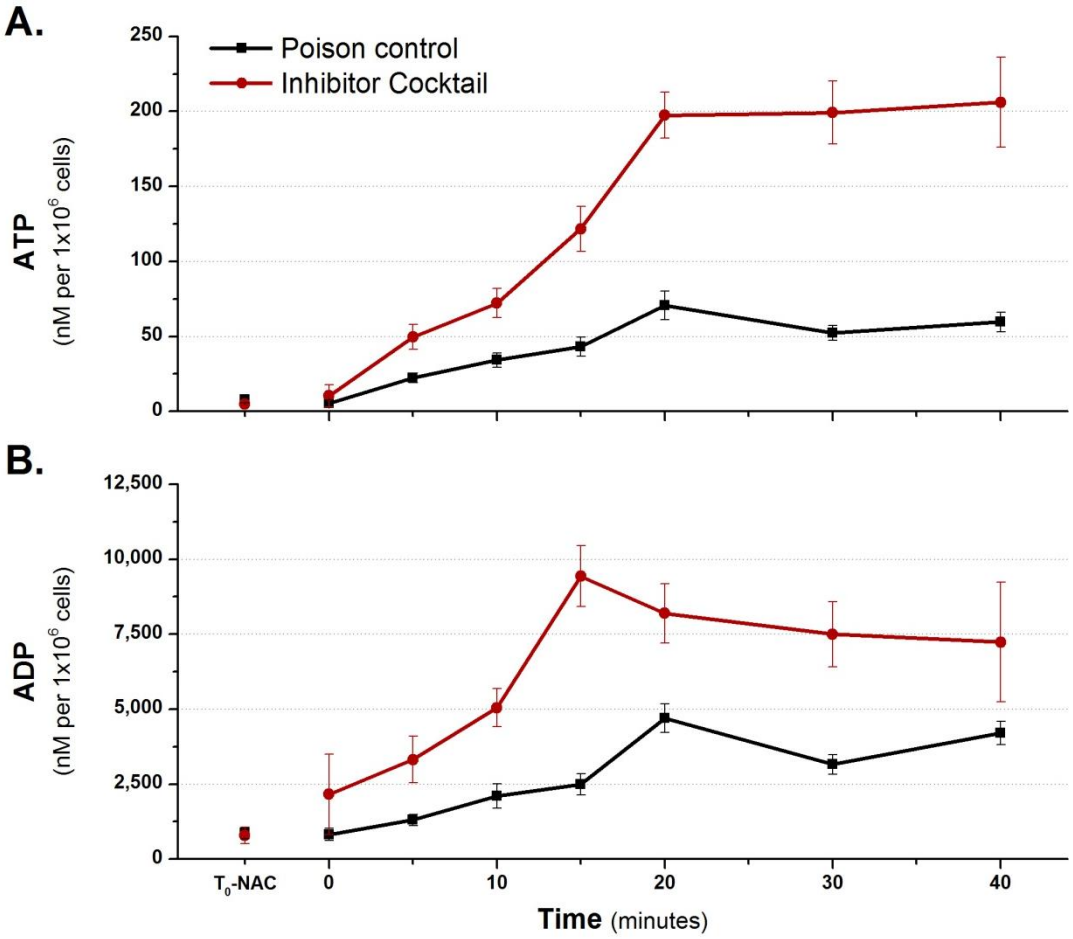

Figure 8-8. Extracellular nucleotide concentration following metabolic poisoning in the presence and absence of the inhibitor cocktail (levamisole, ARL 67156 and ebselen), in EA.hy926 cells.

EA.hy926 cells were cultured in 12 well plates until confluent. Once confluent, nucleotide release in response to poisoning was measured, in HBS, via tube luminometry. The effect of the poison cocktail (4 mM cyanide, 10 mM 2-DG and 5 µM ionomycin) on extracellular nucleotide concentration (A. ATP and B. ADP) was recorded in the presence and absence the inhibitor cocktail (10 mM levamisole, 100µM ARL 67156 and 30 µM ebselen). The data plotted is the mean of 27 (poison control) and 3 (inhibitor cocktail) with S.E.M. error bars. T_0-NAC denotes the time zero nil addition control.

8.6. Cell Permeability

8.6.1. Caspase 3/7

With the observed extracellular ADP not necessarily arising from ecto-enzyme activity mechanisms of release were considered as a source of the nucleotides. Initially the cells permeability was studied using the apoptotic markers caspase 3/7. The caspases are a family of proteases, central to apoptosis but also act as markers for mitochondrial outer membrane permeabilisation [611, 612].

The caspase 3/7 dynamics peaks after 15 minutes of poisoning, coinciding with elevating extracellular ATP concentration, as illustrated in Figure 8-9. The signal appears to diminish at 20 minutes but is again elevated after 30 minutes of poisoning, suggesting that mitochondrial outer membrane permeabilisation and permeability is elevated from about 15 minutes.

8.6.2. Calcein and Propidium iodide staining

As an alternative protocol to measure cell permeability to caspase 3/7, the cells ability to retain calcein and take up PI was investigated during the poisoning protocol, as seen in Figure 8-10. After calcein loading, all living cells exhibited green fluorescence as seen after 0 time in poisoning (Figure 8-10C). Likewise, there was minimal PI staining visible in cells before extended periods of metabolic insult (Figure 8-10F). The cell staining remained near basal levels for the initial 20 minutes of poisoning, before calcein decrease and PI staining is elevated as seen in Figure 8-10A and B, respectively. The calcein and PI staining appears consistent with the observed caspase 3/7 data, suggesting that the cells permeability shifts after 15 to 20 minutes of metabolic poisoning.

Whilst PI uptake has been previously used as an indicator of cell death, it has been shown as a marker of increased cell permeability and the opening of connexin hemichannels [628]. As connexin hemichannels are a proposed mechanism of PI

uptake the cell staining was examined in the presence of the known channel blocker flufenamic acid (FFA) [358].

After 40 minutes in the absence of metabolic poisoning the cells showed calcein retention and minimal PI uptake, whilst decreased calcein and high PI staining is observed in the presence of metabolic poisoning (Figure 8-11A and B and Figure 8-11C and D, respectively). The addition of FFA in combination with metabolic poisoning appeared to have no discernible effect on the cell staining (Figure 8-11E and F). In comparison 5 minutes pre-treatment with EGTA, before the poison and FFA treatment over 40 minutes, the cells calcein staining was dramatically preserved with minimal PI uptake (Figure 8-11G and H).

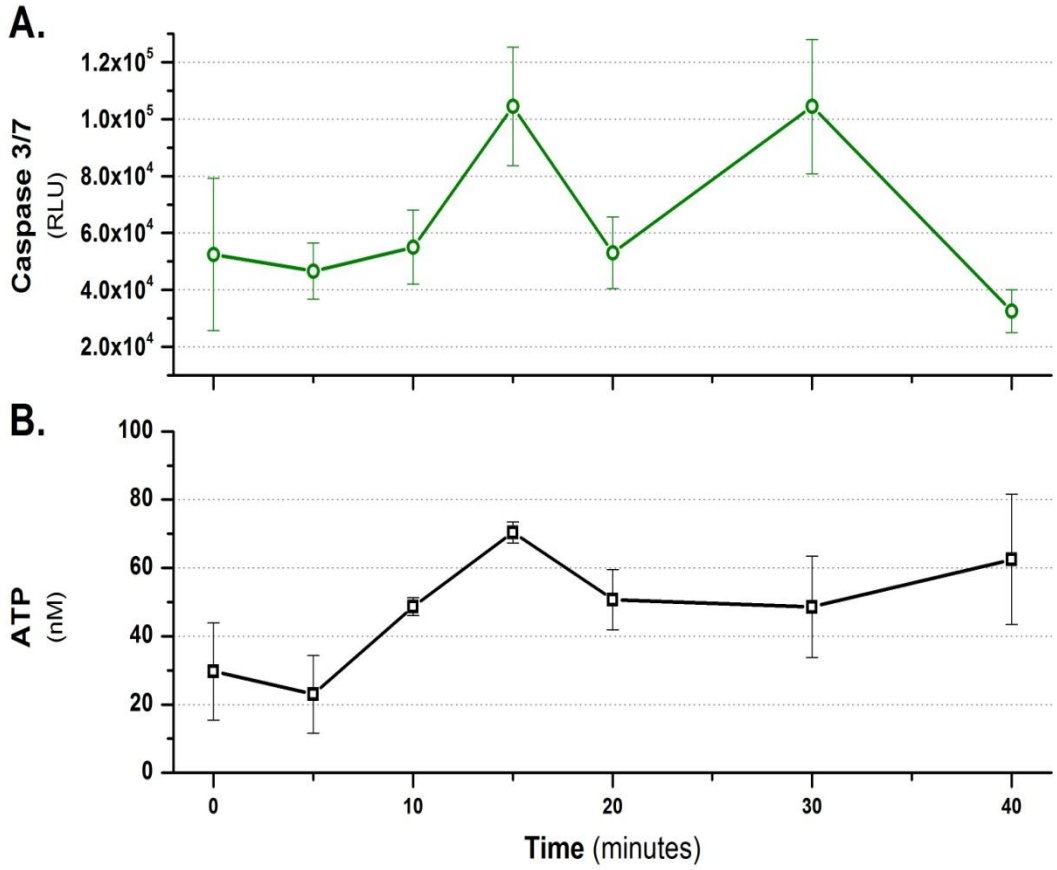

Figure 8-9. Caspase 3/7 dynamics in relation to extracellular ATP concentration following metabolic poisoning, in EA.hy926 cells.

EA.hy926 cells were cultured in 12 well plates until confluent. Once confluent, nucleotide release and caspase 3/7 luminescence was recorded, via tube luminometry, in response to poisoning in HBS. The effect of the poison cocktail (4 mM cyanide, 10 mM 2-DG and 5 µM ionomycin) on A. caspase 3/7 luminescence and B. extracellular ATP concentration. The data plotted is the mean of 3 comparable repeats with S.E.M. error bars.

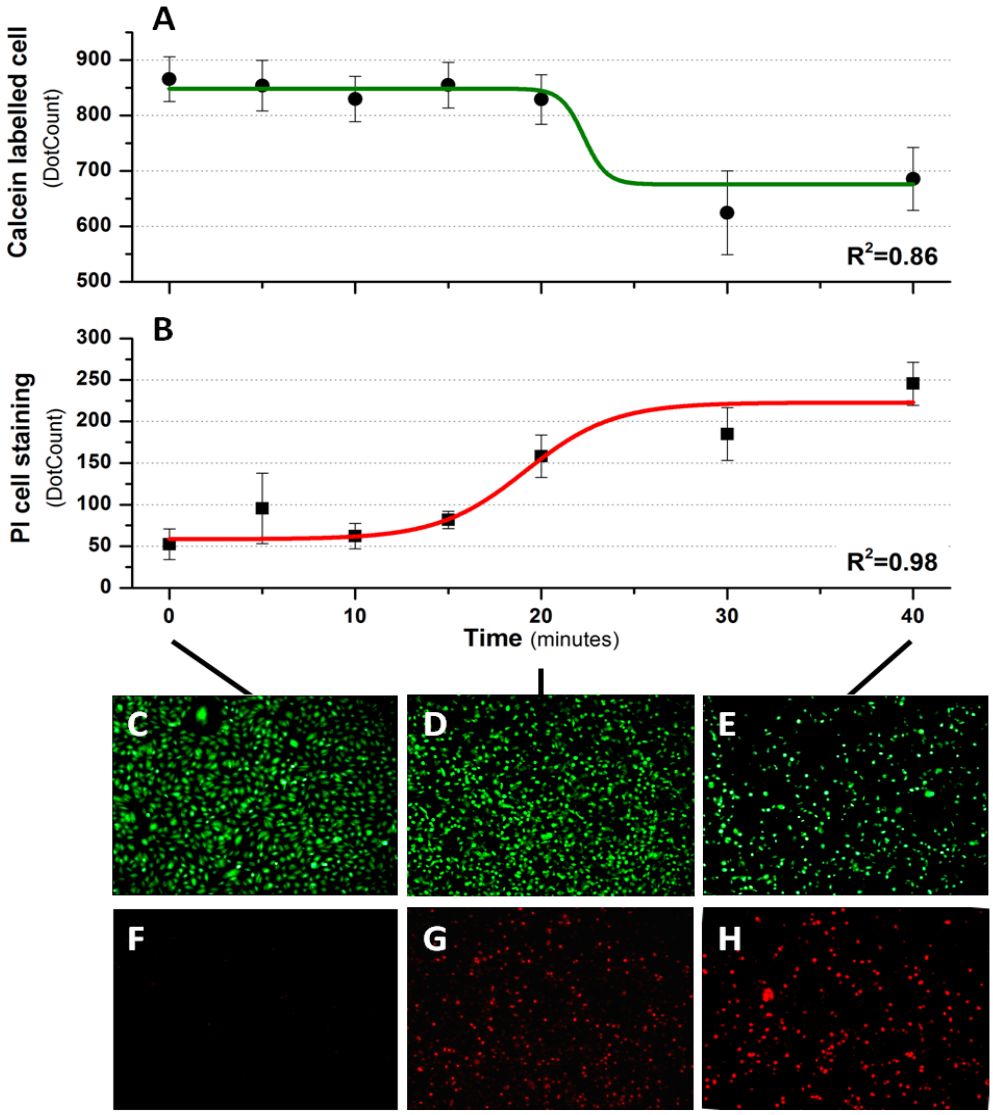

Figure 8-10. Calcein and Propidium Iodide staining during metabolic poisoning over a period of 0 to 40 minutes, in EA.hy926 cells.

EA.hy926 cells were cultured in 12 well plates until confluent. Once confluent, nucleotide release in response to poisoning (4 mM cyanide, 10 mM 2-DG and 5 µM ionomycin) was measured, in HBS containing 150 µM PI. Once the sample were collected the HBS was replaced with 2 µM calcein supplemented HBS. The cells were then imaged. Using a Leica DMIRB microscope calcein and PI were imaged at excitation/emission at 494/517 nm and 535/617 nm, respectively. A. illustrates the calcein dynamics and B. PI during metabolic poisoning over 0 to 40 minutes. Images C to E show typical calcein cell staining and F to H PI, during metabolic poisoning at 0 (C, F), 20 (D, G) and 40 minutes (E, H).

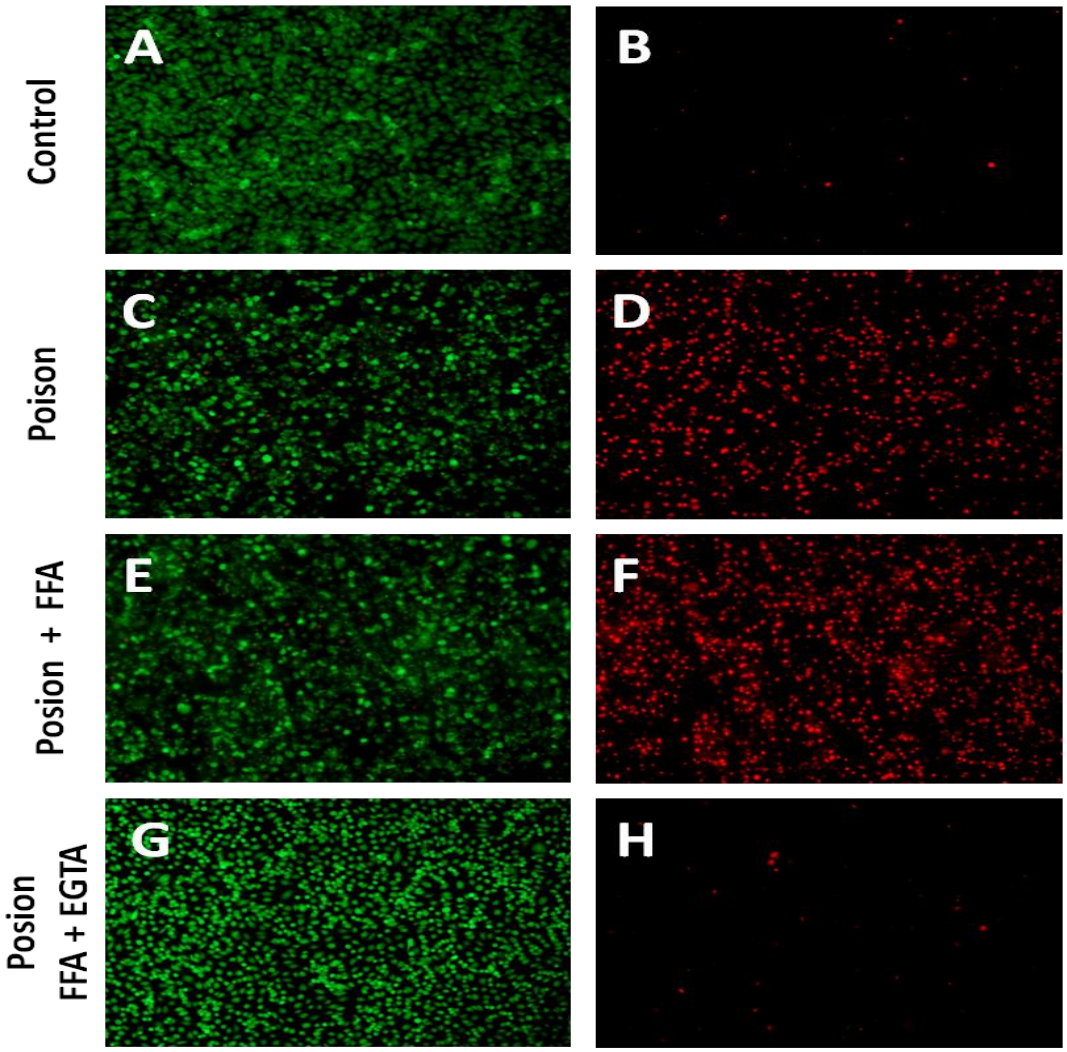

Figure 8-11. Calcein and Propidium Iodide staining after 40 minutes of metabolic poisoning in the presence of flufanamic acid alone and with pretreatment with EGTA, in EA.hy926 cells.

EA.hy926 cells were cultured in 12 well plates until confluent. Once confluent, nucleotide release in response to, A, B) control, C, D) poisoning (4 mM cyanide, 10 mM 2-DG and 5 µM ionomycin), E, F) poisoning in combination with 100 µM FFA and G, H) poisoning in combination with FFA and EGTA pre-treatment; was measured, in HBS containing 150 µM PI. Once the sample were collected the HBS was replaced with 2 µM calcein supplemented HBS. Using a Leica DMIRB microscope calcein (A, C, E and F) and PI (B, D, F and H) were imaged at excitation/emission at 494/517 nm and 535/617 nm, respectively.

8.7. Connexin Hemichannel Release

Connexon hemichannels are a proposed mechanism of nucleotide release as discussed in the introduction (section Nucleotide Release). With modulation of connexin hemichannels exerting such a pronounced effect on calcein and PI staining the channels role on extracellular nucleotide concentration was examined.

Pre-treatment with either EGTA (connexin channel opener) for 5 minutes prior to the 40 minute treatment window or the presence of FFA (channel blocker) showed no modulation of the measured extracellular nucleotide concentration (Figure 8-12). Whilst metabolic poisoning in combination with FFA and EGTA pre-treatment prevented calcein loss and PI uptake there was only a moderate decrease in the initial extracellular nucleotide concentration (0 to 20 minutes, Figure 8-13). It should be noted that pre-treatment with EGTA produced an elevated nucleotide concentration at 0 minutes and so whilst a similar nucleotide concentration were observed, the rate of release over this period had a gradient of 6.4 compared to 9.4 (68%, ATP) and a gradient of 244 compared to 510 (48%, ADP) for poisoning with FFA and EGTA treatment compared to poisoning alone.

The data suggests that whilst the cells' permeability is preserved by the presence of connexin blockers, the extracellular nucleotide concentration is only moderately affected. This suggests that whilst a portion of the measured extracellular ATP and ADP may be derived from connexin release, it does not account for the majority of the observed nucleotide concentration.

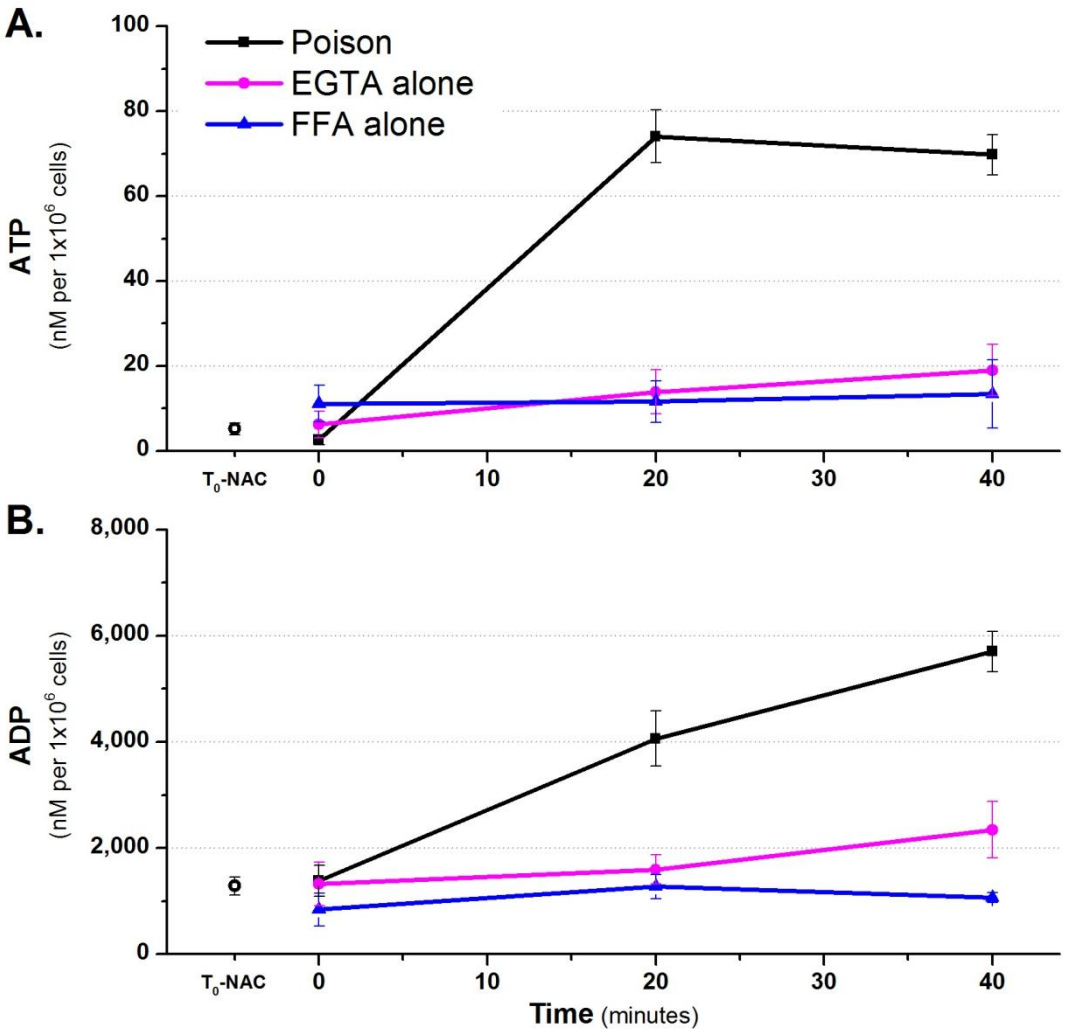

Figure 8-12. Extracellular nucleotide concentration following metabolic poisoning in the presence of FFA and 5 minutes pre treatment with EGTA, in EA.hy926 cells.

EA.hy926 cells were cultured in 12 well plates until confluent. Once confluent, nucleotide release in response to poisoning was measured, in HBS, via tube luminometry. The effect of the poison cocktail (4 mM cyanide, 10 mM 2-DG and 5 µM ionomycin) on extracellular nucleotide concentration (A. ATP and B. ADP) compared to the effect of 5 minutes pre treatment with 10 mM EGTA (pink) or 40 minutes of 100 µM FFA (blue). The data plotted is the mean of 6 repeats with S.E.M. error bars. T_0-NAC denotes the time zero nil addition control.

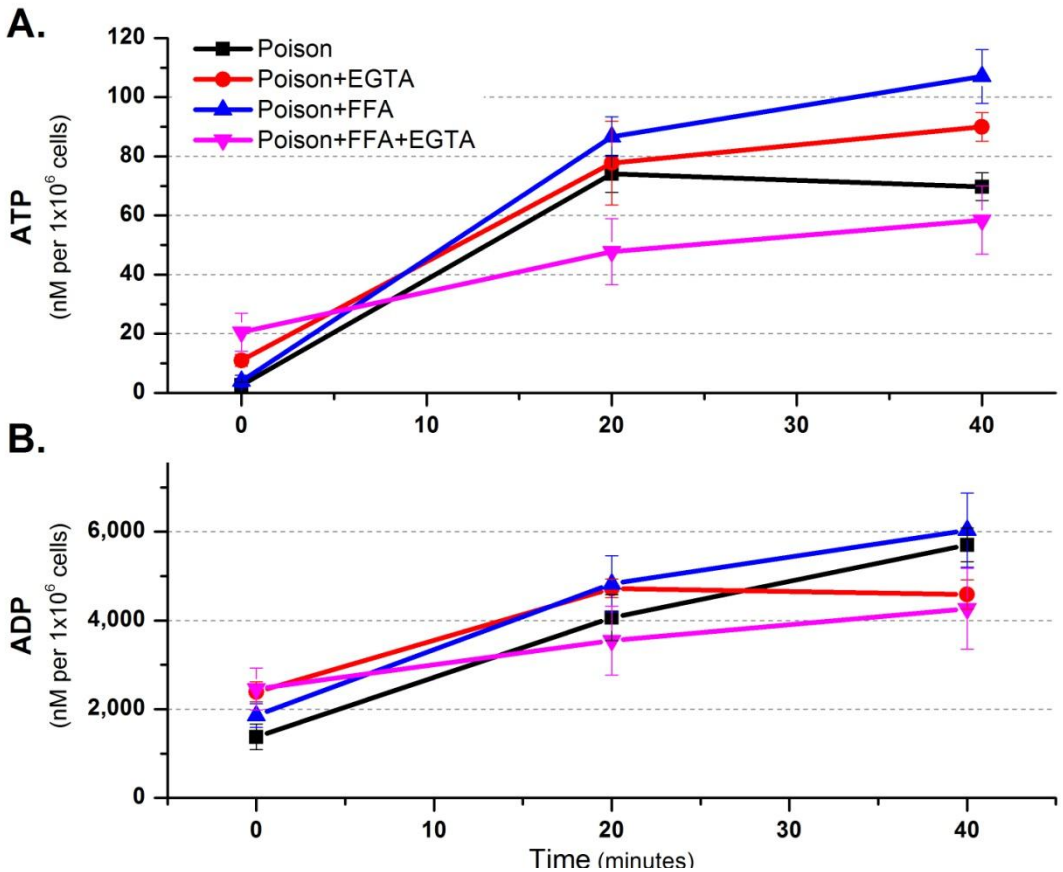

Figure 8-13. Extracellular nucleotide concentration (A. ATP and B. ADP) following metabolic poisoning in the presence and absence of EGTA, FFA alone and in combination, in EA.hy926 cells.

EA.hy926 cells were cultured in 12 well plates until confluent. Once confluent, nucleotide release in response to poisoning was measured, in HBS, via tube luminometry. The effect of the poison cocktail (4 mM cyanide, 10 mM 2-DG and 5 µM ionomycin) on extracellular nucleotide concentration (A. ATP and B. ADP) in the presence of 10 mM EGTA (5 minutes pre-treatment, red), 100 µM FFA (blue) and FFA following EGTA pre-treatment (pink). The data plotted is the mean of 6 repeats with S.E.M. error bars. T_0-NAC denotes the time zero nil addition control.

8.8. $P2X_7$ Release

Since the modulation of the connexin hemichannels appeared to have minimal effect of the observed extracellular nucleotide concretion, the role of the $P2X_7$ channel was examined.

To assess the potential of the $P2X_7$ channel being linked to release ofextracellular nucleotides, the inhibitor oATP was used [608-610]. Oxidised ATP appears to have a marked effect on the measurable ATP and ADP, notably over the first 20 minutes of the poisoning protocol. $P2X_7$ channel inhibition with oATP appears to reduce the extracellular ATP and ADP concentration by 53±16% and 40±32%, respectively.

The data suggest that there is a definite aspect of extracellular ATP and ADP that arises from an oATP inhibited process. Whilst the most likely target and channel is $P2X_7$, like all 'selective' inhibitors it now appears to be less selective than assumed [629]. Consequently, the findings must be taken as preliminary until further studies can confirm the mechanism.

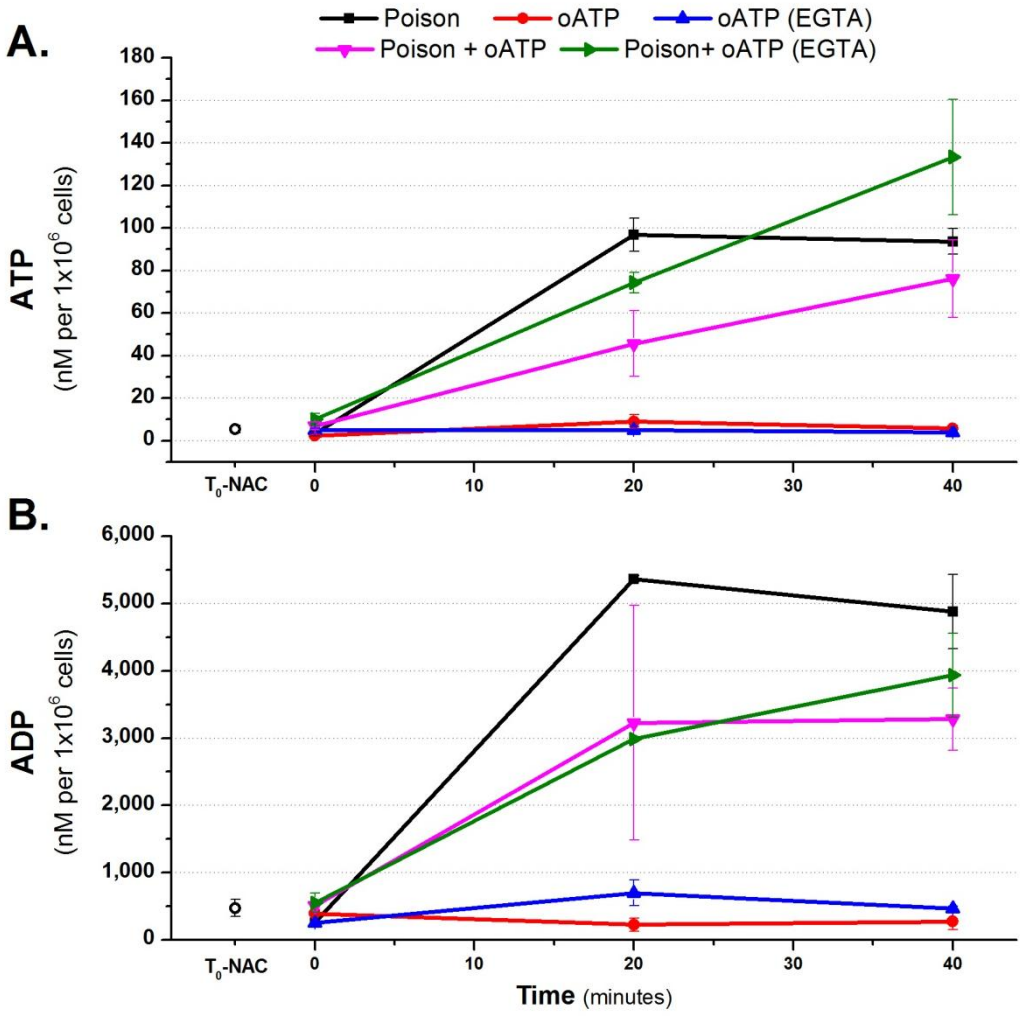

Figure 8-14. Extracellular nucleotide concentration (A. ATP and B. ADP) following metabolic poisoning in the presence and absence of oxidised ATP (oATP), in EA.hy926 cells.

EA.hy926 cells were cultured in 12 well plates until confluent. Once confluent, nucleotide release in response to poisoning was measured, in HBS, via tube luminometry. The effect of the poison cocktail (4 mM cyanide, 10 mM 2-DG and 5 µM ionomycin) on extracellular nucleotide concentration (A. ATP and B. ADP) in the presence of 100 µM oATP, oATP and EGTA pre-treatment and oATP in combination with poisoning with or without EGTA pre-treatment. The data plotted is the mean of 6 repeats with S.E.M. error bars. T_0-NAC denotes the time zero nil addition control.

8.9. Conclusion

Calibration curves were constructed from serial ATP and ADP and used to convert the measured RLU to nucleotide concentrations. The measured extracellular ATP and ADP was in the range of 0 to 40 nM and 0 to 3000 nM, respectively.

To calibrate ATP the known concentrations were plotted against the observed luminescence and a Boltzmann curve of best fit applied. This allowed the data collected to be converted into nanomolar ATP using Equation 6-2. Calculating ADP was more difficult, as it was measured after conversion to ATP. Consequently the serial ADP dilutions were plotted against ATP equivalence rather than using counts directly derived from ADP on the ATP calibration curve. Once converted to their ATP equivalence, the ADP sample concentrations were determined. The ATP equivalence and second calibration curve were used to account for inefficiency with ADP and ATP conversion.

To validate the observed concentrations gained from tube luminometry the nucleotide concentrations were confirmed using HPLC measurement (Figure 8-4). HPLC has been shown to measure ATP and ADP in the picomolar range [334, 614, 630]. Using a Hypersil BDS C18 column, the system afforded sensitivity down to 100 nM. As such HPLC did not provided direct ATP values to compare against tube luminometry results, data published by Lazarowski *et al.* (2000) recorded the extracellular ATP concentration between 0-100 nM, in comparable cells (16HBE14o$^-$ human bronchial epithelial cells and ECV-304 human bladder epithelial cells) [319, 631]. The results gained from HPLC measurements were directly comparable to those seen using luminometry confirming an ADP concentration in EA.hy926 cells in the micro-molar range. This concentration was also in-line with data published by Lazarowski *et al.* (2000), where at the cell surface the ADP concentration was equal to or greater than ATP [319]. Despite lacking the required sensitivity to confirm the observed ATP concentration, HPLC data also measured micro-molar extracellular ADP

8.9.1. Metabolic Poisoning

Cyanide and 2-DG are well documented CIH agents however the addition of ionomycin was required to further stress the cells, promoting nucleotide release [531-534]. Ionomycin can result in $P2X_7$ channel ATP release when used at concentrations above 10 μM, however the ionomycin and CIH induced nucleotide accumulation was more than the additive effects on the metabolic stressors [540].

8.9.2. Cell Permeability

During the 40 minutes of poisoning the overall calcein signal decreased whilst inversely the PI signal increases. Calcein and PI are a measures of cell permeability and not cell lysis [628]. Comparing the cell permeability the nucleotide concentration preceded the shift in calcein and PI staining, as after 10 minutes there was no change in calcein and PI permeability but elevated extracellular nucleotide concentration. The modulation of dye permeability in the presence of FFA is suggestive of a FFA-sensitive mechanism responsible for extracellular nucleotide accumulation.

8.9.3. Mechanism of nucleotide accumulation

With the extracellular nucleotide concentration, notably ADP, increasing during metabolic stressing, the means of the observed accumulation was examined. If extracellular ADP derived from ATP hydrolysis, ecto-enzyme inhibitors would induce a dramatic elevation in observed ATP and reciprocal decrease in ADP.

Levamisole, an inhibitor of ALP, elevated the observed extracellular ATP and ADP [398, 400, 405, 413-420, 423-425]. At the concentration used ebselen has been shown to induce 60% inhibition of ATP hydrolysis but also modulate NDPK activity, as such modulating both hydrolysis and synthesis [410]. With such a large ADP concentration it is unsurprising that the ATP is elevated, as either hydrolysis is inhibited or ebselen has minimal synthesis inhibition on the significant ADP concentration. In the presence of all inhibitors in combination, there was a dramatic elevation of both extracellular nucleotide concentrations. This data coupled with

the large concentration difference (100 fold) between the two nucleotides, it would be energetically difficult for hydrolysis to be the pathway for accumulation, against a large concentration gradient of product. Given the relative concentration of ATP and ADP, ATP synthesis might be expected. If this was the case this process is not inhibited by ebselen since the agent increases both ATP and ADP

The modulation of dye permeability in the presence of FFA (following 5 minutes EGTA pre-treatment) is suggestive of a FFA-sensitive mechanism responsible for extracellular nucleotide accumulation.

The extracellular nucleotide concentration increases in parallel with cell permeability, seen by the respective changes in calcein and PI staining (Figure 8-10). The dye permeability is related to FFA modulated hemi-channels, as the presence of the FFA (maintains staining in poisoned cells comparable to control cells [362, 364]. However, the hemi-channel antagonist FFA had minimal effect on the extracellular nucleotide concentration [408]. Alternatively to hemi-channels, $P2X_7$ channel have been proposed as a nucleotide release pathway, with activation opening ligand-gated ion channel [632-634]. The inhibitor oATP decreased the observed extracellular nucleotide concentrations during the first 20 minutes of metabolic stressing [608].

9. Results - Cardiomyocytes

9.1. Introduction

Ischaemia and ischaemic preconditioning is relevant to cardiac tissue and nucleotide release from the heart is likely to dominate the cardiac vascular pharmacology. To further study the role of $\Delta\psi_m$ in IPC and nucleotide release during metabolic stressing, a CM model that offers a robust system and convenient isolation would be ideal. In striving to generate a viable cell model; CM morphology, immunofluorescence and the presence of spontaneous contractile activity was sought.

Cultured CM cell lines have many advantages over acutely isolated myocytes preparations including, versatility, economy and convenience but are not suited to longer term studies [493, 596]. Alternatively primary CM cultures are more physiologically relevant both structurally and functionally but they can be expensive and isolation procedures are often complex [446-448, 452, 466, 469-475, 479, 481, 597, 598].

In attempting to generate a working CM cell model the HL-1 cell line and primary chick CMs were examined. The HL-1 cell line has been shown to maintain CM phenotype whilst displaying spontaneous contractile activity and have been used in hypoxic studies [472, 475]. With a short embryonic phase and relatively low costs, primary chick CMs offer several advantages over cell lines allowing the study of cardiac physiology, pharmacology and metabolic parameters [443-445].

9.2. Immunofluorescence Controls

Cardiomyocyte specific antibodies were used to identify cells in a primary culture exhibiting a CM-like phenotype. To confirm the validity of the selected antibodies to Troponin T, sarcomeric α-actinin and MF-20, were initially visualised with immunofluorescence labelling using Swiss 3T3 fibroblasts, as a negative control (Figure 9-1) and E8 chick heart sections, as a positive control (Figure 9-2 to Figure 9-4).

9.2.1. Negative Control

These initial experiments also verified that the secondary antibodies (anti-rabbit and anti-mouse Alexa Fluor®) did not exhibit any non-specific cross reactivity or subsequent fluorescence's in the absence of primary antibodies (Figure 9-1A to D). Panels B and D showed the visible staining of mitochondria and cellular nuclei (MitoTracker Red® and DAPI), whilst in panels A and C there was observed immunofluorescence staining.

Pure CM cultures would be an ideal working cell model, as previously discussed, the presence of fibroblasts are required to support CM growth and phenotype [452, 453]. Swiss 3T3 fibroblasts were used as negative controls to ensure the selected markers did not show non-specific labelling (Figure 9-1 Frames E to J) [452, 453].

9.2.2. Positive Control

To confirm antibody specificity and CM marker efficacy, chick heart sections were used as a positive control. Immunofluorescence labelling allowed precise visualisation of any organised cardiac structures (Figure 9-2 and Figure 9-3, respectively). The troponin T antibody ubiquitously stained the isolated heart sections, whilst the sarcomeric α-actinin and MF-20 antibodies offered more distinct staining pattern and as seen at higher magnification (Figure 9-4) allowed the visualisation of the characteristic cardiac substructure (Z-banding and myosin thick filament).

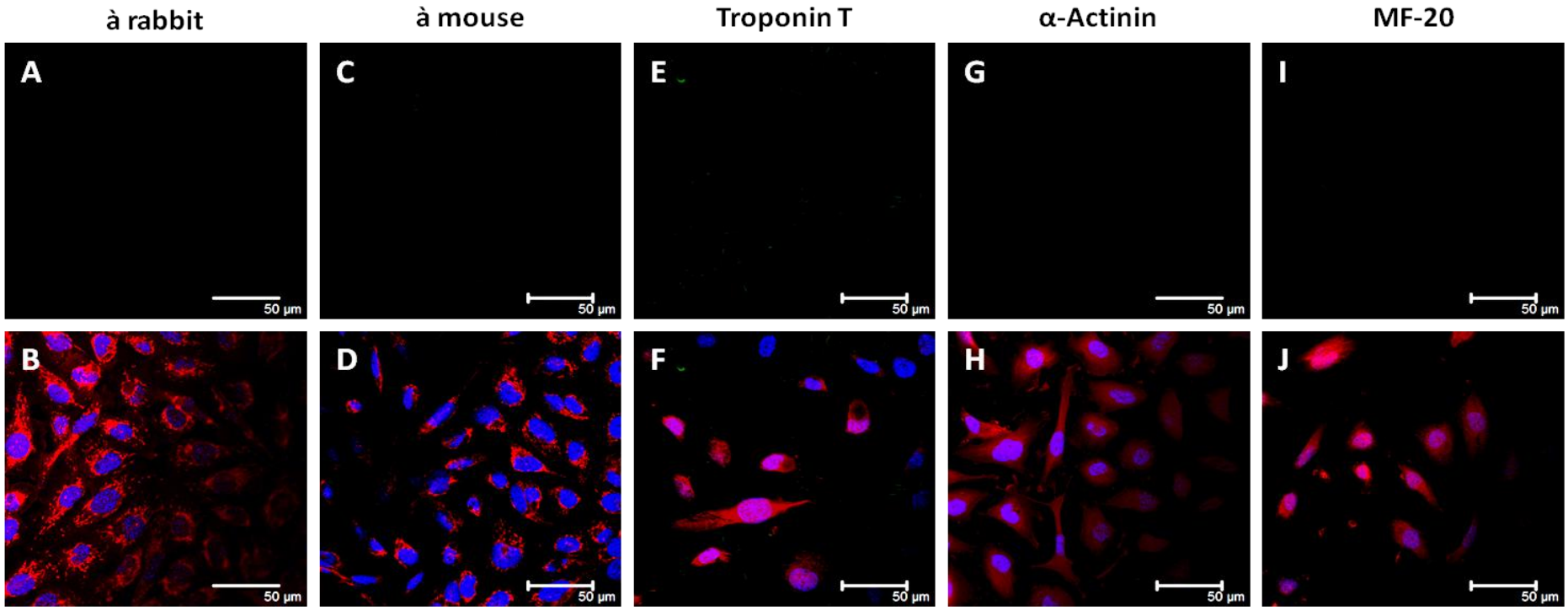

Figure 9-1. Negative control cardiomyocyte immunofluorescence staining in Swiss 3T3 cells.

Swiss 3T3 cells were cultured on 16mm diameter glass coverslips, as described in the methods. Once confluent the cells were loaded with MitoTracker® Red, prior to PFA fixation, as described in the methods. Swiss 3T3 cells were labelled with: anti rabbit (A), anti mouse (C), Troponin T (E), sarcomeric α-actinin (G) , MF-20 (I) and MitoTracker Red® and DAPI (B, D, F, H and J). The tissue was mounted using Moviol containing DAPI and visualised using a Leica SP2 AOBS laser scanning confocal microscope and MaiTai multiphoton system.

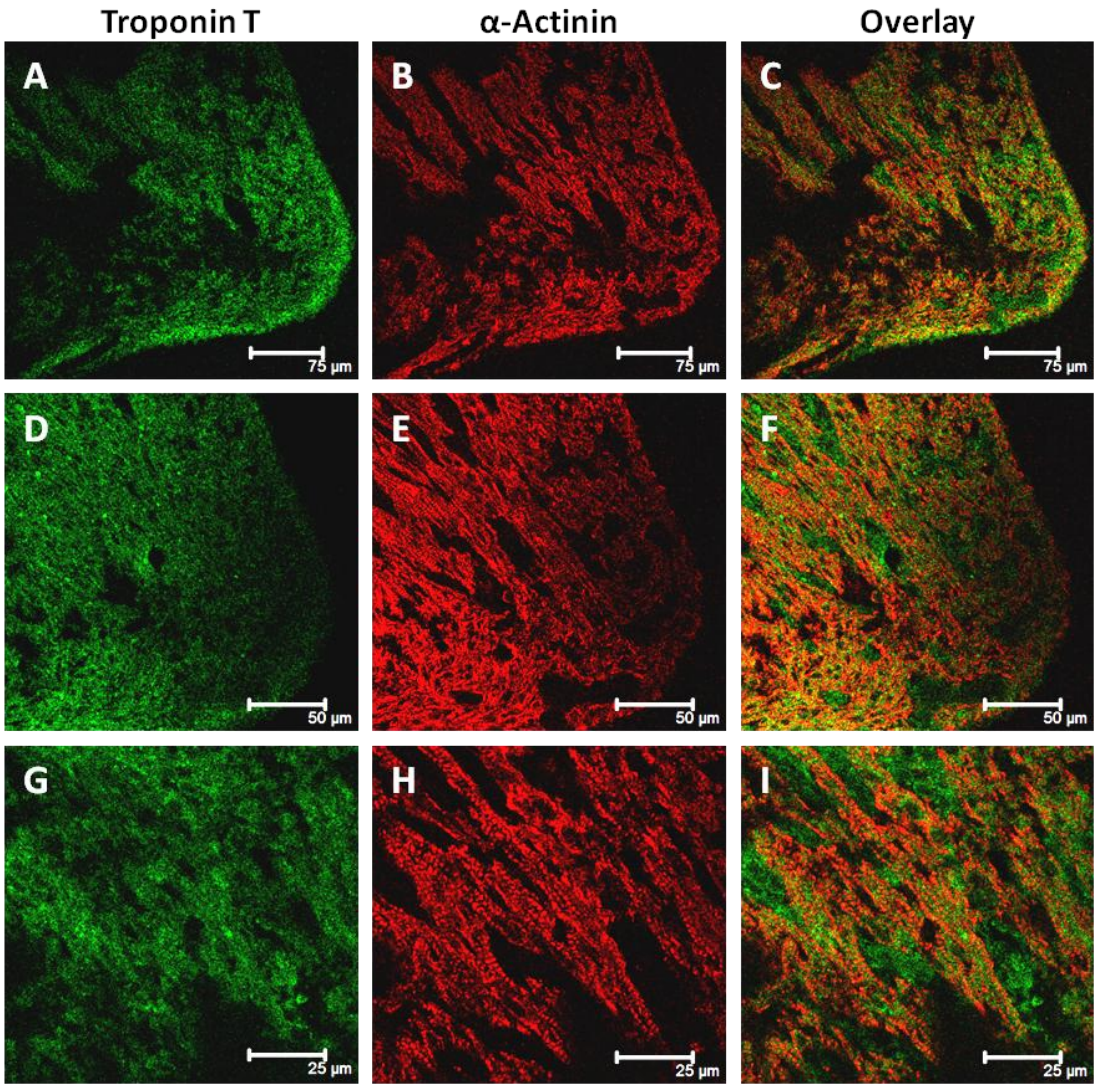

Figure 9-2. Positive cardiomyocyte control immunofluorescence staining (Troponin T and sarcomeric α-actinin) in chick heart section.

Immunofluorescence of cryostat sectioned E8 chick hearts were isolated and fixed in isopropanol. The tissue was stained with: Troponin T (A,D and G), sarcomeric α-actinin (B,E and H) and as an overlay (C,F and I); and shown as enlargement of the same sections (A-C, D-F and G-I). The tissue was mounted using Moviol containing DAPI and visualised using a Leica SP2 AOBS laser scanning confocal microscope and MaiTai multiphoton system.

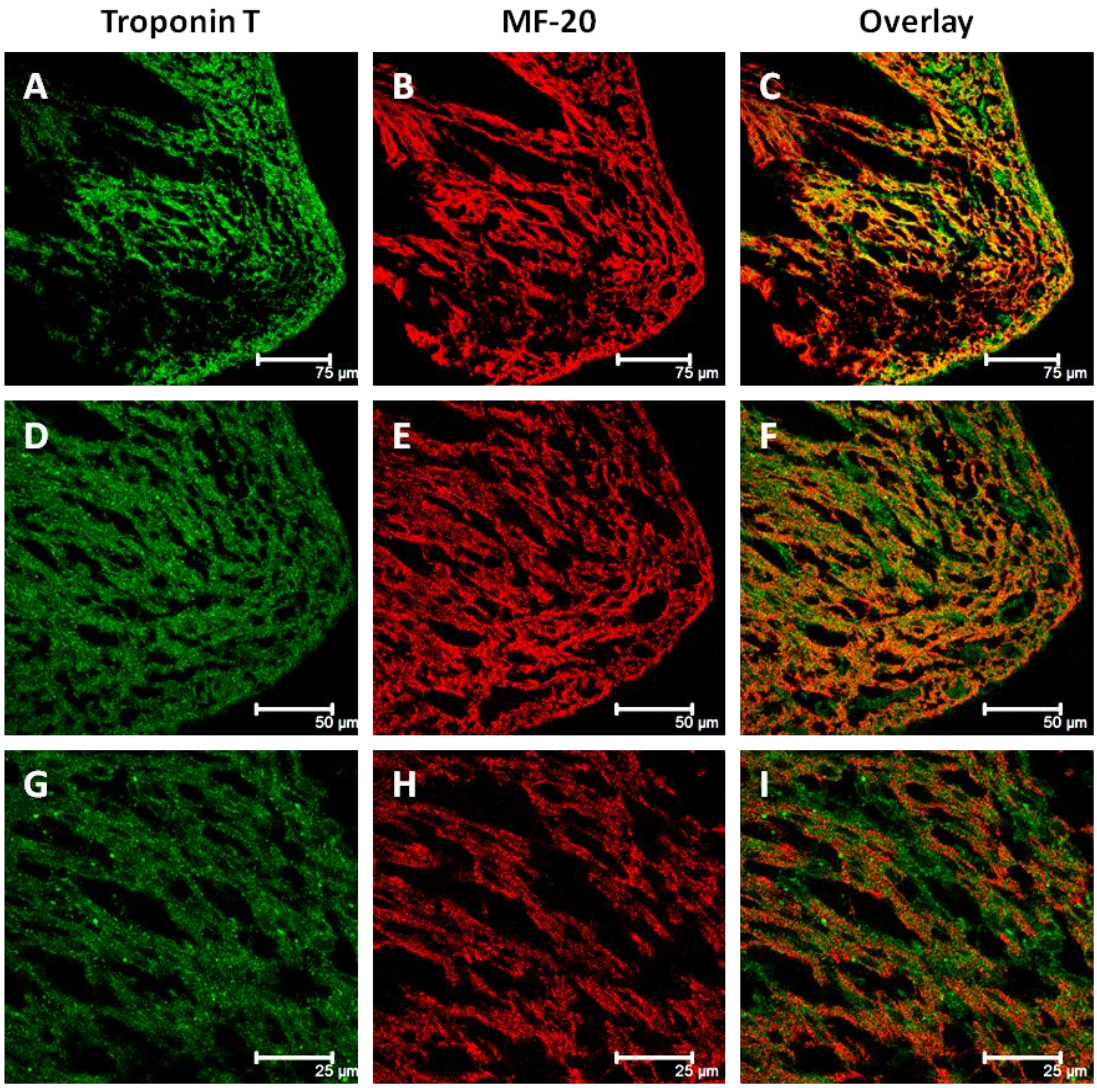

Figure 9-3. Positive cardiomyocyte control immunofluorescence staining (Troponin T and MF-20) in chick heart section.

Immunofluorescence of cryostat sectioned E8 chick hearts were isolated and fixed in isopropanol. The tissue was stained with: Troponin T (A,D and G), MF-20 (B,E and H) and as an overlay (C,F and I); and shown as enlargement of the same sections (A-C, D-F and G-I). The tissue was mounted using Moviol containing DAPI and visualised using a Leica SP2 AOBS laser scanning confocal microscope and MaiTai multiphoton system.

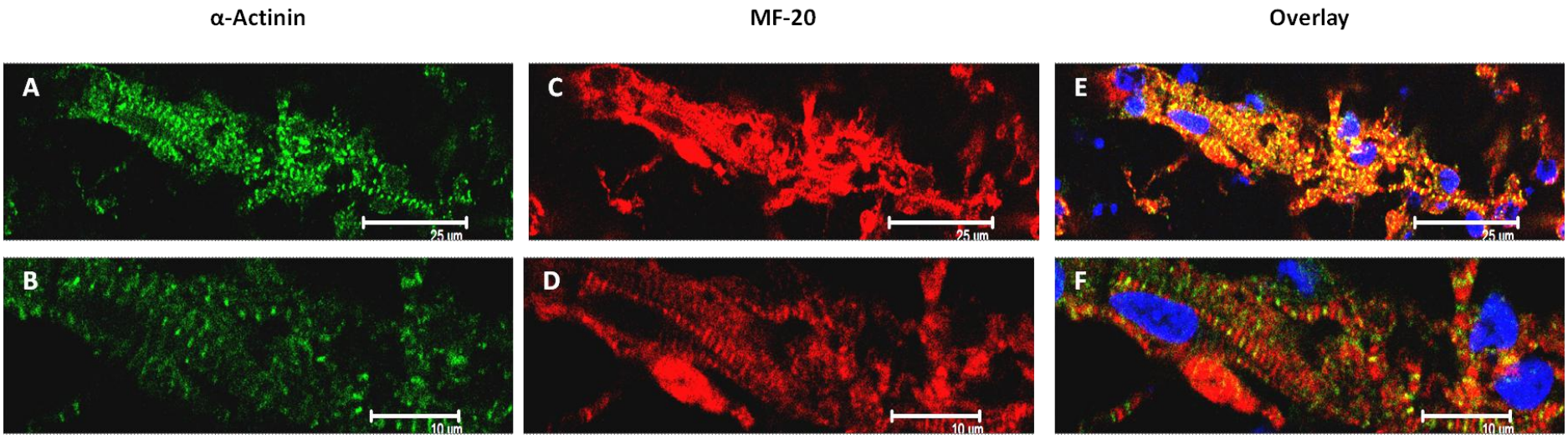

Figure 9-4. Positive cardiomyocyte control immunofluorescence staining (sarcomeric α-actinin and MF-20) in chick heart section.

Immunofluorescence of cryostat sectioned E8 chick hearts were isolated and fixed in isopropanol. The tissue was stained with: sarcomeric α-actinin (A, B), MF-20 (C, D) and as an overlay (E, F); and shown as enlargement of the same sections (A, C ,E and B, D, F). The tissue was mounted using Moviol containing DAPI and visualised using a Leica SP2 AOBS laser scanning confocal microscope and MaiTai multiphoton system.

9.3. HL-1 Cardiomyocytes

When investigating HL-1 CM cell line as a potential myocyte model, the recommended culture protocols and media requirements were used. The presence of CM markers was investigated using CM specific antibodies. Claycomb *et al.* (1998) reported that the maintenance of the CM phenotype required continuous culture in Claycomb Media, whilst they could be maintained for up to 72 hours in basic culture media [472, 475].

9.3.1. Morphology

The typical cell morphology after 72 hours in culture under the different conditions, are presented in Figure 9-5. The cell density of HL-1 cells in DMEM supplemented cultures was much lower in comparison to Claycomb medium. The HL-1 cells that were cultured in Claycomb media showed a near 100% confluent population, whilst those maintained in supplemented DMEM were still less than 50% confluent. In conjunction with the loss of proliferation and resulting lower cell numbers, the appearance of large and disperse hypertrophic cells were observed in the absence of Claycomb media, suggesting Claycomb media is essential.

9.3.2. Immunofluorescence

The HL-1 cells initially exhibited some contractile activity, but in Claycomb media the cells are in the constant presence of 100 µM NE. The cells displayed the typical morphology of immature myocytes.

When maintained in continuous culture the contractile activity was quickly lost and to investigate the retention of a cardiomyocyte phenotype the presence of the CM markers was examined, using the CM markers validated above. MitoTracker® and DAPI staining confirmed the presence of viable and confluent cell populations and was used as controls when examining the CM markers. Despite the strict adhesion to the Claycomb protocol, the cultured HL-1 cells showed no immunofluorescence labelling in the presence of any of the CM antibodies, as seen in Figure 9-6A to C.

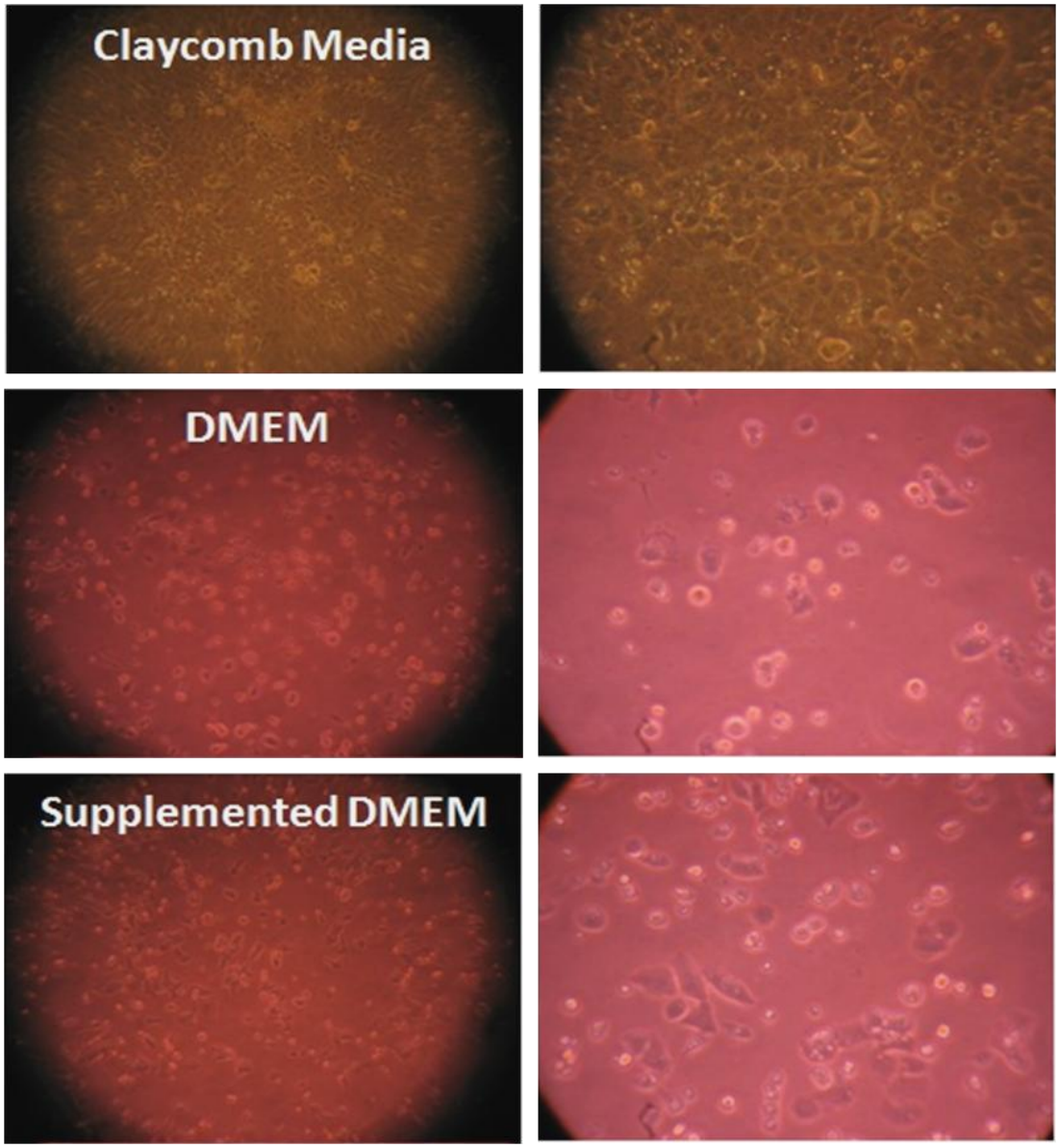

Figure 9-5. Culture media comparison, showing the requirement for Claycomb media in HL-1 cell culture.

HL-1 cells were seeded at ¼ dilution and cultured on fibronectin/gelatine coated, 6 well plates. The cell cultures were maintained in complete claycomb media, DMEM (10% FCS, 1% P/S) and Supplemented DMEM (10% FCS, 1% P/S, 1% L-Glutamine and 1% Noradrenaline). The cells were feed daily and maintained for 72 hours, monitored every 12 hours, with an inverted Nikon Diaphot microscope, 40x objective and imaged.

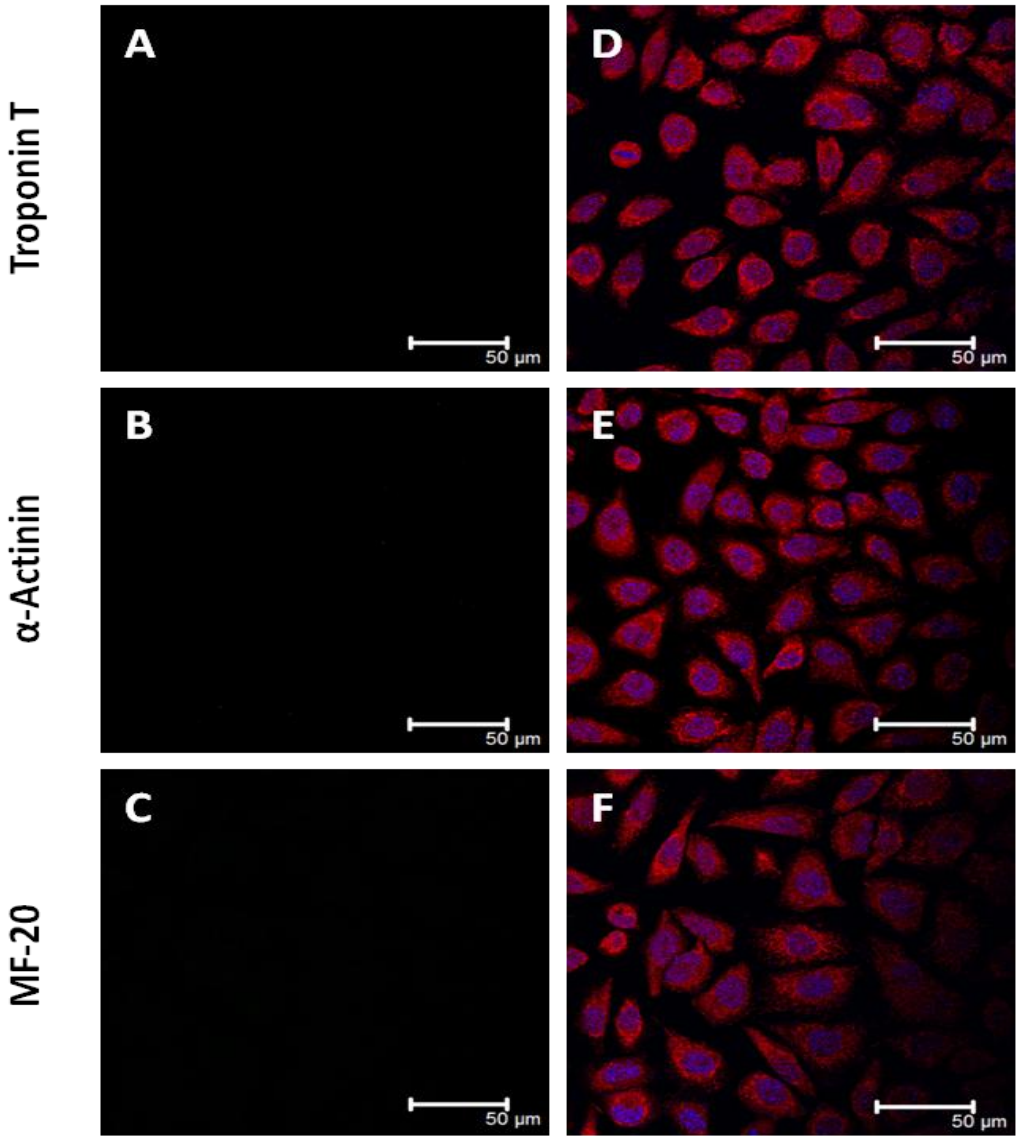

Figure 9-6. Cardiomyocyte conformation using immunofluorescence staining (sarcomeric α-actinin and MF-20) in HL-1 cells.

HL-1 cells were cultured as described in the methods and once confluent loaded with MitoTracker® before being PFA fixed and immunofluorescence labelled for CM markers: Troponin T (A, D), sarcomeric α-actinin (B, E) and MF-20 (C, F) in the absence and presence of MitoTracker® and DAPI. The slides were mounted using Moviol containing DAPI and visualised using a Leica SP2 AOBS laser scanning confocal microscope and MaiTai multiphoton system.

9.4. Primary Cardiomyocytes

Since HL-1 cells did not appear to maintain their CM morphology or spontaneous contractile activity, primary CMs were isolated from chick embryos. Using a technique adapted from Laugwitz *et al.*, isolated primary cardiomyocytes were maintained in culture for periods [494, 498, 600].

Confirmation of CM in the culture was established initially by observation of typical CM morphology (the formation of thick, highly refractive cells, either round or spindle shaped, uni-nuclated cells with a finely granular cytoplasm) alongside the tell-tale spontaneous contractile activity (Figure 9-7) [487-490].The cells formed a monolayer with the appearance of 'myoball' type beating structure [635, 636]. Conformation of CMs being cultured was supported spontaneous contractile activity, as illustrated in relaxed (Figure 9-7B) and contracted (Figure 9-7C) states.

Preliminary observations were indicative of a CM population. The same cardiac specific antibodies for Troponin T, sarcomeric α-actinin and MF-20 (Figure 9-2, 0-3 and 0-4) that were used above in the intact tissue were used here on the cultured cells. The labelling observed, in Figure 9-8 and Figure 9-9, shows distinctive and high immunofluorescence patterns, confirming the presence of CMs with contractile apparatus.[459, 494-497]. At higher magnifications, the highly ordered actin filaments and sarcomeric structure of CMs can be clearly seen [494, 495, 498-500].

The results confirm that the isolation and culture technique can be used to produce viable cultured CMs with contractile activity.

9.5. Cardiomyocyte Culture Purity

With a confirmed CM presence, via the appearance of spontaneous contractile activity, morphology and immunofluorescence labelling, the cell population and proportion of CM compared to non-CMs was examined. The ubiquitous cell marker MitoTracker® (red) stained the entire population, whilst cells expressing CM phenotype were labelled with sarcomeric α-actinin or MF-20 (green). The

immunofluorescence staining shows the appearance of CM aggregating to form ‘myoballs’. These ‘myoballs’ were the predominant site of cardiac activity (Figure 9-10).

The labelling shows that the cultured cells do not form a homogenous population but a heterogeneous culture of CM cells, expressing the sarcomeric α-actinin substructure, along with non-CMs. The alternative cells may be immature CMs, not yet expressing CM markers or fibroblasts, as suggested by their elongated shape and adhesion to the culture surface (Figure 9-10C).

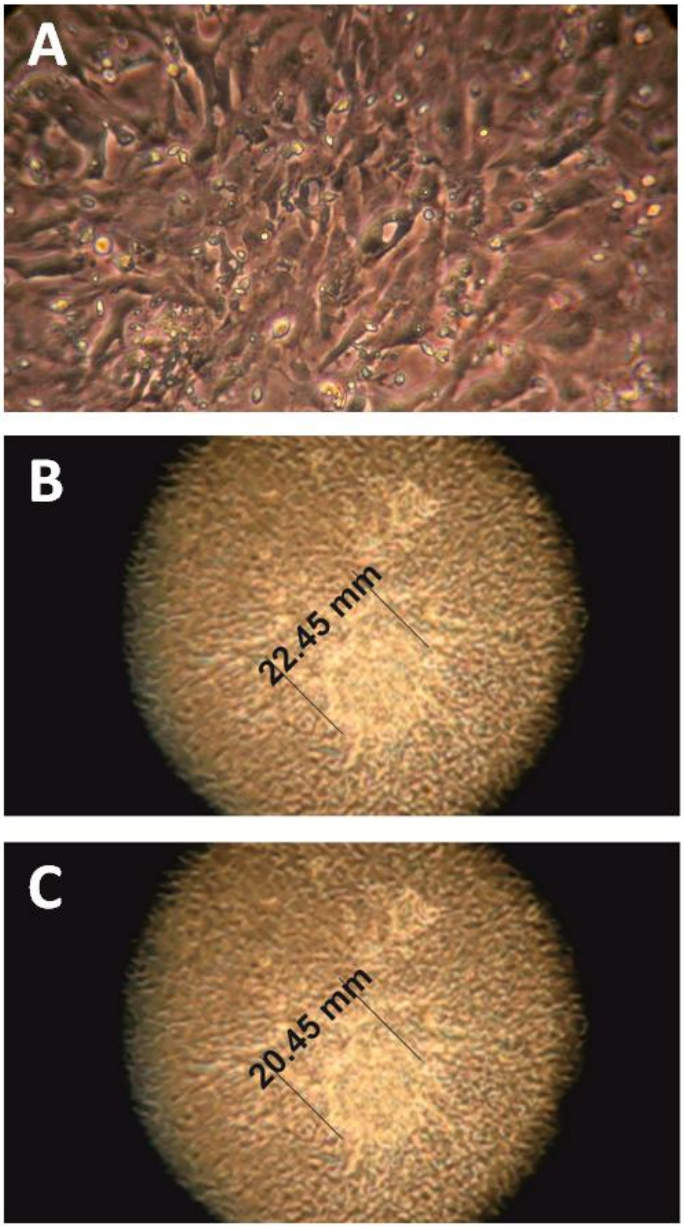

Figure 9-7. Cardiomyocyte morphology and visualisation of spontaneous contractile activity in chick cardiomyocytes.

Cardiomyocytes were cultured from isolated E8 chick hearts as described in the methods. The cells were observed over an extended period and photographed. A) shows the typical morphology of cultured CMs after 4 days in culture. Panels B) and C) illustrate the observed spontaneous activity in CM cells in both their (B, 22.45 mm) and contracted state (20.45 mm), illustrated by the parallel lines.

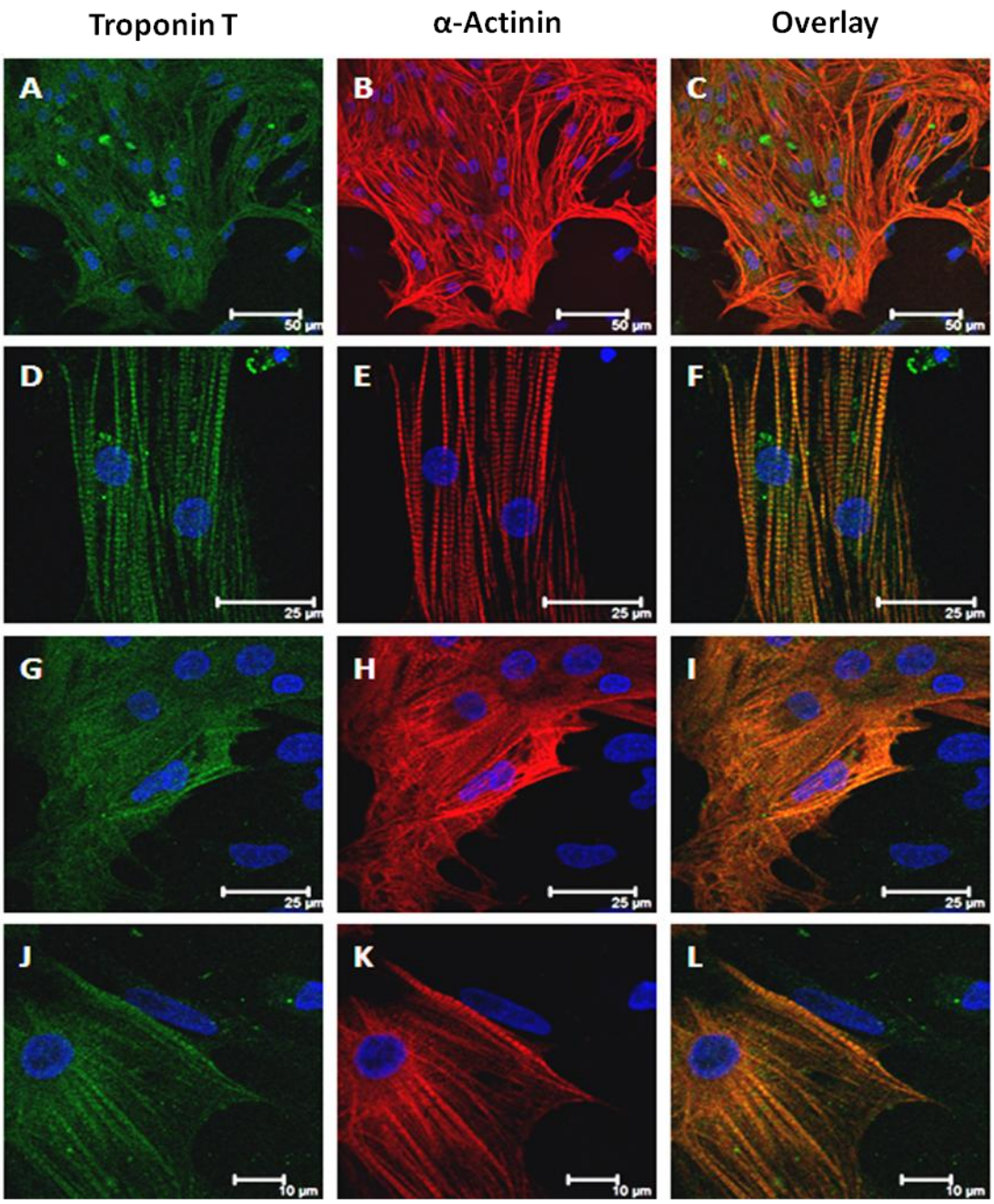

Figure 9-8. Cardiomyocyte immunofluorescence staining with Troponin T and sarcomeric α-actinin in cultured chick cardiomyocytes.

Cardiomyocytes were cultured from isolated E8 chick hearts as described in the methods. With spontaneous cardiac activity observed, cells were PFA fixed and stained with Troponin T (A, D, G and J), sarcomeric α-actinin (B, E, F and K) and as an overlay (C, F, I and L). The slides were mounted using Moviol containing DAPI and visualised using a Leica SP2 AOBS laser scanning confocal microscope and MaiTai multiphoton system.

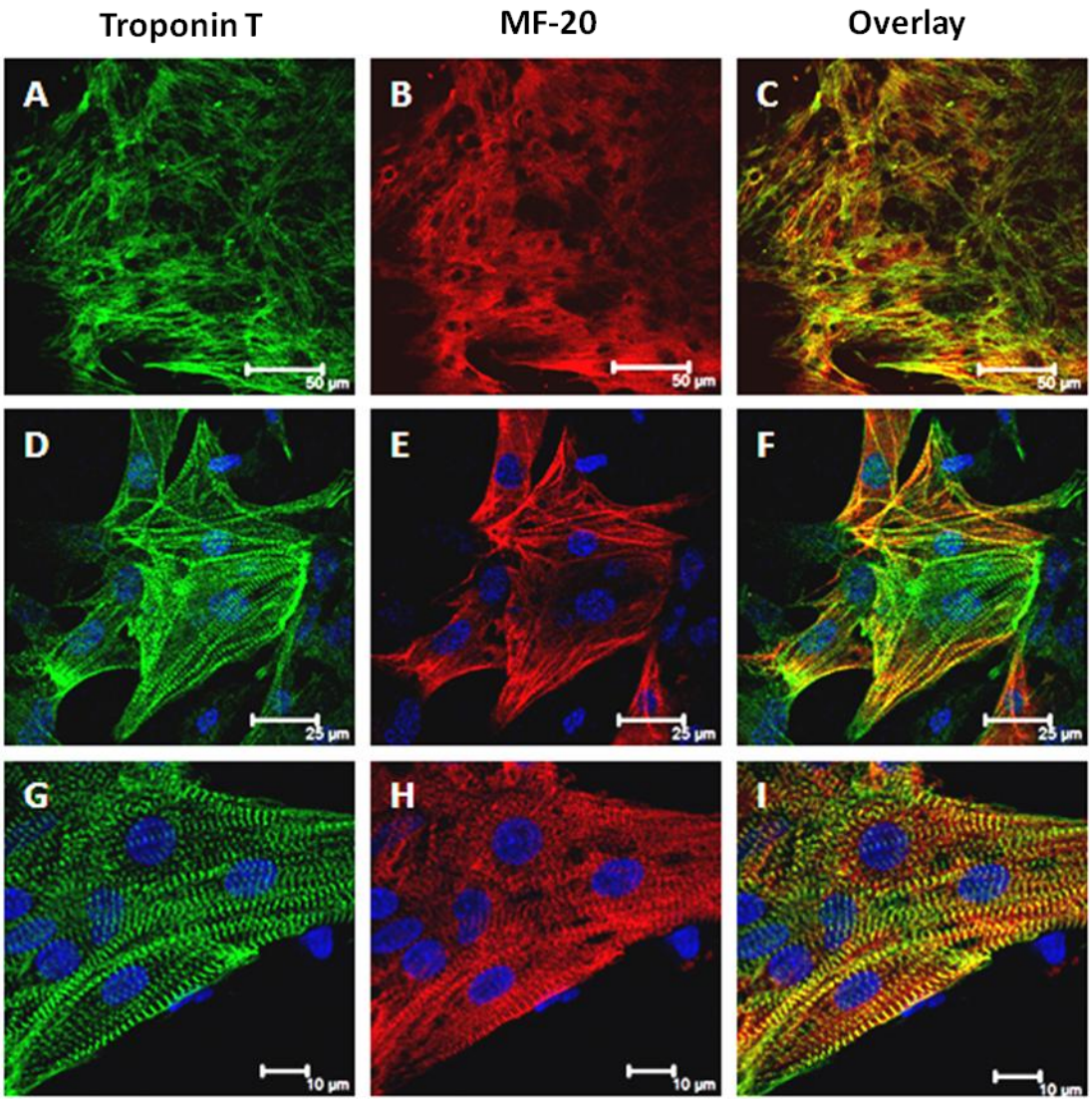

Figure 9-9 Cardiomyocyte immunofluorescence staining using, Troponin T and MF-20 in cultured chick cardiomyocytes.

Cardiomyocytes were cultured from isolated E8 chick hearts as described in the methods. With spontaneous cardiac activity observed, cells were PFA fixed and stained with Troponin T (A, D and G), MF-20 (B, E and F) and as an overlay (C, F and I). The slides were mounted using Moviol containing DAPI and visualised using a Leica SP2 AOBS laser scanning confocal microscope and MaiTai multiphoton system.

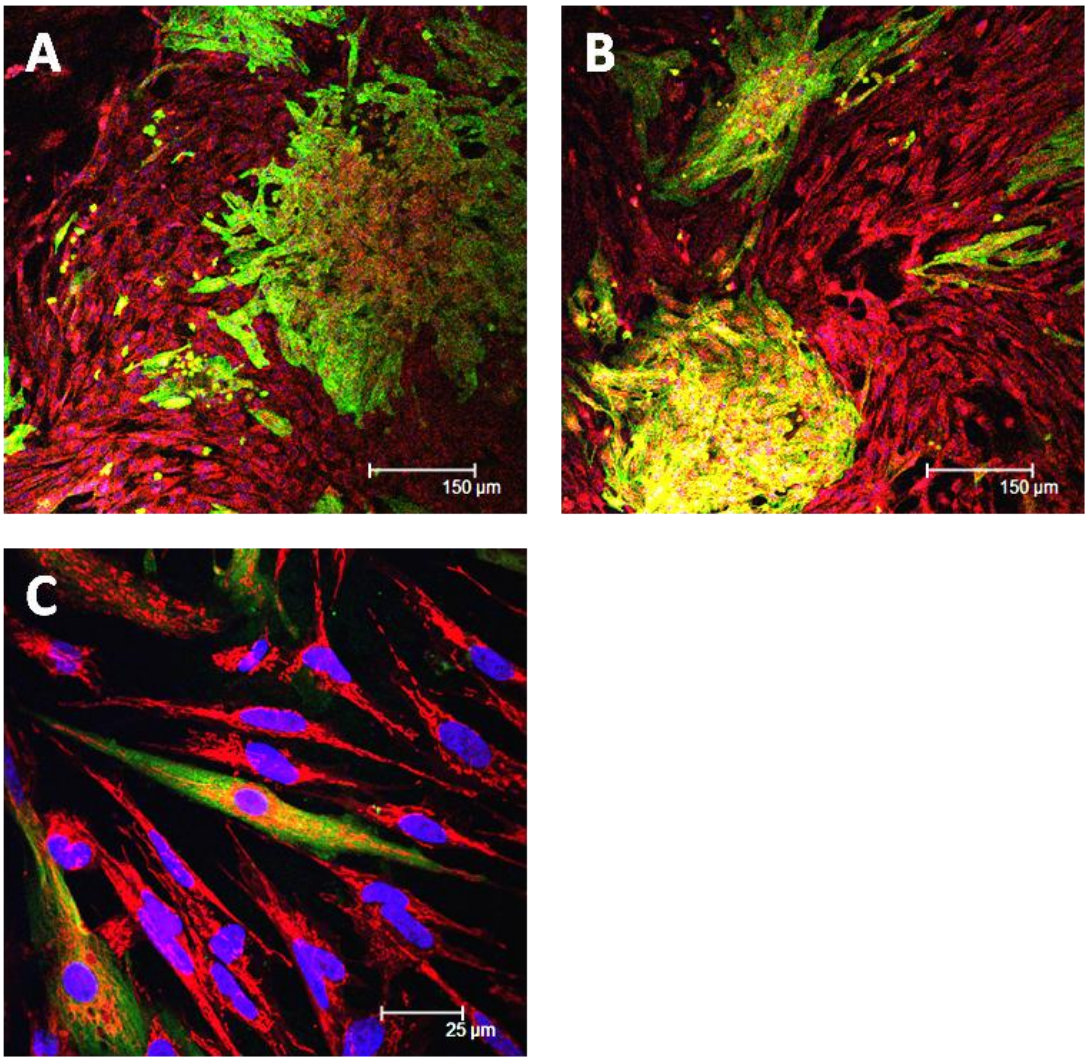

Figure 9-10. Cultured chick cell population phenotypes, CM (green) and alternative cells (red).

CMs were cultured from isolated E8 chick hearts as described in the methods. Once spontaneous cardiac activity was observed the cells were loaded with MitoTracker® before being PFA fixed and immunofluorescence labelled with sarcomeric α-actinin (A and B) and MF-20 (C; green). The slides were mounted using Moviol containing DAPI and visualised using a Leica SP2 AOBS laser scanning confocal microscope and MaiTai multiphoton system.

9.6. Calcium Measurements

To support the immunofluorescence data, and to confirm aspects of normal cell physiology, CM Ca^{2+}-dynamics was measured. The control measurements include the basal $[Ca^{2+}]_c$ and $[Ca^{2+}]_m$ concentration along with the typical calcium cycling events during beating.

To observe cytoplasmic and mitochondrial calcium, the Ca^{2+} sensitive indicators, Fluo-4 and X-Rhod-1 were used, as described in the section 6.5.1. Confluent and contractile CMs were loaded in separated experiments with Fluo-4, X-Rhod-1 and aequorin and the Ca^{2+} dynamics were observed in real time using a Leica SP2 AOBS laser scanning confocal microscope and MaiTai multiphoton system and by luminometry for aequorin [555, 556, 558].

9.6.1. Cytoplasmic Calcium

Chick CMs showed loading with the Fluo-4 Ca^{2+}-indicator, illustrated in Figure 9-11A. This allowed the observation of Ca^{2+} fluctuations in CMs during spontaneous activity. Frame ii. and iv. Illustrate elevated fluorescent intensity during a $[Ca^{2+}]_c$ spike, in comparison to the 'relaxed' state, which is associated with basal $[Ca^{2+}]_c$ levels, Frame i., iii. and v., Figure 9-11A.

The Ca^{2+} signals were illustrated and expressed as a fraction of the basal fluorescence (F/F_0). This enabled the comparison of Ca^{2+}-dynamics across the entire frame and ROI (Figure 9-11B). Across the three ROI, synchronous activity was observed with the $[Ca^{2+}]_c$ peaking together. However, the intensity of this dynamics varies across the ROIs, most notably in ROI 2. In this region the signal amplitude and $[Ca^{2+}]_c$ spiking is much more variable and does not occur all of the time. Figure 9-11C, is a representative trace of the individual $[Ca^{2+}]_c$ spike and illustrates the characteristic appearance of the responses. The peak shows the rapid elevation and slower recovery phase typical of a CM [471].

9.6.2. Mitochondrial Calcium

To measure $[Ca^{2+}]_m$ beating CMs were loaded with X-Rhod-1. Despite being a well-established technique the observed $[Ca^{2+}]_m$ dynamics is poor with no discernible or repeated changes in $[Ca^{2+}]_m$ were difficult to resolve. In ROI 2 there appears to be some periodic fluctuations in X-Rhod-1 fluorescence that could be attributed to changes in $[Ca^{2+}]_m$.

9.6.3. Mitochondrial Aequorin

As an alternative to X-rhod-1, mt[AEQ]WT was utilized. The benefits of using mitochondrial specific aequorin include: organelle targeting and quantification of $[Ca^{2+}]_m$. The luminometer allows the measurement of the entire cell population, and reduces any errors associated with mitochondrial migration out of the plane of focus with confocal microscopy.

The mt[AEQ]WT plasmid was initially tested on HeLa cells to determine if typical aequorin $[Ca^{2+}]_m$ responses could be measured using this approach. The presence of an appropriately sized mitochondrial aequorin insert (770 bp) in the mt[AEQ]WT plasmid was confirmed using the restriction endonucleotide ECOR1. The endonucleotide segments the aequorin insert from the pcDNA3.1 backbone (5500 bp). The agarose gel, using a ladder (columns A, H), the two segments (aequorin and pcDNA3.1) are visualized compared to the uncut larger fragment (column C to F and B, G, Figure 9-13).

With a confirmed aequorin insert, the transfection protocol was tested in the HeLa cell line (Figure 9-14). HeLa cells were transfected in the presence and absence of Ca^{2+} at a plasmid to GeneJuice® ratio of 1:3 or 1:1.5. The observed Ca^{2+}-dynamics illustrates the requirement of Ca^{2+} during aequorin reconstitution. With a working protocol and set transfection ratio the aequorin reconstitution incubation period was studied. Maximal reconstitution and optimal luminescence was observed after four hours, whilst after two hours, 86% of the maximal signal was obtained.

With a working transfection protocol was established CMs exhibiting spontaneous contractile activity were investigated. The $[Ca^{2+}]_m$ waves were observed during spontaneous activity, over a five minute period as illustrated in Figure 9-16. Distinct $[Ca^{2+}]_c$ waves were observed with Fluo-4, however agonist-induce $[Ca^{2+}]_m$ responses were clearly visible in the presence of certain agonists (Figure 9-16).

The transfection was confirmed by the presence of a noisy trace, elevated above the observed baseline or 'dark count' at 10 RLU and the large counts recorded in during lysis induced by calcium chloride ($CaCl_2$). The measured RLU data was then converted to $[Ca^{2+}]_m$ nM using Equation 5-13, generating the trace seen in Figure 9-16. Whilst the noisy trace is indicative of CM Ca^{2+}-dynamics it is not as defined or discrete as the cytoplasmic cycling observed using Flou-4 (Figure 9-11). The lack of clear and distinct Ca^{2+}-spikes may be attributed to the nature of the detection system, as the entire population is measured rather than the observed 'myoballs' to where the contractile activity appears restricted.

To attempt to confirm the presence of CM derived Ca^{2+}-dynamics the aequorin fluorescence was measure in response to cell stimulation with various agonists: 10 µM ATP, 100 µM phenylepinephrine (PE) or NE, 20 µM caffeine and potassium HEPES (Figure 9-17).

The addition of ATP induced multiple, clear and defined Ca^{2+}-spikes. As ATP is a generic agonist the resulting dynamics cannot rule out ATP acting on a fibroblast population (Figure 9-17B). The more CM specific agonists PE and NE had a mixed response. Phenylepinephrine inducing several large and prolonged Ca^{2+}-fluctuations whilst the presence of norepinehrine gave rise to an initial peak but very little in the way of repeatable contractile activity (Figure 9-17C and D, respectively). The presence of either caffeine or potassium HEPES had similar effects on already noisy traces, increasing the frequency but not the amplitude of the dynamics (Figure 9-17E and F, respectively).

Collectively the observed traces in Figure 9-16 and Figure 9-17 are indicative of inducible Ca^{2+}-dynamics. However, the signals appear noisy and the fluctuations in the observed fluorescence maybe just noise or cycling arising from the non-CM cells

within the population. Whilst there is confirmed transfection there is no way of confirming that the CM cells were transfected. With no apparent synchronous contractile activity or transient inhibition of the dynamics using calcium antagonists, such as L-type channel inhibitors, benzothiazepines, or RyR antagonist ruthenium red, these findings require further verification [637, 638].

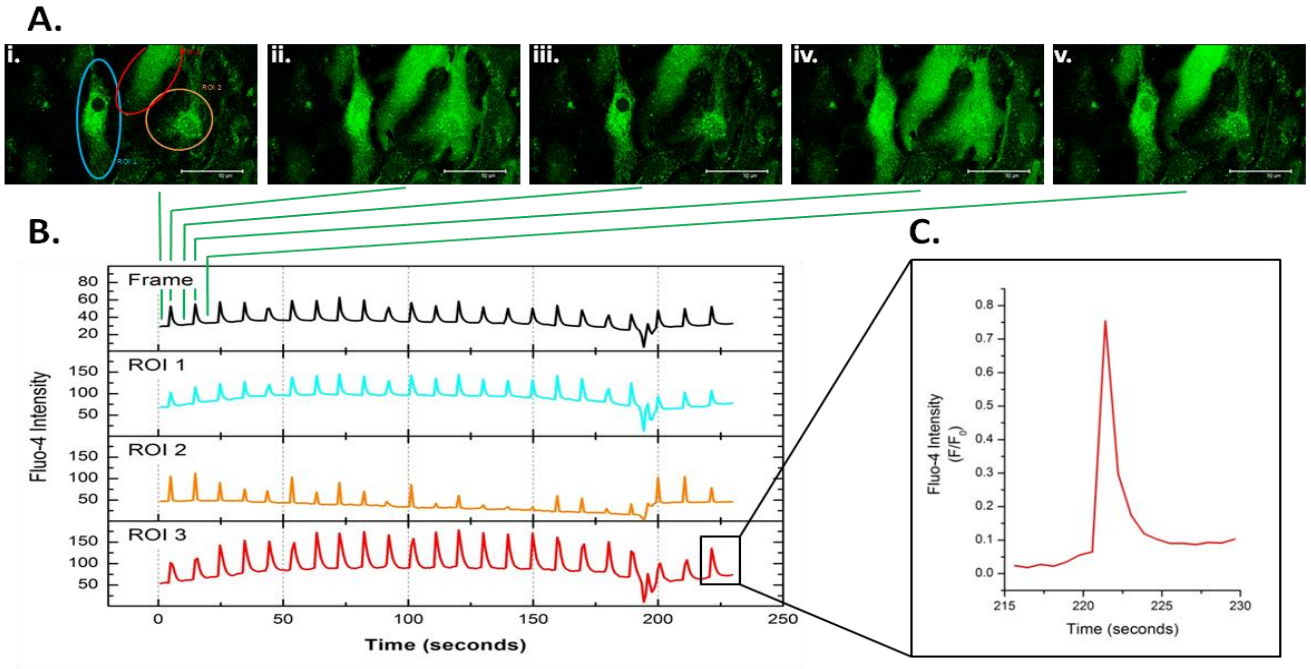

Figure 9-11. Cytoplasmic calcium staining of spontaneous contractile activity in chick cardiomyocytes, using Fluo-4.

CMs were cultured from isolated E8 chick hearts as described in the methods. Once spontaneous cardiac activity was observed the cells were loaded with 2µM Fluo-4 before and observed using a Leica SP2 AOBS laser scanning confocal microscope and MaiTai multiphoton system. A) represents a typical series of fluorescence, illustrating the variation between resting and elevated Ca^{2+} fluorescence intensity. B) data plots representative of real-time fluctuations in $[Ca^{2+}]_c$, across the entire frame and the selected regions of interest. C) the frames of typical$[Ca^{2+}]_c$ wave.

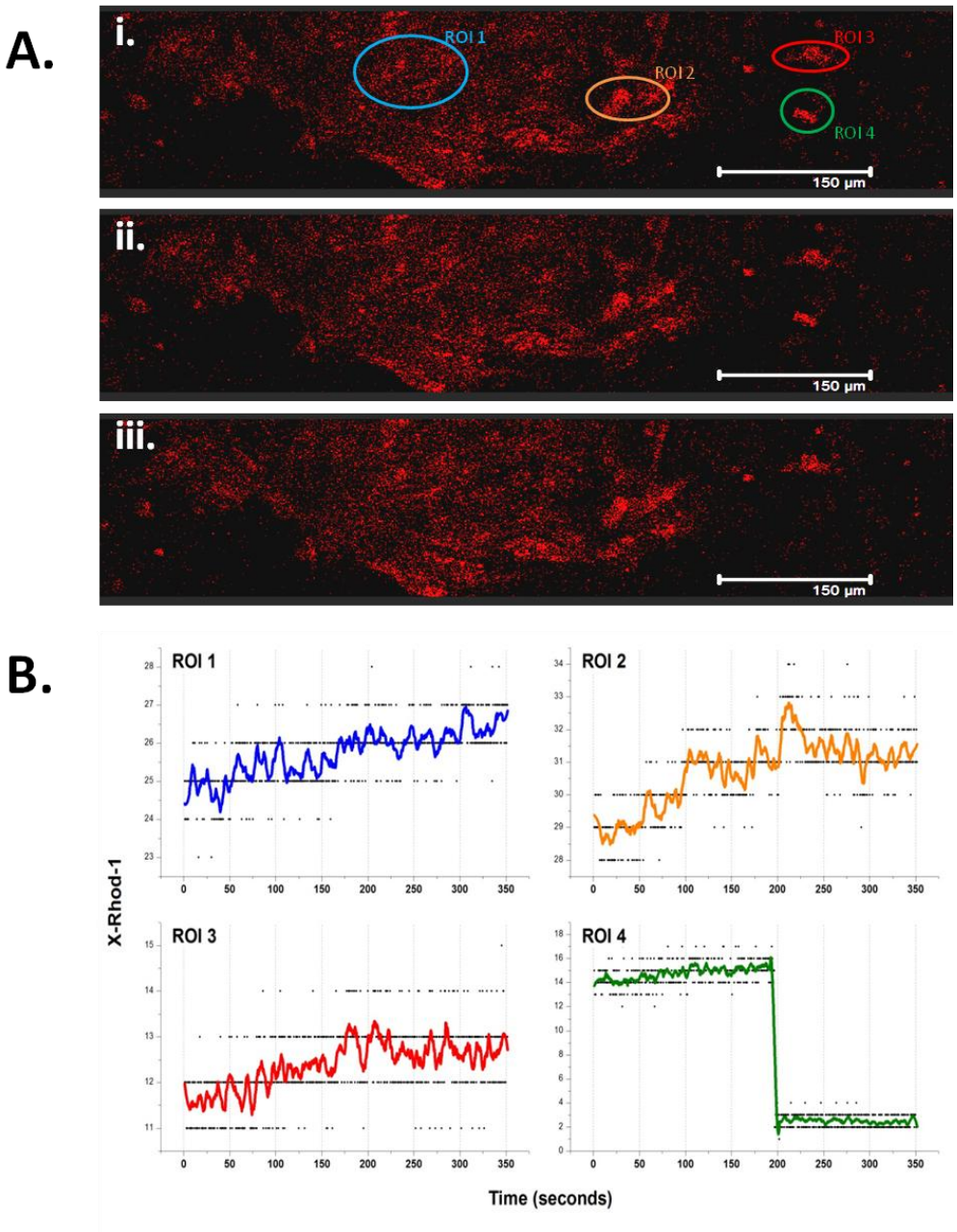

Figure 9-12. Mitochondrial calcium staining of spontaneous contractile activity in chick cardiomyocytes, using X-Rhod-1.

CMs were cultured from isolated E8 chick hearts as described in the methods. Once spontaneous cardiac activity was observed the cells were loaded with 2µM Fluo-4 before and observed using a Leica SP2 AOBS laser scanning confocal microscope and MaiTai multiphoton system. A) represents a typical series of fluorescence, illustrating the variance between resting and elevated Ca^{2+} fluorescence intensity. B) illustrates the real-time fluctuations in $[Ca^{2+}]_m$ across the entire frame and the selected regions of interest.

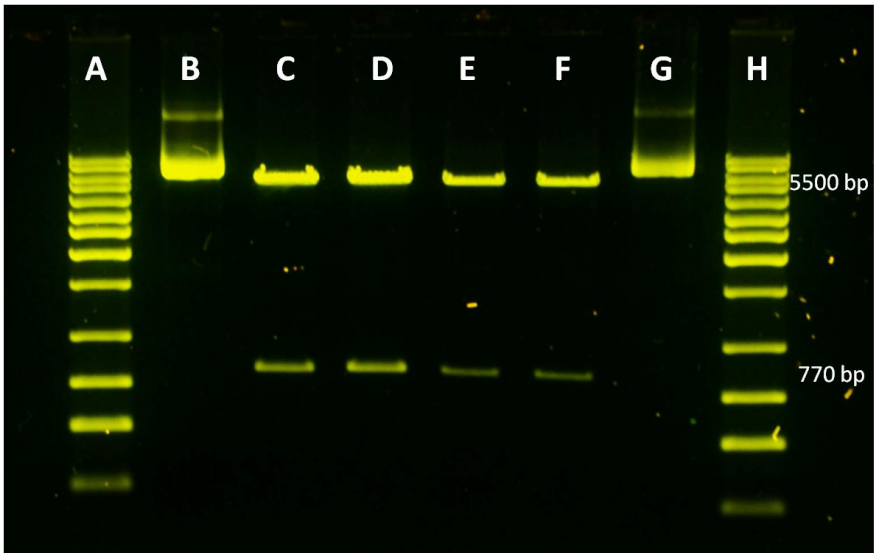

Figure 9-13. Agarose gel, showing the construction of mt[AEQ]WT plasmid.

To confirm the presence of the aequorin insert within the mt[AEQ]WT, the plasmid was incubated for 1 hour with 10 units/µl of EcoR I restriction enzyme, to cleave the aequorin segment from the pcDNA3 backbone. The gel shows the AXYGEN 1Kb ladder (A, H), uncut plasmid (B, G) and then treated plasmids (C-F).

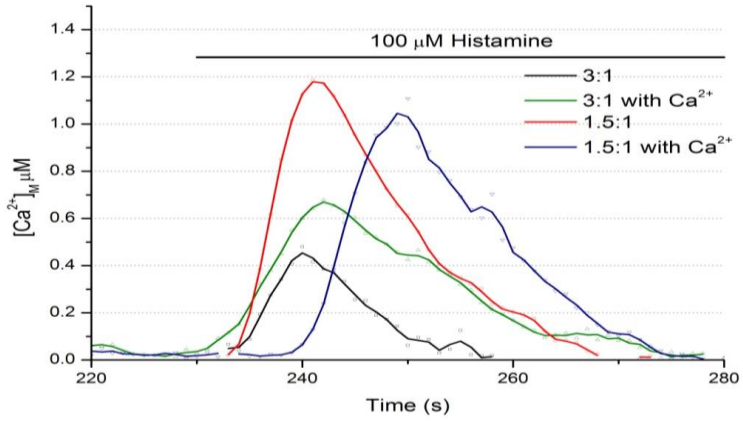

Figure 9-14. Transfection reagent ratios and the requirement of calcium in working with mt[AEQ]WT in HeLa cells.

HeLa cells were cultured on 16mm dia. coverslips, in DMEM. Typical responses to 100µM Histamine are shown in mt[AEQ]WT transfected cells. The experiment was performed in HBS in a 37^{o}C heated chamber in a purpose built luminometer. The line graph is the real time trace of $[Ca^{2+}]_m$ µM, where the solid bar indicated the addition of 100µM Histamine, whilst the bar graph represents the peak observed of $[Ca^{2+}]_m$ µM.

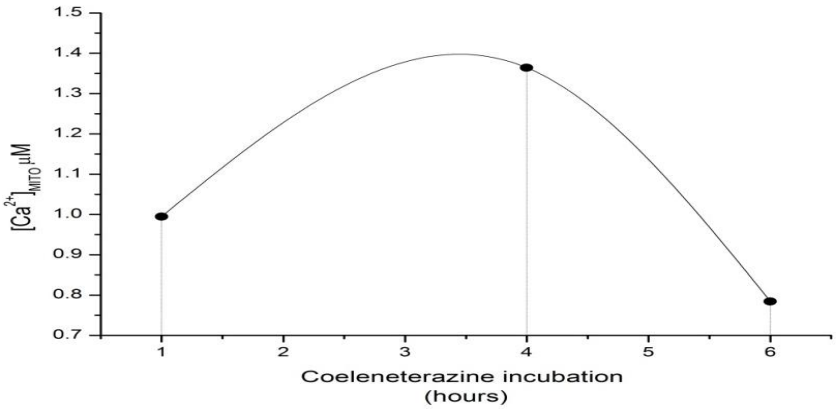

Figure 9-15. Coelenterazine activation of apoaequorin and the subsequent mt[AEQ]WT dynamics in response to histamine stimulation, in HeLa cell.

HeLa cells were cultured in DMEM and once 70% confluent transfected with mt[AEQ]WT plasmid for 48 hours. The cells response to 100µM Histamine stimulation was then measured in a purpose built luminometer. The cells were pre-incubated with 6 µM co-elenterazine prior to Histamine treatment, for 1, 4 and 6 hours.

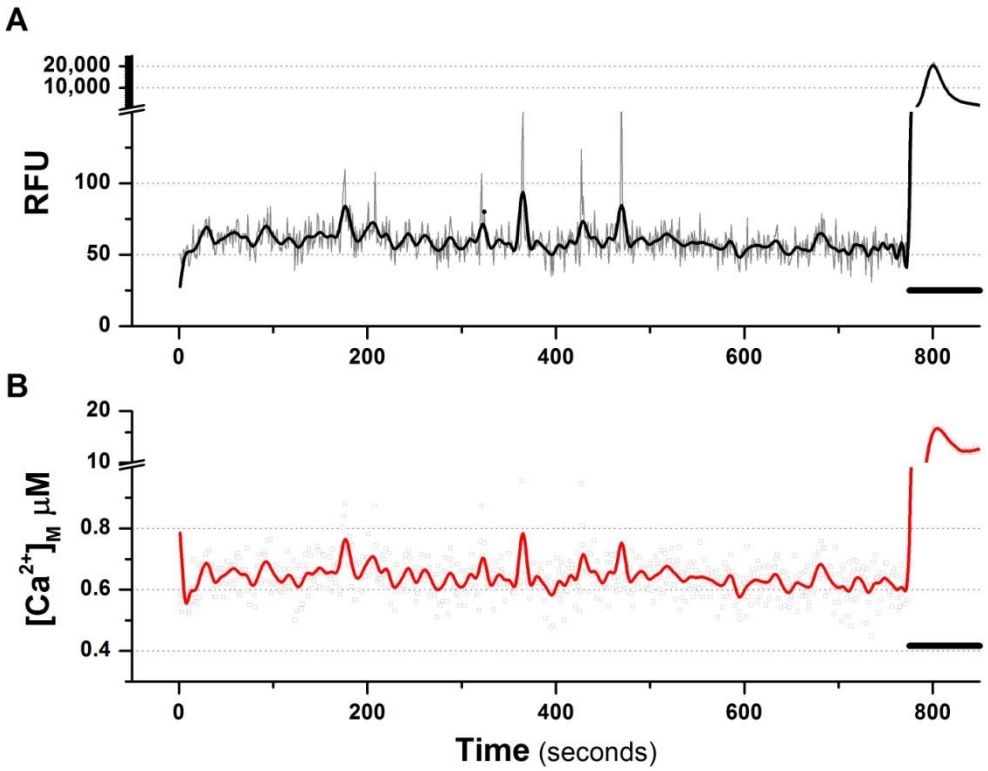

Figure 9-16. Calcium dynamics (mt[AEQ]WT) in cardiac myocytes displaying spontaneous activity.

CMs were cultured from isolated E8 chick hearts and after 72 hours in culture the CMs were transfected with mt[AEQ]WT as described in the methods. Once spontaneous activity was observed the transfected cells were subject to 2 hours incubation with 6 µM coelenterazine. Once ready, coverslips were loaded into the purpose-built perfusion chamber and the $[Ca^{2+}]_m$ was measured. A. illustrates the observed RLU and B. the resulting $[Ca^{2+}]_m$ µM. The bar indicated the addition of 10 mM $CaCl_2$. Fast Fourier Transform (FFT) filter number of data points set at 5.

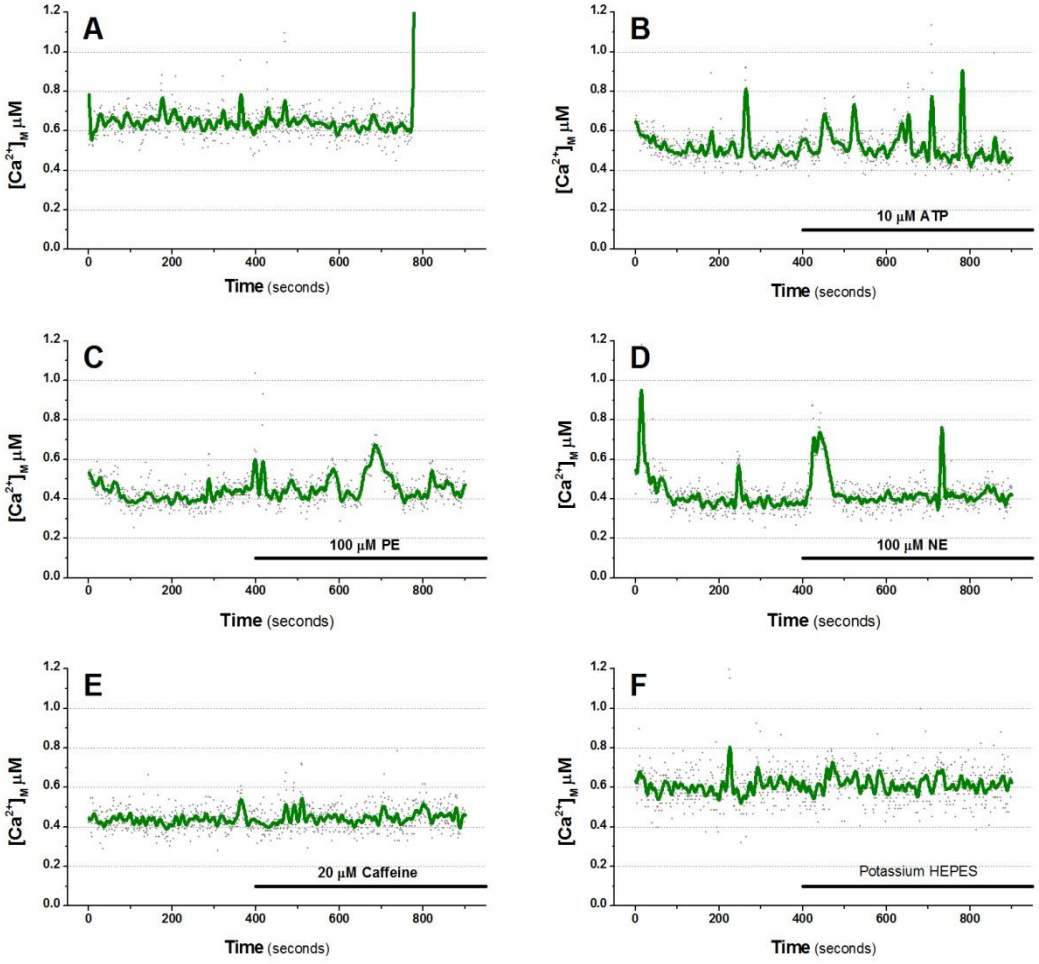

Figure 9-17. Calcium dynamics in cardiomyocytes transfected with mt[AEQ]WT, was measured during spontaneous activity in the absence and presence of various agonists.

CMs were cultured from isolated E8 chick hearts and after 72 hours in culture the CMs were transfected with mt[AEQ]WT as described in the methods. Once spontaneous activity was observed the transfected cells were subject to 2 hours incubation with 6 µM coelenterazine. The coverslips were loaded into the purpose-built perfusion chamber and $[Ca^{2+}]_m$ was measured in response to various agonists; A) control, B) 10 µM ATP, C) 100 µM phenylepinephrine (PE), D) 100 µM norepinephrine (NE), E) 20 µM caffeine and F) potassium HEPES. Fast Fourier Transform (FFT) filter number of data points set at 5.

9.7. Conclusion

Initial immunofluorescence staining using positive and negative controls confirmed that the antibodies, sarcomeric α-actinin, myosin heavy chain MF-20 and Troponin T, are CM specific [459, 494-498]. The antibodies α-actinin and MF-20 showed broad, periodic staining of Z-bands and intercalated discs, while Troponin T was CM specific but generated less distinctive labelling [498, 639-641].

The HL-1 cell line was proposed as a working CM model, reported to survive repeated sub-culturing, whilst maintaining a CM phenotype and contractile ability [472, 475, 483-486]. Despite this, in culture the cells lacked any observable contractile activity, either spontaneous or induced. The HL-1 cells also lacked any CM specific immunofluorescent staining. As an alternative to the HL-1 CM cell line, primary chicks CMs were utilized as a model. Using established isolation techniques involving heart isolation and Collagenase II digestion, a contractile CM cell culture was developed. The isolated chick cells displayed the ability to be maintained in culture, through serial passages (up to two sub-cultures). Alongside the cells ability to survive isolation and to proliferate, the cultured cell population displayed distinct CM immunofluorescence labelling (Figure 9-8 and Figure 9-9). The most important and distinguishing markers was the appearance of maintained spontaneous contractile activity in culture, in the absence of external stimuli.

9.7.1. Cardiomyocyte Culture Purity

The presence of non-CM cells within the population was not surprising as a heterogenous population of CMs and fibroblasts has been shown necessary for proper CM growth and function [452, 453, 457]. However within the heterogeneous populations, the primary chick cultures form distinct, contractile ‘myoballs’ [635, 636].

9.7.2. Calcium dynamics

With spontaneous contractile activity observed in the apparent 'myoballs' Ca^{2+}-dynamics was recorded (Figure 9-11). Whilst Ca^{2+}-cycling is well documented and is not the main focus of this study, the recordings support the validity and usefulness of the chick CM model. Cell labelling with Fluo-4 displayed discrete and repeatable Ca^{2+}-spiking during spontaneous 'myoball' contractile activity. However, mitochondrial Ca^{2+}-dynamics proved more difficult to measure with either, X-Rhod-1 labelling or aequorin transfection.

X-Rhod-1 staining measurements were poor with only periodic $[Ca^{2+}]_m$ fluctuations observed. Mitochondrial target aequorin provides an improved system but still no definitive CM derived signalling was observed. The signalling appears noisy and the responses to ATP maybe derived from non-CM cells such as endothelial and fibroblasts or via $P2Y_{11}$ receptor positive ionotropic activation [321, 585-587, 642]. However, the luminescence observed in response to PE and NE stimulation implies CM specific Ca^{2+}-dynamics.

Beat-to-beat changes in $[Ca^{2+}]_m$ occur during E-C coupling in the heart is believed to be either 'integrating' or 'phasic' uptake [643-646]. Phasic $[Ca^{2+}]_m$-transients, as seen in $[Ca^{2+}]_c$, were not observed as spiking may result from small $[Ca^{2+}]_m$ fluxes or $[Ca^{2+}]_m$ transients only in a minority of the cells and subsequently integrated.

10. Discussion

10.1. Mitochondrial Membrane Potential

The IPC induced by diazoxide is associated with $\Delta\psi_m$ depolarisation via mitoK$_{ATP}$ channel opening, however the precise mechanism of action is still unresolved [254, 647]. The mechanism of action is further dispute as some laboratories have reported that the diazoxide IPC may arise from alternative mechanisms including the modulation of the sarcoK$_{ATP}$ channel or inhibition of succinate dehydrogenase [252-254, 258]. In a similar way the "ischemia selective inhibitor of mitoK$_{ATP}$ channels" 5-HD has been proposed to have other actions including modulation of β-oxidation" [254, 262-264, 270, 272, 274].

10.1.1. Diazoxide and 5-HD

Diazoxide induced substantial depolarisation to approximately -150 mV, consistent with the IPC synonymous with diazoxide (**Figure 7-3**) [15, 120-124, 584]. Diazoxide-induced depolarisation was elevated in the presence cyanide whilst slowed by oligomycin (Figure 7-6). The $\Delta\psi_m$ modulated by cyanide and diazoxide or oligomycin suggests that diazoxide is inducing K^+ influx, potentially via the mitoK$_{ATP}$ opening.

With 5-HD negating diazoxide IPC, how does 5-HD induce mild depolarising whilst also inhibiting diazoxide-induced depolarisation? Does diazoxide IPC arise from ETC inhibition and the resulting depolarisation, which is bypassed by 5-HD (by modulation of β-oxidation for example) or is 5-HD a metabolic agent inducing depolarisation but in the presence of diazoxide also function as a K^+ channel blocker? Alternatively, is the observed IPC the result of a different pathway entirely, such as ROS generation [34, 40, 41, 144, 254-256, 647]? The metabolic effect of 5-HD assumes that in the presence of adequate substrates 5-HD acts as a weak inhibitor of complex II, however in the absence of substrate of during ETC blockages (including the presence of diazoxide) 5-HD acts as a substrate [237, 254, 255, 270-273]. This alternative metabolic mechanism of action has been described by Hanley *et al.* (2002) as illustrated in Figure 10-1 [254]

Diazoxide induces depolarisation and whilst the exact mechanism cannot be defined, the data is consistent with it being a KCO rather than an ETC modulator. Observed depolarisation induced by 5-HD is consistent with it exerting a metabolic role through modulation of β-oxidation or the ETC rather than inhibiting mitoK_{ATP} channel opening. The results suggest that diazoxide-IPC arises from $\Delta\psi_m$ depolarisation, butas 5-HD induces mild depolarisation but does not afford IPC, a degree of depolarisation is required to induce IPC.

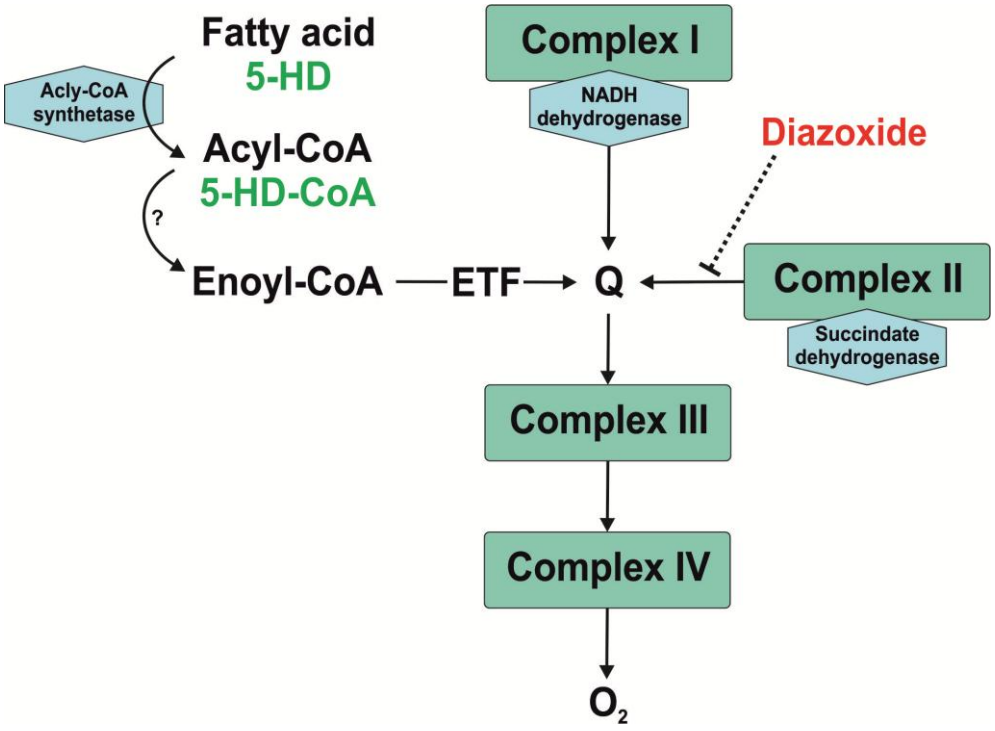

Figure 10-1. Pathway of metabolic IPC via the ETC and the involvement of diazoxide and 5-HD.

It has been suggested that diazoxide inhibits succinate dehydrogenase at Complex II. 5-HD is proposed to act as a substrate for the enzyme acyl-CoA synthetase, feeding into the ETC as depicted. The principal product of this reaction, 5-HD-CoA may inhibit or serve as substrate for acetyl coenzyme A (acyl-CoA) dehydrogenase. ETF denotes electron transferring flavoprotein and Q denotes ubiquinone.

10.1.2. Cyclic GMP & IPC agents

The addition of cGMP modulators all induced mild depolarisation, consistent with cGMP-PKG opening of mitoK$_{ATP}$. The presence of cGMP modulators had minimal effect on diazoxide induced depolarisation. Similarly there was nominal modulation in the presence of 5-HD, however as 5-HD itself induces mild depolarisation of the $\Delta\psi_m$ which may mask any antagonistic effect of 5-HD on cGMP mitoK$_{ATP}$ modulation.

It is well documented that NO activate both cGMP-PKG and cGMP-independent pathways. A major issue is that the NO donors, SNAP and SNP, could induce depolarisation independent of cGMP, such as binding cytochrome C oxidase, competing with O_2 as the final electron acceptor in the ETC, thus directly inducing depolarisation [648]. To confirm that it is cGMP and not direct NO derived effects, the presence of cGMP PKG inhibitors (KT5823, (*Rp*)-8-Br-PETP-cGMPS and (Rp)-pCPT-cGMP) could be used[290, 300]. These would attenuate any cGMP and PKG induced depolarisation. The PDE$_5$ inhibitor zaprinast induces a small depolarisation, suggesting a link between elevated cGMP and depolarisation. How cGMP induces $\Delta\psi_m$ depolarisation is not clear, but the mitoK$_{ATP}$ channel remains as a candidate [275-277].

10.1.3. FCCP Depolarisation

FCCP was initially used as an internal control at the end of each experiment inducing large $\Delta\psi_m$ depolarisation. The presence of diazoxide elevated FCCP-derived depolarisation whilst 5-HD exerted no discernible effects. The modulation of independent depolarising mechanisms such as the ETC (FCCP) and the mitoK$_{ATP}$ channel (diazoxide) could account for additional diazoxide depolarisation.

10.1.4. Concluding Remarks

Considering published data and the results discussed in this thesis, diazoxides actions are consistent with it acting as a K^+ channel opener. The data is consistent

with 5-HD exerting a metabolic effect, possibly modulating β-oxidation as suggested by the literature [237, 254, 262, 263, 270-274]. However, it is not necessarily all or nothing; instead 5-HD actually could act as both a substrate in β-oxidation and exerts the antagonistic effect on diazoxide-induced IPC and depolarisation, as a mitoK_{ATP} channel blocker.

From the results, it is clear that the presence of diazoxide-induced a $\Delta\psi_m$ depolarisation, to similar levels as seen with cyanide, whilst 5-HD exerted a much smaller depolarisation.

10.1.5. Future work

To validate the assumption that diazoxide opens the proposed mitoK_{ATP} channel, the channel needs to be identified and studied using strategies other than the pharmacological agents used here. To determine the involvement of the channel a variety of techniques including mitochondrial patch-clamp experiments, measuring flavoprotein fluorescence, $[K^+]_m$, short interfering RNA (siRNA) silencing, could be used to examine the potential of mitoK_{ATP} modulation by diazoxide.

Flavoprotein fluorescence, resulting from flavoprotein oxidation, has been used as an indicator of mitoK_{ATP} channel opening in response to diazoxide [121]. This is now disputed following the discovery that at concentrations which are known to induce IPC and expected to open the channel, diazoxide failed to increase fluorescence [254, 647, 649]. In any case, flavoprotein fluorescence is not a direct measurement of K^+ influx.

Mitochondrial patch-clamping allows mitochondrial ion channels to be studied [650, 651]. However, due to mitochondrial proximity to the endoplasmic reticulum, and the formation of physical tethers between the organelles, mitochondrial patching can be hindered. Also, in these studies it is not a mitochondria but a mitoplast (isolated mitochondria with no OMM), reconstituted into proteo- or giant-liposomes that are used. Whilst oxidative phosphorylation remains, other

properties such as the pathway of β-oxidation are interrupted [231, 652-654]. Certainly channel function is not being assessed in its natural environment.

Measuring K^+-dynamics in response to the presence of the proposed channel modulators would be helpful. It would not confirm the mitoK_{ATP} channel, but exclude K^+-independent pathways from being associated IPC and depolarisation. Observing the K^+-fluctuations would enable the antagonistic effect of 5-HD to be examined and the concept of mutual or isolated pathways responsible for the measured responses. However measuring $[K^+]_m$ proves to be an ambitious challenge, with small concentrations and changes difficult to accurately record. The K^+ indicator, potassium-binding benzofuran isophthalate (PBFI) exhibits a K_d of 10 to 100 mM (room temperature at pH 7.05) [556, 655, 656]. Whilst this provides a system for measuring K^+ concentrations via fluorescence activated cell sorting, even in apoptotic cells the PBFI increase was only 4 fold [655]. Without improved fluorescent probes and detection systems, it may be impossible to measure the small change in $[K^+]_m$ associated with small depolarisation.

De Stefani *et al.* (2011) used siRNA silencing screening to knock down expression of the mitochondrial calcium uniporter (MCU) protein. This approach could be used to identify the mitoK_{ATP} channel or silence other potential channels and see the effect exerted by diazoxide, 5-HD and other proposed channel modulators [657].

Coming back to using pharmacological agents is not ideal, but in the immediate future they provide a parallel pathway in trying to ascertain the involvement of the mitoK_{ATP} channel and the modulators, diazoxide and 5-HD.

Multiple ETC inhibitors such as myxothiazol (acts on complex II) and cyanide (acts on complex IV) could be compared to the effects of diazoxide and cyanide on $\Delta\psi_m$ [513]. If the resulting shifts in $\Delta\psi_m$ are comparable and blocking of the ETC at multiple sites induces accumulative depolarisation, diazoxide may act via oxidative phosphorylation modulation. However, if multiple blockers do not induce additive effects on depolarisation then the proposed KCO pathway remains a candidate for diazoxide-induced depolarisation. Alternatively rotenone, an inhibitor of complex I

of the ETC, could be used to inhibit electron transport at the start of the chain and as such negate any subsequent inhibition [658, 659]. If diazoxide affects IPC in presence of rotenone, it would imply that a change in $\Delta\psi_m$ arises from KCO mediated actions rather than ETC modulation.

To look at the involvement of ROS within IPC as the key factor, rather than mitoK_{ATP} opening, they need to be sequestered or their generation needs to be inhibited. To achieve this inhibitors of complex I (rotenone) or II (myxothiazol) of the ETC could be used to generate ROS species or IPC [513, 658-660]. However in this approach the $\Delta\psi_m$ would already be altered and as such, using the ROS scavengers (such as sodium pyruvate, mannitol and carboxy-PTIO; for full review of ROS scavengers see Franco *et al.* (2007)), would provide a more prudent and beneficial way to assess ROS involvement in $\Delta\psi_m$ and IPC [661-663]. An alternative and more direct approach would be to look at the effect of direct ROS signalling using H_20_2 and potential IPC or $\Delta\psi_m$ modulation. If diazoxide IPC resulted from ROS generation, then the importance of the $\Delta\psi_m$ modulation needs to be reconsidered.

Whilst the data is conclusive that diazoxide induces greater depolarisation than 5-HD, the data was expressed as F/F_0 and not as actual $\Delta\psi_m$ in millivolts. As such, the exact shift in the $\Delta\psi_m$ can only be estimated and whilst the degree of depolarisation may appear significant its scale is unknown. At quenching mode concentration, TMRE exhibits non-liner fluorescence, however without directly measuring the F/F_0 at known $\Delta\psi_m$ the actual membrane potential cannot be determined [504, 509-512]. To resolve this issue it would be prudent to repeat the experiments whilst using a mitochondrial patch clamp technique (see Kirichok *et al.* and Sorgato *et al.* for further details) [650, 664]. This would offer precise $\Delta\psi_m$ readings which could be used to generate an accurate and reliable calibration curve of TMRE (saturated) as a measure of $\Delta\psi_m$ in HeLa cells. However, plotting F/F_0 against $\Delta\psi_m$ at set points, FCCP (-60 mV), resting (-180 mV) and oligomycin (-200 mV) suggests that the relationship between F/F_0 and $\Delta\psi_m$ is fairly close to linear.

A potential secondary issue arising from the use of TMRE was the assumption that it reported $\Delta\psi_m$ and not cytoplasmic membrane potential. This is highly relevant since evidence suggests that diazoxide IPC is mediated via sarcoK_{ATP} channel modulation [252, 253]. Whilst the response elicited by the controls, cyanide and oligomycin, confirmed TMRE as an indicator of $\Delta\psi_m$, they did not exclude the potential that cytoplasmic membrane potential may also be reported. To confirm that TMRE was localised to mitochondria, TMRE loaded cells were co-labelled with a mitochondrial membrane dye, such as MitoTracker® Green. The dual staining showed co-localisation of the probes and absence of plasma membrane signal.

10.2. Extracellular Nucleotides

With ATP and ADP having unique pharmacology and resulting receptor activation the extracellular nucleotide concentration during metabolic stressing is important. As such the aim of this section was to look at the extracellular nucleotide concentration during CIH and determine if ADP is present alongside ATP. The cause of extracellular nucleotide accumulation was also examined with regard to ecto-enzyme activity and release.

10.2.1. Chemical Induced Hypoxia

Cyanide and 2-DG are well documented CIH agents however induced minimal metabolic stressing prior to the addition of ionomycin. Imamura *et al.* (2009) have shown that, in proliferating cancer cell lines (such as HeLa), ATP synthesis is derived from glycolysis and β-oxidation and not pyruvate-derived metabolism [665, 666]. Subsequently CIH induced partial reduction in cytoplasmic ATP [666].

The addition of ionomycin induces a large increase in $[Ca^{2+}]_c$ resulting in activation of SERCA PMCA and other energy dependant processes. The addition of ionomycin needs to be considered, especially for metabolically active CMs and be avoidable by replacing glucose within the media with galactose. Changing to galactose elevates oxidative phosphorylation and mitochondrial respiration which would exacerbate CIH-induced stressing, potentially removing the requirement for ionomycin [667, 668].

10.2.2. Permeability and cell lysis

Calcein and PI do not show catastrophic cell lysis but rather increased permeability over the course of the experiment. The modulation of dye permeability in the presence of FFA is suggestive of a FFA-sensitive mechanism responsible for extracellular nucleotide accumulation.

The calcein and PI staining also confirmed that there was no sudden cell death as there was no dramatic change in staining. As the dye can permeate hemichannels the change in dye retention and uptake does not necessarily represent cell lysis. The presence of FFA, an inhibitor of hemichannels, prevented dye permeability but not extracellular nucleotide accumulation, suggesting that neither cell lysis or FFA-sensative release is the mechanism of nucleotide accumulation.

10.2.3. Nucleotide Calibration Curves

Calibration curves were constructed from serial ATP and ADP and used to convert the measured RLU to nucleotide concentrations.

The sensitivity of the HPLC system was not sufficient to accurately measure the concentration of ATP and ADP, as afforded by tube luminometry. Despite not being able to measure the exact nucleotide concentration both systems suggest that the concentration of ATP and ADP fell within the range of 0 to 40 nM and 0 to 3000 nM, respectively. Other laboratories have been able to use HPLC to measure nucleotides down to the picomolar range, which could be attributed to the use of radioactive species, ^{3}H or ^{32}P, rather than fluorescence [334, 614, 630].

10.2.4. Extracellular Concentration

Elevated extracellular ATP was expected, however the concentration of ADP was surprisingly high, approximately 100 fold greater than the prevailing ATP. This implies ADP signalling and resulting pharmacology maybe more significant than ATP under hypoxic conditions as they act via $P2Y_{1,\ 6,\ 11}$ and $P2Y_{2,\ 11,}$ P2X, respectively [316, 317].

ADP signalling is primarily associated with platelet aggregation, P2y signalling also can activate vasodilation, platelet aggregation, proinflamatory action, ion channels (either directly or indirectly), phospholipases, regulate cAMP levels and tyrosine kinase mitogen-activated protein kinase cascades [82, 83, 301, 316, 323, 383, 385, 386, 588-594, 669-671].

10.2.5. Mechanism of extracellular accumulation

As CIH elevated the extracellular nucleotide concentration, the next step was to examine the mechanism of accumulation. There are two predominant mechanisms which may account for elevated concentrations; ecto-enzyme activity or release.

10.2.5.1. Ecto-enzyme activity

If the extracellular ADP was derived from ATP hydrolysis ecto-enzyme inhibitors (levamisole, ARL 67156 or ebselen) would be expected to induce a dramatic increase in ATP and reciprocal decrease in ADP concentration.

The data from ecto-nucleotide inhibition does not confirm the precise effects of extracellular enzymes, it does confirm that there is no rapid hydrolysis between release and recording, which would have been abolished. With both nucleotides increasing in the presence of ecto-enzyme inhibition, two options remain to explain the presence of ADP, either extracellular synthesis or cellular release.

The relative specificity of the ecto-nucleotidase is an issue as inhibiting ATP hydrolysis should elevate ATP. However, the ecto-nucleotide enzymes are not specific and can inhibit the forward and backward reaction in the equilibrium between ATP, ADP and AMP. Unfortunately without precise K_i data for inhibitors and knowledge of equilibrium constants for the substrates and products, it is very difficult to establish the degree of enzyme activity being inhibited and the precise amount of ADP derived from ATP.

AK activity can be inhibit by Ap_5A [409]. However commercial supplies of Ap_5A contain mononucleotides and clearly the presence of either ATP or ADP would interfere with the assays. To measure AK activity commercially available sources of Ap_5A were used but were contaminated with mononucleotides leading to misleading results, if not treated before use [605]. To remove nucleotide phosphates contaminants the Ap_5A stock was treated with alkaline phosphatise however Ap_5A remained contaminated and consequently it was not possible to

determine if AK was displaying a role in determining the relative ATP:ADP concentrations [605-607].

10.2.5.2. Release mechanisms

As discussed in section 5.5.2 Nucleotide Release, the potential release mechanisms for nucleotides are; ABC transporters, vesicle trafficking and channels. As the calcein and PI staining (Figure 8-10) was FFA-sensitive, connexins and or pannexins were implicated as a likely channel, however the presence of FFA had minimal effect on the observed nucleotide concentration. Another putative release mechanism is the oATP-sensitive $P2X_7$ channel. The addition of oATP decreased the observed extracellular ATP and ADP concentrations during the initial 20 minutes of poisoning (Figure 8-14).

In the presence of oATP (100 µM oATP for 0 to 40 minutes) extracellular nucleotides were reduced, despite being used at a lower concentrations and reduced period than the 1 to 2 hours incubation at 300 µM used by others [610]. Further work using oATP at a higher concentration and longer incubation period may induce further or complete inhibition of the extracellular nucleotides release. Secondary to an extended incubation period, as with most 'selective' inhibitors oATP may be less specific than proposed or required and as such alternative channel blockers needs to be examined [629]. The presence of ionomycin has been shown to induce ATP release via exocytosis activation of $P2X_7$ channels [540]. As such the effects of ionomycin need to be examined in combination with oATP to see if ATP release results from the presence of ionomycin [667, 668, 672].

Alongside hemi-channels and $P2X_7$ channels, vesicle trafficking is a proposed mechanism of nucleotide release, which might be a significant contributor to the observed extracellular accumulation. As a potential release mechanism Kreda *et al.* 2010 paper supports the observed nucleotide concentrations and this release pathway, as they showed within secretary granules the nucleotide pool by concentration was ADP > AMP >>ATP [673]. Bodin *et al.* (2001) reported ATP release from endothelia to be via exocytosis [323].

10.2.6. Concluding Remarks

In this study, the data confirms that ADP is present alongside ATP in the extracellular environment. What is surprising is the concentration of the observed nucleotides.

One explanation is that the observed nucleotides both arise from cellular release since it is difficult to reconcile the generation of such large amounts of ADP. Whilst the exact release mechanism remains elusive the data presented here implicates the involvement of the $P2X_7$ channel in some ways and not connexin or pannexins hemichannels. Further characterisation of hypoxia and nucleotide release is clearly needed. Such characterisation should not be restricted to ATP as occurs in most studies.

One interesting scenarios is that since $P2X_7$ activation may be coupled to exocytosis by way of signalling at micro-domains [540]. This may explain the sensitivity of the extracellular nucleotide elevations to oATP. The presence of large amount ADP is secretary vesicles would explain the large amount of extracellular ADP seen in these studies.

10.2.7. Future Work

Molecular approaches such as siRNA to establish if extracellular nucleotide elevation is arising from hemichannel or $P2X_7$ linked exocytosis would provide valuable insight. Additional approaches to inducing CIH are needed.

Finally measurements of intracellular ATP or the ATP to ADP ratio to link with measurement of extracellular nucleotide elevation would be insightful. The ATeam probe, a genetically-encoded FRET-based indicators for ATP, that exhibits high selectivity to ATP (ε subunit) over other nucleotides; offering sensitivity to ATP in the range of 2 μM to 8 mM [666]. Perceval is a fluorescent sensor constructed in 2009 by Berg *et al.*, Perceval allows the measurement of an ATP:ADP ratio [627]. The sensor function is executed by the backbone of Perceval whilst the fluorescent characteristics are mediated by using circularly permuted24 monomeric Venus

(cpmVenus). Perceval has a prominent emission peak at 530 nm when excited at 490 nm and an additional smaller peak at 405 nm excitation and the F_{490}/F_{405} ratio increases threefold and only 1.4 times in the presence of ATP (saturated) and ADP (saturated), respectively. As such the probe allows the measurement of both ATP and ADP, for a full review please see Berg *et al.* (2009) [627]. Extracellular nucleotide could be measured by these probes of they were attached to cell surface proteins. However, they may lack the sensitivity and range of luciferase [666].

10.3. Cardiomyocytes

To further study nucleotide release in metabolic poisoning and the role of $\Delta\psi_m$ in IPC a working CM model was sought.

The immunofluorescence labelling results confirmed the presence of cardiomyocyte specific markers (sarcomeric α-actinin, myosin heavy chain MF-20 and Troponin T) in chick cardiomyocyte heart sections. These markers were not present in Swiss 3T3 fibroblast cells. The antibodies selected showed CM specific staining in line with previously published papers [459, 494-498].

Whilst HL-1 cells were a proposed functional CM model in culture the cells lacked contractile activity or immunofluorescent staining [472, 475, 483-486]. In contrast the primary chicks CMs offered a viable cell model with specific CM immunofluorescence labelling and spontaneous contractile activity.

10.3.1. Cardiomyocyte Culture Purity

The presence of non-CM cells (presumably fibroblasts or endothelial cells) within the population was not surprising as a heterogenous population has been shown essential for proper CM growth and function [452, 453, 457]. Without fibroblast specific staining, using antibodies such as anti-vimentin or CD31, CD34 it is only speculation that these non-CM cells are fibroblasts or endothelial cells [674, 675].

Homogenous populations remove interference from non-CM cells and are achievable using pluripotent stem cells, however fibroblasts are necessary in primary cultures [452, 453, 469, 676]. Despite the heterogeneous cell populations, the primary chick cultures form distinct, contractile 'myoballs' [635, 636].

10.3.2. Calcium dynamics

Spontaneous contractile activity was observed in the apparent 'myoballs' Ca^{2+}-dynamics and was recorded to validate CM physiology. The cell population displayed discrete and repeatable $[Ca^{2+}]_c$-dynamics, whilst not discernible from

background traces. Mitochondrial target aequorin offered an improved system compared to X-Rhod-1 labelling, but still no definitive CM derived signalling was observed. The signalling appears noisy and whilst the responses to ATP may derived from non-CM, the luminescence observed in response to PE and NE stimulation implies CM specific Ca^{2+}-dynamics [321, 585-587, 642].

The poor $[Ca^{2+}]_m$-dynamics may arise from a loss of contractile activity whilst maintained for an extended period in transfection media (Opti-MEM, which lacks FBS and glucose) as opposed to normal culture media. Whilst Opti-MEM media is sufficient to support cells, it may not have been sufficient to support co-ordinated or synchronous beating. The media change may affect transfection efficacy, toxicity was minimised using GeneJuice® as compared to alternative reagents it is apparently nontoxic [677].

With a heterogeneous population the exact cellular source of observed Ca^{2+}-dynamics needs confirming. Transient inhibition using calcium antagonists (L-type channel inhibitors, benzothiazepines, or RyR antagonist ruthenium red) could confirm if the signalling was derived from CM cells within the population [637, 638]. Alternatively mapping the transfected cells, using HA-tagged fusion or mitochondrial targeted GFP could be used to monitor the specific cells transfected and as such the origin of the observed $[Ca^{2+}]_m$ dynamics [678].

Cardiomyocyte and notably primary cell culture transfection using chemical techniques has remained an obstacle, with reagents such as lipofection generating only 15% transfection [679-683]. Viral transduction may provide an improved substitute to plasmid transfection, to introduce mitochondrial targeted aequorin and other reporters. Adeno-associated viral (AAV) vectors have received considerable attention and appear to be a reliable and effective system giving high efficiency of infection and protein expression (88.1% efficacy in rat CMs) [677, 684].

The low aequorin luminescence and lack of measurable Ca^{2+}-dynamics may be attributed to contractile activity being restricted to ‘myoballs’ whilst the detection system measured the entire population. In recording the signalling from the entire

population contractile rhythmic $[Ca^{2+}]_m$-dynamics may be difficult to assess when spiking in distinct regions or non-CMs occurs. To overcome this problem either pure CM populations displaying contractile ability or an alternative detection system allow regions of interest to be measured is required.

The luminescence photometer system however does not allow the measurement of distinct regions such as the contractile 'myoballs' and so measuring $[Ca^{2+}]_m$ changes present a major difficulty. As a solution an imaging approach could be adopted however imaging is better suited to fluorescence rather than luminescence. Confluent CM cultures displaying synchronous activity offer an alternative and overcome these issues, as reported by Kucera *et al.* [685]. The more viable option for immediate research using the chick CM model would be to adapt the detection system in a manner to enable the 'myoballs' to be highlighted as regions of interest, as achieved using the confocal microscope to measure $[Ca^{2+}]_c$.

10.3.3. Concluding Remarks

The long term aim is to take the protocols and initial findings from the work with mitoK_{ATP} channel modulators and nucleotide release in HeLa and EA.hy926 cells and transfer them to the chick CM cells. These cells have the potential to provide a useful model for investigating many aspects of myocyte function. However, monitoring of function must take place at the cellular level and not by population. It would certainly be interesting to monitor intracellular ATP and ADP during hypoxia in these cells.

11. References

1. Halestrap, A.P. and P. Pasdois, *The role of the mitochondrial permeability transition pore in heart disease.* Biochim Biophys Acta, 2009. **1787**(11): p. 1402-15.
2. Nesto, R.W. and G.J. Kowalchuk, *The ischemic cascade: temporal sequence of hemodynamic, electrocardiographic and symptomatic expressions of ischemia.* Am J Cardiol, 1987. **59**(7): p. 23C-30C.
3. Colin Mathers, D.M.F., J. T. Boerma and WHO, *The Global Burden of Disease: 2004 Update.* 2004.
4. Suh, S.H., G. Droogmans, and B. Nilius, *Effects of cyanide and deoxyglucose on Ca2+ signalling in macrovascular endothelial cells.* Endothelium, 2000. **7**(3): p. 155-68.
5. Arnould, T., et al., *Effect of hypoxia upon intracellular calcium concentration of human endothelial cells.* J Cell Physiol, 1992. **152**(1): p. 215-21.
6. Hansson, G.K., *Mechanisms of disease - Inflammation, atherosclerosis, and coronary artery disease.* New England Journal of Medicine, 2005. **352**(16): p. 1685-1695.
7. Libby, P., P.M. Ridker, and A. Maseri, *Inflammation and atherosclerosis.* Circulation, 2002. **105**(9): p. 1135-43.
8. Navab, M., et al., *The Yin and Yang of oxidation in the development of the fatty streak. A review based on the 1994 George Lyman Duff Memorial Lecture.* Arterioscler Thromb Vasc Biol, 1996. **16**(7): p. 831-42.
9. Bird, D.A., et al., *Receptors for oxidized low-density lipoprotein on elicited mouse peritoneal macrophages can recognize both the modified lipid moieties and the modified protein moieties: implications with respect to macrophage recognition of apoptotic cells.* Proc Natl Acad Sci U S A, 1999. **96**(11): p. 6347-52.
10. Toth, P.P., *An urgent matter-identifying your patients' cardiovascular risk and improving their outcomes. Atherosclerosis: the underlying disease.* J Fam Pract, 2009. **58**(11 Suppl Urgent): p. S19-25.
11. Ibanez, B., G. Vilahur, and J.J. Badimon, *Plaque progression and regression in atherothrombosis.* J Thromb Haemost, 2007. **5 Suppl 1**: p. 292-9.
12. Stocker, R. and J.F. Keaney, Jr., *Role of oxidative modifications in atherosclerosis.* Physiol Rev, 2004. **84**(4): p. 1381-478.
13. de Winther, M.P. and M.H. Hofker, *Scavenging new insights into atherogenesis.* J Clin Invest, 2000. **105**(8): p. 1039-41.
14. Glass, C.K. and J.L. Witztum, *Atherosclerosis. the road ahead.* Cell, 2001. **104**(4): p. 503-16.
15. Garlid, K.D., et al., *Mitochondrial potassium transport: the role of the mitochondrial ATP-sensitive K(+) channel in cardiac function and cardioprotection.* Biochim Biophys Acta, 2003. **1606**(1-3): p. 1-21.
16. Millane, T., et al., *ABC of heart failure. Acute and chronic management strategies.* BMJ, 2000. **320**(7234): p. 559-62.

17. Koenig, W. and N. Khuseyinova, *Biomarkers of atherosclerotic plaque instability and rupture.* Arterioscler Thromb Vasc Biol, 2007. **27**(1): p. 15-26.
18. Kristian, T. and B.K. Siesjo, *Calcium in ischemic cell death.* Stroke, 1998. **29**(3): p. 705-18.
19. Peng, T.I. and M.J. Jou, *Oxidative stress caused by mitochondrial calcium overload.* Ann N Y Acad Sci, 2010. **1201**: p. 183-8.
20. Denton, R.M. and J.G. McCormack, *Ca2+ as a second messenger within mitochondria of the heart and other tissues.* Annu Rev Physiol, 1990. **52**: p. 451-66.
21. Robson, S.C., J. Sevigny, and H. Zimmermann, *The E-NTPDase family of ectonucleotidases: Structure function relationships and pathophysiological significance.* Purinergic Signal, 2006. **2**(2): p. 409-30.
22. Varadarajan, S.G., et al., *Changes in [Na(+)](i), compartmental [Ca(2+)], and NADH with dysfunction after global ischemia in intact hearts.* Am J Physiol Heart Circ Physiol, 2001. **280**(1): p. H280-93.
23. Carvalho, B.M., et al., *Enhanced calcium mobilization in rat ventricular myocytes during the onset of pressure overload-induced hypertrophy.* Am J Physiol Heart Circ Physiol, 2006. **291**(4): p. H1803-13.
24. Fowler, M.R., et al., *Decreased Ca2+ extrusion via Na+/Ca2+ exchange in epicardial left ventricular myocytes during compensated hypertrophy.* Am J Physiol Heart Circ Physiol, 2005. **288**(5): p. H2431-8.
25. Wickenden, A.D., et al., *The role of action potential prolongation and altered intracellular calcium handling in the pathogenesis of heart failure.* Cardiovasc Res, 1998. **37**(2): p. 312-23.
26. Dorn, G.W., 2nd and J.D. Molkentin, *Manipulating cardiac contractility in heart failure: data from mice and men.* Circulation, 2004. **109**(2): p. 150-8.
27. Nicholls, D.G., *A role for the mitochondrion in the protection of cells against calcium overload?* Prog Brain Res, 1985. **63**: p. 97-106.
28. Duchen, M.R., *Roles of mitochondria in health and disease.* Diabetes, 2004. **53 Suppl 1**: p. S96-102.
29. Zhang, D., et al., *Mitochondrial DNA mutations activate the mitochondrial apoptotic pathway and cause dilated cardiomyopathy.* Cardiovasc Res, 2003. **57**(1): p. 147-57.
30. Cairns, C.B., *Rude unhinging of the machinery of life: metabolic approaches to hemorrhagic shock.* Curr Opin Crit Care, 2001. **7**(6): p. 437-43.
31. Roderick, H.L., et al., *Calcium in the heart: when it's good, it's very very good, but when it's bad, it's horrid.* Biochem Soc Trans, 2007. **35**(Pt 5): p. 957-61.
32. Duchen, M.R., et al., *On the involvement of a cyclosporin A sensitive mitochondrial pore in myocardial reperfusion injury.* Cardiovasc Res, 1993. **27**(10): p. 1790-4.
33. Halestrap, A.P., *What is the mitochondrial permeability transition pore?* J Mol Cell Cardiol, 2009. **46**(6): p. 821-31.
34. Zoratti, M. and I. Szabo, *The mitochondrial permeability transition.* Biochim Biophys Acta, 1995. **1241**(2): p. 139-76.
35. Ichas, F., L.S. Jouaville, and J.P. Mazat, *Mitochondria are excitable organelles capable of generating and conveying electrical and calcium signals.* Cell, 1997. **89**(7): p. 1145-53.

36. Gustafsson, A.B. and R.A. Gottlieb, *Mechanisms of apoptosis in the heart.* J Clin Immunol, 2003. **23**(6): p. 447-59.
37. Gustafsson, A.B. and R.A. Gottlieb, *Heart mitochondria: gates of life and death.* Cardiovasc Res, 2008. **77**(2): p. 334-43.
38. Martinou, J.C. and D.R. Green, *Breaking the mitochondrial barrier.* Nat Rev Mol Cell Biol, 2001. **2**(1): p. 63-7.
39. Gunter, T.E. and D.R. Pfeiffer, *Mechanisms by which mitochondria transport calcium.* Am J Physiol, 1990. **258**(5 Pt 1): p. C755-86.
40. Pain, T., et al., *Opening of mitochondrial K(ATP) channels triggers the preconditioned state by generating free radicals.* Circ Res, 2000. **87**(6): p. 460-6.
41. Forbes, R.A., C. Steenbergen, and E. Murphy, *Diazoxide-induced cardioprotection requires signaling through a redox-sensitive mechanism.* Circ Res, 2001. **88**(8): p. 802-9.
42. Heyndrickx, G.R., et al., *Regional myocardial functional and electrophysiological alterations after brief coronary artery occlusion in conscious dogs.* J Clin Invest, 1975. **56**(4): p. 978-85.
43. Maxwell, S.R. and G.Y. Lip, *Reperfusion injury: a review of the pathophysiology, clinical manifestations and therapeutic options.* Int J Cardiol, 1997. **58**(2): p. 95-117.
44. Reffelmann, T., et al., *No-reflow phenomenon persists long-term after ischemia/reperfusion in the rat and predicts infarct expansion.* Circulation, 2003. **108**(23): p. 2911-7.
45. Agati, L., *Microvascular integrity after reperfusion therapy.* Am Heart J, 1999. **138**(2 Pt 2): p. S76-8.
46. Park, J.L. and B.R. Lucchesi, *Mechanisms of myocardial reperfusion injury.* Ann Thorac Surg, 1999. **68**(5): p. 1905-12.
47. Granger, D.N., *Ischemia-reperfusion: mechanisms of microvascular dysfunction and the influence of risk factors for cardiovascular disease.* Microcirculation, 1999. **6**(3): p. 167-78.
48. Collard, C.D., et al., *Neutrophil-derived glutamate regulates vascular endothelial barrier function.* J Biol Chem, 2002. **277**(17): p. 14801-11.
49. Eltzschig, H.K. and C.D. Collard, *Vascular ischaemia and reperfusion injury.* Br Med Bull, 2004. **70**: p. 71-86.
50. Carden, D.L. and D.N. Granger, *Pathophysiology of ischaemia-reperfusion injury.* J Pathol, 2000. **190**(3): p. 255-66.
51. Kaminski, K.A., et al., *Oxidative stress and neutrophil activation--the two keystones of ischemia/reperfusion injury.* Int J Cardiol, 2002. **86**(1): p. 41-59.
52. Gross, G.J., J.R. Kersten, and D.C. Warltier, *Mechanisms of postischemic contractile dysfunction.* Ann Thorac Surg, 1999. **68**(5): p. 1898-904.
53. Rao, V., et al., *Lactate release during reperfusion predicts low cardiac output syndrome after coronary bypass surgery.* Ann Thorac Surg, 2001. **71**(6): p. 1925-30.
54. Taegtmeyer, H., P. Razeghi, and M.E. Young, *Mitochondrial proteins in hypertrophy and atrophy: a transcript analysis in rat heart.* Clin Exp Pharmacol Physiol, 2002. **29**(4): p. 346-50.

55. Young, M.E., et al., *Uncoupling protein 3 transcription is regulated by peroxisome proliferator-activated receptor (alpha) in the adult rodent heart.* FASEB J, 2001. **15**(3): p. 833-45.
56. Douette, P. and F.E. Sluse, *Mitochondrial uncoupling proteins: new insights from functional and proteomic studies.* Free Radic Biol Med, 2006. **40**(7): p. 1097-107.
57. Vidal-Puig, A.J., et al., *Energy metabolism in uncoupling protein 3 gene knockout mice.* J Biol Chem, 2000. **275**(21): p. 16258-66.
58. McLeod, C.J., et al., *Uncoupling proteins 2 and 3 function in concert to augment tolerance to cardiac ischemia.* J Biol Chem, 2005. **280**(39): p. 33470-6.
59. Laskowski, K.R. and R.R. Russell, 3rd, *Uncoupling proteins in heart failure.* Curr Heart Fail Rep, 2008. **5**(2): p. 75-9.
60. Pacher, P., J.S. Beckman, and L. Liaudet, *Nitric oxide and peroxynitrite in health and disease.* Physiol Rev, 2007. **87**(1): p. 315-424.
61. Brookes, P.S. and V.M. Darley-Usmar, *Role of calcium and superoxide dismutase in sensitizing mitochondria to peroxynitrite-induced permeability transition.* Am J Physiol Heart Circ Physiol, 2004. **286**(1): p. H39-46.
62. Brown, G.C. and V. Borutaite, *Nitric oxide, cytochrome c and mitochondria.* Biochem Soc Symp, 1999. **66**: p. 17-25.
63. Bolli, R., et al., *Direct evidence that oxygen-derived free radicals contribute to postischemic myocardial dysfunction in the intact dog.* Proc Natl Acad Sci U S A, 1989. **86**(12): p. 4695-9.
64. Jordan, J.E., Z.Q. Zhao, and J. Vinten-Johansen, *The role of neutrophils in myocardial ischemia-reperfusion injury.* Cardiovasc Res, 1999. **43**(4): p. 860-78.
65. Berry, C.E. and J.M. Hare, *Xanthine oxidoreductase and cardiovascular disease: molecular mechanisms and pathophysiological implications.* J Physiol, 2004. **555**(Pt 3): p. 589-606.
66. Li, C. and R.M. Jackson, *Reactive species mechanisms of cellular hypoxia-reoxygenation injury.* Am J Physiol Cell Physiol, 2002. **282**(2): p. C227-41.
67. Toyokuni, S., *Reactive oxygen species-induced molecular damage and its application in pathology.* Pathol Int, 1999. **49**(2): p. 91-102.
68. Beckman, J.S., *Ischaemic injury mediator.* Nature, 1990. **345**(6270): p. 27-8.
69. Beckman, J.S. and W.H. Koppenol, *Nitric oxide, superoxide, and peroxynitrite: the good, the bad, and ugly.* Am J Physiol, 1996. **271**(5 Pt 1): p. C1424-37.
70. Brown, G.C. and V. Borutaite, *Inhibition of mitochondrial respiratory complex I by nitric oxide, peroxynitrite and S-nitrosothiols.* Biochim Biophys Acta, 2004. **1658**(1-2): p. 44-9.
71. Murray, J., et al., *Oxidative damage to mitochondrial complex I due to peroxynitrite: identification of reactive tyrosines by mass spectrometry.* J Biol Chem, 2003. **278**(39): p. 37223-30.
72. Cassina, A. and R. Radi, *Differential inhibitory action of nitric oxide and peroxynitrite on mitochondrial electron transport.* Arch Biochem Biophys, 1996. **328**(2): p. 309-16.
73. Guidarelli, A., M. Fiorani, and O. Cantoni, *Enhancing effects of intracellular ascorbic acid on peroxynitrite-induced U937 cell death are mediated by*

mitochondrial events resulting in enhanced sensitivity to peroxynitrite-dependent inhibition of complex III and formation of hydrogen peroxide. Biochem J, 2004. **378**(Pt 3): p. 959-66.

74. Radi, R., et al., *Peroxynitrite reactions and formation in mitochondria.* Free Radic Biol Med, 2002. **33**(11): p. 1451-64.
75. Pearce, L.L., et al., *The catabolic fate of nitric oxide: the nitric oxide oxidase and peroxynitrite reductase activities of cytochrome oxidase.* J Biol Chem, 2002. **277**(16): p. 13556-62.
76. Castro, L., M. Rodriguez, and R. Radi, *Aconitase is readily inactivated by peroxynitrite, but not by its precursor, nitric oxide.* J Biol Chem, 1994. **269**(47): p. 29409-15.
77. Han, D., et al., *Sites and mechanisms of aconitase inactivation by peroxynitrite: modulation by citrate and glutathione.* Biochemistry, 2005. **44**(36): p. 11986-96.
78. Borutaite, V., R. Morkuniene, and G.C. Brown, *Release of cytochrome c from heart mitochondria is induced by high Ca2+ and peroxynitrite and is responsible for Ca(2+)-induced inhibition of substrate oxidation.* Biochim Biophys Acta, 1999. **1453**(1): p. 41-8.
79. Bonfoco, E., et al., *Apoptosis and necrosis: two distinct events induced, respectively, by mild and intense insults with N-methyl-D-aspartate or nitric oxide/superoxide in cortical cell cultures.* Proc Natl Acad Sci U S A, 1995. **92**(16): p. 7162-6.
80. Scarlett, J.L., et al., *Alterations to glutathione and nicotinamide nucleotides during the mitochondrial permeability transition induced by peroxynitrite.* Biochem Pharmacol, 1996. **52**(7): p. 1047-55.
81. Vieira, H.L., et al., *The adenine nucleotide translocator: a target of nitric oxide, peroxynitrite, and 4-hydroxynonenal.* Oncogene, 2001. **20**(32): p. 4305-16.
82. Eltzschig, H.K., et al., *Coordinated adenine nucleotide phosphohydrolysis and nucleoside signaling in posthypoxic endothelium: role of ectonucleotidases and adenosine A2B receptors.* J Exp Med, 2003. **198**(5): p. 783-96.
83. Eltzschig, H.K., et al., *Endogenous adenosine produced during hypoxia attenuates neutrophil accumulation: coordination by extracellular nucleotide metabolism.* Blood, 2004. **104**(13): p. 3986-92.
84. Medzhitov, R. and C.A. Janeway, Jr., *An ancient system of host defense.* Curr Opin Immunol, 1998. **10**(1): p. 12-5.
85. Hill, J.H. and P.A. Ward, *The phlogistic role of C3 leukotactic fragments in myocardial infarcts of rats.* J Exp Med, 1971. **133**(4): p. 885-900.
86. Vlaicu, R., et al., *Immunoglobulins and complement components in human aortic atherosclerotic intima.* Atherosclerosis, 1985. **55**(1): p. 35-50.
87. Spain, D.A., et al., *Complement activation mediates intestinal injury after resuscitation from hemorrhagic shock.* J Trauma, 1999. **46**(2): p. 224-33.
88. Mulligan, M.S., et al., *Requirement and role of C5a in acute lung inflammatory injury in rats.* J Clin Invest, 1996. **98**(2): p. 503-12.
89. Rus, H., C. Cudrici, and F. Niculescu, *The role of the complement system in innate immunity.* Immunol Res, 2005. **33**(2): p. 103-12.

90. Nakase, T., et al., *The impact of inflammation on the pathogenesis and prognosis of ischemic stroke.* J Neurol Sci, 2008. **271**(1-2): p. 104-9.
91. Hashimoto, H., et al., *C-reactive protein is an independent predictor of the rate of increase in early carotid atherosclerosis.* Circulation, 2001. **104**(1): p. 63-7.
92. Trial, J., et al., *Inflammation and ischemia: macrophages activated by fibronectin fragments enhance the survival of injured cardiac myocytes.* Exp Biol Med (Maywood), 2004. **229**(6): p. 538-45.
93. Collard, C.D., et al., *Complement activation following oxidative stress.* Mol Immunol, 1999. **36**(13-14): p. 941-8.
94. Kilgore, K.S., et al., *Neutrophils and reactive oxygen intermediates mediate glucan-induced pulmonary granuloma formation through the local induction of monocyte chemoattractant protein-1.* Lab Invest, 1997. **76**(2): p. 191-201.
95. Dreyer, W.J., et al., *Kinetics of C5a release in cardiac lymph of dogs experiencing coronary artery ischemia-reperfusion injury.* Circ Res, 1992. **71**(6): p. 1518-24.
96. Vogt, W., et al., *Non-enzymic activation of the fifth component of human complement, by oxygen radicals. Some properties of the activation product, C5b-like C5.* Mol Immunol, 1989. **26**(12): p. 1133-42.
97. Murry, C.E., R.B. Jennings, and K.A. Reimer, *Preconditioning with ischemia: a delay of lethal cell injury in ischemic myocardium.* Circulation, 1986. **74**(5): p. 1124-36.
98. O'Rourke, B., *Myocardial K(ATP) channels in preconditioning.* Circ Res, 2000. **87**(10): p. 845-55.
99. Lundberg, K.C. and L.I. Szweda, *Preconditioning prevents loss in mitochondrial function and release of cytochrome c during prolonged cardiac ischemia/reperfusion.* Arch Biochem Biophys, 2006. **453**(1): p. 130-4.
100. Minamino, T., et al., *Cardioprotection due to preconditioning correlates with increased ecto-5'-nucleotidase activity.* Am J Physiol, 1996. **270**(1 Pt 2): p. H238-44.
101. Vinten-Johansen, J., et al., *Broad-spectrum cardioprotection with adenosine.* Ann Thorac Surg, 1999. **68**(5): p. 1942-8.
102. Ostadal, B., I. Ostadalova, and N.S. Dhalla, *Development of cardiac sensitivity to oxygen deficiency: comparative and ontogenetic aspects.* Physiol Rev, 1999. **79**(3): p. 635-59.
103. Loubani, M., A. Hassouna, and M. Galiñanes, *Delayed preconditioning of the human myocardium: signal transduction and clinical implications.* Cardiovascular Research, 2004. **61**(3): p. 600-609.
104. Baxter, G.F. and P. Ferdinandy, *Delayed preconditioning of myocardium: current perspectives.* Basic Res Cardiol, 2001. **96**(4): p. 329-44.
105. DeFily, D.V. and W.M. Chilian, *Preconditioning protects coronary arteriolar endothelium from ischemia-reperfusion injury.* Am J Physiol, 1993. **265**(2 Pt 2): p. H700-6.
106. Thourani, V.H., et al., *Ischemic preconditioning attenuates postischemic coronary artery endothelial dysfunction in a model of minimally invasive direct coronary artery bypass grafting.* J Thorac Cardiovasc Surg, 1999. **117**(2): p. 383-9.

107. Nakamura, M., et al., *Preconditioning decreases Bax expression, PMN accumulation and apoptosis in reperfused rat heart.* Cardiovasc Res, 2000. **45**(3): p. 661-70.
108. Kloner, R.A. and R.B. Jennings, *Consequences of brief ischemia: stunning, preconditioning, and their clinical implications: part 2.* Circulation, 2001. **104**(25): p. 3158-67.
109. Wu, Z.K., et al., *Ischemic preconditioning suppresses ventricular tachyarrhythmias after myocardial revascularization.* Circulation, 2002. **106**(24): p. 3091-6.
110. Meldrum, D.R., et al., *Protein kinase C mediates Ca2(+)-induced cardioadaptation to ischemia-reperfusion injury.* Am J Physiol, 1996. **271**(3 Pt 2): p. R718-26.
111. Meldrum, D.R., et al., *Cardiac preconditioning with calcium: clinically accessible myocardial protection.* J Thorac Cardiovasc Surg, 1996. **112**(3): p. 778-86.
112. Miyawaki, H., X. Zhou, and M. Ashraf, *Calcium preconditioning elicits strong protection against ischemic injury via protein kinase C signaling pathway.* Circ Res, 1996. **79**(1): p. 137-46.
113. Sewell, W.H., D.R. Koth, and C.E. Huggins, *Ventricular fibrillation in dogs after sudden return of flow to the coronary artery.* Surgery, 1955. **38**(6): p. 1050-3.
114. Tsang, A., D.J. Hausenloy, and D.M. Yellon, *Myocardial postconditioning: reperfusion injury revisited.* Am J Physiol Heart Circ Physiol, 2005. **289**(1): p. H2-7.
115. Zhao, H., *The protective effect of ischemic postconditioning against ischemic injury: from the heart to the brain.* J Neuroimmune Pharmacol, 2007. **2**(4): p. 313-8.
116. Zhao, H., *Ischemic postconditioning as a novel avenue to protect against brain injury after stroke.* J Cereb Blood Flow Metab, 2009. **29**(5): p. 873-885.
117. Zhao, Z.Q., et al., *Inhibition of myocardial injury by ischemic postconditioning during reperfusion: comparison with ischemic preconditioning.* Am J Physiol Heart Circ Physiol, 2003. **285**(2): p. H579-88.
118. Galagudza, M., et al., *Ischemic postconditioning: brief ischemia during reperfusion converts persistent ventricular fibrillation into regular rhythm.* European Journal of Cardio-Thoracic Surgery, 2004. **25**(6): p. 1006-1010.
119. Stojnic, N., et al., *Potassium channel opener pinacidil induces relaxation of the isolated human radial artery.* J Pharmacol Sci, 2007. **104**(2): p. 122-9.
120. Costa, A.D., et al., *The direct physiological effects of mitoK(ATP) opening on heart mitochondria.* Am J Physiol Heart Circ Physiol, 2006. **290**(1): p. H406-15.
121. Liu, Y., et al., *Mitochondrial ATP-dependent potassium channels: novel effectors of cardioprotection?* Circulation, 1998. **97**(24): p. 2463-9.
122. Garlid, K.D., et al., *Cardioprotective effect of diazoxide and its interaction with mitochondrial ATP-sensitive K+ channels. Possible mechanism of cardioprotection.* Circ Res, 1997. **81**(6): p. 1072-82.

123. Sato, T., et al., *Adenosine primes the opening of mitochondrial ATP-sensitive potassium channels: a key step in ischemic preconditioning?* Circulation, 2000. **102**(7): p. 800-5.
124. Gross, G.J., D.C. Warltier, and H.F. Hardman, *Comparative effects of nicorandil, a nicotinamide nitrate derivative, and nifedipine on myocardial reperfusion injury in dogs.* J Cardiovasc Pharmacol, 1987. **10**(5): p. 535-42.
125. Grover, G.J., et al., *Anti-ischemic effects of the potassium channel activators pinacidil and cromakalim and the reversal of these effects with the potassium channel blocker glyburide.* J Pharmacol Exp Ther, 1989. **251**(1): p. 98-104.
126. Imai, N., et al., *Comparative effects of nitroprusside and pinacidil on myocardial blood flow and infarct size in awake dogs with acute myocardial infarction.* Circulation, 1988. **77**(3): p. 705-11.
127. Chiang, N., et al., *Leukotriene B4 receptor transgenic mice reveal novel protective roles for lipoxins and aspirin-triggered lipoxins in reperfusion.* J Clin Invest, 1999. **104**(3): p. 309-16.
128. Panes, J., M. Perry, and D.N. Granger, *Leukocyte-endothelial cell adhesion: avenues for therapeutic intervention.* Br J Pharmacol, 1999. **126**(3): p. 537-50.
129. Shinmura, K., et al., *Inducible Nitric Oxide Synthase Modulates Cyclooxygenase-2 Activity in the Heart of Conscious Rabbits During the Late Phase of Ischemic Preconditioning.* Circulation Research, 2002. **90**(5): p. 602-608.
130. Atochin, D.N., et al., *Rapid cerebral ischemic preconditioning in mice deficient in endothelial and neuronal nitric oxide synthases.* Stroke, 2003. **34**(5): p. 1299-303.
131. Park, K.M., et al., *Inducible nitric-oxide synthase is an important contributor to prolonged protective effects of ischemic preconditioning in the mouse kidney.* J Biol Chem, 2003. **278**(29): p. 27256-66.
132. Barry, O.P., et al., *Arachidonic acid in platelet microparticles up-regulates cyclooxygenase-2-dependent prostaglandin formation via a protein kinase C/mitogen-activated protein kinase-dependent pathway.* J Biol Chem, 1999. **274**(11): p. 7545-56.
133. Blanco, A., et al., *Involvement of tyrosine kinases in the induction of cyclo-oxygenase-2 in human endothelial cells.* Biochem J, 1995. **312 (Pt 2)**: p. 419-23.
134. von Knethen, A., D. Callsen, and B. Brune, *Superoxide attenuates macrophage apoptosis by NF-kappa B and AP-1 activation that promotes cyclooxygenase-2 expression.* J Immunol, 1999. **163**(5): p. 2858-66.
135. Schmedtje, J.F., Jr., et al., *Hypoxia induces cyclooxygenase-2 via the NF-kappaB p65 transcription factor in human vascular endothelial cells.* J Biol Chem, 1997. **272**(1): p. 601-8.
136. Shinmura, K., et al., *Cyclooxygenase-2 mediates the cardioprotective effects of the late phase of ischemic preconditioning in conscious rabbits.* Proc Natl Acad Sci U S A, 2000. **97**(18): p. 10197-202.

137. Guo, Y., et al., *Evidence for an essential role of cyclooxygenase-2 as a mediator of the late phase of ischemic preconditioning in mice.* Basic Res Cardiol, 2000. **95**(6): p. 479-84.
138. Marzi, I., et al., *Value of superoxide dismutase for prevention of multiple organ failure after multiple trauma.* J Trauma, 1993. **35**(1): p. 110-9; discussion 119-20.
139. Land, W., et al., *The beneficial effect of human recombinant superoxide dismutase on acute and chronic rejection events in recipients of cadaveric renal transplants.* Transplantation, 1994. **57**(2): p. 211-7.
140. Przyklenk, K., *Pharmacologic treatment of the stunned myocardium: the concepts and the challenges.* Coron Artery Dis, 2001. **12**(5): p. 363-9.
141. Weisman, H.F., et al., *Soluble human complement receptor type 1: in vivo inhibitor of complement suppressing post-ischemic myocardial inflammation and necrosis.* Science, 1990. **249**(4965): p. 146-51.
142. Altmann, R., *Die Elementarorganismen und ihre Beziehungen zu den Zellen. Zweite vermehrte Auflage (The Elementary Organisms and Their Relationships to the Cells. Second Extended Edition).* Verlag Von Veit & Comp, Leipzig., 1894. **160**: p. 34.
143. Ernster, L. and G. Schatz, *Mitochondria: a historical review.* J Cell Biol, 1981. **91**(3 Pt 2): p. 227s-255s.
144. Garlid, K.D. and A.P. Halestrap, *The mitochondrial K(ATP) channel--fact or fiction?* J Mol Cell Cardiol, 2012. **52**(3): p. 578-83.
145. McBride, H.M., M. Neuspiel, and S. Wasiak, *Mitochondria: more than just a powerhouse.* Curr Biol, 2006. **16**(14): p. R551-60.
146. Hajnoczky, G., et al., *Mitochondrial calcium signalling and cell death: approaches for assessing the role of mitochondrial Ca2+ uptake in apoptosis.* Cell Calcium, 2006. **40**(5-6): p. 553-60.
147. Green, D.R., *Apoptotic pathways: the roads to ruin.* Cell, 1998. **94**(6): p. 695-8.
148. Herrmann, J.M. and W. Neupert, *Protein transport into mitochondria.* Curr Opin Microbiol, 2000. **3**(2): p. 210-4.
149. Schein, S.J., M. Colombini, and A. Finkelstein, *Reconstitution in planar lipid bilayers of a voltage-dependent anion-selective channel obtained from paramecium mitochondria.* J Membr Biol, 1976. **30**(2): p. 99-120.
150. Shoshan-Barmatz, V. and D. Ben-Hail, *VDAC, a multi-functional mitochondrial protein as a pharmacological target.* Mitochondrion, 2012. **12**(1): p. 24-34.
151. Shimizu, S., M. Narita, and Y. Tsujimoto, *Bcl-2 family proteins regulate the release of apoptogenic cytochrome c by the mitochondrial channel VDAC.* Nature, 1999. **399**(6735): p. 483-7.
152. Costantini, P., et al., *Mitochondrion as a novel target of anticancer chemotherapy.* J Natl Cancer Inst, 2000. **92**(13): p. 1042-53.
153. Baines, C.P., et al., *Voltage-dependent anion channels are dispensable for mitochondrial-dependent cell death.* Nat Cell Biol, 2007. **9**(5): p. 550-5.
154. Madesh, M. and G. Hajnoczky, *VDAC-dependent permeabilization of the outer mitochondrial membrane by superoxide induces rapid and massive cytochrome c release.* J Cell Biol, 2001. **155**(6): p. 1003-15.

155. Rousset, S., et al., *The biology of mitochondrial uncoupling proteins.* Diabetes, 2004. **53 Suppl 1**: p. S130-5.
156. Goglia, F. and V.P. Skulachev, *A function for novel uncoupling proteins: antioxidant defense of mitochondrial matrix by translocating fatty acid peroxides from the inner to the outer membrane leaflet.* FASEB J, 2003. **17**(12): p. 1585-91.
157. Rial, E., et al., *Retinoids activate proton transport by the uncoupling proteins UCP1 and UCP2.* EMBO J, 1999. **18**(21): p. 5827-33.
158. Raha, S. and B.H. Robinson, *Mitochondria, oxygen free radicals, disease and ageing.* Trends Biochem Sci, 2000. **25**(10): p. 502-8.
159. Chevet, E., et al., *The endoplasmic reticulum: integration of protein folding, quality control, signaling and degradation.* Curr Opin Struct Biol, 2001. **11**(1): p. 120-4.
160. Palade, G., *Intracellular aspects of the process of protein synthesis.* Science, 1975. **189**(4200): p. 347-58.
161. Bootman, M.D., O.H. Petersen, and A. Verkhratsky, *The endoplasmic reticulum is a focal point for co-ordination of cellular activity.* Cell Calcium, 2002. **32**(5-6): p. 231-4.
162. Verkhratsky, A. and O.H. Petersen, *The endoplasmic reticulum as an integrating signalling organelle: from neuronal signalling to neuronal death.* Eur J Pharmacol, 2002. **447**(2-3): p. 141-54.
163. Rizzuto, R., et al., *Mitochondria as biosensors of calcium microdomains.* Cell Calcium, 1999. **26**(5): p. 193-9.
164. Csordas, G., et al., *Structural and functional features and significance of the physical linkage between ER and mitochondria.* J Cell Biol, 2006. **174**(7): p. 915-21.
165. Giorgi, C., et al., *Structural and functional link between the mitochondrial network and the endoplasmic reticulum.* Int J Biochem Cell Biol, 2009. **41**(10): p. 1817-27.
166. Rizzuto, R., et al., *Close contacts with the endoplasmic reticulum as determinants of mitochondrial Ca2+ responses.* Science, 1998. **280**(5370): p. 1763-6.
167. Mannella, C.A., et al., *Electron microscopic tomography of rat-liver mitochondria and their interaction with the endoplasmic reticulum.* Biofactors, 1998. **8**(3-4): p. 225-8.
168. Lebiedzinska, M., et al., *Interactions between the endoplasmic reticulum, mitochondria, plasma membrane and other subcellular organelles.* Int J Biochem Cell Biol, 2009. **41**(10): p. 1805-16.
169. Berridge, M.J., *The endoplasmic reticulum: a multifunctional signaling organelle.* Cell Calcium, 2002. **32**(5-6): p. 235-49.
170. Stone, S.J. and J.E. Vance, *Phosphatidylserine synthase-1 and -2 are localized to mitochondria-associated membranes.* J Biol Chem, 2000. **275**(44): p. 34534-40.
171. Vance, J.E., *Phospholipid synthesis in a membrane fraction associated with mitochondria.* J Biol Chem, 1990. **265**(13): p. 7248-56.
172. Da Poian, A.T., El-Bacha, T. & Luz, M. R, *Nutrient Utilization in Humans: Metabolism Pathways.* Nature Education, 2010. **3**(9): p. 11.

173. Jouaville, L.S., et al., *Regulation of mitochondrial ATP synthesis by calcium: evidence for a long-term metabolic priming.* Proc Natl Acad Sci U S A, 1999. **96**(24): p. 13807-12.
174. Berridge, M.J., *Elementary and global aspects of calcium signalling.* J Physiol, 1997. **499 (Pt 2)**: p. 291-306.
175. Bell, C.J., et al., *ATP regulation in adult rat cardiomyocytes: time-resolved decoding of rapid mitochondrial calcium spiking imaged with targeted photoproteins.* J Biol Chem, 2006. **281**(38): p. 28058-67.
176. Gaspers, L.D. and A.P. Thomas, *Calcium-dependent activation of mitochondrial metabolism in mammalian cells.* Methods, 2008. **46**(3): p. 224-32.
177. Eaton, R.P., *Glucagon and lipoproteins.* Metabolism, 1976. **25**(11 Suppl 1): p. 1415-7.
178. Eaton, R.P., *Synthesis of plasma triglycerides in endogenous hypertriglyceridemia.* J Lipid Res, 1971. **12**(4): p. 491-7.
179. van der Vusse, G.J., M. van Bilsen, and J.F. Glatz, *Cardiac fatty acid uptake and transport in health and disease.* Cardiovasc Res, 2000. **45**(2): p. 279-93.
180. Grynberg, A. and L. Demaison, *Fatty Acid Oxidation in the Heart.* Journal of Cardiovascular Pharmacology, 1996. **28**: p. 11-17.
181. Lopaschuk, G.D., et al., *Regulation of fatty acid oxidation in the mammalian heart in health and disease.* Biochim Biophys Acta, 1994. **1213**(3): p. 263-76.
182. Neely, J.R. and H.E. Morgan, *Relationship between carbohydrate and lipid metabolism and the energy balance of heart muscle.* Annu Rev Physiol, 1974. **36**: p. 413-59.
183. Saddik, M. and G.D. Lopaschuk, *Myocardial triglyceride turnover and contribution to energy substrate utilization in isolated working rat hearts.* J Biol Chem, 1991. **266**(13): p. 8162-70.
184. Bing, R.J., et al., *Metabolism of the human heart. II. Studies on fat, ketone and amino acid metabolism.* Am J Med, 1954. **16**(4): p. 504-15.
185. Opie, L.H., *Metabolism of the heart in health and disease. Part I.* American Heart Journal, 1968. **76**(5): p. 685-698.
186. Opie, L.H., *Metabolism of the heart in health and disease. Part II.* American Heart Journal, 1969. **77**(1): p. 100-122.
187. Wisneski, J.A., et al., *Effects of acute hyperglycemia on myocardial glycolytic activity in humans.* J Clin Invest, 1990. **85**(5): p. 1648-56.
188. Mootha, V.K., A.E. Arai, and R.S. Balaban, *Maximum oxidative phosphorylation capacity of the mammalian heart.* Am J Physiol, 1997. **272**(2 Pt 2): p. H769-75.
189. Harris, D.A. and A.M. Das, *Control of mitochondrial ATP synthesis in the heart.* Biochem J, 1991. **280 (Pt 3)**: p. 561-73.
190. Balaban, R.S., *Cardiac energy metabolism homeostasis: role of cytosolic calcium.* J Mol Cell Cardiol, 2002. **34**(10): p. 1259-71.
191. Berridge, M.J., M.D. Bootman, and H.L. Roderick, *Calcium signalling: dynamics, homeostasis and remodelling.* Nat Rev Mol Cell Biol, 2003. **4**(7): p. 517-29.
192. Knoop, F., *Der Abbau aromatischer Fettsa¨uren im*

Tierko¨rper. Chem. Physiol. Pathol., 1904/05. **6**: p. 150–162.
193. Dakin, H.D., *THE CATALYTIC ACTION OF AMINO-ACIDS, PEPTONES AND PROTEINS IN EFFECTING CERTAIN SYNTHESES.* Journal of Biological Chemistry, 1909. **7**(1): p. 49-55.
194. Lipmann, F., *On chemistry and function of coenzyme A.* Bacteriol Rev, 1953. **17**(1): p. 1-16.
195. Lynen, F. and S. Ochoa, *Enzymes of fatty acid metabolism.* Biochim Biophys Acta, 1953. **12**(1-2): p. 299-314.
196. Vinnars, E., J. Bergstom, and P. Furst, *Influence of the postoperative state on the intracellular free amino acids in human muscle tissue.* Ann Surg, 1975. **182**(6): p. 665-71.
197. Moller, P., et al., *Electrolytes and free amino acids in leg skeletal muscle of young and elderly women.* Gerontology, 1983. **29**(1): p. 1-8.
198. Roth, E., et al., *Amino acid concentrations in plasma and skeletal muscle of patients with acute hemorrhagic necrotizing pancreatitis.* Clin Chem, 1985. **31**(8): p. 1305-9.
199. Askanazi, J., et al., *Muscle and plasma amino acids following injury. Influence of intercurrent infection.* Ann Surg, 1980. **192**(1): p. 78-85.
200. MacLean, D.A., T.E. Graham, and B. Saltin, *Branched-chain amino acids augment ammonia metabolism while attenuating protein breakdown during exercise.* Am J Physiol, 1994. **267**(6 Pt 1): p. E1010-22.
201. Kovacevic, Z. and J.D. McGivan, *Mitochondrial metabolism of glutamine and glutamate and its physiological significance.* Physiol Rev, 1983. **63**(2): p. 547-605.
202. Smith, R.J., *Glutamine metabolism and its physiologic importance.* JPEN J Parenter Enteral Nutr, 1990. **14**(4 Suppl): p. 40S-44S.
203. Stumvoll, M., et al., *Role of glutamine in human carbohydrate metabolism in kidney and other tissues.* Kidney Int, 1999. **55**(3): p. 778-92.
204. Krebs, H.A., *THE INTERMEDIATE METABOLISM OF CARBOHYDRATES.* The Lancet, 1937. **230**(5952): p. 736-738.
205. Mitchell, P., *Coupling of phosphorylation to electron and hydrogen transfer by a chemi-osmotic type of mechanism.* Nature, 1961. **191**: p. 144-8.
206. Mitchell, P. and J. Moyle, *Chemiosmotic Hypothesis of Oxidative Phosphorylation.* Nature, 1967. **213**(5072): p. 137-139.
207. Boyer, P.D., R.L. Cross, and W. Momsen, *A new concept for energy coupling in oxidative phosphorylation based on a molecular explanation of the oxygen exchange reactions.* Proc Natl Acad Sci U S A, 1973. **70**(10): p. 2837-9.
208. Berg JM, T.J.S.L., *Chapter 18, Oxidative Phosphorylation.* Biochemistry., 2002. **5th edition.** .
209. Lenaz, G., et al., *Mitochondrial Complex I: structural and functional aspects.* Biochim Biophys Acta, 2006. **1757**(9-10): p. 1406-20.
210. Heinemeyer, J., et al., *A structural model of the cytochrome C reductase/oxidase supercomplex from yeast mitochondria.* J Biol Chem, 2007. **282**(16): p. 12240-8.
211. Schagger, H. and K. Pfeiffer, *Supercomplexes in the respiratory chains of yeast and mammalian mitochondria.* EMBO J, 2000. **19**(8): p. 1777-83.

212. Schagger, H., *Respiratory chain supercomplexes of mitochondria and bacteria.* Biochim Biophys Acta, 2002. **1555**(1-3): p. 154-9.
213. Hirst, J., *Energy transduction by respiratory complex I--an evaluation of current knowledge.* Biochem Soc Trans, 2005. **33**(Pt 3): p. 525-9.
214. Hirst, J., *Towards the molecular mechanism of respiratory complex I.* Biochem J, 2010. **425**(2): p. 327-39.
215. Cecchini, G., *Function and structure of complex II of the respiratory chain.* Annu Rev Biochem, 2003. **72**: p. 77-109.
216. Ramsay, R.R., D.J. Steenkamp, and M. Husain, *Reactions of electron-transfer flavoprotein and electron-transfer flavoprotein: ubiquinone oxidoreductase.* Biochem J, 1987. **241**(3): p. 883-92.
217. Zhang, J., F.E. Frerman, and J.J. Kim, *Structure of electron transfer flavoprotein-ubiquinone oxidoreductase and electron transfer to the mitochondrial ubiquinone pool.* Proc Natl Acad Sci U S A, 2006. **103**(44): p. 16212-7.
218. Ikeda, Y., C. Dabrowski, and K. Tanaka, *Separation and properties of five distinct acyl-CoA dehydrogenases from rat liver mitochondria. Identification of a new 2-methyl branched chain acyl-CoA dehydrogenase.* J Biol Chem, 1983. **258**(2): p. 1066-76.
219. Ruzicka, F.J. and H. Beinert, *A new iron-sulfur flavoprotein of the respiratory chain. A component of the fatty acid beta oxidation pathway.* J Biol Chem, 1977. **252**(23): p. 8440-5.
220. Berry, E.A., et al., *Structure and function of cytochrome bc complexes.* Annu Rev Biochem, 2000. **69**: p. 1005-75.
221. Trumpower, B.L., *The protonmotive Q cycle. Energy transduction by coupling of proton translocation to electron transfer by the cytochrome bc1 complex.* J Biol Chem, 1990. **265**(20): p. 11409-12.
222. Schultz, B.E. and S.I. Chan, *Structures and proton-pumping strategies of mitochondrial respiratory enzymes.* Annu Rev Biophys Biomol Struct, 2001. **30**: p. 23-65.
223. Hunte, C., H. Palsdottir, and B.L. Trumpower, *Protonmotive pathways and mechanisms in the cytochrome bc1 complex.* FEBS Lett, 2003. **545**(1): p. 39-46.
224. Calhoun, M.W., J.W. Thomas, and R.B. Gennis, *The cytochrome oxidase superfamily of redox-driven proton pumps.* Trends Biochem Sci, 1994. **19**(8): p. 325-30.
225. Boyer, P.D., *The ATP synthase--a splendid molecular machine.* Annu Rev Biochem, 1997. **66**: p. 717-49.
226. Nicholls, D.G. and M.W. Ward, *Mitochondrial membrane potential and neuronal glutamate excitotoxicity: mortality and millivolts.* Trends Neurosci, 2000. **23**(4): p. 166-74.
227. Nicholls, D.G. and V.S. Bernson, *Inter-relationships between proton electrochemical gradient, adenine-nucleotide phosphorylation potential and respiration, during substrate-level and oxidative phosphorylation by mitochondria from brown adipose tissue of cold-adapted guinea-pigs.* Eur J Biochem, 1977. **75**(2): p. 601-12.

228. Garlid, K.D. and P. Paucek, *The mitochondrial potassium cycle.* IUBMB Life, 2001. **52**(3-5): p. 153-8.
229. Garlid, K.D., A.D. Beavis, and S.K. Ratkje, *On the nature of ion leaks in energy-transducing membranes.* Biochim Biophys Acta, 1989. **976**(2-3): p. 109-20.
230. Gross, G.J. and R.M. Fryer, *Sarcolemmal versus mitochondrial ATP-sensitive K+ channels and myocardial preconditioning.* Circ Res, 1999. **84**(9): p. 973-9.
231. Inoue, I., et al., *ATP-sensitive K+ channel in the mitochondrial inner membrane.* Nature, 1991. **352**(6332): p. 244-7.
232. Jang, Y., et al., *NO mobilizes intracellular Zn2+ via cGMP/PKG signaling pathway and prevents mitochondrial oxidant damage in cardiomyocytes.* Cardiovasc Res, 2007. **75**(2): p. 426-33.
233. Brennan, J.P., et al., *Mitochondrial uncoupling, with low concentration FCCP, induces ROS-dependent cardioprotection independent of KATP channel activation.* Cardiovasc Res, 2006. **72**(2): p. 313-21.
234. Holmuhamedov, E.L., et al., *Mitochondrial ATP-sensitive K+ channels modulate cardiac mitochondrial function.* Am J Physiol, 1998. **275**(5 Pt 2): p. H1567-76.
235. Xu, W., et al., *Cytoprotective role of Ca2+- activated K+ channels in the cardiac inner mitochondrial membrane.* Science, 2002. **298**(5595): p. 1029-33.
236. Garlid, K.D., *Cation transport in mitochondria--the potassium cycle.* Biochim Biophys Acta, 1996. **1275**(1-2): p. 123-6.
237. Jaburek, M., et al., *State-dependent inhibition of the mitochondrial KATP channel by glyburide and 5-hydroxydecanoate.* J Biol Chem, 1998. **273**(22): p. 13578-82.
238. Beavis, A.D., *Properties of the inner membrane anion channel in intact mitochondria.* J Bioenerg Biomembr, 1992. **24**(1): p. 77-90.
239. Kowaltowski, A.J., et al., *Bioenergetic consequences of opening the ATP-sensitive K(+) channel of heart mitochondria.* Am J Physiol Heart Circ Physiol, 2001. **280**(2): p. H649-57.
240. Holmuhamedov, E.L., L. Wang, and A. Terzic, *ATP-sensitive K+ channel openers prevent Ca2+ overload in rat cardiac mitochondria.* J Physiol, 1999. **519 Pt 2**: p. 347-60.
241. Sasaki, N., et al., *Activation of mitochondrial ATP-dependent potassium channels by nitric oxide.* Circulation, 2000. **101**(4): p. 439-45.
242. Oldenburg, O., M.V. Cohen, and J.M. Downey, *Mitochondrial K(ATP) channels in preconditioning.* J Mol Cell Cardiol, 2003. **35**(6): p. 569-75.
243. Baines, C.P., M. Goto, and J.M. Downey, *Oxygen radicals released during ischemic preconditioning contribute to cardioprotection in the rabbit myocardium.* J Mol Cell Cardiol, 1997. **29**(1): p. 207-16.
244. Tritto, I., et al., *Oxygen radicals can induce preconditioning in rabbit hearts.* Circ Res, 1997. **80**(5): p. 743-8.
245. Griffiths, E.J. and A.P. Halestrap, *Mitochondrial non-specific pores remain closed during cardiac ischaemia, but open upon reperfusion.* Biochem J, 1995. **307 (Pt 1)**: p. 93-8.

246. Korge, P., H.M. Honda, and J.N. Weiss, *Regulation of the mitochondrial permeability transition by matrix Ca(2+) and voltage during anoxia/reoxygenation.* Am J Physiol Cell Physiol, 2001. **280**(3): p. C517-26.
247. Garlid, K.D., et al., *The mitochondrial KATP channel as a receptor for potassium channel openers.* J Biol Chem, 1996. **271**(15): p. 8796-9.
248. Ardehali, H. and B. O'Rourke, *Mitochondrial K(ATP) channels in cell survival and death.* J Mol Cell Cardiol, 2005. **39**(1): p. 7-16.
249. Moreau, C., et al., *SUR, ABC proteins targeted by KATP channel openers.* J Mol Cell Cardiol, 2005. **38**(6): p. 951-63.
250. Moreau, C., et al., *SUR, ABC proteins targeted by KATP channel openers.* Journal of Molecular and Cellular Cardiology, 2005. **38**(6): p. 951-963.
251. Ashcroft, F.M. and F.M. Gribble, *New windows on the mechanism of action of K(ATP) channel openers.* Trends Pharmacol Sci, 2000. **21**(11): p. 439-45.
252. D'Hahan, N., et al., *Pharmacological plasticity of cardiac ATP-sensitive potassium channels toward diazoxide revealed by ADP.* Proc Natl Acad Sci U S A, 1999. **96**(21): p. 12162-7.
253. Suzuki, M., et al., *Cardioprotective effect of diazoxide is mediated by activation of sarcolemmal but not mitochondrial ATP-sensitive potassium channels in mice.* Circulation, 2003. **107**(5): p. 682-5.
254. Hanley, P.J., et al., *K(ATP) channel-independent targets of diazoxide and 5-hydroxydecanoate in the heart.* J Physiol, 2002. **542**(Pt 3): p. 735-41.
255. Ockaili, R.A., P. Bhargava, and R.C. Kukreja, *Chemical preconditioning with 3-nitropropionic acid in hearts: role of mitochondrial K(ATP) channel.* Am J Physiol Heart Circ Physiol, 2001. **280**(5): p. H2406-11.
256. Han, J., et al., *Opening of mitochondrial ATP-sensitive potassium channels evokes oxygen radical generation in rabbit heart slices.* J Biochem, 2002. **131**(5): p. 721-7.
257. Drose, S., U. Brandt, and P.J. Hanley, *K+-independent actions of diazoxide question the role of inner membrane KATP channels in mitochondrial cytoprotective signaling.* J Biol Chem, 2006. **281**(33): p. 23733-9.
258. Ovide-Bordeaux, S., R. Ventura-Clapier, and V. Veksler, *Do modulators of the mitochondrial K(ATP) channel change the function of mitochondria in situ?* J Biol Chem, 2000. **275**(47): p. 37291-5.
259. Grimmsmann, T. and I. Rustenbeck, *Direct effects of diazoxide on mitochondria in pancreatic B-cells and on isolated liver mitochondria.* Br J Pharmacol, 1998. **123**(5): p. 781-8.
260. Schafer, G., et al., *Diazoxide, an inhibitor of succinate oxidation.* Biochem Pharmacol, 1969. **18**(10): p. 2678-81.
261. Schafer, J.A. and E. Heinz, *The effect of reversal on Na + and K + electrochemical potential gradients on the active transport of amino acids in Ehrlich ascites tumor cells.* Biochim Biophys Acta, 1971. **249**(1): p. 15-33.
262. Kis, B., et al., *Diazoxide induces delayed pre-conditioning in cultured rat cortical neurons.* J Neurochem, 2003. **87**(4): p. 969-80.
263. Dzeja, P.P., et al., *Targeting nucleotide-requiring enzymes: implications for diazoxide-induced cardioprotection.* Am J Physiol Heart Circ Physiol, 2003. **284**(4): p. H1048-56.

264. McCullough, J.R., et al., *Specific block of the anti-ischemic actions of cromakalim by sodium 5-hydroxydecanoate.* Circ Res, 1991. **69**(4): p. 949-58.
265. Baxter, G.F. and D.M. Yellon, *ATP-sensitive K+ channels mediate the delayed cardioprotective effect of adenosine A1 receptor activation.* J Mol Cell Cardiol, 1999. **31**(5): p. 981-9.
266. Ockaili, R., et al., *Opening of mitochondrial KATP channel induces early and delayed cardioprotective effect: role of nitric oxide.* Am J Physiol, 1999. **277**(6 Pt 2): p. H2425-34.
267. Minners, J., et al., *Dinitrophenol, cyclosporin A, and trimetazidine modulate preconditioning in the isolated rat heart: support for a mitochondrial role in cardioprotection.* Cardiovasc Res, 2000. **47**(1): p. 68-73.
268. Kantor, P.F., et al., *The antianginal drug trimetazidine shifts cardiac energy metabolism from fatty acid oxidation to glucose oxidation by inhibiting mitochondrial long-chain 3-ketoacyl coenzyme A thiolase.* Circ Res, 2000. **86**(5): p. 580-8.
269. Lehtihet, M., et al., *Glibenclamide inhibits islet carnitine palmitoyltransferase 1 activity, leading to PKC-dependent insulin exocytosis.* Am J Physiol Endocrinol Metab, 2003. **285**(2): p. E438-46.
270. Lim, K.H., et al., *The effects of ischaemic preconditioning, diazoxide and 5-hydroxydecanoate on rat heart mitochondrial volume and respiration.* J Physiol, 2002. **545**(Pt 3): p. 961-74.
271. Eaton, S., K. Bartlett, and M. Pourfarzam, *Mammalian mitochondrial beta-oxidation.* Biochem J, 1996. **320 (Pt 2)**: p. 345-57.
272. Hanley, P.J., et al., *Beta-oxidation of 5-hydroxydecanoate, a putative blocker of mitochondrial ATP-sensitive potassium channels.* J Physiol, 2003. **547**(Pt 2): p. 387-93.
273. Hanley, P.J., et al., *5-Hydroxydecanoate is metabolised in mitochondria and creates a rate-limiting bottleneck for beta-oxidation of fatty acids.* J Physiol, 2005. **562**(Pt 2): p. 307-18.
274. Das, M., J.E. Parker, and A.P. Halestrap, *Matrix volume measurements challenge the existence of diazoxide/glibencamide-sensitive KATP channels in rat mitochondria.* J Physiol, 2003. **547**(Pt 3): p. 893-902.
275. Ping, P., et al., *Ischemic preconditioning induces selective translocation of protein kinase C isoforms epsilon and eta in the heart of conscious rabbits without subcellular redistribution of total protein kinase C activity.* Circ Res, 1997. **81**(3): p. 404-14.
276. Qiu, Y., et al., *Direct evidence that protein kinase C plays an essential role in the development of late preconditioning against myocardial stunning in conscious rabbits and that epsilon is the isoform involved.* J Clin Invest, 1998. **101**(10): p. 2182-98.
277. Ahlner, J., et al., *Organic nitrate esters: clinical use and mechanisms of actions.* Pharmacol Rev, 1991. **43**(3): p. 351-423.
278. Yan, L., et al., *Decreasing cyclic GMP exerts similar positive functional effects on cardiac myocytes regardless of initial level.* Pharmacology, 2000. **61**(1): p. 51-6.
279. Weiss, H.R., et al., *Cyclic GMP and cyclic AMP induced changes in control and hypertrophic cardiac myocyte function interact through cyclic GMP affected*

cyclic-AMP phosphodiesterases. Can J Physiol Pharmacol, 1999. **77**(6): p. 422-31.

280. Mohan, P., S.U. Sys, and D.L. Brutsaert, *Positive inotropic effect of nitric oxide in myocardium.* Int J Cardiol, 1995. **50**(3): p. 233-7.
281. Yamaguchi, F., et al., *Activation of cardiac muscarinic receptor and ischemic preconditioning effects in in situ rat heart.* Heart Vessels, 1997. **12**(2): p. 74-83.
282. Billman, G.E., *Effect of carbachol and cyclic GMP on susceptibility to ventricular fibrillation.* FASEB J, 1990. **4**(6): p. 1668-73.
283. Iliodromitis, E.K., et al., *Alterations in circulating cyclic guanosine monophosphate (c-GMP) during short and long ischemia in preconditioning.* Basic Res Cardiol, 1996. **91**(3): p. 234-9.
284. Nakanishi, K., et al., *Intracoronary L-arginine during reperfusion improves endothelial function and reduces infarct size.* Am J Physiol, 1992. **263**(6 Pt 2): p. H1650-8.
285. Xie, Y.W., et al., *Role of endothelium-derived nitric oxide in the modulation of canine myocardial mitochondrial respiration in vitro. Implications for the development of heart failure.* Circ Res, 1996. **79**(3): p. 381-7.
286. Cleeter, M.W., et al., *Reversible inhibition of cytochrome c oxidase, the terminal enzyme of the mitochondrial respiratory chain, by nitric oxide. Implications for neurodegenerative diseases.* FEBS Lett, 1994. **345**(1): p. 50-4.
287. Vegh, A., L. Szekeres, and J. Parratt, *Preconditioning of the ischaemic myocardium; involvement of the L-arginine nitric oxide pathway.* Br J Pharmacol, 1992. **107**(3): p. 648-52.
288. Zolle, O., A.M. Lawrie, and A.W. Simpson, *Activation of the particulate and not the soluble guanylate cyclase leads to the inhibition of Ca2+ extrusion through localized elevation of cGMP.* J Biol Chem, 2000. **275**(34): p. 25892-9.
289. Abraham, E.H., et al., *The multidrug resistance (mdr1) gene product functions as an ATP channel.* Proc Natl Acad Sci U S A, 1993. **90**(1): p. 312-6.
290. Han, J., et al., *Modulation of ATP-sensitive potassium channels by cGMP-dependent protein kinase in rabbit ventricular myocytes.* J Biol Chem, 2001. **276**(25): p. 22140-7.
291. Costa, A.D., et al., *cGMP signalling in pre- and post-conditioning: the role of mitochondria.* Cardiovasc Res, 2008. **77**(2): p. 344-52.
292. Francis, S.H., I.V. Turko, and J.D. Corbin, *Cyclic nucleotide phosphodiesterases: relating structure and function.* Prog Nucleic Acid Res Mol Biol, 2001. **65**: p. 1-52.
293. Ziolo, M.T., et al., *Inhibition of cyclic GMP hydrolysis with zaprinast reduces basal and cyclic AMP-elevated L-type calcium current in guinea-pig ventricular myocytes.* Br J Pharmacol, 2003. **138**(5): p. 986-94.
294. Bolli, R., et al., *The nitric oxide hypothesis of late preconditioning.* Basic Res Cardiol, 1998. **93**(5): p. 325-38.
295. Shinbo, A. and T. Iijima, *Potentiation by nitric oxide of the ATP-sensitive K+ current induced by K+ channel openers in guinea-pig ventricular cells.* Br J Pharmacol, 1997. **120**(8): p. 1568-74.

296. Tsuura, Y., et al., *Nitric oxide opens ATP-sensitive K+ channels through suppression of phosphofructokinase activity and inhibits glucose-induced insulin release in pancreatic beta cells.* J Gen Physiol, 1994. **104**(6): p. 1079-98.
297. Southam, E. and J. Garthwaite, *Comparative effects of some nitric oxide donors on cyclic GMP levels in rat cerebellar slices.* Neurosci Lett, 1991. **130**(1): p. 107-11.
298. Croen, K.D., *Evidence for antiviral effect of nitric oxide. Inhibition of herpes simplex virus type 1 replication.* J Clin Invest, 1993. **91**(6): p. 2446-52.
299. Nisoli, E., et al., *Mitochondrial biogenesis in mammals: the role of endogenous nitric oxide.* Science, 2003. **299**(5608): p. 896-9.
300. Butt, E., et al., *Inhibition of cyclic GMP-dependent protein kinase-mediated effects by (Rp)-8-bromo-PET-cyclic GMPS.* Br J Pharmacol, 1995. **116**(8): p. 3110-6.
301. Drury, A.N. and A. Szent-Gyorgyi, *The physiological activity of adenine compounds with especial reference to their action upon the mammalian heart.* J Physiol, 1929. **68**(3): p. 213-37.
302. Ralevic, V. and G. Burnstock, *Receptors for purines and pyrimidines.* Pharmacol Rev, 1998. **50**(3): p. 413-92.
303. Abbracchio, M.P. and G. Burnstock, *Purinergic signalling: pathophysiological roles.* Jpn J Pharmacol, 1998. **78**(2): p. 113-45.
304. Zimmermann, H., *Extracellular metabolism of ATP and other nucleotides.* Naunyn Schmiedebergs Arch Pharmacol, 2000. **362**(4-5): p. 299-309.
305. Burnstock, G., *The past, present and future of purine nucleotides as signalling molecules.* Neuropharmacology, 1997. **36**(9): p. 1127-39.
306. Picher, M. and R.C. Boucher, *Human airway ecto-adenylate kinase. A mechanism to propagate ATP signaling on airway surfaces.* J Biol Chem, 2003. **278**(13): p. 11256-64.
307. Gillespie, J.H., *The biological significance of the linkages in adenosine triphosphoric acid.* J Physiol, 1934. **80**(4): p. 345-59.
308. Burnstock, G., *A basis for distinguishing two types of purinergic receptor.* Cell Membrane Receptors for Drugs and Hormones, 1978: p. 107-118.
309. Sattin, A. and T.W. Rall, *The effect of adenosine and adenine nucleotides on the cyclic adenosine 3', 5'-phosphate content of guinea pig cerebral cortex slices.* Mol Pharmacol, 1970. **6**(1): p. 13-23.
310. Jacobson, K.A. and Z.G. Gao, *Adenosine receptors as therapeutic targets.* Nat Rev Drug Discov, 2006. **5**(3): p. 247-64.
311. Benham, C.D. and R.W. Tsien, *A novel receptor-operated Ca2+-permeable channel activated by ATP in smooth muscle.* Nature, 1987. **328**(6127): p. 275-8.
312. Dubyak, G.R., *Signal transduction by P2-purinergic receptors for extracellular ATP.* Am J Respir Cell Mol Biol, 1991. **4**(4): p. 295-300.
313. Abbracchio, M.P. and G. Burnstock, *Purinoceptors: are there families of P2X and P2Y purinoceptors?* Pharmacol Ther, 1994. **64**(3): p. 445-75.
314. North, R.A., *Molecular physiology of P2X receptors.* Physiol Rev, 2002. **82**(4): p. 1013-67.

315. Lazarowski, E.R., R.C. Boucher, and T.K. Harden, *Mechanisms of release of nucleotides and integration of their action as P2X- and P2Y-receptor activating molecules.* Mol Pharmacol, 2003. **64**(4): p. 785-95.
316. Boarder, M.R. and S.M.O. Hourani, *The regulation of vascular function by P2 receptors: multiple sites and multiple receptors.* Trends in Pharmacological Sciences, 1998. **19**(3): p. 99-107.
317. Communi, D., et al., *Cloning of a human purinergic P2Y receptor coupled to phospholipase C and adenylyl cyclase.* J Biol Chem, 1997. **272**(51): p. 31969-73.
318. Leon, C., et al., *The P2Y(1) receptor is involved in the maintenance of glucose homeostasis and in insulin secretion in mice.* Purinergic Signal, 2005. **1**(2): p. 145-51.
319. Lazarowski, E.R., R.C. Boucher, and T.K. Harden, *Constitutive release of ATP and evidence for major contribution of ecto-nucleotide pyrophosphatase and nucleoside diphosphokinase to extracellular nucleotide concentrations.* J Biol Chem, 2000. **275**(40): p. 31061-8.
320. Donaldson, S.H., et al., *Basal nucleotide levels, release, and metabolism in normal and cystic fibrosis airways.* Mol Med, 2000. **6**(11): p. 969-82.
321. Vassort, G., *Adenosine 5'-triphosphate: a P2-purinergic agonist in the myocardium.* Physiol Rev, 2001. **81**(2): p. 767-806.
322. Yegutkin, G.G., *Nucleotide- and nucleoside-converting ectoenzymes: Important modulators of purinergic signalling cascade.* Biochim Biophys Acta, 2008. **1783**(5): p. 673-94.
323. Bodin, P. and G. Burnstock, *Purinergic signalling: ATP release.* Neurochem Res, 2001. **26**(8-9): p. 959-69.
324. Williams, C. and T. Forrester, *Loss of ATP in micromolar amounts after perchloric acid treatment.* Pflugers Arch, 1976. **366**(2-3): p. 281-3.
325. Zuo, P., et al., *Mathematical model of nucleotide regulation on airway epithelia. Implications for airway homeostasis.* J Biol Chem, 2008. **283**(39): p. 26805-19.
326. Lazarowski, E.R., et al., *Release of cellular UDP-glucose as a potential extracellular signaling molecule.* Mol Pharmacol, 2003. **63**(5): p. 1190-7.
327. Forrester, T., *An estimate of adenosine triphosphate release into the venous effluent from exercising human forearm muscle.* J Physiol, 1972. **224**(3): p. 611-28.
328. Milner, P., et al., *Rapid release of endothelin and ATP from isolated aortic endothelial cells exposed to increased flow.* Biochem Biophys Res Commun, 1990. **170**(2): p. 649-56.
329. Milner, P., et al., *Increased shear stress leads to differential release of endothelin and ATP from isolated endothelial cells from 4- and 12-month-old male rabbit aorta.* J Vasc Res, 1992. **29**(6): p. 420-5.
330. Milner, P., et al., *Endothelial cells cultured from human umbilical vein release ATP, substance P and acetylcholine in response to increased flow.* Proc Biol Sci, 1990. **241**(1302): p. 245-8.
331. Yegutkin, G., P. Bodin, and G. Burnstock, *Effect of shear stress on the release of soluble ecto-enzymes ATPase and 5'-nucleotidase along with endogenous ATP from vascular endothelial cells.* Br J Pharmacol, 2000. **129**(5): p. 921-6.

332. Burnstock, G., *Release of vasoactive substances from endothelial cells by shear stress and purinergic mechanosensory transduction.* J Anat, 1999. **194 (Pt 3)**: p. 335-42.
333. Grygorczyk, R. and J.W. Hanrahan, *CFTR-independent ATP release from epithelial cells triggered by mechanical stimuli.* Am J Physiol, 1997. **272**(3 Pt 1): p. C1058-66.
334. Watt, W.C., E.R. Lazarowski, and R.C. Boucher, *Cystic fibrosis transmembrane regulator-independent release of ATP. Its implications for the regulation of P2Y2 receptors in airway epithelia.* J Biol Chem, 1998. **273**(22): p. 14053-8.
335. Homolya, L., T.H. Steinberg, and R.C. Boucher, *Cell to cell communication in response to mechanical stress via bilateral release of ATP and UTP in polarized epithelia.* J Cell Biol, 2000. **150**(6): p. 1349-60.
336. Guyot, A. and J.W. Hanrahan, *ATP release from human airway epithelial cells studied using a capillary cell culture system.* J Physiol, 2002. **545**(Pt 1): p. 199-206.
337. Reisin, I.L., et al., *The cystic fibrosis transmembrane conductance regulator is a dual ATP and chloride channel.* J Biol Chem, 1994. **269**(32): p. 20584-91.
338. Grygorczyk, R., J.A. Tabcharani, and J.W. Hanrahan, *CFTR channels expressed in CHO cells do not have detectable ATP conductance.* J Membr Biol, 1996. **151**(2): p. 139-48.
339. Reddy, M.M., et al., *Failure of the cystic fibrosis transmembrane conductance regulator to conduct ATP.* Science, 1996. **271**(5257): p. 1876-9.
340. Braunstein, G.M., et al., *Cystic fibrosis transmembrane conductance regulator facilitates ATP release by stimulating a separate ATP release channel for autocrine control of cell volume regulation.* J Biol Chem, 2001. **276**(9): p. 6621-30.
341. Hazama, A., et al., *Swelling-induced, CFTR-independent ATP release from a human epithelial cell line: lack of correlation with volume-sensitive cl(-) channels.* J Gen Physiol, 1999. **114**(4): p. 525-33.
342. Schwiebert, E.M., *ABC transporter-facilitated ATP conductive transport.* Am J Physiol, 1999. **276**(1 Pt 1): p. C1-8.
343. Guthrie, P.B., et al., *ATP released from astrocytes mediates glial calcium waves.* J Neurosci, 1999. **19**(2): p. 520-8.
344. Queiroz, G., et al., *A study of the mechanism of the release of ATP from rat cortical astroglial cells evoked by activation of glutamate receptors.* Neuroscience, 1999. **91**(3): p. 1171-81.
345. Yegutkin, G.G., T. Henttinen, and S. Jalkanen, *Extracellular ATP formation on vascular endothelial cells is mediated by ecto-nucleotide kinase activities via phosphotransfer reactions.* FASEB J, 2001. **15**(1): p. 251-260.
346. Schwiebert, L.M., et al., *Extracellular ATP signaling and P2X nucleotide receptors in monolayers of primary human vascular endothelial cells.* Am J Physiol Cell Physiol, 2002. **282**(2): p. C289-301.
347. Boudreault, F. and R. Grygorczyk, *Cell swelling-induced ATP release and gadolinium-sensitive channels.* Am J Physiol Cell Physiol, 2002. **282**(1): p. C219-26.
348. Knight, G.E., et al., *ATP is released from guinea pig ureter epithelium on distension.* Am J Physiol Renal Physiol, 2002. **282**(2): p. F281-8.

349. Sabirov, R.Z., A.K. Dutta, and Y. Okada, *Volume-dependent ATP-conductive large-conductance anion channel as a pathway for swelling-induced ATP release.* J Gen Physiol, 2001. **118**(3): p. 251-66.
350. Hisadome, K., et al., *Volume-regulated anion channels serve as an auto/paracrine nucleotide release pathway in aortic endothelial cells.* J Gen Physiol, 2002. **119**(6): p. 511-20.
351. Okada, S.F., et al., *Voltage-dependent anion channel-1 (VDAC-1) contributes to ATP release and cell volume regulation in murine cells.* J Gen Physiol, 2004. **124**(5): p. 513-26.
352. Sridharan, M., et al., *Prostacyclin receptor-mediated ATP release from erythrocytes requires the voltage-dependent anion channel.* American Journal of Physiology - Heart and Circulatory Physiology, 2012. **302**(3): p. H553-H559.
353. Okada, S.F., et al., *Physiological regulation of ATP release at the apical surface of human airway epithelia.* J Biol Chem, 2006. **281**(32): p. 22992-3002.
354. Sabirov, R. and Y. Okada, *ATP release via anion channels.* Purinergic Signalling, 2005. **1**(4): p. 311-328.
355. Kang, J., et al., *Connexin 43 hemichannels are permeable to ATP.* J Neurosci, 2008. **28**(18): p. 4702-11.
356. Harris, A.L., *Emerging issues of connexin channels: biophysics fills the gap.* Q Rev Biophys, 2001. **34**(3): p. 325-472.
357. Retamal, M.A., et al., *Opening of connexin 43 hemichannels is increased by lowering intracellular redox potential.* Proc Natl Acad Sci U S A, 2007. **104**(20): p. 8322-7.
358. Knight, M.M., et al., *Articular chondrocytes express connexin 43 hemichannels and P2 receptors - a putative mechanoreceptor complex involving the primary cilium?* J Anat, 2009. **214**(2): p. 275-83.
359. Saez, J.C., et al., *Connexin-based gap junction hemichannels: gating mechanisms.* Biochim Biophys Acta, 2005. **1711**(2): p. 215-24.
360. Contreras, J.E., et al., *Gating and regulation of connexin 43 (Cx43) hemichannels.* Proc Natl Acad Sci U S A, 2003. **100**(20): p. 11388-93.
361. Arcuino, G., et al., *Intercellular calcium signaling mediated by point-source burst release of ATP.* Proc Natl Acad Sci U S A, 2002. **99**(15): p. 9840-5.
362. Gomes, P., et al., *ATP release through connexin hemichannels in corneal endothelial cells.* Invest Ophthalmol Vis Sci, 2005. **46**(4): p. 1208-18.
363. Saez, J.C., et al., *Gap junction hemichannels in astrocytes of the CNS.* Acta Physiol Scand, 2003. **179**(1): p. 9-22.
364. Stout, C.E., et al., *Intercellular calcium signaling in astrocytes via ATP release through connexin hemichannels.* J Biol Chem, 2002. **277**(12): p. 10482-8.
365. Zhao, H.B., N. Yu, and C.R. Fleming, *Gap junctional hemichannel-mediated ATP release and hearing controls in the inner ear.* Proc Natl Acad Sci U S A, 2005. **102**(51): p. 18724-9.
366. Bao, L., F. Sachs, and G. Dahl, *Connexins are mechanosensitive.* Am J Physiol Cell Physiol, 2004. **287**(5): p. C1389-95.

367. Eltzschig, H.K., et al., *ATP release from activated neutrophils occurs via connexin 43 and modulates adenosine-dependent endothelial cell function.* Circ Res, 2006. **99**(10): p. 1100-8.
368. Faigle, M., et al., *ATP release from vascular endothelia occurs across Cx43 hemichannels and is attenuated during hypoxia.* PLoS One, 2008. **3**(7): p. e2801.
369. Tong, D., et al., *In vivo analysis of undocked connexin43 gap junction hemichannels in ovarian granulosa cells.* J Cell Sci, 2007. **120**(Pt 22): p. 4016-24.
370. Anselmi, F., et al., *ATP release through connexin hemichannels and gap junction transfer of second messengers propagate Ca2+ signals across the inner ear.* Proceedings of the National Academy of Sciences, 2008. **105**(48): p. 18770-18775.
371. Li, A., et al., *Pathways for ATP release by bovine ciliary epithelial cells, the initial step in purinergic regulation of aqueous humor inflow.* American Journal of Physiology - Cell Physiology, 2010. **299**(6): p. C1308-C1317.
372. Shahidullah, M., A. Mandal, and N.A. Delamere, *TRPV4 in porcine lens epithelium regulates hemichannel-mediated ATP release and Na-K-ATPase activity.* American Journal of Physiology - Cell Physiology, 2012. **302**(12): p. C1751-C1761.
373. Pearson, R.A., et al., *ATP Released via Gap Junction Hemichannels from the Pigment Epithelium Regulates Neural Retinal Progenitor Proliferation.* Neuron, 2005. **46**(5): p. 731-744.
374. Scemes, E., S.O. Suadicani, and D.C. Spray, *Intercellular communication in spinal cord astrocytes: fine tuning between gap junctions and P2 nucleotide receptors in calcium wave propagation.* J Neurosci, 2000. **20**(4): p. 1435-45.
375. Coco, S., et al., *Storage and release of ATP from astrocytes in culture.* J Biol Chem, 2003. **278**(2): p. 1354-62.
376. Seminario-Vidal, L., et al., *Thrombin Promotes Release of ATP from Lung Epithelial Cells through Coordinated Activation of Rho- and Ca2+-dependent Signaling Pathways.* Journal of Biological Chemistry, 2009. **284**(31): p. 20638-20648.
377. Gaddum, J.H. and P. Holtz, *The localization of the action of drugs on the pulmonary vessels of dogs and cats.* J Physiol, 1933. **77**(2): p. 139-58.
378. Folkow, B., *The vasodilator action of adenosine triphosphate.* Acta Physiol Scand, 1949. **17**(4): p. 311-6.
379. Born, G.V., *Aggregation of blood platelets by adenosine diphosphate and its reversal.* Nature, 1962. **194**: p. 927-9.
380. Weissmuller, T., H.K. Eltzschig, and S.P. Colgan, *Dynamic purine signaling and metabolism during neutrophil-endothelial interactions.* Purinergic Signal, 2005. **1**(3): p. 229-39.
381. Winbury, M.M., et al., *Coronary dilator action of the adenine-ATP series.* J Pharmacol Exp Ther, 1953. **109**(3): p. 255-60.
382. Burnstock, G. and M. Williams, *P2 purinergic receptors: modulation of cell function and therapeutic potential.* J Pharmacol Exp Ther, 2000. **295**(3): p. 862-9.

383. Fredholm, B.B. and A. Sollevi, *Cardiovascular effects of adenosine.* Clin Physiol, 1986. **6**(1): p. 1-21.
384. Sparks, H.V., Jr. and H. Bardenheuer, *Regulation of adenosine formation by the heart.* Circ Res, 1986. **58**(2): p. 193-201.
385. Berne, R.M., *Cardiac nucleotides in hypoxia: possible role in regulation of coronary blood flow.* Am J Physiol, 1963. **204**: p. 317-22.
386. Gerlach, E., et al., *[on the Behavior of Nucleotides and Their Dephosphorylation Degradation Products in the Kidney in Ischemia and Short-Term Post-Ischemic Re-Establishment of Blood Circulation].* Pflugers Arch Gesamte Physiol Menschen Tiere, 1963. **278**: p. 296-315.
387. Dubyak, G.R. and C. el-Moatassim, *Signal transduction via P2-purinergic receptors for extracellular ATP and other nucleotides.* Am J Physiol, 1993. **265**(3 Pt 1): p. C577-606.
388. Groschel-Stewart, U., et al., *Localisation of P2X5 and P2X7 receptors by immunohistochemistry in rat stratified squamous epithelia.* Cell Tissue Res, 1999. **296**(3): p. 599-605.
389. Hollopeter, G., et al., *Identification of the platelet ADP receptor targeted by antithrombotic drugs.* Nature, 2001. **409**(6817): p. 202-7.
390. Jantzen, H.M., et al., *Evidence for two distinct G-protein-coupled ADP receptors mediating platelet activation.* Thromb Haemost, 1999. **81**(1): p. 111-7.
391. Fabre, J.E., et al., *Decreased platelet aggregation, increased bleeding time and resistance to thromboembolism in P2Y1-deficient mice.* Nat Med, 1999. **5**(10): p. 1199-202.
392. Rapaport, E., *ATP in the treatment of cancer, in Purinergic Approaches.* Experimental Therapeutics, WileyLiss, New York., 1997: p. 545–553.
393. Lazarowski, E.R., et al., *Direct demonstration of mechanically induced release of cellular UTP and its implication for uridine nucleotide receptor activation.* J Biol Chem, 1997. **272**(39): p. 24348-54.
394. Moser, T.L., et al., *Endothelial cell surface F1-F0 ATP synthase is active in ATP synthesis and is inhibited by angiostatin.* Proc Natl Acad Sci U S A, 2001. **98**(12): p. 6656-61.
395. Handa, M. and G. Guidotti, *Purification and cloning of a soluble ATP-diphosphohydrolase (apyrase) from potato tubers (Solanum tuberosum).* Biochem Biophys Res Commun, 1996. **218**(3): p. 916-23.
396. Zimmermann, H., *Two novel families of ectonucleotidases: molecular structures, catalytic properties and a search for function.* Trends Pharmacol Sci, 1999. **20**(6): p. 231-6.
397. Mulero, J.J., et al., *CD39-L4 is a secreted human apyrase, specific for the hydrolysis of nucleoside diphosphates.* J Biol Chem, 1999. **274**(29): p. 20064-7.
398. Kukulski, F., et al., *Comparative hydrolysis of P2 receptor agonists by NTPDases 1, 2, 3 and 8.* Purinergic Signal, 2005. **1**(2): p. 193-204.
399. Picher, M. and R.C. Boucher, *Biochemical evidence for an ecto alkaline phosphodiesterase I in human airways.* Am J Respir Cell Mol Biol, 2000. **23**(2): p. 255-61.

400. Mihaylova-Todorova, S.T., L.D. Todorov, and D.P. Westfall, *Enzyme kinetics and pharmacological characterization of nucleotidases released from the guinea pig isolated vas deferens during nerve stimulation: evidence for a soluble ecto-nucleoside triphosphate diphosphohydrolase-like ATPase and a soluble ecto-5'-nucleotidase-like AMPase.* J Pharmacol Exp Ther, 2002. **302**(3): p. 992-1001.
401. Gijsbers, R., et al., *The hydrolysis of lysophospholipids and nucleotides by autotaxin (NPP2) involves a single catalytic site.* FEBS Lett, 2003. **538**(1-3): p. 60-4.
402. Cimpean, A., et al., *Substrate-specifying determinants of the nucleotide pyrophosphatases/phosphodiesterases NPP1 and NPP2.* Biochem J, 2004. **381**(Pt 1): p. 71-7.
403. Stefan, C., S. Jansen, and M. Bollen, *Modulation of purinergic signaling by NPP-type ectophosphodiesterases.* Purinergic Signal, 2006. **2**(2): p. 361-70.
404. Jansen, S., et al., *Proteolytic maturation and activation of autotaxin (NPP2), a secreted metastasis-enhancing lysophospholipase D.* J Cell Sci, 2005. **118**(Pt 14): p. 3081-9.
405. Picher, M., et al., *Ecto 5'-nucleotidase and nonspecific alkaline phosphatase. Two AMP-hydrolyzing ectoenzymes with distinct roles in human airways.* J Biol Chem, 2003. **278**(15): p. 13468-79.
406. Strater, N., *Ecto-5'-nucleotidase: Structure function relationships.* Purinergic Signal, 2006. **2**(2): p. 343-50.
407. Seminario-Vidal, L., E.R. Lazarowski, and S.F. Okada, *Assessment of extracellular ATP concentrations.* Methods Mol Biol, 2009. **574**: p. 25-36.
408. Burrell, H.E., et al., *Human keratinocytes release ATP and utilize three mechanisms for nucleotide interconversion at the cell surface.* J Biol Chem, 2005. **280**(33): p. 29667-76.
409. Dixon, C.J., J.F. Hall, and M.R. Boarder, *ADP stimulation of inositol phosphates in hepatocytes: role of conversion to ATP and stimulation of P2Y2 receptors.* Br J Pharmacol, 2003. **138**(1): p. 272-8.
410. Furstenau, C.R., et al., *The effect of ebselen on adenine nucleotide hydrolysis by platelets from adult rats.* Chem Biol Interact, 2004. **148**(1-2): p. 93-9.
411. Semianrio-Vidal, L., et al., *Ebselen is a potent non-competitive inhibitor of extracellular nucleoside diphosphokinase.* Purinergic Signal, 2010. **6**(4): p. 383-91.
412. Seminario-Vidal, L., et al., *Erratum to: Ebselen is a potent non-competitive inhibitor of extracellular nucleoside diphosphokinase.* Purinergic Signal, 2011.
413. Farahbakhsh, N.A., *Ectonucleotidases of the rabbit ciliary body nonpigmented epithelium.* Invest Ophthalmol Vis Sci, 2003. **44**(9): p. 3952-60.
414. He, M.L., et al., *Release and extracellular metabolism of ATP by ecto-nucleotidase eNTPDase 1-3 in hypothalamic and pituitary cells.* Purinergic Signal, 2005. **1**(2): p. 135-44.
415. Westfall, T.D., et al., *Release of a soluble ATPase from the rabbit isolated vas deferens during nerve stimulation.* Br J Pharmacol, 2000. **131**(5): p. 909-14.

416. Machida, T., et al., *Ectonucleoside triphosphate diphosphohydrolase 1/CD39, localized in neurons of human and porcine heart, modulates ATP-induced norepinephrine exocytosis.* J Pharmacol Exp Ther, 2005. **313**(2): p. 570-7.
417. Silva, G., W.H. Beierwaltes, and J.L. Garvin, *Extracellular ATP stimulates NO production in rat thick ascending limb.* Hypertension, 2006. **47**(3): p. 563-7.
418. Drakulich, D.A., C. Spellmon, and T.D. Hexum, *Effect of the ecto-ATPase inhibitor, ARL 67156, on the bovine chromaffin cell response to ATP.* Eur J Pharmacol, 2004. **485**(1-3): p. 137-40.
419. Crack, B.E., et al., *Pharmacological and biochemical analysis of FPL 67156, a novel, selective inhibitor of ecto-ATPase.* Br J Pharmacol, 1995. **114**(2): p. 475-81.
420. Connolly, G.P. and J.A. Duley, *Ecto-nucleotidase of cultured rat superior cervical ganglia: dipyridamole is a novel inhibitor.* Eur J Pharmacol, 2000. **397**(2-3): p. 271-7.
421. Levesque, S.A., et al., *Specificity of the ecto-ATPase inhibitor ARL 67156 on human and mouse ectonucleotidases.* Br J Pharmacol, 2007. **152**(1): p. 141-50.
422. Westfall, T.D., et al., *The interaction of diadenosine polyphosphates with P2x-receptors in the guinea-pig isolated vas deferens.* Br J Pharmacol, 1997. **121**(1): p. 57-62.
423. Constantopoulos, A., et al., *The effect of levamisole on phosphodiesterase activity.* Experientia, 1977. **33**(3): p. 395-6.
424. Picher, M., et al., *Ecto 5'-Nucleotidase and Nonspecific Alkaline Phosphatase.* Journal of Biological Chemistry, 2003. **278**(15): p. 13468-13479.
425. Kaulich, M., R. Qurishi, and C.E. Muller, *Extracellular metabolism of nucleotides in neuroblastoma x glioma NG108-15 cells determined by capillary electrophoresis.* Cell Mol Neurobiol, 2003. **23**(3): p. 349-64.
426. Nagy, A.K., T.A. Shuster, and A.V. Delgado-Escueta, *Rat brain synaptosomal ATP:AMP-phosphotransferase activity.* J Neurochem, 1989. **53**(4): p. 1166-72.
427. Lienhard, G.E. and Secemski, II, *P 1 ,P 5 -Di(adenosine-5')pentaphosphate, a potent multisubstrate inhibitor of adenylate kinase.* J Biol Chem, 1973. **248**(3): p. 1121-3.
428. Song, L.S., et al., *Calcium biology of the transverse tubules in heart.* Ann N Y Acad Sci, 2005. **1047**: p. 99-111.
429. Bers, D.M., *Cardiac excitation-contraction coupling.* Nature, 2002. **415**(6868): p. 198-205.
430. Maack, C. and B. O'Rourke, *Excitation-contraction coupling and mitochondrial energetics.* Basic Res Cardiol, 2007. **102**(5): p. 369-92.
431. Fabiato, A., *Simulated calcium current can both cause calcium loading in and trigger calcium release from the sarcoplasmic reticulum of a skinned canine cardiac Purkinje cell.* J Gen Physiol, 1985. **85**(2): p. 291-320.
432. Fabiato, A., *Time and calcium dependence of activation and inactivation of calcium-induced release of calcium from the sarcoplasmic reticulum of a skinned canine cardiac Purkinje cell.* J Gen Physiol, 1985. **85**(2): p. 247-89.
433. Lopaschuk, G.D., et al., *Myocardial fatty acid metabolism in health and disease.* Physiol Rev, 2010. **90**(1): p. 207-58.

434. Su, X. and N.A. Abumrad, *Cellular fatty acid uptake: a pathway under construction.* Trends Endocrinol Metab, 2009. **20**(2): p. 72-7.
435. Whitmer, J.T., et al., *Control of fatty acid metabolism in ischemic and hypoxic hearts.* J Biol Chem, 1978. **253**(12): p. 4305-9.
436. Lloyd, S.G., et al., *Impact of low-flow ischemia on substrate oxidation and glycolysis in the isolated perfused rat heart.* Am J Physiol Heart Circ Physiol, 2004. **287**(1): p. H351-62.
437. Burrows, M.T., *Rhythmical Activity of Isolated Heart Muscle Cells in Vitro.* Science, 1912. **36**(916): p. 90-2.
438. Moscona, A. and H. Moscona, *The dissociation and aggregation of cells from organ rudiments of the early chick embryo.* J Anat, 1952. **86**(3): p. 287-301.
439. Bkaily, G., N. Sperelakis, and J. Doane, *A new method for preparation of isolated single adult myocytes.* Am J Physiol, 1984. **247**(6 Pt 2): p. H1018-26.
440. Cavanaugh, M.W., *Pulsation, migration and division in dissociated chick embryo heart cells in vitro.* Journal of Experimental Zoology, 1955. **128**(3): p. 573-589.
441. Patten, B.M. and T.C. Kramer, *The initiation of contraction in the embryonic chick heart.* American Journal of Anatomy, 1933. **53**(3): p. 349-375.
442. Meda, E. and A. Ferroni, *Early functional differentiation of heart muscle cells.* Cellular and Molecular Life Sciences, 1959. **15**(11): p. 427-428.
443. Kim, D. and T.W. Smith, *Cellular mechanisms underlying calcium-proton interactions in cultured chick ventricular cells.* J Physiol, 1988. **398**: p. 391-410.
444. McLean, M.J. and N. Sperelakis, *Retention of fully differentiated electrophysiological properties of chick embryonic heart cells in culture.* Dev Biol, 1976. **50**(1): p. 134-41.
445. Murphy, E., A. LeFurgey, and M. Lieberman, *Biochemical and structural changes in cultured heart cells induced by metabolic inhibition.* Am J Physiol, 1987. **253**(5 Pt 1): p. C700-6.
446. Estevez, M.D., A. Wolf, and U. Schramm, *Effect of PSC 833, verapamil and amiodarone on adriamycin toxicity in cultured rat cardiomyocytes.* Toxicol In Vitro, 2000. **14**(1): p. 17-23.
447. Limaye, D.A. and Z.A. Shaikh, *Cytotoxicity of cadmium and characteristics of its transport in cardiomyocytes.* Toxicol Appl Pharmacol, 1999. **154**(1): p. 59-66.
448. Acosta, D. and K. Ramos, *Cardiotoxicity of tricyclic antidepressants in primary cultures of rat myocardial cells.* J Toxicol Environ Health, 1984. **14**(2-3): p. 137-43.
449. Wenzel, D.G., J.W. Wheatley, and G.D. Byrd, *Effects of nicotine on cultured rat heart cells.* Toxicol Appl Pharmacol, 1970. **17**(3): p. 774-85.
450. Ray, M., et al., *The hamster heart is resistant to calcium paradox.* Pharmacol Res, 2000. **41**(4): p. 475-81.
451. Yamashita, N., et al., *Induction of manganese superoxide dismutase in rat cardiac myocytes increases tolerance to hypoxia 24 hours after preconditioning.* J Clin Invest, 1994. **94**(6): p. 2193-9.
452. Seymour, E.M., et al., *HL-1 myocytes exhibit PKC and K(ATP) channel-dependent delta opioid preconditioning.* J Surg Res, 2003. **114**(2): p. 187-94.

453. Vanden Hoek, T.L., et al., *Reperfusion injury on cardiac myocytes after simulated ischemia.* Am J Physiol, 1996. **270**(4 Pt 2): p. H1334-41.
454. Ieda, M., et al., *Cardiac Fibroblasts Regulate Myocardial Proliferation through β1 Integrin Signaling.* Developmental Cell, 2009. **16**(2): p. 233-244.
455. Miragoli, M., G. Gaudesius, and S. Rohr, *Electrotonic modulation of cardiac impulse conduction by myofibroblasts.* Circ Res, 2006. **98**(6): p. 801-10.
456. Baudino, T.A., et al., *Cardiac fibroblasts: friend or foe?* Am J Physiol Heart Circ Physiol, 2006. **291**(3): p. H1015-26.
457. Camelliti, P., T.K. Borg, and P. Kohl, *Structural and functional characterisation of cardiac fibroblasts.* Cardiovasc Res, 2005. **65**(1): p. 40-51.
458. Egorova, M.V., S.A. Afanas'ev, and S.V. Popov, *A simple method for isolation of cardiomyocytes from adult rat heart.* Bull Exp Biol Med, 2005. **140**(3): p. 370-3.
459. Rodgers, L.S., et al., *An improved protocol for the isolation and cultivation of embryonic mouse myocytes.* Cytotechnology, 2009. **59**(2): p. 93-102.
460. Yang, B.C., D.S. Zander, and J.L. Mehta, *Hypoxia-reoxygenation-induced apoptosis in cultured adult rat myocytes and the protective effect of platelets and transforming growth factor-beta(1).* J Pharmacol Exp Ther, 1999. **291**(2): p. 733-8.
461. Powell, T. and V.W. Twist, *A rapid technique for the isolation and purification of adult cardiac muscle cells having respiratory control and a tolerance to calcium.* Biochem Biophys Res Commun, 1976. **72**(1): p. 327-33.
462. Doetschman, T.C., et al., *The in vitro development of blastocyst-derived embryonic stem cell lines: formation of visceral yolk sac, blood islands and myocardium.* J Embryol Exp Morphol, 1985. **87**: p. 27-45.
463. Wobus, A.M., G. Wallukat, and J. Hescheler, *Pluripotent mouse embryonic stem cells are able to differentiate into cardiomyocytes expressing chronotropic responses to adrenergic and cholinergic agents and Ca2+ channel blockers.* Differentiation, 1991. **48**(3): p. 173-182.
464. Williams, R.L., et al., *Myeloid leukaemia inhibitory factor maintains the developmental potential of embryonic stem cells.* Nature, 1988. **336**(6200): p. 684-7.
465. Robbins, J., et al., *Mouse embryonic stem cells express the cardiac myosin heavy chain genes during development in vitro.* J Biol Chem, 1990. **265**(20): p. 11905-9.
466. Hescheler, J., et al., *Embryonic stem cells: a model to study structural and functional properties in cardiomyogenesis.* Cardiovasc Res, 1997. **36**(2): p. 149-62.
467. Kleppisch, T., et al., *Voltage-dependent L-type Ca channels and a novel type of non-selective cation channel activated by cAMP-dependent phosphorylation in mesoderm-like (MES-1) cells.* Cellular Signalling, 1993. **5**(6): p. 727-734.
468. Maltsev, V.A., et al., *Cardiomyocytes differentiated in vitro from embryonic stem cells developmentally express cardiac-specific genes and ionic currents.* Circ Res, 1994. **75**(2): p. 233-44.

469. McCormack, J.G., A.P. Halestrap, and R.M. Denton, *Role of calcium ions in regulation of mammalian intramitochondrial metabolism.* Physiol Rev, 1990. **70**(2): p. 391-425.
470. Nguyen, S.V. and W.C. Claycomb, *Hypoxia regulates the expression of the adrenomedullin and HIF-1 genes in cultured HL-1 cardiomyocytes.* Biochem Biophys Res Commun, 1999. **265**(2): p. 382-6.
471. Robert, V., et al., *Beat-to-beat oscillations of mitochondrial [Ca2+] in cardiac cells.* EMBO J, 2001. **20**(17): p. 4998-5007.
472. White, S.M., P.E. Constantin, and W.C. Claycomb, *Cardiac physiology at the cellular level: use of cultured HL-1 cardiomyocytes for studies of cardiac muscle cell structure and function.* Am J Physiol Heart Circ Physiol, 2004. **286**(3): p. H823-9.
473. Anisimov, S.V., et al., *SAGE identification of differentiation responsive genes in P19 embryonic cells induced to form cardiomyocytes in vitro.* Mech Dev, 2002. **117**(1-2): p. 25-74.
474. Klug, M.G., et al., *Genetically selected cardiomyocytes from differentiating embronic stem cells form stable intracardiac grafts.* J Clin Invest, 1996. **98**(1): p. 216-24.
475. Claycomb, W.C., et al., *HL-1 cells: a cardiac muscle cell line that contracts and retains phenotypic characteristics of the adult cardiomyocyte.* Proc Natl Acad Sci U S A, 1998. **95**(6): p. 2979-84.
476. Mestril, R., et al., *Isolation of a novel inducible rat heat-shock protein (HSP70) gene and its expression during ischaemia/hypoxia and heat shock.* Biochem J, 1994. **298 Pt 3**: p. 561-9.
477. Mizukami, Y., et al., *Nuclear mitogen-activated protein kinase activation by protein kinase czeta during reoxygenation after ischemic hypoxia.* J Biol Chem, 2000. **275**(26): p. 19921-7.
478. Tanno, M., et al., *Diverse mechanisms of myocardial p38 mitogen-activated protein kinase activation: evidence for MKK-independent activation by a TAB1-associated mechanism contributing to injury during myocardial ischemia.* Circ Res, 2003. **93**(3): p. 254-61.
479. Hescheler, J., et al., *Morphological, biochemical, and electrophysiological characterization of a clonal cell (H9c2) line from rat heart.* Circ Res, 1991. **69**(6): p. 1476-86.
480. Sipido, K.R. and E. Marban, *L-type calcium channels, potassium channels, and novel nonspecific cation channels in a clonal muscle cell line derived from embryonic rat ventricle.* Circ Res, 1991. **69**(6): p. 1487-99.
481. Delcarpio, J.B., et al., *Morphological characterization of cardiomyocytes isolated from a transplantable cardiac tumor derived from transgenic mouse atria (AT-1 cells).* Circ Res, 1991. **69**(6): p. 1591-600.
482. Sartiani, L., et al., *Functional expression of the hyperpolarization-activated, non-selective cation current I(f) in immortalized HL-1 cardiomyocytes.* J Physiol, 2002. **545**(Pt 1): p. 81-92.
483. Kitta, K., et al., *Hepatocyte growth factor protects cardiac myocytes against oxidative stress-induced apoptosis.* Free Radic Biol Med, 2001. **31**(7): p. 902-10.

484. Kitta, K., et al., *Hepatocyte growth factor induces GATA-4 phosphorylation and cell survival in cardiac muscle cells.* J Biol Chem, 2003. **278**(7): p. 4705-12.
485. Lanson, N.A., Jr., et al., *The MRE11-NBS1-RAD50 pathway is perturbed in SV40 large T antigen-immortalized AT-1, AT-2 and HL-1 cardiomyocytes.* Nucleic Acids Res, 2000. **28**(15): p. 2882-92.
486. George, C.H., G.V. Higgs, and F.A. Lai, *Ryanodine receptor mutations associated with stress-induced ventricular tachycardia mediate increased calcium release in stimulated cardiomyocytes.* Circ Res, 2003. **93**(6): p. 531-40.
487. Gordon, W.E., 3rd, *Immunofluorescent and ultrastructural studies of "sarcomeric" units in stress fibers of cultured non-muscle cells.* Exp Cell Res, 1978. **117**(2): p. 253-60.
488. Ishikawa, H., R. Bischoff, and H. Holtzer, *Mitosis and intermediate-sized filaments in developing skeletal muscle.* J Cell Biol, 1968. **38**(3): p. 538-55.
489. Konigsberg, I.R., *Clonal analysis of myogenesis.* Science, 1963. **140**(3573): p. 1273-84.
490. Clark, W.A., Jr., *Selective control of fibroblast proliferation and its effect on cardiac muscle differentiation in vitro.* Dev Biol, 1976. **52**(2): p. 263-82.
491. Engler, A.J., et al., *Embryonic cardiomyocytes beat best on a matrix with heart-like elasticity: scar-like rigidity inhibits beating.* J Cell Sci, 2008. **121**(Pt 22): p. 3794-802.
492. Lipp, P., et al., *Spatially non-uniform Ca2+ signals induced by the reduction of transverse tubules in citrate-loaded guinea-pig ventricular myocytes in culture.* J Physiol, 1996. **497 (Pt 3)**: p. 589-97.
493. Mitcheson, J.S., J.C. Hancox, and A.J. Levi, *Cultured adult cardiac myocytes: future applications, culture methods, morphological and electrophysiological properties.* Cardiovasc Res, 1998. **39**(2): p. 280-300.
494. Laugwitz, K.L., et al., *Postnatal isl1+ cardioblasts enter fully differentiated cardiomyocyte lineages.* Nature, 2005. **433**(7026): p. 647-53.
495. Schultheiss, T., et al., *Differential distribution of subsets of myofibrillar proteins in cardiac nonstriated and striated myofibrils.* J Cell Biol, 1990. **110**(4): p. 1159-72.
496. Dlugosz, A.A., et al., *The relationship between stress fiber-like structures and nascent myofibrils in cultured cardiac myocytes.* J Cell Biol, 1984. **99**(6): p. 2268-78.
497. Lin, Z.X., et al., *Polygons and adhesion plaques and the disassembly and assembly of myofibrils in cardiac myocytes.* J Cell Biol, 1989. **108**(6): p. 2355-67.
498. Jones, S.P. and S.W. Kennedy, *Chicken embryo cardiomyocyte cultures--a new approach for studying effects of halogenated aromatic hydrocarbons in the avian heart.* Toxicol Sci, 2009. **109**(1): p. 66-74.
499. Bin, Z., et al., *Efficient cardiomyocyte differentiation of embryonic stem cells by bone morphogenetic protein-2 combined with visceral endoderm-like cells.* Cell Biol Int, 2006. **30**(10): p. 769-76.

500. Zhu, D., et al., *Icariin-mediated modulation of cell cycle and p53 during cardiomyocyte differentiation in embryonic stem cells.* European Journal of Pharmacology, 2005. **514**(2–3): p. 99-110.
501. Childs, A.C., et al., *Doxorubicin treatment in vivo causes cytochrome C release and cardiomyocyte apoptosis, as well as increased mitochondrial efficiency, superoxide dismutase activity, and Bcl-2:Bax ratio.* Cancer Res, 2002. **62**(16): p. 4592-8.
502. Maxwell, M.H., G.W. Robertson, and D. Moseley, *Potential role of serum troponin T in cardiomyocyte injury in the broiler ascites syndrome.* Br Poult Sci, 1994. **35**(5): p. 663-7.
503. Eatman, D., et al., *Phenotypic stability of chick cardiomyocytes in serum-free media. Preservation of muscarinic receptor expression.* J Pharmacol Toxicol Methods, 2000. **44**(3): p. 533-42.
504. Scaduto, R.C., Jr. and L.W. Grotyohann, *Measurement of mitochondrial membrane potential using fluorescent rhodamine derivatives.* Biophys J, 1999. **76**(1 Pt 1): p. 469-77.
505. Loew, L.M., et al., *Imaging in five dimensions: time-dependent membrane potentials in individual mitochondria.* Biophys J, 1993. **65**(6): p. 2396-407.
506. Ehrenberg, B., et al., *Membrane potential can be determined in individual cells from the nernstian distribution of cationic dyes.* Biophys J, 1988. **53**(5): p. 785-94.
507. Perry, S.W., et al., *Mitochondrial membrane potential probes and the proton gradient: a practical usage guide.* Biotechniques, 2011. **50**(2): p. 98-115.
508. Emaus, R.K., R. Grunwald, and J.J. Lemasters, *Rhodamine 123 as a probe of transmembrane potential in isolated rat-liver mitochondria: spectral and metabolic properties.* Biochim Biophys Acta, 1986. **850**(3): p. 436-48.
509. Duchen, M.R., *Mitochondria in health and disease: perspectives on a new mitochondrial biology.* Mol Aspects Med, 2004. **25**(4): p. 365-451.
510. Duchen, M.R., A. Leyssens, and M. Crompton, *Transient mitochondrial depolarizations reflect focal sarcoplasmic reticular calcium release in single rat cardiomyocytes.* J Cell Biol, 1998. **142**(4): p. 975-88.
511. Ward, M.W., et al., *Mitochondrial membrane potential and glutamate excitotoxicity in cultured cerebellar granule cells.* J Neurosci, 2000. **20**(19): p. 7208-19.
512. O'Reilly, C.M., et al., *Quantitative analysis of spontaneous mitochondrial depolarizations.* Biophys J, 2003. **85**(5): p. 3350-7.
513. Wyatt, C.N. and K.J. Buckler, *The effect of mitochondrial inhibitors on membrane currents in isolated neonatal rat carotid body type I cells.* J Physiol, 2004. **556**(Pt 1): p. 175-91.
514. van Gelder, B.F. and A.O. Muijsers, *On cytochrome c oxidase. II. The ratio of cytochrome a to cytochrome a3.* Biochim Biophys Acta, 1966. **118**(1): p. 47-57.
515. Kamishima, T. and J.M. Quayle, *Mitochondrial Ca2+ uptake is important over low [Ca2+]i range in arterial smooth muscle.* Am J Physiol Heart Circ Physiol, 2002. **283**(6): p. H2431-9.
516. Heytler, P.G., *Uncouplers of oxidative phosphorylation.* Methods Enzymol, 1979. **55**: p. 462-42.

517. Brennan, J.P., et al., *Mitochondrial uncoupling, with low concentration FCCP, induces ROS-dependent cardioprotection independent of KATP channel activation.* Cardiovascular Research, 2006. **72**(2): p. 313-321.
518. Mitchell, P. and J. Moyle, *Respiratory-chain protonmotive stoicheiometry.* Biochem Soc Trans, 1979. **7**(5): p. 887-94.
519. Mitchell, P., *Protonmotive cytochrome system of mitochondria.* Ann N Y Acad Sci, 1980. **341**: p. 564-84.
520. Ting, H.P., D.F. Wilson, and B. Chance, *Effects of uncouplers of oxidative phosphorylation on the specific conductance of bimolecular lipid membranes.* Arch Biochem Biophys, 1970. **141**(1): p. 141-6.
521. Wilson, D.F. and B. Chance, *Reversal of azide inhibition by uncouplers.* Biochem Biophys Res Commun, 1966. **23**(5): p. 751-6.
522. Slater, E.C., *Mechanism of oxidative phosphorylation.* Annu Rev Biochem, 1977. **46**: p. 1015-26.
523. Gunter, T.E., et al., *Mitochondrial calcium transport: physiological and pathological relevance.* Am J Physiol, 1994. **267**(2 Pt 1): p. C313-39.
524. Yuan, X.J., et al., *A mitochondrial uncoupler increases KCa currents but decreases KV currents in pulmonary artery myocytes.* Am J Physiol, 1996. **270**(1 Pt 1): p. C321-31.
525. Schuchmann, S., et al., *A relative energy failure is associated with low-Mg2+ but not with 4-aminopyridine induced seizure-like events in entorhinal cortex.* J Neurophysiol, 1999. **81**(1): p. 399-403.
526. Duchen, M.R., *Ca(2+)-dependent changes in the mitochondrial energetics in single dissociated mouse sensory neurons.* Biochem J, 1992. **283 (Pt 1)**: p. 41-50.
527. Duchen, M.R., *Contributions of mitochondria to animal physiology: from homeostatic sensor to calcium signalling and cell death.* J Physiol, 1999. **516 (Pt 1)**: p. 1-17.
528. Duchen, M.R. and T.J. Biscoe, *Relative mitochondrial membrane potential and [Ca2+]i in type I cells isolated from the rabbit carotid body.* J Physiol, 1992. **450**: p. 33-61.
529. Brown, J., *Effects of 2-deoxyglucose on carbohydrate metablism: review of the literature and studies in the rat.* Metabolism, 1962. **11**: p. 1098-112.
530. Weindruch, R., et al., *Caloric restriction mimetics: metabolic interventions.* J Gerontol A Biol Sci Med Sci, 2001. **56 Spec No 1**: p. 20-33.
531. Facundo, H.T., J.G. de Paula, and A.J. Kowaltowski, *Mitochondrial ATP-sensitive K+ channels prevent oxidative stress, permeability transition and cell death.* J Bioenerg Biomembr, 2005. **37**(2): p. 75-82.
532. Baczko, I., W.R. Giles, and P.E. Light, *Resting membrane potential regulates Na(+)-Ca2+ exchange-mediated Ca2+ overload during hypoxia-reoxygenation in rat ventricular myocytes.* J Physiol, 2003. **550**(Pt 3): p. 889-98.
533. Jovanovic, A., et al., *Recombinant cardiac ATP-sensitive K+ channel subunits confer resistance to chemical hypoxia-reoxygenation injury.* Circulation, 1998. **98**(15): p. 1548-55.
534. Allshire, A. and P. Cobbold, *Ca2+ flux into metabolically deprived cardiomyocytes.* Biochemical Society Transactions, 1987.

535. Putney, J.W., Jr., *Inositol phosphates and calcium entry.* Adv Second Messenger Phosphoprotein Res, 1992. **26**: p. 143-60.
536. Jacob, R., *Agonist-stimulated divalent cation entry into single cultured human umbilical vein endothelial cells.* J Physiol, 1990. **421**: p. 55-77.
537. Schilling, W.P., O.A. Cabello, and L. Rajan, *Depletion of the inositol 1,4,5-trisphosphate-sensitive intracellular Ca2+ store in vascular endothelial cells activates the agonist-sensitive Ca(2+)-influx pathway.* Biochem J, 1992. **284 (Pt 2)**: p. 521-30.
538. Morgan, A.J. and R. Jacob, *Ionomycin enhances Ca2+ influx by stimulating store-regulated cation entry and not by a direct action at the plasma membrane.* Biochem J, 1994. **300 (Pt 3)**: p. 665-72.
539. Mason, M.J. and S. Grinstein, *Ionomycin activates electrogenic Ca2+ influx in rat thymic lymphocytes.* Biochem J, 1993. **296 (Pt 1)**: p. 33-9.
540. Gutierrez-Martin, Y., et al., *P2X7 receptors trigger ATP exocytosis and modify secretory vesicle dynamics in neuroblastoma cells.* J Biol Chem, 2011. **286**(13): p. 11370-81.
541. Taylor, A.L., et al., *Bioluminescence detection of ATP release mechanisms in epithelia.* Am J Physiol, 1998. **275**(5 Pt 1): p. C1391-406.
542. Beigi, R., et al., *Detection of local ATP release from activated platelets using cell surface-attached firefly luciferase.* Am J Physiol, 1999. **276**(1 Pt 1): p. C267-78.
543. Beigi, R.D. and G.R. Dubyak, *Endotoxin activation of macrophages does not induce ATP release and autocrine stimulation of P2 nucleotide receptors.* J Immunol, 2000. **165**(12): p. 7189-98.
544. Joseph, S.M., M.R. Buchakjian, and G.R. Dubyak, *Colocalization of ATP release sites and ecto-ATPase activity at the extracellular surface of human astrocytes.* J Biol Chem, 2003. **278**(26): p. 23331-42.
545. Arakaki, N., et al., *Possible role of cell surface H+ -ATP synthase in the extracellular ATP synthesis and proliferation of human umbilical vein endothelial cells.* Mol Cancer Res, 2003. **1**(13): p. 931-9.
546. Rizzuto, R., M. Brini, and T. Pozzan, *Intracellular targeting of the photoprotein aequorin: a new approach for measuring, in living cells, Ca2+ concentrations in defined cellular compartments.* Cytotechnology, 1993. **11 Suppl 1**: p. S44-6.
547. Brini, M., et al., *Transfected aequorin in the measurement of cytosolic Ca2+ concentration ([Ca2+]c). A critical evaluation.* J Biol Chem, 1995. **270**(17): p. 9896-903.
548. Tsien, R.Y., T. Pozzan, and T.J. Rink, *T-cell mitogens cause early changes in cytoplasmic free Ca2+ and membrane potential in lymphocytes.* Nature, 1982. **295**(5844): p. 68-71.
549. Grynkiewicz, G., M. Poenie, and R.Y. Tsien, *A new generation of Ca2+ indicators with greatly improved fluorescence properties.* J Biol Chem, 1985. **260**(6): p. 3440-50.
550. Malgaroli, A., et al., *Fura-2 measurement of cytosolic free Ca2+ in monolayers and suspensions of various types of animal cells.* J Cell Biol, 1987. **105**(5): p. 2145-55.

551. Sanchez-Bueno, A., R. Yoshida, and F.I. Tsuji, *Regeneration and luminescence of aequorin in Chinese hamster ovary cells transformed with cDNA for apoaequorin.* Int J Biochem Cell Biol, 1996. **28**(9): p. 1045-9.
552. Filippin, L., et al., *Improved strategies for the delivery of GFP-based Ca2+ sensors into the mitochondrial matrix.* Cell Calcium, 2005. **37**(2): p. 129-36.
553. Tsien, R.Y., *New tetracarboxylate chelators for fluorescence measurement and photochemical manipulation of cytosolic free calcium concentrations.* Soc Gen Physiol Ser, 1986. **40**: p. 327-45.
554. Tsien, R.Y., *Measuring and manipulating cytosolic Ca2+ with trapped indicators.* Kroc Found Ser, 1984. **17**: p. 147-55.
555. Gerencser, A.A. and V. Adam-Vizi, *Selective, high-resolution fluorescence imaging of mitochondrial Ca2+ concentration.* Cell Calcium, 2001. **30**(5): p. 311-21.
556. Minta, A., J.P. Kao, and R.Y. Tsien, *Fluorescent indicators for cytosolic calcium based on rhodamine and fluorescein chromophores.* J Biol Chem, 1989. **264**(14): p. 8171-8.
557. Parker, I., J. Choi, and Y. Yao, *Elementary events of InsP3-induced Ca2+ liberation in Xenopus oocytes: hot spots, puffs and blips.* Cell Calcium, 1996. **20**(2): p. 105-21.
558. Hollingworth, S., K.R. Gee, and S.M. Baylor, *Low-affinity Ca2+ indicators compared in measurements of skeletal muscle Ca2+ transients.* Biophys J, 2009. **97**(7): p. 1864-72.
559. Fast, V.G., et al., *Effects of electrical shocks on Cai2+ and Vm in myocyte cultures.* Circ Res, 2004. **94**(12): p. 1589-97.
560. Button, D. and M. Brownstein, *Aequorin-expressing mammalian cell lines used to report Ca2+ mobilization.* Cell Calcium, 1993. **14**(9): p. 663-71.
561. Shimomura, O. and F.H. Johnson, *Peroxidized coelenterazine, the active group in the photoprotein aequorin.* Proc Natl Acad Sci U S A, 1978. **75**(6): p. 2611-5.
562. Shimomura, O. and F.H. Johnson, *Regeneration of the photoprotein aequorin.* Nature, 1975. **256**(5514): p. 236-8.
563. Shimomura, O., *Luminescence of aequorin is triggered by the binding of two calcium ions.* Biochem Biophys Res Commun, 1995. **211**(2): p. 359-63.
564. Head, J.F., et al., *The crystal structure of the photoprotein aequorin at 2.3 A resolution.* Nature, 2000. **405**(6784): p. 372-6.
565. Rizzuto, R., et al., *Rapid changes of mitochondrial Ca2+ revealed by specifically targeted recombinant aequorin.* Nature, 1992. **358**(6384): p. 325-7.
566. Rizzuto, R., et al., *A gene specifying subunit VIII of human cytochrome c oxidase is localized to chromosome 11 and is expressed in both muscle and non-muscle tissues.* J Biol Chem, 1989. **264**(18): p. 10595-600.
567. Colella, M. and T. Pozzan, *Cardiac cell hypertrophy in vitro: role of calcineurin/NFAT as Ca2+ signal integrators.* Ann N Y Acad Sci, 2008. **1123**: p. 64-8.
568. Rimessi, A., et al., *The versatility of mitochondrial calcium signals: from stimulation of cell metabolism to induction of cell death.* Biochim Biophys Acta, 2008. **1777**(7-8): p. 808-16.

569. De Giorgi, F., et al., *Targeting aequorin and green fluorescent protein to intracellular organelles.* Gene, 1996. **173**(1 Spec No): p. 113-7.
570. Allen, D.G., J.R. Blinks, and F.G. Prendergast, *Aequorin luminescence: relation of light emission to calcium concentration--a calcium-independent component.* Science, 1977. **195**(4282): p. 996-8.
571. Mithofer, A. and C. Mazars, *Aequorin-based measurements of intracellular Ca2+-signatures in plant cells.* Biol Proced Online, 2002. **4**: p. 105-118.
572. Edgell, C.J., C.C. McDonald, and J.B. Graham, *Permanent cell line expressing human factor VIII-related antigen established by hybridization.* Proc Natl Acad Sci U S A, 1983. **80**(12): p. 3734-7.
573. Kilsdonk, E.P., A.N. Dorsman, and A. van Tol, *Net transport of cholesterol from cells of the human EA.hy 926 endothelial cell line to high density lipoproteins.* Experientia, 1993. **49**(6-7): p. 561-6.
574. Emeis, J.J. and C.J. Edgell, *Fibrinolytic properties of a human endothelial hybrid cell line (Ea.hy 926).* Blood, 1988. **71**(6): p. 1669-75.
575. Eremeeva, M.E. and D.J. Silverman, *Rickettsia rickettsii infection of the EA.hy 926 endothelial cell line: morphological response to infection and evidence for oxidative injury.* Microbiology, 1998. **144 (Pt 8)**: p. 2037-48.
576. Edgell, C.J., et al., *Endothelium specific Weibel-Palade bodies in a continuous human cell line, EA.hy926.* In Vitro Cell Dev Biol, 1990. **26**(12): p. 1167-72.
577. Macville, M., et al., *Comprehensive and definitive molecular cytogenetic characterization of HeLa cells by spectral karyotyping.* Cancer Res, 1999. **59**(1): p. 141-50.
578. Rahbari, R., et al., *A novel L1 retrotransposon marker for HeLa cell line identification.* Biotechniques, 2009. **46**(4): p. 277-84.
579. Tseeb, V., et al., *Highly thermosensitive Ca dynamics in a HeLa cell through IP(3) receptors.* HFSP J, 2009. **3**(2): p. 117-23.
580. Lui, P.P., et al., *The rise of nuclear and cytosolic Ca2+ can be uncoupled in HeLa cells.* Pflugers Arch, 1998. **436**(3): p. 371-6.
581. Bulotta, S., et al., *Activation of the endothelial nitric-oxide synthase by tumor necrosis factor-alpha. A novel feedback mechanism regulating cell death.* J Biol Chem, 2001. **276**(9): p. 6529-36.
582. Todaro, G.J. and H. Green, *Quantitative studies of the growth of mouse embryo cells in culture and their development into established lines.* J Cell Biol, 1963. **17**: p. 299-313.
583. Todaro, G.J., S.R. Wolman, and H. Green, *Rapid Transformation of Human Fibroblasts with Low Growth Potential into Established Cell Lines by Sv40.* J Cell Physiol, 1963. **62**: p. 257-65.
584. Garlid, K.D., *Opening mitochondrial K(ATP) in the heart--what happens, and what does not happen.* Basic Res Cardiol, 2000. **95**(4): p. 275-9.
585. Zheng, J.S., et al., *Extracellular ATP inhibits adrenergic agonist-induced hypertrophy of neonatal cardiac myocytes.* Circ Res, 1996. **78**(4): p. 525-35.
586. Danziger, R.S., et al., *Extracellular ATP has a potent effect to enhance cytosolic calcium and contractility in single ventricular myocytes.* Cell Calcium, 1988. **9**(4): p. 193-9.

587. Balogh, J., et al., *Phospholipase C and cAMP-dependent positive inotropic effects of ATP in mouse cardiomyocytes via P2Y11-like receptors.* Journal of Molecular and Cellular Cardiology, 2005. **39**(2): p. 223-230.
588. Erlinge, D. and G. Burnstock, *P2 receptors in cardiovascular regulation and disease.* Purinergic Signal, 2008. **4**(1): p. 1-20.
589. Burnstock, G., *Purinergic signaling and vascular cell proliferation and death.* Arterioscler Thromb Vasc Biol, 2002. **22**(3): p. 364-73.
590. Wihlborg, A.K., et al., *ADP receptor P2Y12 is expressed in vascular smooth muscle cells and stimulates contraction in human blood vessels.* Arterioscler Thromb Vasc Biol, 2004. **24**(10): p. 1810-5.
591. Ralevic, V. and G. Burnstock, *Involvement of purinergic signaling in cardiovascular diseases.* Drug News Perspect, 2003. **16**(3): p. 133-40.
592. Hechler, B., M. Cattaneo, and C. Gachet, *The P2 receptors in platelet function.* Seminars in thrombosis and hemostasis, 2005. **31**(2): p. 150-161.
593. Jin, J. and S.P. Kunapuli, *Coactivation of two different G protein-coupled receptors is essential for ADP-induced platelet aggregation.* Proc Natl Acad Sci U S A, 1998. **95**(14): p. 8070-4.
594. Peroutka, S.J., *Migraine: a chronic sympathetic nervous system disorder.* Headache, 2004. **44**(1): p. 53-64.
595. Bowers, K.C., A.P. Allshire, and P.H. Cobbold, *Continuous measurements of cytoplasmic ATP in single cardiomyocytes during simulation of the "oxygen paradox".* Cardiovasc Res, 1993. **27**(10): p. 1836-9.
596. Decker, M.L., et al., *Morphometric evaluation of the contractile apparatus in primary cultures of rabbit cardiac myocytes.* Circ Res, 1991. **69**(1): p. 86-94.
597. Louch, W.E., K.A. Sheehan, and B.M. Wolska, *Methods in cardiomyocyte isolation, culture, and gene transfer.* J Mol Cell Cardiol, 2011. **51**(3): p. 288-98.
598. Diaz, R.J. and G.J. Wilson, *Studying ischemic preconditioning in isolated cardiomyocyte models.* Cardiovasc Res, 2006. **70**(2): p. 286-96.
599. Vogel, A., et al., *Coordinate control of 3T3 cell proliferation by platelet-derived growth factor and plasma components.* Proc Natl Acad Sci U S A, 1978. **75**(6): p. 2810-4.
600. DeHann, R.L., *Regulation of spontaneous activity and growth of embryonic chick heart cells in tissue culture.* Dev Biol, 1967. **16**(3): p. 216-49.
601. Blondel, B., I. Roijen, and J.P. Cheneval, *Heart cells in culture: a simple method for increasing the proportion of myoblasts.* Experientia, 1971. **27**(3): p. 356-8.
602. Fox, C.H., et al., *Formaldehyde fixation.* J Histochem Cytochem, 1985. **33**(8): p. 845-53.
603. Rizzuto, R., et al., *Photoprotein-mediated measurement of calcium ion concentration in mitochondria of living cells.* Methods Enzymol, 1995. **260**: p. 417-28.
604. Higa, A. and M. Mandel, *Factors influencing competence of Escherichia coli for lambda-phage deoxyribonucleic acid infection.* Jpn J Microbiol, 1972. **16**(4): p. 251-7.

605. Conant, A.R., et al., *Diadenosine polyphosphates are selective vasoconstrictors in human coronary artery bypass grafts.* Vascular Pharmacology, 2008. **48**(4–6): p. 157-164.
606. Conant, A.R., et al., *Characterization of the P2 receptors on the human umbilical vein endothelial cell line ECV304.* British Journal of Pharmacology, 1998. **125**(2): p. 357-364.
607. Conant, A.R., W.C. Dihmis, and A.W.M. Simpson, *Diadenosine polyphosphates are potential mediators of post-operative contraction in human coronary artery bypass grafts.* Journal of Molecular and Cellular Cardiology, 2006. **40**(6): p. 1013.
608. Murgia, M., et al., *Oxidized ATP. An irreversible inhibitor of the macrophage purinergic P2Z receptor.* J Biol Chem, 1993. **268**(11): p. 8199-203.
609. Morelli, A., et al., *Extracellular ATP causes ROCK I-dependent bleb formation in P2X7-transfected HEK293 cells.* Mol Biol Cell, 2003. **14**(7): p. 2655-64.
610. Di Virgilio, F., *Novel data point to a broader mechanism of action of oxidized ATP: the P2X7 receptor is not the only target.* Br J Pharmacol, 2003. **140**(3): p. 441-3.
611. van Loo, G., et al., *The role of mitochondrial factors in apoptosis: a Russian roulette with more than one bullet.* Cell Death Differ, 2002. **9**(10): p. 1031-42.
612. Lakhani, S.A., et al., *Caspases 3 and 7: key mediators of mitochondrial events of apoptosis.* Science, 2006. **311**(5762): p. 847-51.
613. Cobbold, P.H.a.L., J. A. C., *Cellular Calcium: A Practical Approach (McCormack, J. G. and Cobbold, P. H., eds.).* 1991: p. 54-81.
614. Lazarowski, E.R., et al., *Pharmacological selectivity of the cloned human P2U-purinoceptor: potent activation by diadenosine tetraphosphate.* Br J Pharmacol, 1995. **116**(1): p. 1619-27.
615. Bacallao, R., S. Sohrab, and C. Phillips, *Guiding Principles of Specimen Preservation for Confocal Fluorescence Microscopy Handbook Of Biological Confocal Microscopy*, J.B. Pawley, Editor. 2006, Springer US. p. 368-380.
616. Malouf, N.N., et al., *A cardiac troponin T epitope conserved across phyla.* J Biol Chem, 1992. **267**(13): p. 9269-74.
617. Bader, D., T. Masaki, and D.A. Fischman, *Immunochemical analysis of myosin heavy chain during avian myogenesis in vivo and in vitro.* J Cell Biol, 1982. **95**(3): p. 763-70.
618. Hartley, R.S. and Z. Yablonka-Reuveni, *Long-term maintenance of primary myogenic cultures on a reconstituted basement membrane.* In Vitro Cell Dev Biol, 1990. **26**(10): p. 955-61.
619. Grubbs, F., *Procedures for detecting outlying observations in samples.* Technometrics., 1969. **11**: p. 1-21.
620. Oubrahim, H., E.R. Stadtman, and P.B. Chock, *Mitochondria play no roles in Mn(II)-induced apoptosis in HeLa cells.* Proc Natl Acad Sci U S A, 2001. **98**(17): p. 9505-10.
621. Murata, M., et al., *Mitochondrial ATP-sensitive potassium channels attenuate matrix Ca(2+) overload during simulated ischemia and reperfusion: possible mechanism of cardioprotection.* Circ Res, 2001. **89**(10): p. 891-8.

622. Gaspar, T., et al., *ROS-independent preconditioning in neurons via activation of mitoK(ATP) channels by BMS-191095.* J Cereb Blood Flow Metab, 2008. **28**(6): p. 1090-103.
623. Biagini, G.A., et al., *Functional characterization and target validation of alternative complex I of Plasmodium falciparum mitochondria.* Antimicrob Agents Chemother, 2006. **50**(5): p. 1841-51.
624. Chalmers, S. and J.G. McCarron, *The mitochondrial membrane potential and Ca2+ oscillations in smooth muscle.* J Cell Sci, 2008. **121**(Pt 1): p. 75-85.
625. Gerstenberger, J.P., P. Occhipinti, and A.S. Gladfelter, *Heterogeneity in mitochondrial morphology and membrane potential is independent of the nuclear division cycle in multinucleate fungal cells.* Eukaryot Cell, 2012. **11**(3): p. 353-67.
626. Rego, A.C., S. Vesce, and D.G. Nicholls, *The mechanism of mitochondrial membrane potential retention following release of cytochrome c in apoptotic GT1-7 neural cells.* Cell Death Differ, 2001. **8**(10): p. 995-1003.
627. Berg, J., Y.P. Hung, and G. Yellen, *A genetically encoded fluorescent reporter of ATP:ADP ratio.* Nat Methods, 2009. **6**(2): p. 161-6.
628. Anderberg, E.K. and P. Artursson, *Epithelial transport of drugs in cell culture. VIII: Effects of sodium dodecyl sulfate on cell membrane and tight junction permeability in human intestinal epithelial (Caco-2) cells.* Journal of Pharmaceutical Sciences, 1993. **82**(4): p. 392-398.
629. Beigi, R.D., et al., *Oxidized ATP (oATP) attenuates proinflammatory signaling via P2 receptor-independent mechanisms.* Br J Pharmacol, 2003. **140**(3): p. 507-19.
630. Lazarowski, E.R., et al., *UDP activates a mucosal-restricted receptor on human nasal epithelial cells that is distinct from the P2Y2 receptor.* Proc Natl Acad Sci U S A, 1997. **94**(6): p. 2599-603.
631. Brown, J., et al., *Critical evaluation of ECV304 as a human endothelial cell model defined by genetic analysis and functional responses: a comparison with the human bladder cancer derived epithelial cell line T24/83.* Lab Invest, 2000. **80**(1): p. 37-45.
632. Volonte, C., et al., *P2X7 Receptors: Channels, Pores and More.* CNS & Neurological Disorders - Drug Targets, 2012. **11**(6): p. 705-721.
633. Cheewatrakoolpong, B., et al., *Identification and characterization of splice variants of the human P2X7 ATP channel.* Biochem Biophys Res Commun, 2005. **332**(1): p. 17-27.
634. Yan, Z., et al., *The P2X7 receptor channel pore dilates under physiological ion conditions.* J Gen Physiol, 2008. **132**(5): p. 563-73.
635. Horn, R. and M.S. Brodwick, *Acetylcholine-induced current in perfused rat myoballs.* J Gen Physiol, 1980. **75**(3): p. 297-321.
636. Wu, F.S. and K. Zierler, *Calcium currents in rat myoballs and their inhibition by insulin.* Endocrinology, 1989. **125**(5): p. 2563-72.
637. Percival, A.L., et al., *Chicken skeletal muscle ryanodine receptor isoforms: ion channel properties.* Biophysical journal, 1994. **67**(5): p. 1834-1850.
638. Lukyanenko, V., et al., *Inhibition of Ca(2+) sparks by ruthenium red in permeabilized rat ventricular myocytes.* Biophys J, 2000. **79**(3): p. 1273-84.

639. Carroll, S., et al., *N-RAP scaffolds I-Z-I assembly during myofibrillogenesis in cultured chick cardiomyocytes.* J Cell Sci, 2004. **117**(Pt 1): p. 105-14.
640. Dabiri, G.A., et al., *Myofibrillogenesis visualized in living embryonic cardiomyocytes.* Proc Natl Acad Sci U S A, 1997. **94**(17): p. 9493-8.
641. E, L.L., et al., *Enrichment of cardiomyocytes derived from mouse embryonic stem cells.* J Heart Lung Transplant, 2006. **25**(6): p. 664-74.
642. Homolya, L., et al., *Nucleotide-regulated calcium signaling in lung fibroblasts and epithelial cells from normal and P2Y(2) receptor (-/-) mice.* J Biol Chem, 1999. **274**(37): p. 26454-60.
643. Andrienko, T.N., E. Picht, and D.M. Bers, *Mitochondrial free calcium regulation during sarcoplasmic reticulum calcium release in rat cardiac myocytes.* Journal of Molecular and Cellular Cardiology, 2009. **46**(6): p. 1027-1036.
644. Sedova, M., E.N. Dedkova, and L.A. Blatter, *Integration of rapid cytosolic Ca2+ signals by mitochondria in cat ventricular myocytes.* Am J Physiol Cell Physiol, 2006. **291**(5): p. C840-50.
645. Maack, C., et al., *Elevated cytosolic Na + decreases mitochondrial Ca 2+ uptake during excitation-contraction coupling and impairs energetic adaptation in cardiac myocytes.* Circulation Research, 2006. **99**(2): p. 172-182.
646. Dedkova, E.N. and L.A. Blatter, *Mitochondrial Ca2+ and the heart.* Cell Calcium, 2008. **44**(1): p. 77-91.
647. Standen, N.B., *Cardioprotection by preconditioning: K(ATP) channels, metabolism, or both?* J Physiol, 2002. **542**(Pt 3): p. 666.
648. Erusalimsky, J.D. and S. Moncada, *Nitric oxide and mitochondrial signaling: from physiology to pathophysiology.* Arterioscler Thromb Vasc Biol, 2007. **27**(12): p. 2524-31.
649. Lawrence, C.L., et al., *The KATP channel opener diazoxide protects cardiac myocytes during metabolic inhibition without causing mitochondrial depolarization or flavoprotein oxidation.* Br J Pharmacol, 2001. **134**(3): p. 535-42.
650. Kirichok, Y., G. Krapivinsky, and D.E. Clapham, *The mitochondrial calcium uniporter is a highly selective ion channel.* Nature, 2004. **427**(6972): p. 360-4.
651. Zoratti, M. and I. Szabo, *Electrophysiology of the inner mitochondrial membrane.* J Bioenerg Biomembr, 1994. **26**(5): p. 543-53.
652. Garcia-Perez, C., G. Hajnoczky, and G. Csordas, *Physical coupling supports the local Ca2+ transfer between sarcoplasmic reticulum subdomains and the mitochondria in heart muscle.* J Biol Chem, 2008. **283**(47): p. 32771-80.
653. Lohret, T.A., R.E. Jensen, and K.W. Kinnally, *Tim23, a protein import component of the mitochondrial inner membrane, is required for normal activity of the multiple conductance channel, MCC.* J Cell Biol, 1997. **137**(2): p. 377-86.
654. Lohret, T.A., et al., *Activity of the mitochondrial multiple conductance channel is independent of the adenine nucleotide translocator.* J Biol Chem, 1996. **271**(9): p. 4846-9.

655. Bortner, C.D., F.M. Hughes, Jr., and J.A. Cidlowski, *A primary role for K+ and Na+ efflux in the activation of apoptosis.* J Biol Chem, 1997. **272**(51): p. 32436-42.
656. Schwartzman, R.A. and J.A. Cidlowski, *Apoptosis: the biochemistry and molecular biology of programmed cell death.* Endocr Rev, 1993. **14**(2): p. 133-51.
657. De Stefani, D., et al., *A forty-kilodalton protein of the inner membrane is the mitochondrial calcium uniporter.* Nature, 2011. **476**(7360): p. 336-40.
658. Ichikawa, H., et al., *Rotenone, a mitochondrial electron transport inhibitor, ameliorates ischemia-reperfusion-induced intestinal mucosal damage in rats.* Redox Rep, 2004. **9**(6): p. 313-6.
659. Koopman, W.J., et al., *Inhibition of complex I of the electron transport chain causes O2-. -mediated mitochondrial outgrowth.* Am J Physiol Cell Physiol, 2005. **288**(6): p. C1440-50.
660. Tada-Oikawa, S., et al., *Mechanism for generation of hydrogen peroxide and change of mitochondrial membrane potential during rotenone-induced apoptosis.* Life Sci, 2003. **73**(25): p. 3277-88.
661. Franco, R., M.I. Panayiotidis, and J.A. Cidlowski, *Glutathione depletion is necessary for apoptosis in lymphoid cells independent of reactive oxygen species formation.* J Biol Chem, 2007. **282**(42): p. 30452-65.
662. Walford, G.A., et al., *Hypoxia potentiates nitric oxide-mediated apoptosis in endothelial cells via peroxynitrite-induced activation of mitochondria-dependent and -independent pathways.* J Biol Chem, 2004. **279**(6): p. 4425-32.
663. Gauuan, P.J., et al., *Superoxide dismutase mimetics: synthesis and structure-activity relationship study of MnTBAP analogues.* Bioorg Med Chem, 2002. **10**(9): p. 3013-21.
664. Sorgato, M.C., B.U. Keller, and W. Stuhmer, *Patch-clamping of the inner mitochondrial membrane reveals a voltage-dependent ion channel.* Nature, 1987. **330**(6147): p. 498-500.
665. Warburg, O., *On respiratory impairment in cancer cells.* Science, 1956. **124**(3215): p. 269-70.
666. Imamura, H., et al., *Visualization of ATP levels inside single living cells with fluorescence resonance energy transfer-based genetically encoded indicators.* Proc Natl Acad Sci U S A, 2009. **106**(37): p. 15651-6.
667. Reitzer, L.J., B.M. Wice, and D. Kennell, *Evidence that glutamine, not sugar, is the major energy source for cultured HeLa cells.* J Biol Chem, 1979. **254**(8): p. 2669-76.
668. Rossignol, R., et al., *Energy substrate modulates mitochondrial structure and oxidative capacity in cancer cells.* Cancer Res, 2004. **64**(3): p. 985-93.
669. Von der Weid, P.Y., et al., *Effects of ATP on cultured smooth muscle cells from rat aorta.* British Journal of Pharmacology, 1993. **108**(3): p. 638-645.
670. Strøbæk, D., et al., *ATP activates K and Cl channels via purinoceptor-mediated release of Ca2+ in human coronary artery smooth muscle.* American Journal of Physiology - Cell Physiology, 1996. **271**(5 40-5): p. C1463-C1471.

671. Ikeuchi, Y. and T. Nishizaki, *ATP activates the potassium channel and enhances cytosolic Ca2+ release via a P(2y) purinoceptor linked to pertussis toxin-insensitive G-protein in brain artery endothelial cells.* Biochemical and Biophysical Research Communications, 1995. **215**(3): p. 1022-1028.
672. Dedkova, E.N., A.A. Sigova, and V.P. Zinchenko, *Mechanism of action of calcium ionophores on intact cells: ionophore-resistant cells.* Membr Cell Biol, 2000. **13**(3): p. 357-68.
673. Kreda, S.M., et al., *Receptor-promoted exocytosis of airway epithelial mucin granules containing a spectrum of adenine nucleotides.* J Physiol, 2010. **588**(Pt 12): p. 2255-67.
674. Goodpaster, T., et al., *An immunohistochemical method for identifying fibroblasts in formalin-fixed, paraffin-embedded tissue.* J Histochem Cytochem, 2008. **56**(4): p. 347-58.
675. Miettinen, M., A.E. Lindenmayer, and A. Chaubal, *Endothelial cell markers CD31, CD34, and BNH9 antibody to H- and Y-antigens--evaluation of their specificity and sensitivity in the diagnosis of vascular tumors and comparison with von Willebrand factor.* Modern pathology : an official journal of the United States and Canadian Academy of Pathology, Inc, 1994. **7**(1): p. 82-90.
676. Lian, X., et al., *Robust cardiomyocyte differentiation from human pluripotent stem cells via temporal modulation of canonical Wnt signaling.* Proc Natl Acad Sci U S A, 2012. **109**(27): p. E1848-57.
677. Djurovic, S., et al., *Comparison of nonviral transfection and adeno-associated viral transduction on cardiomyocytes.* Molecular Biotechnology, 2004. **28**(1): p. 21-31.
678. Tu, Y., F. Li, and C. Wu, *Nck-2, a novel Src homology2/3-containing adaptor protein that interacts with the LIM-only protein PINCH and components of growth factor receptor kinase-signaling pathways.* Mol Biol Cell, 1998. **9**(12): p. 3367-82.
679. Albert, N. and J.P. Tremblay, *Evaluation of various gene transfection methods into human myoblast clones.* Transplant Proc, 1992. **24**(6): p. 2784-6.
680. Dodds, E., et al., *Lipofection of cultured mouse muscle cells: a direct comparison of Lipofectamine and DOSPER.* Gene Ther, 1998. **5**(4): p. 542-51.
681. Trivedi, R.A. and G. Dickson, *Liposome-mediated gene transfer into normal and dystrophin-deficient mouse myoblasts.* J Neurochem, 1995. **64**(5): p. 2230-8.
682. Vitiello, L., et al., *Transfection of cultured myoblasts in high serum concentration with DODAC:DOPE liposomes.* Gene Ther, 1998. **5**(10): p. 1306-13.
683. Kott, M., et al., *A new efficient method for transfection of neonatal cardiomyocytes using histone H1 in combination with DOSPER liposomal transfection reagent.* Somat Cell Mol Genet, 1998. **24**(4): p. 257-61.
684. Monahan, P.E. and R.J. Samulski, *Adeno-associated virus vectors for gene therapy: more pros than cons?* Mol Med Today, 2000. **6**(11): p. 433-40.
685. Kucera, J.P., et al., *Power-law behavior of beat-rate variability in monolayer cultures of neonatal rat ventricular myocytes.* Circ Res, 2000. **86**(11): p. 1140-5.